2015

# Influence of heterocycle substitution in π-functional materials for organic photovoltaics

Benjamin James Hale
*Iowa State University*

# Influence of heterocycle substitution in π-functional materials for organic photovoltaics

by

**Benjamin J. Hale**

A dissertation submitted to the graduate faculty

in partial fulfillment of the requirements for the degree of

DOCTOR OF PHILOSOPHY

Major: Organic Chemistry

Program of Study Committee:
Malika Jeffries-EL, Major Professor
William Jenks
Javier Vela
Arthur Winter
Sumit Chaudhary

Iowa State University

Ames, Iowa

2015

# DEDICATION

To Aunt Pat, we miss you.

TABLE OF CONTENTS

# CHAPTER 1

# GENERAL INTRODUCTION

## 1.1 Dissertation Overview

This dissertation details the work performed by the author in the Jeffries-EL group from 2009-2015. The work discussed is centered around the design, synthesis, and characterization of various π-conjugated materials and their use in organic photovoltaic (OPV) solar cells. Chapter 1 is a general introduction to the physical and electronic properties of organic semiconducting materials, as well as the synthetic principals toward designing narrow band gap materials. An overview of the history, physics, and engineering requirements of OPV solar cells is also discussed.

Chapter 2 is a paper that has been submitted to *Chemistry – A European Journal* for publication and discusses the impact of nitrogen substitution for the sulfur atom of the widely used thienopyrroledione (TPD) acceptor unit. The majority of the synthetic work was performed by the author. Additional monomer precursors were synthesized by Jon Stoffer. The device fabrication and testing was performed by Moneim Elshobaki and Ryan Gebhardt. Computational work was performed by David Wheeler. The computational section was written by Aimée Tomlinson. The remainder of the manuscript was written by the author of this dissertation.

Chapter 3 is a manuscript in preparation for *Macromolecules* and reports the synthesis of a series of donor-acceptor-donor-acceptor-donor (D1-A-D2-A-D1) based molecular donors and the impact of the variation of D1 and D2 on the physical and electronic

properties of the materials, as well as their performance in organic photovoltaic devices. All of the synthetic work was performed by the author. The device fabrication, testing, and characterization was performed by Ryan Gebhardt. The manuscript was written by the author of this dissertation.

Chapter 4 is a manuscript in preparation for *Polymer Chemistry* and reports the synthesis, characterization, and the impact of heteroatom substitution and side chain variation on the photovoltaic performance of four dithienosilole-*alt*-diketopyrrolopyrrole based polymers. All of the synthetic work was performed by the author. Some of the intermediate 3,3'-dibromo-5,5'-bis(trimethylsilyl)-2,2'-bithiophene was recrystallized by Dr. Achala Bhuwalka. The device fabrication is currently being performed by Ian Pelse under the supervision of Dr. John Reynolds. The manuscript was written by the author of this dissertation.

Chapter 5 is a manuscript that is in preparation for *Macromolecular Rapid Communications* and expands upon the pyrrolopyrroledione (PPD) unit described in Chapter 4 by using PPD as a donor in donor-acceptor copolymers with both TPD and diketopyrrolopyrrole as acceptors. The majority of the synthetic work was performed by the author. Additional monomer precursors were synthesized by Jon Stoffer. The manuscript was written by the author of this dissertation.

Chapter 6 draws some general conclusions of the work performed The chapter concludes with acknowledgements from the author of this dissertation, followed by an appendix of terms used in this dissertation.

## 1.2 Origins of Organic Semiconductors

Nearly forty years ago, Shirakawa, MacDiarmid, and Heeger et al. reported the first instance of an organic semiconductor with the discovery of electrical conductivity in doped polyacetylene.[1, 2] Since that time, interest in organic semiconductors has grown exponentially, with progress in the research of these materials taking them from being merely an academic curiosity to being commercially viable in a variety of applications, such as organic photovoltaics (OPVs),[3-7] light-emitting diodes (OLEDs),[8-11] field-effect transistors (OFETs),[12-19] non-linear optics,[20-24] electrochemical cells (batteries),[25-27] and sensor devices.[28-30] Although interest in organic semiconductors is at an all-time high, inorganic semiconductors are still predominantly used in devices, yet organics offer numerous potential advantages over inorganics.

Most materials commonly used in inorganic semiconductors, including silicon, germanium, gallium arsenide, cadmium telluride, and lead (pervoskites), require high cost-processing on an industrial scale and face various issues in terms of extreme toxicity and air stability, particularly in photovoltaics.[31] For efficient silicon-based devices, ultra-high purity silicon is required as well as expensive processing techniques, such as vapor deposition and lithographic printing, due to the detrimental impact of defects on device performance.[32-35] Perovskite-based photovoltaics suffer heavily from air stability issues and the toxicity of lead salts. Cadmium telluride photovoltaics, while less sensitive to defects and having significantly cheaper fabrication costs than silicon, suffer from lower efficiencies, the extreme toxicity of cadmium, and the toxicity and low availability of tellurium. Even after accounting for recovery from recycling, recent projections suggest

that the capacity for manufacturing thin-film photovoltaic cells from cadmium telluride is very near the maximum supply of tellurium available.[36]

On the other hand, organic semiconductors, while currently less efficient than their inorganic counterparts (Figure 1.1), offer several advantages. Organic semiconductors, made from petroleum products, can be fabricated into devices using low-cost techniques, such as spin-coating,[37] inkjet printing,[38] dip coating,[39] and screen printing[40] due to their solubility in common organic solvents. These techniques lend well to commercial applications, for instance roll-to-roll processing, as they are easily scaled up and allow the fabrication of large area panels on flexible substrates.[41] Even with recent developments in flexible silicon-based photovoltaics,[42] the ability to fine-tune the physical and electronic properties of organic semiconductors through structural modification gives rise to a wide

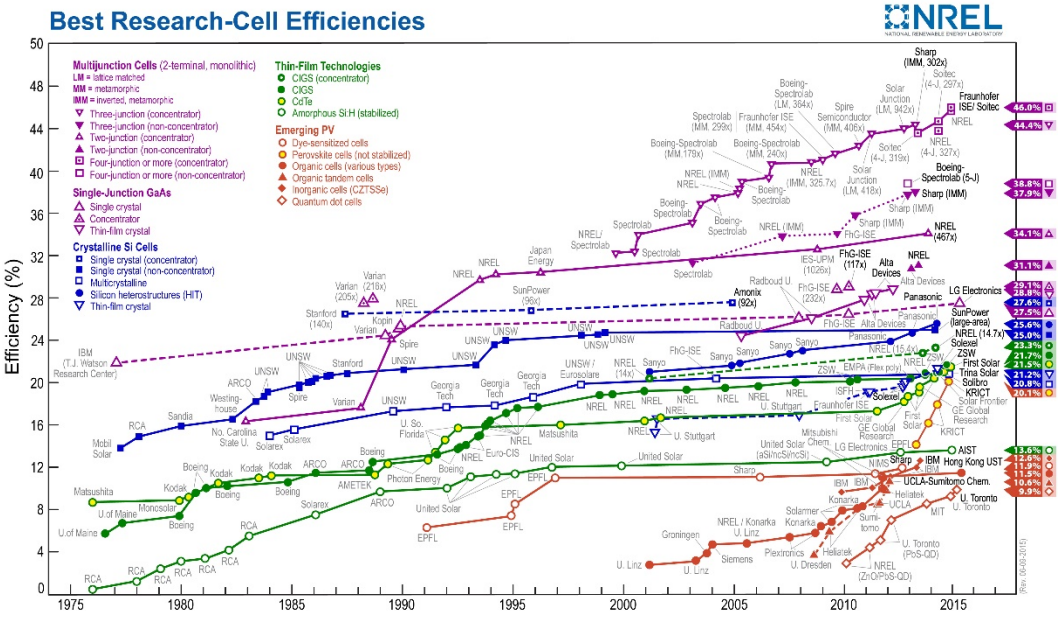


**Figure 1.1.** Best efficiencies of research solar cells. Organics are in red (bottom right).[43]

range of properties not attainable in inorganics. Synthetic structural modifications of an organic molecule can be used to specifically design a material for an application that it would best be suited and control the performance in a semiconducting device.[44]

The origin of electrical conductivity in organic materials is a direct result of an extended π-system created by alternating single and double bonds. The formation of band-like structures is dependent on the extent of π-conjugation in a system. Figure 1.2 shows how these band structures are formed in polyacetylene. As the chain length increases from ethylene to butadiene to octatetraene to the *n*-ene, the number of π- and π*-molecular orbitals (MOs) increases from 1 to 2 to 4 to *n*-π and π* orbitals. With the addition of each successive π- and π*-orbital, the highest occupied molecular orbital (HOMO) increases

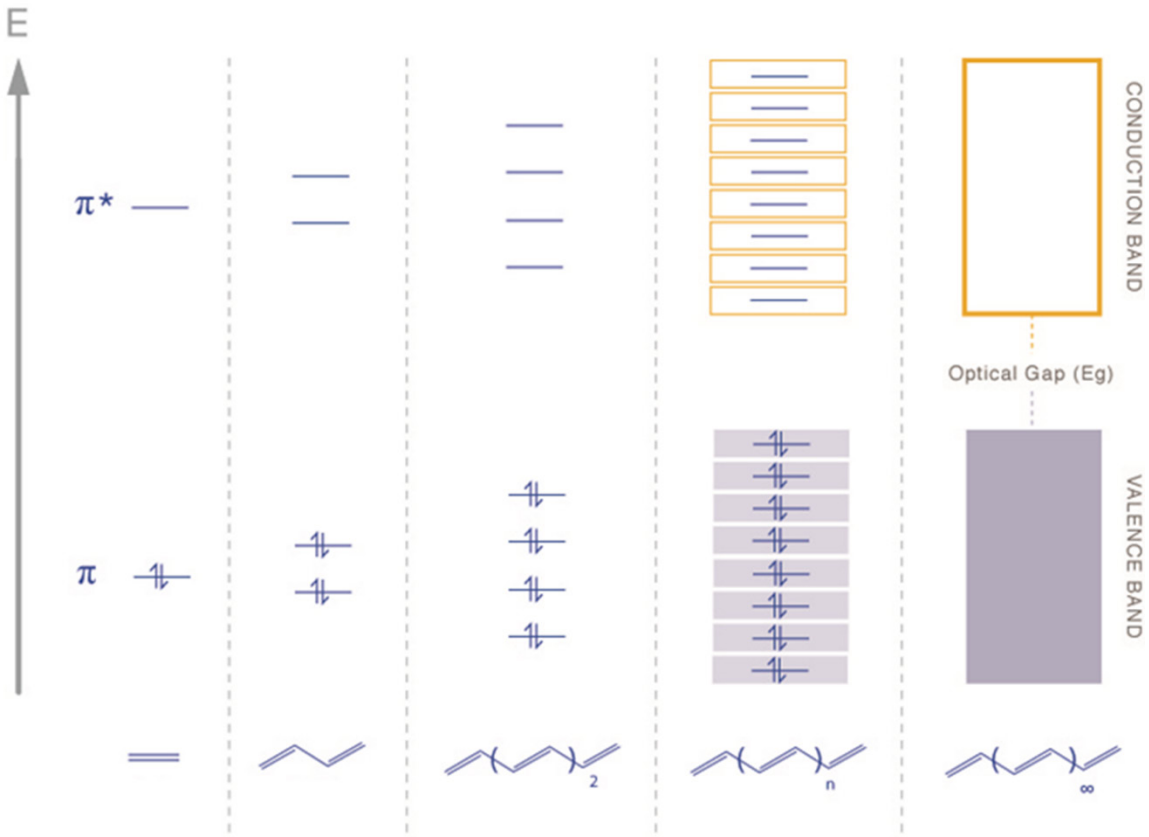


**Figure 1.2.** Origin of the band structure of polyacetylene from π-molecular orbitals.

while the lowest occupied molecular orbital (LUMO) decreases.[45] When the number of π-MOs increases, the range of energies they occupy becomes wider, and the MOs become closer in energy. As the conjugation approaches infinity, the energy difference between the filled π- and empty π*-MOs becomes so small that the orbitals begin to resemble the traditional band-like structures that are common with inorganic semiconductors, with the π- and π*-orbitals being analogous to the valence and conduction bands, respectively, and the distance between them corresponding to the bandgap.[1] Both the location of the band structure and the size of the bandgap determine the properties of the semiconducting materials, but, as discussed later, this band structure can be fine-tuned through material design to have the necessary properties for the desired application.

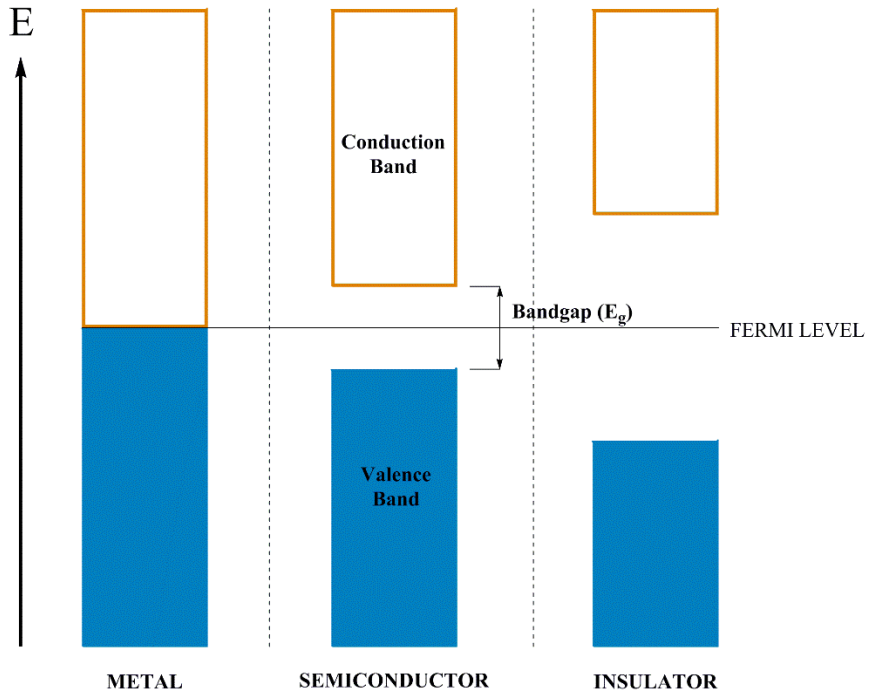


**Figure 1.3.** Simplified band diagrams for metals, semiconductors, and insulators.

While the formation of band structures is necessary for high electrical conductivity, the magnitude of the bandgap primarily determines whether a material is a conductor,

semiconductor, or insulator, as depicted in Figure 1.3. In the case of metals, there is only a partially-filled band, as opposed to two discreet bands with a bandgap, which allows for the free flow of electrons and holes. Insulators, on the other hand, possess a very large bandgap that prevents all conduction, as electrons are unable to be thermally promoted to states capable of carrying current. Semiconductors also have a bandgap, but it is much narrower, enabling a dilute number of thermally excited carriers to reside near the conduction band edge.[46, 47] While in theory polymer conjugation could extend from one end of the chain to the other, in practice defects in the structure or steric interactions can cause twisting in the backbone. If the degree of twisting is enough, this can limit the delocalization of π-electrons to smaller segments, reducing the effective conjugation length of the material, which in turn increases the bandgap.

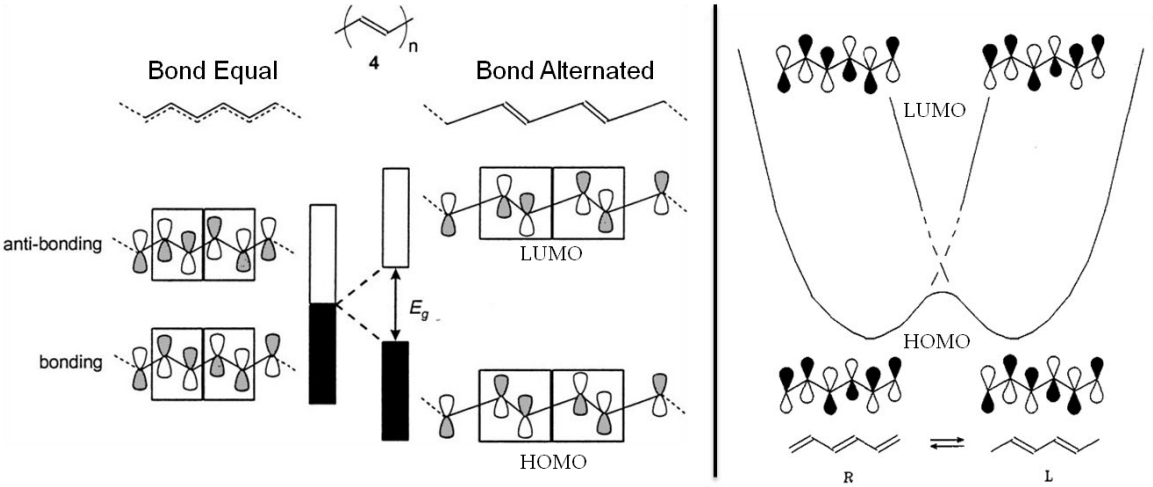


**Figure 1.4.** Bandgap formation due to Peierls distortion in polyacetylene.

In an ideal world, polyacetylene would be able to increase its conjugation to the point where the HOMO and LUMO converged, making it an organic metal with an effective conjugation length running the entirety of the polymer. In this scenario, the fully

delocalized π-system (Bond Equal, Figure 1.4) along the polymer backbone would cause every bond to be the same length. The full delocalization of the π-electrons would allow them to freely move throughout the length of the polymer, resulting in the band structure of a metal. In reality, polyacetylene experiences a geometric deformation, known as Peierls distortion, that results in alternating short and long bonds, caused by the interactions of bonding and non-bonding π-orbitals (Bond Alternated, Figure 1.4).[48] This difference in bond length is observable in nuclear magnetic resonance and x-ray diffraction spectroscopy, and has been measured to be 1.35 Å and 1.45 Å.[48, 49] This distortion prevents full delocalization of the π-electrons, causing a splitting of the energy levels and the formation of a bandgap.[50]

The two bond lengths of polyacetylene arise due to the two degenerate ground states of polyacetylene. These states, labeled as R and L in Figure 1.4, have HOMOs having π-bonding interactions between the double bonds and π-antibonding interactions between the single bonds, with the only difference between R and L being the position of the double and single bonds. Conversely, the LUMOs experience π-bonding interactions between the single bonds and π-antibonding interactions between the double bonds. Both the HOMO and LUMO of R are energetically equivalent to the respective HOMO and LUMO of L. Further examination shows the HOMO of the R form corresponds to the LUMO of the L form, and the HOMO of the L form corresponds to the LUMO of the R form. This relationship leads to a thermally forbidden transition between the two forms, resulting in a dimerization of the polymer and the alternating bonds.[51] The Peierls distortion caused by these two forms result in the formation of the two bands and a medium bandgap of 1.5 eV, making polyacetylene an organic semiconductor.[52]

Unfortunately, most conjugated materials aren't as simple as polyacetylene, such as the case of poly(*p*-phenylene) (PPP) shown in Figure 1.5. The backbones of more complex polyaromatic conjugated materials can be defined as "a series of consecutive carbon-carbon double bonds linked together by carbon-carbon single bonds."[53] Using this definition, there are two possible resonance structures for the ground state with nondegenerate energy. The first resonance structure is called the aromatic form. In the

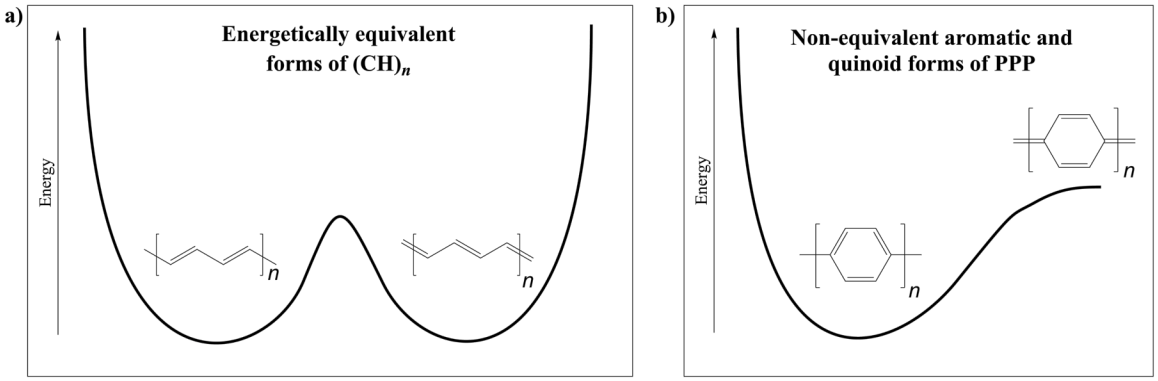


**Figure 1.5.** Potential energy diagrams of polyacetylene (a) and poly(*p*-phenylene) (b)

aromatic form, each carbocycle or heterocycle confines its π-electrons within the ring, maintaining aromaticity. Delocalization of the π-electrons along the backbone converts all double bonds to single bonds and single bonds to double bonds, resulting in the quinoid form. The quinoid form is less stable, having lost the stabilizing effects of aromaticity, and has a higher HOMO and lower LUMO, resulting in a reduced bandgap. This change in energy is represented in Figure 1.5b.

The ratio of aromatic population to quinoid can be expressed in terms of the parameter bond length alternation (BLA), which is defined as the average of the difference in length between adjacent carbon-carbon bonds in a polyene chain.[54] The higher the aromatic

contribution in the ground state, the larger the BLA value.[55] When quinoid contribution increases, the single bonds begin to shorten as they gain more double bond character, and the BLA begins to decrease. As BLA decreases, quinoid character increases linearly, and the bandgap decreases.[56]

Given the relationship between BLA and bandgap, along with the high dependence of the BLA on the aromatic stabilization resonance energy of an aromatic unit, structural modifications introduced along the conjugated backbone can be used to widen or narrow the bandgap. The effect of aromaticity on bandgap is shown in Figure 1.6. Due to the high degree of aromaticity in benzene rings, poly(*p*-phenylene) has a large bandgap of approximately 3.2 eV. With the introduction of something as simple as a double bond

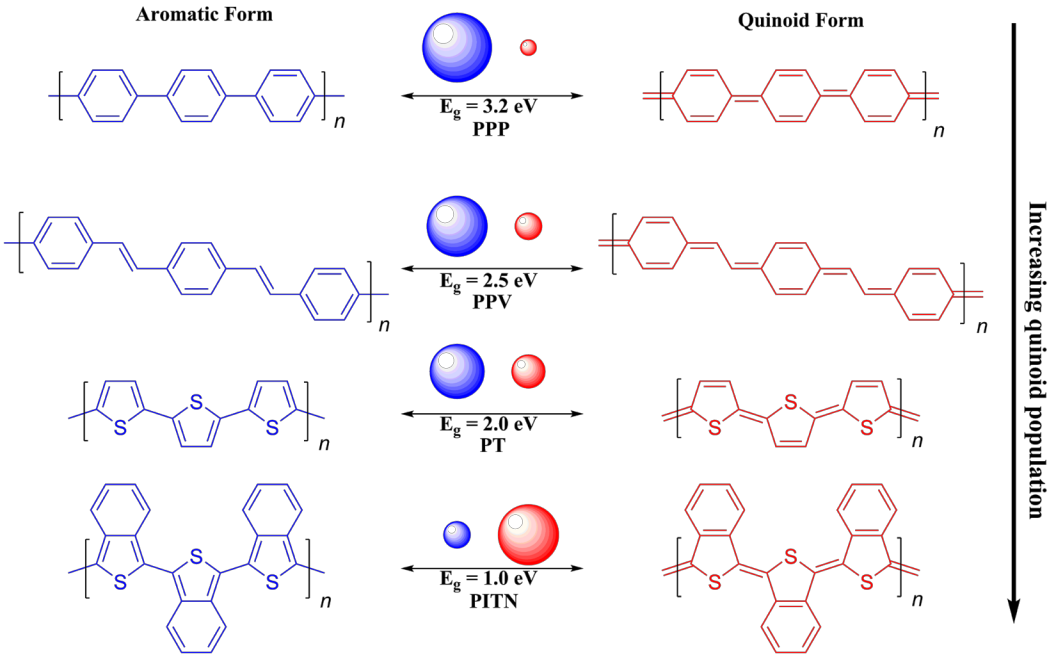


**Figure 1.6.** Aromatic and quinoid resonance forms of poly(*p*-phenylene) (PPP), poly(*p*-phenylenevinylene) (PPV), polythiophene (PT), and poly(isothianaphthene) (PITN) with relative contribution of each form represented by the colored circles.

between the rings, giving poly(*p*-phenylenevinylene), the aromaticity of the benzene rings is diluted and a reduction in the bandgap down to 2.4 eV is observed. The inclusion of aromatic units with lower aromaticity, such as thiophene, can further lower the bandgap. If all of the benzene units are replaced to give polythiophene, the bandgap is lowered to 2.0 eV.[57] The first truly low bandgap material reported was poly(isothianaphthene) (PITN), with a bandgap of 1.0 eV.[58] The remarkably low bandgap of PITN was achieved by placing benzene rings on the [3,4-*c*] edge of the thiophene. Benzene aromaticity, having a greater aromatic resonance energy than thiophene (1.56 vs 1.26 eV, respectively), is preferred over thiophene aromaticity.[59, 60] This preference allows the main chain of PITN to favor the quinoid form to maintain benzene aromaticity, narrowing the bandgap.

As previously mentioned, the effective conjugation length of a material is an important parameter in determining the bandgap. The effective conjugation length is highly dependent on the nature and, in many cases, the order of the aromatic units in the conjugated backbone, therefore the effective conjugation length varies drastically between materials.[61-63] The downside of this approach is it possesses only so much utility, due to the inevitable leveling off of the bandgap due to Peierls distortion.

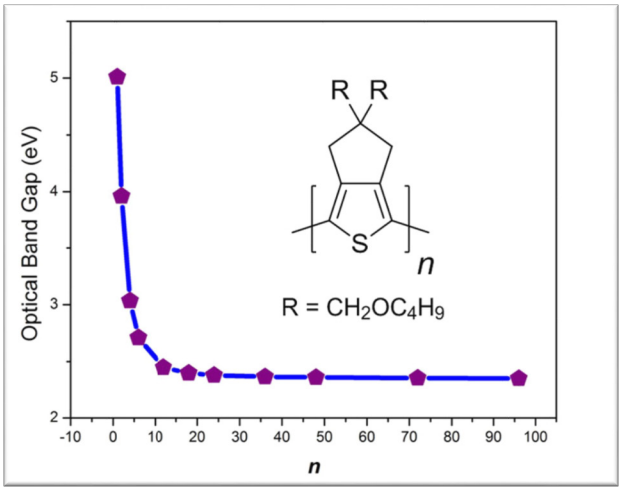


**Figure 1.7.** Relationship between chain length and bandgap in oligiothiophene.

The relationship between bandgap reduction and conjugation length was demonstrated in a study by Otsubo, et al., where the bandgap of functionalized oligiothiophene was measured in the dimer to the 96-mer.[64] As seen in Figure 1.7, there is a drastic reduction of 1.51 eV in bandgap going from n=2 (3.95 eV) to n=12 (2.43 eV). The addition of each new repeat unit shows diminishing returns, with n=1 to n=2, n=2 to n=3, and so on, showing a smaller and smaller reduction in bandgap. While n=2 to n=12 had a reduction of 1.51 eV, extension from n=12 to n=24 gave only a 0.15 eV reduction. Quadrupling the chain length from the 24-mer to the 96-mer gave a bandgap reduction of only 0.11 eV. The varying properties of conjugated materials allows for the effective conjugation length to be as short as 8 repeat units, with many falling in the 11 – 20 repeat unit range.[65-67] Even though increasing conjugation length has a limited effect on bandgap, other important properties, such as film-forming ability and charge transport mobility, are benefited by increased length, and will be discussed later.[68, 69]

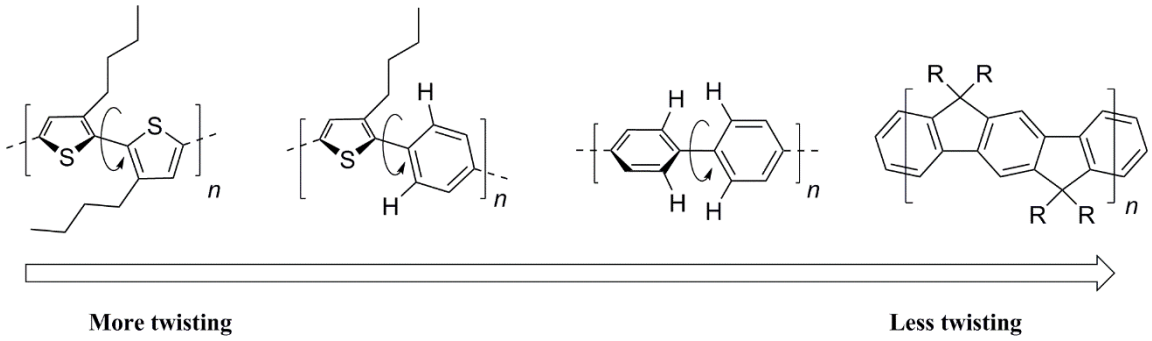


**Figure 1.8.** Effect of steric interactions on planarity of conjugated materials.

Steric defects in a material can have a detrimental impact on planarity, causing a reduction in the bandgap. One approach to guaranteeing a narrow bandgap is to reduce steric interactions between adjacent aromatic units. Reduction in steric interactions increases planarization between adjacent aromatic units. This increased planarization

allows parallel p-orbital interactions to extend conjugation and further facilitate delocalization. This increased delocalization leads to a decrease in BLA and reduction in bandgap. Various causes of backbone twisting are shown in Figure 1.8. The biggest culprit to breaking main chain planarity is the interaction of alkyl chains on two adjacent rings. Inclusion of 6-membered rings in the backbone can also lead to issues, particularly when alkyl chains are present and allow for alkyl – H interactions. A lesser degree of twisting can be see with H – H interactions on adjacent 6-membered rings. Chemical rigidification is one of the most effective ways to decrease steric interactions between adjacent aromatic units. Rigidification is best achieved through the introduction of functionalized methylene or heteroatom bridges to form ladder-type structures. This forces planarity, which decreases BLA, and, in turn, reduces the bandgap.[70, 71]

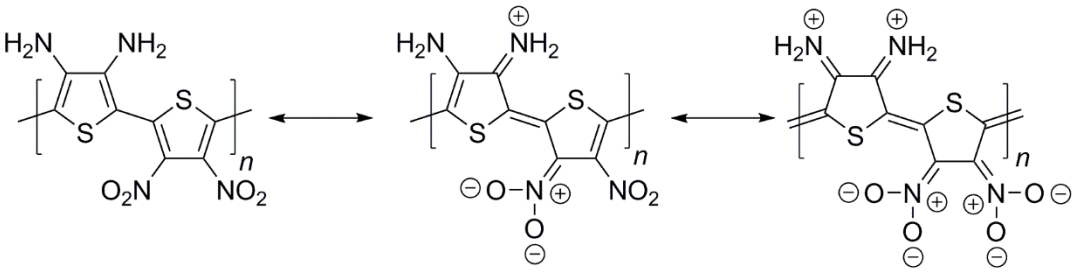

**Figure 1.9.** Promotion of the quinoid form through functional group resonance.

The addition of electron donating groups (EDGs) or electron withdrawing groups (EWGs) directly onto the aromatic units in the main chain is an effective way of perturbing the molecular orbitals, through either inductive or mesomeric effects.[72] In the example shown in Figure 1.9, the addition of electron-donating amines and electron-withdrawing nitro groups on the neighboring thiophene results in a very low bandgap of 1.1 eV due to the high degree of zwitterionic and quinoid character.[73] Some examples of common

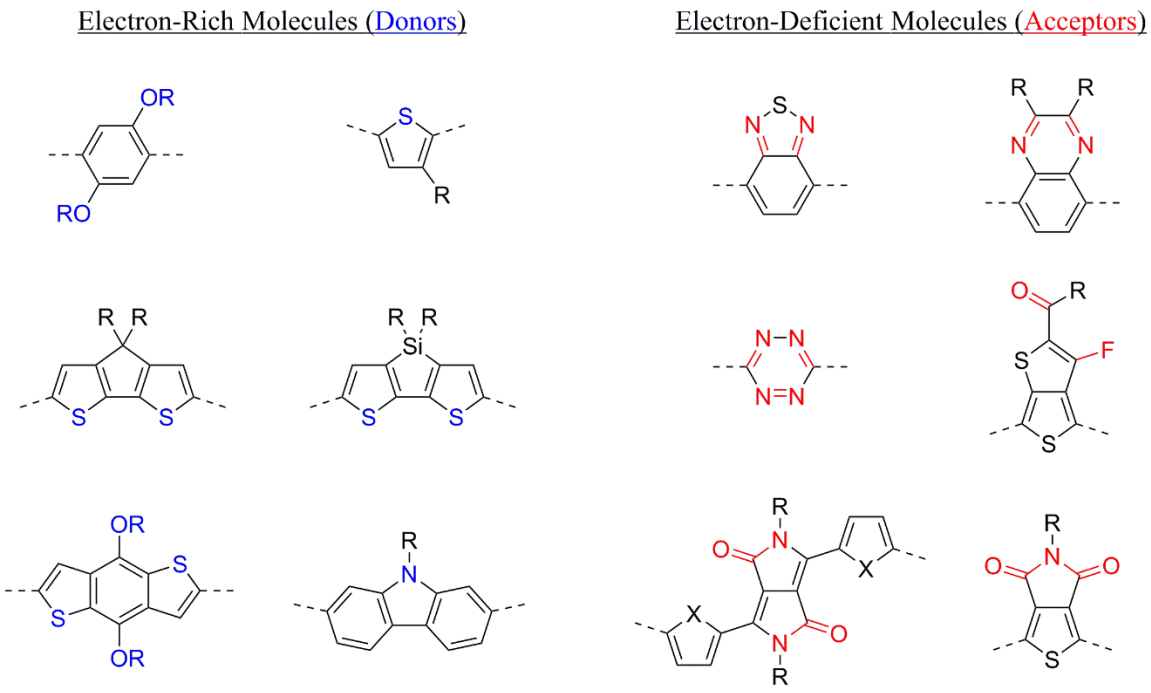


**Figure 1.10.** Common electron-rich donors and electron-deficient acceptors.

electron-donating and electron-accepting units are shown in Figure 1.10. Generally, the addition of electron-donating substituents such as alkyls, alkoxys, amines, and electron rich heteroatoms increase the ionization potential, raising the HOMO energy level of the molecule. The opposite holds true with the addition of electron-withdrawing substituents. The incorporation of fluorines, imines, nitriles, amides, imides, ketones, esters, and nitro groups tend to increase the electron affinity, resulting in lower LUMO levels.[74]

To date, the most effective and widely used method in reducing bandgaps has been the design of materials with alternating conjugated electron-rich donors (D) and a conjugated electron-deficient acceptor (A) in the same backbone.[75-78] The use of this D–A system creates a push-pull driving force, helping facilitate electron delocalization and stabilize mesomeric quinoid structures (D–A → $D^{+}$=$A^{-}$) over the material, reducing BLA. In the case of materials for photovoltaics, photoinduced intramolecular charge transfer (ICT),

correlated with the high-lying HOMO of the donor unit and the low-lying LUMO of the acceptor unit can also account for a reduced bandgap.[78]

The simplest and most explicit explanation for the bandgap reduction in D–A systems, illustrated in Figure 1.11, involves the hybridization of the molecular orbital between the donor and acceptor in the D–A material.[79] In these systems, the HOMO of the donor unit interacts with the HOMO of the acceptor unit, according to the rules of perturbation theory, to give two new HOMOs for the D–A system.[52, 80, 81] In a similar fashion, the LUMO of the donor unit interacts with the LUMO of the acceptor unit to give two new LUMOs for the D–A system. The result, after redistribution of the electrons to these new hybridized orbitals, is a higher lying HOMO, lower lying LUMO, and a smaller bandgap. This allows energy level and bandgap tuning by careful choice of the donor-acceptor combination.

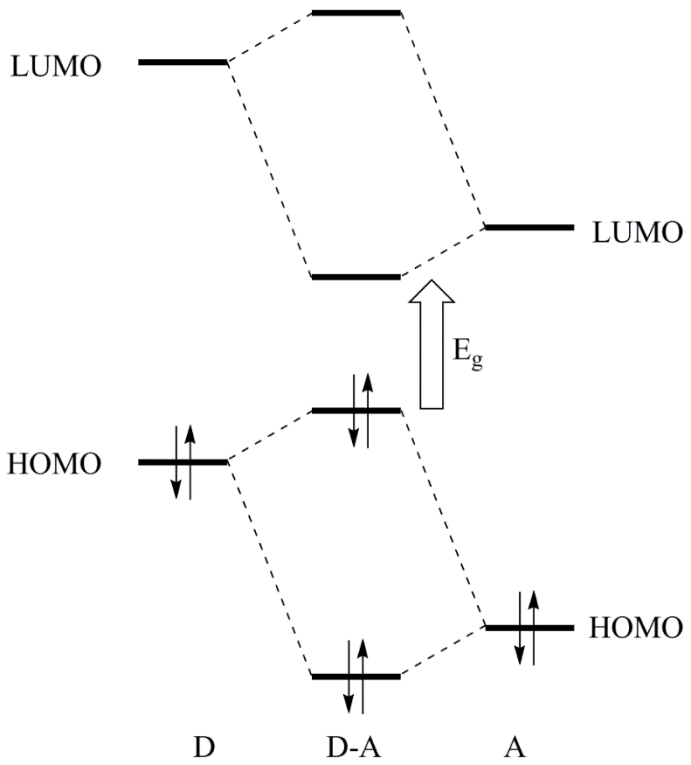


**Figure 1.11.** Orbital mixing of donor (D) and acceptor (A) units in a D–A system leading to a reduced bandgap.

The most important property of a π-conjugated material that can be viable in electronics is solubility in organic solvents. If a material is completely insoluble, there is no way for it to be processed or utilized in a device. On the other hand, the material must have sufficient π-character to maintain reasonable charge transport capabilities. In the case of polymers, charge transport ability is directly related to the molecular weight of the polymer, or degree of polymerization.[69, 82] A significant factor influencing solubility in both polymeric and molecular conjugated materials are intermolecular interactions caused by greater rigidity along the backbone and stacking through π–π interactions between molecules.[83] Increasing the length of the π-system, backbone rigidity, and intermolecular π-stacking can have beneficial impacts on the film forming properties and increasing charge carrier ability, yet unfortunately, also have a negative impact on the solubility of a material.

Strong intermolecular π–π stacking is the predominant cause of poor solubility in polyaromatic systems. The introduction of aliphatic side-chains to the conjugated backbone has, thus far, been one of the easiest and most effective ways to combat solubility issues. Nearly all reasonably effective conjugated materials require aliphatic chains to be solution-processable. The selection of appropriate alkyl chains is necessary, as they can have a large impact on the performance of an organic semiconductor through both imparting varying degrees of order in a thin film, but also modifying the energy levels as well.[84] Materials utilizing short, linear side chains tend to suffer from poor solubility, while the use of long or branched alkyl chains results in higher solubility, but at a cost.[85] The use of bulky branched chains can disrupt intermolecular π-stacking, thereby reducing photoconductivity in photovoltaics. Although detrimental to OPVs, this is beneficial to OLEDs due to the tendency to limit fluorescence quenching through excimer formation.[86]

To attain a high degree of charge carrier mobility, the minimum number of insulating alkyl chains required to impart solubility should be used. One option is the use of short, branched chains as a way to increase solubility while minimizing the chance of interfering with thin film order and π-stacking.[87] The final consideration in alkyl chain selection is the thermal stability of the material. Increasing the number of alkyl chains tends to reduce the thermal stability of the material, although, the onset of thermal decomposition tends to be well above the operating temperature of devices.[88]

The ability to effectively transport charges is important in any material that is to be used in electronics. In materials for OPVs, the ability to transport charges in the solid state is one of the most desired properties.[82] The mechanism by which organic semiconductors transport charges, charge-hopping, can be influenced by many properties, such as material shape,[89] regioregularity,[39] solubilizing alkyl chains,[90] and, with polymers, molecular weight.[91] In a charge-hopping mechanism, holes and electrons are transported throughout a film by "hopping" from one chain to the next.[92-94] This charge-hopping mechanism results in lower mobilities and makes charge transport susceptible to charge traps caused by material defects, functional end-groups, and impurities, such as metal catalysts.[69, 95-97] When measured, conjugated organic materials tend to have imbalanced charge transport, with hole mobilities significantly higher than electron mobilities in most materials.[98] While this is believed to be due to the electron rich nature of the organic π-systems, there is growing evidence that the n- or p-type properties observed in organics does not reflect the intrinsic abilities of the material to transport holes or electrons.[99] Theoretical studies have suggested that the hole and electron mobilities for many organic semiconductors should be comparable.[100, 101] Low n-type mobility is typically linked to extrinsic effects, such as the

instability of radical-anions with respect to water, hydroxyl groups, or oxygen, and the presence of specific traps for electrons that are the result of photo-oxidation of the π-conjugated backbone.[102-105]

The relationship between solubility and charge transport is a double edged sword, as charge carrier ability is dependent upon the ability of the molecules to order themselves and the extent of π-stacking they display, both of which decrease solubility.[95] A careful balance must be met so that materials are solution processable, yet still have strong inter-chain interactions allowing self-assembly into well-ordered regions of π-stacked molecules.[106] Solvent selection can have a massive impact on the resulting film morphology, which, in turn, impacts charge mobility.[107] Due to discrepancies in how mobilities are measured, it can be difficult to directly correlate device performance and measured mobility.

### 1.3 Organic Photovoltaics

In recent years, academic and public interest has shifted toward the research and commercialization of alternative energy sources, such as solar, wind, hydroelectric, and geothermal, for power generation for public utilities.[108-110] The possible energy output from solar energy is rivaled by no other currently existing source, renewable or nonrenewable. More solar energy strikes Earth in an hour and a half than is consumed in a year.[111] Although the use of solar energy is slowly becoming more widespread, the upfront cost of photovoltaics (PVs) is still prohibitively high for many, due to the manufacturing cost and technical barriers that exist in large-scale commercial implementation. The high fabrication

costs of silicon-based PVs, which make up a majority of terrestrial devices, results in a high cost per kilowatt hour.

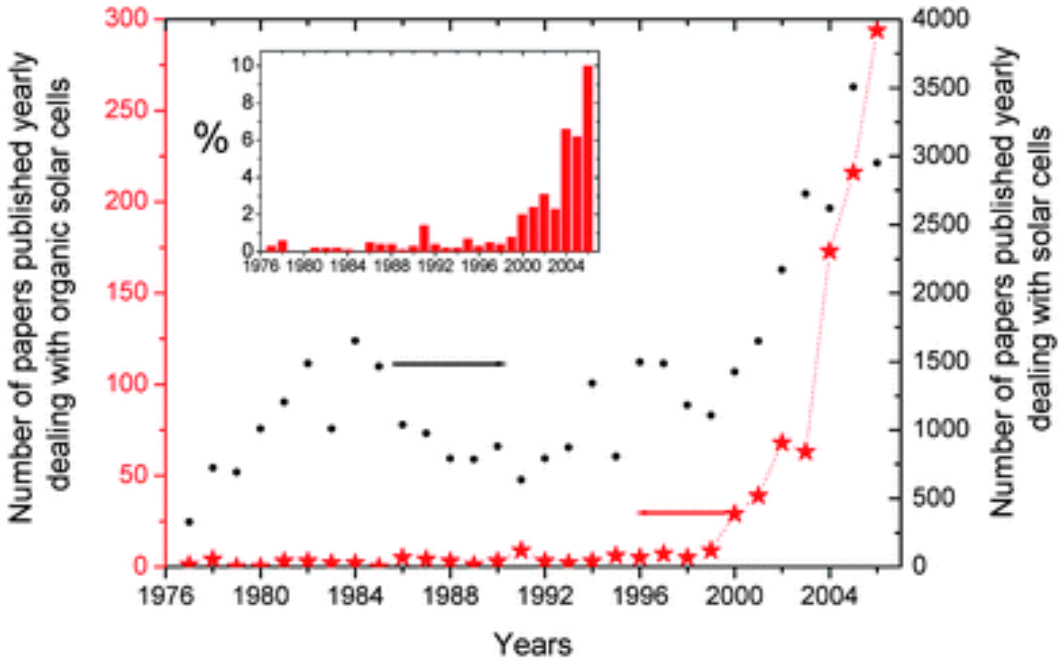


**Figure 1.12.** Number of publications on photovoltaics and organic photovoltaics since 1976.

In the last fifteen years, research interest in organic semiconductors for PV applications has exploded, as seen in Figure 1.12.[112] This dramatic increase in research interest has been driven by the potential to replace high purity silicon with materials made from cheap, renewable materials; the opportunity for low-cost, large area fabrication; and the ability to be used in light-weight, flexible devices.[6, 113, 114] This increase in research has led to the development of many molecular and polymer based OPVs, with high power conversion efficiency (PCE) well over 8%.[115-122] Although the overall efficiency of OPVs has crossed into the realm of commercial viability, further development is needed to reduce the cost of devices.

Original OPV architecture was based off of a very simple design comprised of a semiconducting organic between two electrodes. Early studies were performed on anthracene, metal-phthalocyanines, and chlorophyll-*a*, each giving low photocurrent.[123-125] Work by Delacote et al. showed an improved effect when magnesium phthalocyanines were placed between two different metals.[126] Early work on polymeric materials were performed on polyacetylene and polythiophene, with limited results.[127, 128] The first major improvement in efficiency was reported by Karg et al. in 1993, using polyacetylene sandwiched between semi-transparent indium tin oxide (ITO) and aluminum.[129] An open circuit voltage ($V_{OC}$) of 1 V and a PCE of 0.1% were achieved upon illumination with white light, and the system was further studied by Marks et al.[130] and Antoniadis et al.[131]

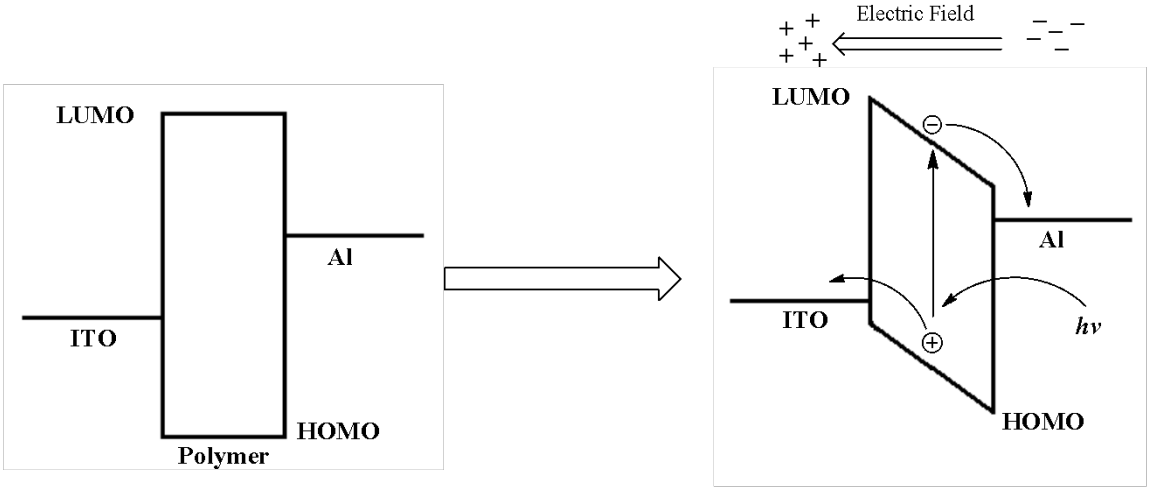


**Figure 1.13.** Schematic of a single layer OPV cell.

A schematic of these single layer devices is shown in Figure 1.13. The differing work functions of the metal electrodes results in band bending of the active layer, creating an electric field. Photoexcitation of the organic layer by a photon promotes an electron from $S_0 \rightarrow S_1$, generating a coulombically bound electron-hole pair, known as an exciton, due to

the generally low dielectric of organic materials. Due to the electric field, these excitons can dissociate to free holes and electrons, which then travel to the anode and cathode, respectfully. The potential difference, along with the created current, generates power, which can be utilized for energy applications.[132]

The most important factor with a PV cell, along with cost, is the overall efficiency. The PCE of a PV cell cannot be directly measured, therefore it is governed by a variety of parameters. A typical current density vs. voltage (*J*-*V*) curve is shown in Figure 1.14 with the critical parameters highlighted. These parameters are defined as:[133]

**Short circuit current density ($J_{SC}$)** – The short circuit current ($I_{SC}$) per area of the cell surface. The $I_{SC}$ is the current that flows when there is no external field applied; the charges drift due to the internal field. $I_{SC}$ is determined by the number of photons absorbed, the quantum efficiency of charge separation, and the transport of charge carriers through the material.

**Open circuit voltage ($V_{OC}$)** – The maximum voltage delivered by the solar cell under illumination. At this voltage, the current is zero. The $V_{OC}$ is determined by the difference in quasi-Fermi levels of the components of the active layer. This parameter will be discussed in further detail later.

**Fill factor (FF)** – The ratio of maximum power of the solar cell ($V_m \cdot J_m$) to the product of $V_{OC}$ and $J_{SC}$. The FF is determined by the competition between sweep-out of the photogenerated carriers and the recombination carriers to the ground state.[134] Both shunt ($R_{sh}$) and series ($R_s$) resistance can have a sizable impact on FF.

**PCE** – The ratio of maximum power generated by the cell ($P_{out}$) to the power of incident light ($P_{in}$). The incident light power is, usually, standardized to be equivalent to the air-mass (AM) 1.5 solar spectrum. The AM 1.5 solar spectrum is defined as the spectrum of solar radiation received on the surface of the earth (100 mW $cm^{-2}$).

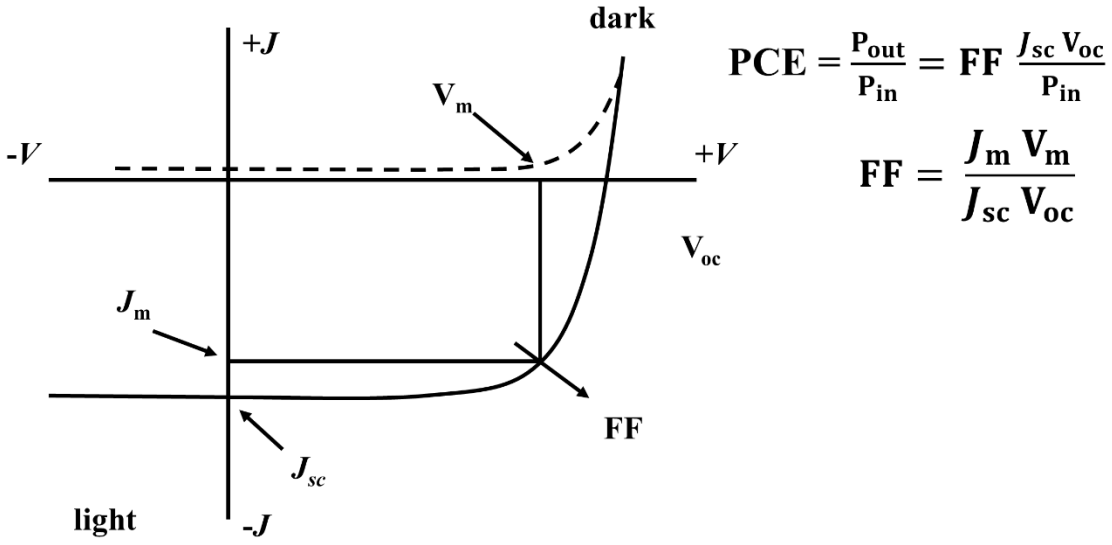


**Figure 1.14.** Current density vs voltage (*J-V*) of a solar cell, with critical parameters highlighted.

While capable of generating some power, single layer OPVs suffer from many drawbacks. One such shortcoming is the poor rate of exciton dissociation in the active layer. The generated electric field isn't strong enough to dissociate the bound pair quickly enough, allowing them to decay, usually through recombination.[135] Factors such as poor morphology and imbalanced charge transport also degrade PCE.[136] In an attempt to overcome the low exciton dissociation of single layer devices, bilayer devices, with an active layer comprised of an electron-rich (p-type) material, with a high lying HOMO, and an electron-deficient (n-type) material, with a low lying LUMO, sandwiched between two metal electrodes, were developed.[137, 138] The principal behind these bilayer devices is

shown in Figure 1.15. Upon excitation in the p-type material, the formed exciton can diffuse to the p-n interface. The lower LUMO energy of the n-type material allows for a greater driving force for dissociation than just the electric field, alone. For efficient dissociation, an energy gap of at least 0.2 eV is required.[139] The newly formed free charges are then capable of transporting through the p-type and n-type materials, to their respective electrodes, generating a photocurrent.

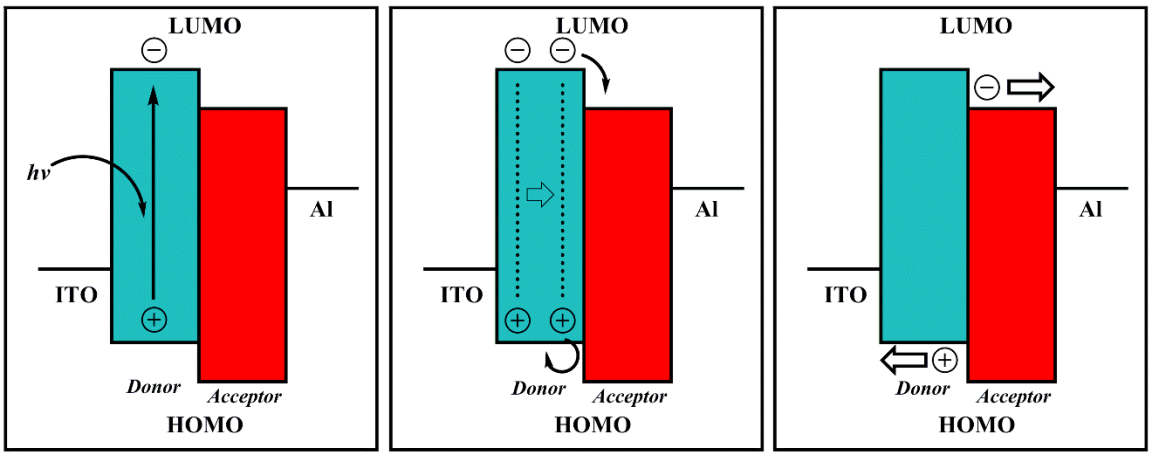


**Figure 1.15.** Mechanism of free charge generation in a bilayer photovoltaic cell.

While more efficient than single layer OPVs with their inclusion of a p-n junction, bilayer OPVs generally have relatively low efficiencies, particularly due to the required thickness of each layer. Efficient light absorption in OPVs requires an active layer, with a thickness of at least 100 nm, to be significantly thicker than the diffusion length of an exciton.[139] This short diffusion length of approximately 10 nm is due to short exciton lifetimes.[140-142] The combination of short exciton diffusion length and the need for a thick active layer results in excitons formed within the bulk of either material to recombine, decreasing quantum efficiency and, in turn, PCE. One solution to this issue is the

fabrication of a highly-ordered heterojunction with interdigitated donor and acceptor domains on the scale of 10 – 20 nm thick. This design allows for a readily available D-A interface for all generated excitons and pathways to each electrode. Very recently, devices fabricated with such architecture by nanoimprinting deterministic aperiodic nanostructures into each layer, resulting in a PCE of over 10% and high photocurrent.[121]

To date, the most widely used architecture for OPVs has been that of the bulk-heterojunction (BHJ) device, first introduced by Yu et al. and Halls et al.[76, 143, 144] The active layer in BHJ devices is formed by spin casting a blend of the donor and acceptor materials onto a substrate, creating an interpenetrating, single active layer with a very large D-A interface surface area (Figure 1.16). Optimized processing conditions, such as solvent, solvent concentration, spin rate, donor to acceptor ratio, solvent additives, annealing, etc., create an interpenetrating network of donor and acceptor running from electrode to electrode, allowing nearly all exciton formation to occur within 10 nm of a p-n junction. The use of a single active layer eliminates the need for the donor and acceptor materials to have different solvent profiles. Early devices achieved PCEs as high as 1.9% through the mixing of two polymers with different energy levels, marking a major improvement over previous OPVs.[145]

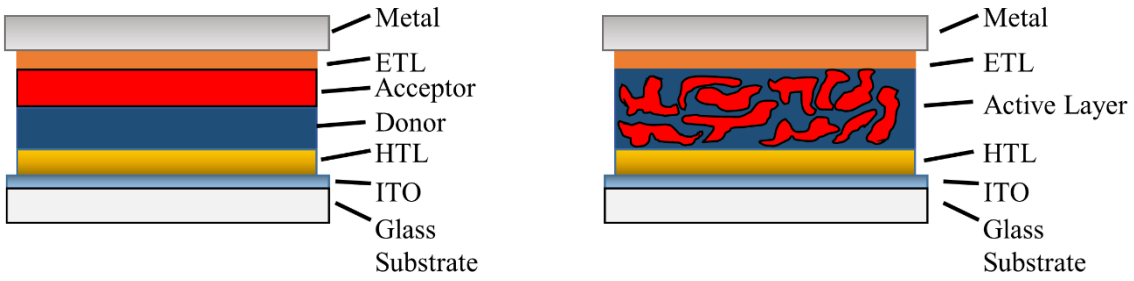


**Figure 1.16.** Device architecture of bilayer (left) vs. bulk heterojunction (right) solar cells.

While promising, BHJs using two different π-conjugated polymers suffered from various morphology issues. The use of large π-systems led to little phase separation between the materials, resulting in a decrease in free charges due to geminate recombination of excitons.[146-148] Without a clear way to induce a reasonable amount of phase separation, BHJ solar cells would have made little progress if it were not for the discovery of ultra-fast electron transfer from polymers to buckminsterfullerene, $C_{60}$, by Sariciftci et al. in late 1992.[149] The ultra-fast charge transfer to fullerenes was orders of magnitude faster than any radiative or non-radiative pathway for decay of an exciton, allowing for the possibility of highly efficient OPVs.

Fullerenes present many properties making them ideal for use in OPVs as an n-type material. They possess a relatively low lying LUMO, aiding in driving electron injection from donor materials.[150] Along with having a low lying LUMO, it is also triply-degenerate, allowing for the injection of six electrons. The ultra-fast electron transfer to fullerenes occurs on a time scale of 45 fs, orders of magnitude faster than photoluminescence or back electron transfer.[151] This fast electron transfer allows for quickly quenching the excited state of the donor material, reducing the chance for photooxidation.[152, 153] Lastly, fullerenes also possess high electron mobility, as shown with their use in OFETs, of 1.0 $cm^2\ V^{-1}\ s^{-1}$, which is ideal for rapid transfer of the free charges to the cathode.[154]

One drawback of fullerenes are their low degree of solubility in organic solvents. To circumvent this issue, functionalized fullerenes are used. The two most popular fullerene isomers used are the symmetric [6,6]-phenyl-$C_{60}$-butyric acid methyl ester (PC[60]BM) and the asymmetric [6,6]-phenyl-$C_{70}$-butyric acid methyl ester (PC[70]BM), shown in Figure 1.17.[155] PC[70]BM can be substituted for PC[60]BM easily, due to both fullerenes

having the same LUMO.[150] The asymmetry of PC[70]BM results an increased number of lower energy transitions, allowing in increased absorption in the visible spectrum. The

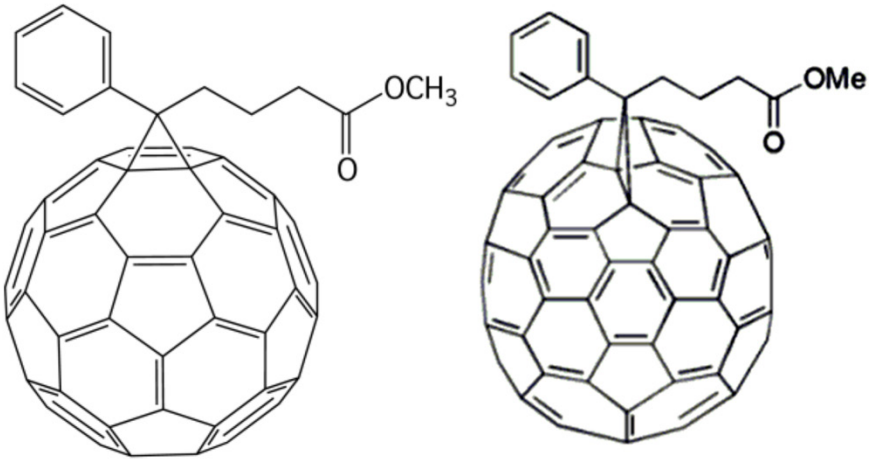


**PC[60]BM** **PC[70]BM**

**Figure 1.17.** The structures of [6,6]-phenyl-$C_{60}$-butyric acid methyl ester (PC[60]BM) and [6,6]-phenyl-$C_{70}$-butyric acid methyl ester (PC[70]BM).

increased absorption of PC[70]BM, along with having the same LUMO, has led to devices with consistently increased PCEs and is becoming the dominant acceptor used with low bandgap materials.

As appealing as PCBM is, it is not without its own disadvantages. The tendency of PCBM to self-assemble can lead to large domain sizes if either the PCBM or donor come out of solution too quickly.[120, 156] If the domains become larger than the average exciton diffusion length, the number of excitons reaching a p-n junction will decrease, which will reduce the number of free charges available to generate current. In addition, fast self-assembly may lead to domains becoming "trapped" within the other material, preventing free charges generated at the p-n junction of the trapped domain from reaching their respective electrode. There has been a large effort in developing techniques to prevent large

and isolated domains.[157] Many processing conditions and film treatments have been developed and implemented with varying degrees of success. Examples include attempts to control self-assembly through solvent selection;[107, 158-160] the use of high-boiling solvent additives during film casting, such as 1,8-diiodooctane and 1-chloronaphthalene;[161-163] the development of block copolymers;[164-166] the use of nanostructures to influence film morphology,[167-169] thermal annealing,[170] and incorporation of PCBM directly on to polymer backbones.[171-173] Even with these drawbacks, to date, a better acceptor material for OPVs than PCBM has yet to be discovered.

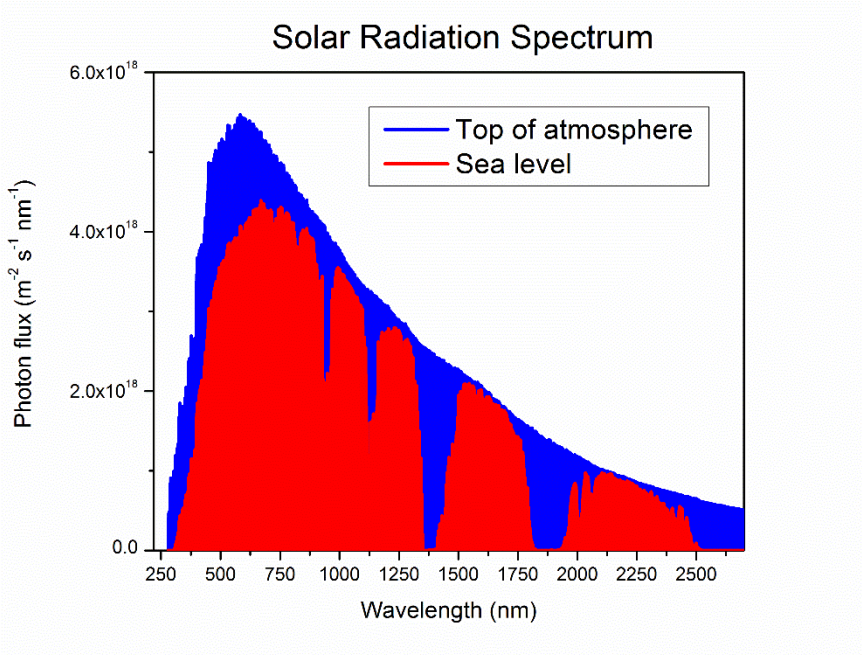


**Figure 1.18.** Photon flux from sunlight at the top of the atmosphere and at sea level.

The inability of PCBM to absorb much, if any, visible light means that nearly all photon absorption in an OPV occurs in the p-type material. To fully maximize photon absorption, a donor would have an absorption profile that covers as much of the visible spectrum as

possible, particularly in the areas of greatest photon flux. As seen in Figure 1.18, the region of greatest flux are in range of 500 – 900 nm, with the peak at approximately 700 nm, with the number of photons trailing off until around 1400 nm. To fully utilize the high density of photons, the donor material must have a bandgap below 1.7 eV. These narrow bandgaps lead to an increased number of excitons generated, resulting in the generation of more potential charge carriers, and an increase in $J_{SC}$, improving PCE.[174] As mentioned in the previous section, the bandgap can be tuned, through synthetic modifications to the donor material, by raising the HOMO and/or lowering the LUMO, which also impacts the absorption profile.[53, 175] The final location of the HOMO and LUMO is vital to the efficiency of the resulting OPV.

In OPVs, the location of the HOMO and LUMO impacts more than just the size of the bandgap; some of the critical parameters of the BHJ solar cell are determined by their position. The LUMO of the donor material, as previously mentioned, needs to be at least 0.2 – 0.3 eV higher than that of PCBM to effectively drive electron transfer between the two materials, as well as an efficient Schottky barrier to prevent back electron transfer into the LUMO of the donor.[176-178] Efficient electron injection as well as electron transport through the BHJ have been found to be the limiting parameter toward high PCE in OPV devices.[179] The other critical parameter heavily influenced by energy level position is $V_{OC}$. The $V_{OC}$ can be approximated by Equation 1.1:

$$V_{\mathrm{OC}} \approx (1/e)\,(E_{\mathrm{LUMO}}^{\mathrm{acceptor}} - E_{\mathrm{HOMO}}^{\mathrm{donor}}) + (k_B T/e)\ln\left(\frac{n_e n_h}{N_c^2}\right), \qquad (1.1)$$

where $e$ is the electron charge; $k_B$ is the Boltzmann constant; $T$ is the absolute temperature; $n_e$ and $n_h$ are the electron and hole densities, respectively; and $N_c$ is the density of states near the acceptor LUMO and the donor HOMO, which are assumed to be equal.[180] The third term in Equation 1.1, which accounts for the temperature dependence of $V_{OC}$, is approximately 0.3 V, giving Equation 1.2.[181]

$$V_{OC} \approx (1/e)\,(E_{LUMO}^{acceptor} - E_{HOMO}^{donor}) - 0.3\ \mathrm{V} \tag{1.2}$$

While obtaining a very high $V_{OC}$ is possible, doing so is not without drawbacks. As $V_{OC}$ increases, the HOMO of the donor material decreases. Since the LUMO of the donor must remain at least 0.3 eV greater than the LUMO of the acceptor, decreasing the HOMO of the donor material widens the bandgap of the material, as illustrated in Figure 1.19. There have been attempts to alter the LUMO of PCBM through structural modification, for example the popular indene-$C_{60}$ bisadduct (ICBA), but they have led to mixed results, due to the change in packing and crystallinity compared to PCBM.[182-186] Ultimately, a balance of a large $LUMO_{acceptor}$ – $HOMO_{donor}$ gap (increase $V_{OC}$), narrow bandgap, and adequate $LUMO_{donor}$ – $LUMO_{acceptor}$ difference (promote exciton dissociation) is required to maximize PCE.

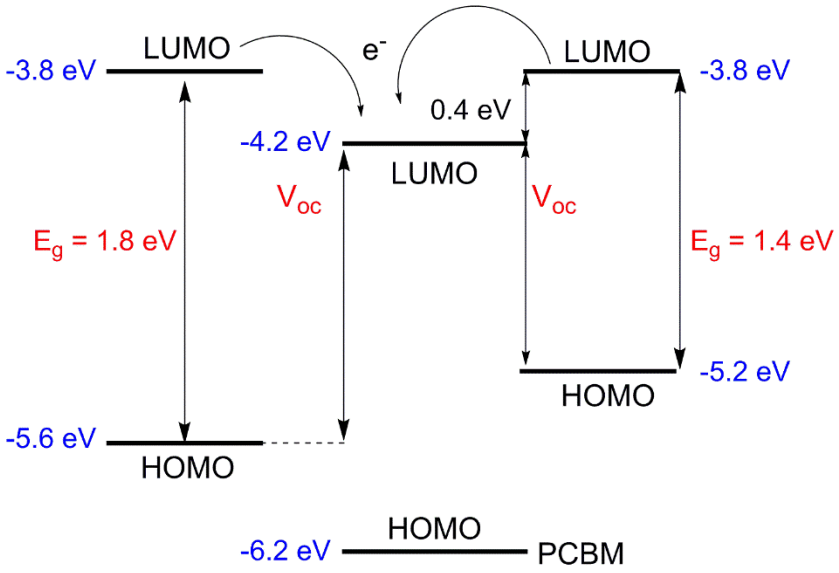


**Figure 1.19.** Impact of raising the donor HOMO on $V_{OC}$ and bandgap ($E_g$).

### 1.4 Design Rules for High Efficiency Solar Cells

As previously discussed, the general mechanism of charge generation in an OPV is comprised of four steps: (1) light absorption and exciton formation, (2) exciton migration to a p-n junction, (3) charge separation, and (4) charge transport and collection. The active layer of OPVs, having a low carrier mobility and high absorption coefficient, tend to have a thickness of around 100 nm. Organic semiconductors, with their low dielectric constants, form excitons upon photon absorption, therefore the active layer must be composed of a interpenetrating network of donor material and PCBM to maximize exciton dissociation. Control of the morphology of these BHJs is essential for high performance OPVs.

The magnitude of the donor bandgap determines how much light can absorbed. A material with a bandgap of 1.1 eV (1100 nm) has the potential to harvest nearly 77% of the solar photons at sea level, whereas many semiconducting organics, having bandgaps over 2 eV (620 nm), can only absorb 30% of solar photons.[176] To achieve high PCE values in

OPVs, the tuning of energy levels, as well as the solubility, of the donor is of the utmost importance. Both solubility and energy levels can be tuned by attaching various substituents to the polyaromatic backbone, altering the morphology in the solid state and/or the electronics of the material. Several building blocks that have been used in high performance materials are shown in Figure 1.20.

The use of fused heterocycles can have multiple benefits. As mentioned in section 1.2, the addition of fused aromatic units outside of the main conjugation pathway, such as with PITN, can help stabilize the quinoidal mesomeric structure, resulting in a very low bandgap. The electron-deficient building block thieno[3,4-*b*]thiophene (TT) is the most

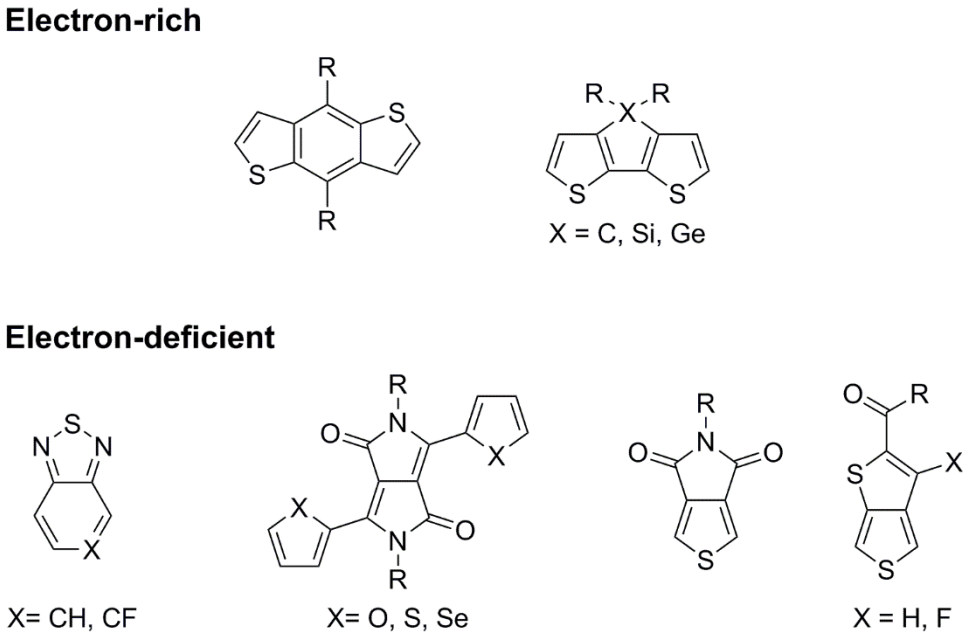


**Figure 1.20.** Common building blocks in high performance OPV materials.

widely used and successful building block possessing this type of structure. The use of TT with the electron rich benzodithiophene (BDT) has led to a series of materials with PCEs over 5% called PTBs.[187-189] Use of the electron-deficient 2,1,3-benzothiadiazoles (BT) has resulted in numerous high performance materials with optimized efficiencies in the range

of 5-7%.[190-197] An added benefit of fused rings is the increased coplanarity, which aides in increased π-overlap and increased delocalization. For example, the use of two fused BTs lead to an enhanced OPV performance from 2.1% to 6.0% for the fused naphthobisthiadiazole.[198, 199]

The incorporation of a fluorine atom has shown many benefits. The strong electron withdrawing ability of fluorine, due to its high electronegativity, and similar size to hydrogen has led to materials with drastically different properties. The biggest benefit is that the substitution of one fluorine for a hydrogen along the backbone of a material can tune the energy levels of the material without introducing additional steric hindrance. It has been observed that, in polymers, the HOMO and LUMO of the donor material drop with the addition of fluorine, and the HOMO drops by approximately 0.1 eV per fluorine in the repeat unit.[189, 200-202] Unfortunately, the effect of fluorination is significantly more complicated than merely altering energy levels. Fluorination has a large impact on the dipole moment changes between the ground state and excited state and fullerene compatibility. Yu et al. established a relationship between the magnitude of dipolar change in materials containing fluorinated-TT, and the resulting performance in OPVs.[203, 204] Further studies on fluoro- and difluoro-BT containing materials have shown similar results, with increased change in dipole giving higher PCEs.[202, 205-208]

As previously stated in this chapter, the use of insulating alkyl side chains is required to make materials that are solution processable. While this does somewhat limit charge transport, this also opens the possibility of utilizing further substituent effects. These substitutions can be used as effective ways of perturbing molecular orbitals or fine tuning the solubility of a material. The substitution of the alkyl chain on BDT for an alkoxy side

group has resulted in a decrease of 0.1 eV in the HOMO of PTB polymers.[189] The use of 5-alkylthienyl groups has led to even larger decreases in the HOMO level and resulted in high efficiency materials through improved π-stacking.[209-212] Choice of substituent can also influence physical properties of materials including phase behavior, charge transport properties, and structural order.[87] While branched alkyl chains impart higher solubility, they can have a large effect on π-π stacking and charge mobility as large branched chains can lengthen *p-p* stacking distance, reducing mobility.[87, 213] Electron-deficient building blocks such as diketopyrrolopyrrole, thienopyrroledione, and TT bearing an ester group offer opportunities for side chain modification with relative ease.[4, 214, 215]

The final structural modification that is commonly used is the incorporation of a bridging atom between two aromatic rings. These bridging atoms rigidify the material, leading to a smaller chance of twisting. The most popular choice for bridging atoms are the group 14 atoms C, Si, and Ge. As the atomic radii increases going down the group, the ionization energy decreases.[216] Use of Si and Ge, as opposed to C, have led to increased structural order in films. Unlike C, the σ*-orbitals of Si and Ge overlap with the π-orbitals of the flanking aromatic rings and are able to play a part in aromaticity and act as an internal acceptor in a D-A-D fashion within a building block.[217, 218]

Compared to synthetic alterations, there are relatively few general strategies toward device optimization. Very low concentrations of solvent additives can have a drastic impact on the nanoscale morphology of the active layer. Use of additives such as 1,8-diiodooctane and 1-chloronaphthalene can help increase the solubility of the fullerene or polymer, respectively, leading to an increase in short circuit current density and fill factor.[162, 219-222] The use of interfacial layers, such as the hole transport layer PEDOT:PSS or the electron

transporting lithium fluoride can drastically improve performance and help align energy levels with the anode and cathode, respectively.[223] These interfacial layers help prevent reactions with the metal electrodes, which can cause the formation of an insulating buffer layer, and diffusion of the metals into the active layer.[224] Conjugated polyelectrolytes, with the benefit of being solution processable, have also been utilized effectively as electron transport materials in high efficiency OPVs.[178, 225-228]

## 1.5 Conclusions

In summary, many important considerations must be made when designing p-type materials for organic photovoltaic applications:

- Bandgap
    - Caused by Peierls distortion.
    - Minimized by increasing effective conjugation length.
        - Stabilizing the mesomeric quinoid form decreases the bandgap.
        - Increased by decreasing steric twists in the π-backbone.
            - Increased planarity achieved through fused aromatic rings or bridging atoms.
    - Fine-tuned utilizing donor-acceptor perturbation of MOs.
        - HOMO primarily determined by donor.
        - LUMO primarily determined by acceptor.
    - Sufficiently narrow (<1.8 eV).
        - Broad absorption over the solar spectrum.

- Maximize number of photons absorbed.
- Increases $J_{SC}$ by increasing quantum efficiency.

- Appropriate HOMO and LUMO energy levels.
  - HOMO and LUMO can be adjusted by addition of EWG or EDG.
  - Inclusion of fluorine atoms lower both HOMO and LUMO.
  - HOMO as low as possible to maximize $V_{OC}$.
  - LUMO within 0.2 – 0.4 eV of PCBM to promote efficient electron transfer.
  - Close enough to guarantee a narrow bandgap.
  - HOMO below 5.2 eV for oxidative stability.[229]

- Good film forming properties
  - Ordered films increase charge mobility.
  - Selective use of side chains to balance π-π stacking and solubility.
    - Short linear chains increase crystallinity while reducing solubility.
    - Branched chains can disrupt π-π stacking while increasing solubility.
    - Alkyl chain density can negatively impact charge mobility.
  - Inclusion of heteroatoms (Si, Ge, etc.) can increase inter-chain π-stacking.
  - Increased planarity improves π-stacking and charge mobility.

- Forms sufficiently sized domains when blended with PCBM.

- Domains approximately 15 – 20 nm in size to allow efficient exciton migration to p-n junction.
- Interpenetrating network necessary to maximize free charge collection.

The overall performance of a material is intimately tied to all of the parameters discussed in this chapter in such a way that the change of one aspect of a material can lead to numerous consequences in all other aspects. Until our understanding of these relationships is more complete, widespread commercialization will remain just out of reach.

## 1.6 References


1. Shirakawa, H.; Louis, E. J.; Macdiarmid, A. G.; Chiang, C. K.; Heeger, A. J., *J Chem Soc Chem Comm* **1977**, DOI 10.1039/c39770000578 (16), 578-580.
2. Chiang, C. K.; Fincher, C. R.; Park, Y. W.; Heeger, A. J.; Shirakawa, H.; Louis, E. J.; Gau, S. C.; MacDiarmid, A. G., *Phys. Rev. Lett.* **1977,** *39* (17), 1098-1101.
3. Kobilka, B. M.; Hale, B. J.; Ewan, M. D.; Dubrovskiy, A. V.; Nelson, T. L.; Duzhko, V.; Jeffries-El, M., *Polymer Chemistry* **2013,** *4* (20), 5329.
4. Zou, Y.; Najari, A.; Berrouard, P.; Beaupré, S.; Réda Aïch, B.; Tao, Y.; Leclerc, M., *J. Am. Chem. Soc.* **2010,** *132* (15), 5330-5331.
5. Beaujuge, P. M.; Fréchet, J. M. J., *J. Am. Chem. Soc.* **2011,** *133* (50), 20009-20029.
6. Brabec, C. J.; Sariciftci, N. S.; Hummelen, J. C., *Adv. Funct. Mater.* **2001,** *11* (1), 15-26.
7. Hoth, C. N.; Schilinsky, P.; Choulis, S. A.; Brabec, C. J., *Nano Lett.* **2008,** *8* (9), 2806-2813.
8. Shinar, J.; Shinar, R., 1.04 - An Overview of Organic Light-Emitting Diodes and their Applications. In *Comprehensive Nanoscience and Technology*, Wiederrecht, D. L. A. D. S. P., Ed. Academic Press: Amsterdam, 2011, pp 73-107.
9. Intemann, J. J.; Mike, J. F.; Cai, M.; Bose, S.; Xiao, T.; Mauldin, T. C.; Roggers, R. A.; Shinar, J.; Shinar, R.; Jeffries-El, M., *Macromolecules* **2010,** *44* (2), 248-255.

10. Friend, R. H.; Gymer, R. W.; Holmes, A. B.; Burroughes, J. H.; Marks, R. N.; Taliani, C.; Bradley, D. D. C.; Santos, D. A. D.; Bredas, J. L.; Logdlund, M.; Salaneck, W. R., *Nature* **1999,** *397* (6715), 121-128.

11. Ego, C.; Marsitzky, D.; Becker, S.; Zhang, J.; Grimsdale, A. C.; Müllen, K.; MacKenzie, J. D.; Silva, C.; Friend, R. H., *J. Am. Chem. Soc.* **2003,** *125* (2), 437-443.

12. Briseno, A. L.; Kim, F. S.; Babel, A.; Xia, Y. N.; Jenekhe, S. A., *J. Mater. Chem.* **2011,** *21* (41), 16461-16466.

13. Dimitrakopoulos, C. D.; Malenfant, P. R. L., *Adv. Mater.* **2002,** *14* (2), 99-117.

14. Facchetti, A., *Chem. Mater.* **2010,** *23* (3), 733-758.

15. Guo, X.; Puniredd, S. R.; Baumgarten, M.; Pisula, W.; Mullen, K., *Adv. Mater.* **2013,** *25* (38), 5467-72.

16. Ortiz, R. o. P.; Facchetti, A.; Marks, T. J., *Chem. Rev.* **2009,** *110* (1), 205-239.

17. Usta, H.; Facchetti, A.; Marks, T. J., *J. Am. Chem. Soc.* **2008,** *130* (27), 8580-8581.

18. Usta, H.; Facchetti, A.; Marks, T. J., *Acc. Chem. Res.* **2011,** *44* (7), 501-510.

19. Wang, C.; Dong, H.; Hu, W.; Liu, Y.; Zhu, D., *Chem. Rev.* **2011,** *112* (4), 2208-2267.

20. Camposeo, A.; Del Carro, P.; Persano, L.; Pisignano, D., *Adv. Mater.* **2012,** *24* (35), OP221-OP225.

21. Cho, M. J.; Choi, D. H.; Sullivan, P. A.; Akelaitis, A. J. P.; Dalton, L. R., *Prog. Polym. Sci.* **2008,** *33* (11), 1013-1058.

22. Janiak, C., *Dalton Transactions* **2003**, 10.1039/b305705b (14), 2781-2804.

23. Ling, Q.-D.; Liaw, D.-J.; Zhu, C.; Chan, D. S.-H.; Kang, E.-T.; Neoh, K.-G., *Prog. Polym. Sci.* **2008,** *33* (10), 917-978.

24. Yesodha, S. K.; Sadashiva Pillai, C. K.; Tsutsumi, N., *Prog. Polym. Sci.* **2004,** *29* (1), 45-74.

25. Mike, J. F.; Lutkenhaus, J. L., *J. Polym. Sci., Part B: Polym. Phys.* **2013,** *51* (7), 468-480.

26. Mike, J. F.; Lutkenhaus, J. L., *ACS Macro Letters* **2013,** *2* (9), 839-844.

27. Mike, J. F.; Shao, L.; Jeon, J.-W.; Lutkenhaus, J. L., *Macromolecules* **2014,** *47* (1), 79-88.

28. Yoon, J.; Chae, S. K.; Kim, J.-M., *J. Am. Chem. Soc.* **2007,** *129* (11), 3038-3039.

29. M. Goldenberg, L.; R. Bryce, M.; C. Petty, M., *J. Mater. Chem.* **1999,** *9* (9), 1957-1974.

30. McQuade, D. T.; Pullen, A. E.; Swager, T. M., *Chem. Rev.* **2000,** *100* (7), 2537-2574.

31. Darling, S. B.; You, F., *RSC Advances* **2013,** *3* (39), 17633-17648.

32. Klaver, A.; van Swaaij, R. A. C. M. M., *Sol. Energy Mater. Sol. Cells* **2008,** *92* (1), 50-60.

33. Sarti, D.; Einhaus, R., *Sol. Energy Mater. Sol. Cells* **2002,** *72* (1–4), 27-40.

34. Spear, W. E.; Willeke, G.; Le Comber, P. G.; Fitzgerald, A. G., *Le Journal de Physique Colloques* **1981,** *42* (C4), C4-257-C4-260.

35. Gribov, B. G.; Zinov'ev, K. V., *Inorg. Mater.* **2003,** *39* (7), 653-662.

36. Woodhouse, M.; Goodrich, A.; Margolis, R.; James, T.; Dhere, R.; Gessert, T.; Barnes, T.; Eggert, R.; Albin, D., *Sol. Energy Mater. Sol. Cells* **2013,** *115*, 199-212.

37. Woo, H. Y.; Shim, H.-K.; Lee, K.-S., *Polym. J.* **2000,** *32* (1), 8-14.

38. Li, B.; Santhanam, S.; Schultz, L.; Jeffries-El, M.; Iovu, M. C.; Sauvé, G.; Cooper, J.; Zhang, R.; Revelli, J. C.; Kusne, A. G.; Snyder, J. L.; Kowalewski, T.; Weiss, L. E.; McCullough, R. D.; Fedder, G. K.; Lambeth, D. N., *Sensors and Actuators B: Chemical* **2007,** *123* (2), 651-660.

39. Wang, G.; Swensen, J.; Moses, D.; Heeger, A. J., *J. Appl. Phys.* **2003,** *93* (10), 6137-6141.

40. Shaheen, S. E.; Radspinner, R.; Peyghambarian, N.; Jabbour, G. E., *Appl. Phys. Lett.* **2001,** *79* (18), 2996-2998.

41. Coakley, K. M.; McGehee, M. D., *Chem. Mater.* **2004,** *16* (23), 4533-4542.

42. He, R.; Day, T. D.; Krishnamurthi, M.; Sparks, J. R.; Sazio, P. J. A.; Gopalan, V.; Badding, J. V., *Adv. Mater.* **2013,** *25* (10), 1461-1467.

43. NREL http://rredc.nrel.gov/solar/spectra/am1.5/ (accessed August 27, 2015).

44. Hilberer, A.; Moroni, M.; Gill, R. E.; Brouwer, H. J.; Krasnikov, V. V.; Pham, T. A.; Malliaras, G. G.; Veenstra, S.; Werts, M. P. L.; van Hutten, P. F.; Hadziioannou, G., *Macromolecular Symposia* **1998,** *125* (1), 99-109.

45. Moliton, A.; Hiorns, R. C., *Polym. Int.* **2004,** *53* (10), 1397-1412.

46. Harrison, W. A., *Elementary Electronic Structure*. World Scientific: 2004.

47. Sze, S. M.; Ng, K. K., *Physics of Semiconductor Devices*. Wiley: 2006.

48. Peierls, R. E., *Quantum theory of solids*. Oxford University Press: Oxford, 2001, p 240.

49. Yannoni, C. S.; Clarke, T. C., *Phys. Rev. Lett.* **1983,** *51* (13), 1191-1193.

50. Blythe, A. R.; Bloor, D., *Electrical Properties of Polymers*. Cambridge University Press: 2005.

51. Tolbert, L. M., *Acc. Chem. Res.* **1992,** *25* (12), 561-568.

52. Anslyn, E. V.; Dougherty, D. A., *Modern Physical Organic Chemistry*. University Science: 2006.

53. Cheng, Y.-J.; Yang, S.-H.; Hsu, C.-S., *Chem. Rev.* **2009,** *109* (11), 5868-5923.

54. Körzdörfer, T.; Parrish, R. M.; Sears, J. S.; Sherrill, C. D.; Brédas, J.-L., *The Journal of Chemical Physics* **2012,** *137* (12), 124305.

55. Brédas, J. L., *The Journal of Chemical Physics* **1985,** *82* (8), 3808-3811.

56. Lee, Y. S.; Kertesz, M., *The Journal of Chemical Physics* **1988,** *88* (4), 2609-2617.

57. Hoogmartens, I.; Adriaensens, P.; Vanderzande, D.; Gelan, J.; Quattrocchi, C.; Lazzaroni, R.; Bredas, J. L., *Macromolecules* **1992,** *25* (26), 7347-7356.

58. Wudl, F.; Kobayashi, M.; Heeger, A. J., *J. Org. Chem.* **1984,** *49* (18), 3382-3384.

59. Dewar, M. J. S.; Trinajstic, N., *J. Am. Chem. Soc.* **1970,** *92* (6), 1453-1459.

60. Subramanian, G.; von Ragué Schleyer, P.; Jiao, H., *Angewandte Chemie International Edition in English* **1996,** *35* (22), 2638-2641.

61. Wohlgenannt, M.; Jiang, X. M.; Vardeny, Z. V., *Physical Review B* **2004,** *69* (24).

62. Klaerner, G.; Miller, R. D., *Macromolecules* **1998,** *31* (6), 2007-2009.

63. Elandaloussi, E. H.; Frère, P.; Richomme, P.; Orduna, J.; Garin, J.; Roncali, J., *J. Am. Chem. Soc.* **1997,** *119* (44), 10774-10784.

64. Izumi, T.; Kobashi, S.; Takimiya, K.; Aso, Y.; Otsubo, T., *J. Am. Chem. Soc.* **2003,** *125* (18), 5286-5287.

65. Ten Hoeve, W.; Wynberg, H.; Havinga, E. E.; Meijer, E. W., *J. Am. Chem. Soc.* **1991,** *113* (15), 5887-5889.

66. Havinga, E. E.; Rotte, I.; Meijer, E. W.; Hoeve, W. T.; Wynberg, H., *Synth. Met.* **1991,** *41* (1–2), 473-478.

67. Meier, H.; Stalmach, U.; Kolshorn, H., *Acta Polym.* **1997,** *48* (9), 379-384.

68. Kline, R. J.; McGehee, M. D.; Kadnikova, E. N.; Liu, J.; Fréchet, J. M. J.; Toney, M. F., *Macromolecules* **2005,** *38* (8), 3312-3319.

69. Kline, R. J.; McGehee, M. D.; Kadnikova, E. N.; Liu, J.; Fréchet, J. M. J., *Adv. Mater.* **2003,** *15* (18), 1519-1522.

70. Brisset, H.; Thobie-Gautier, C.; Jubault, M.; Gorgues, A.; Roncali, J., *J. Chem. Soc., Chem. Commun.* **1994**, 10.1039/C39940001765 (15), 1765-1766.

71. Blanchard, P.; Verlhac, P.; Michaux, L.; Frère, P.; Roncali, J., *Chemistry – A European Journal* **2006,** *12* (4), 1244-1255.

72. Brocks, G.; Tol, A., *Synth. Met.* **1996,** *76* (1–3), 213-216.

73. Zhang, Q. T.; Tour, J. M., *J. Am. Chem. Soc.* **1998,** *120* (22), 5355-5362.

74. van Mullekom, H. A. M.; Vekemans, J. A. J. M.; Havinga, E. E.; Meijer, E. W., *Materials Science and Engineering: R: Reports* **2001,** *32* (1), 1-40.

75. Kitamura, C.; Tanaka, S.; Yamashita, Y., *Chem. Mater.* **1996,** *8* (2), 570-578.

76. Yu, G.; Gao, J.; Hummelen, J. C.; Wudl, F.; Heeger, A. J., *Science* **1995,** *270* (5243), 1789-1791.

77. Colladet, K.; Fourier, S.; Cleij, T. J.; Lutsen, L.; Gelan, J.; Vanderzande, D.; Huong Nguyen, L.; Neugebauer, H.; Sariciftci, S.; Aguirre, A.; Janssen, G.; Goovaerts, E., *Macromolecules* **2007,** *40* (1), 65-72.

78. Yamamoto, T.; Zhou, Z.-h.; Kanbara, T.; Shimura, M.; Kizu, K.; Maruyama, T.; Nakamura, Y.; Fukuda, T.; Lee, B.-L.; Ooba, N.; Tomaru, S.; Kurihara, T.; Kaino, T.; Kubota, K.; Sasaki, S., *J. Am. Chem. Soc.* **1996,** *118* (43), 10389-10399.

79. Brocks, G.; Tol, A., *J. Phys. Chem.* **1996,** *100* (5), 1838-1846.

80. Rauk, A., *Orbital Interaction Theory of Organic Chemistry*. Wiley: 2004.

81. Carey, F. A.; Sundberg, R. J., *Advanced Organic Chemistry: Part A: Structure and Mechanisms*. Springer US: 2007.

82. Tsao, H. N.; Cho, D. M.; Park, I.; Hansen, M. R.; Mavrinskiy, A.; Yoon do, Y.; Graf, R.; Pisula, W.; Spiess, H. W.; Müllen, K., *J. Am. Chem. Soc.* **2011,** *133* (8), 2605-2612.

83. Kim, J., *Pure Appl. Chem.* **2002,** *74* (11).

84. Yang, L.; Zhou, H.; You, W., *The Journal of Physical Chemistry C* **2010,** *114* (39), 16793-16800.

85. Gadisa, A.; Mammo, W.; Andersson, L. M.; Admassie, S.; Zhang, F.; Andersson, M. R.; Inganäs, O., *Adv. Funct. Mater.* **2007,** *17* (18), 3836-3842.

86. Egbe, D. A. M.; Roll, C. P.; Birckner, E.; Grummt, U.-W.; Stockmann, R.; Klemm, E., *Macromolecules* **2002,** *35* (10), 3825-3837.

87. Szarko, J. M.; Guo, J.; Liang, Y.; Lee, B.; Rolczynski, B. S.; Strzalka, J.; Xu, T.; Loser, S.; Marks, T. J.; Yu, L.; Chen, L. X., *Adv. Mater.* **2010,** *22* (48), 5468-72.

88. Mike, J. F.; Makowski, A. J.; Mauldin, T. C.; Jeffries-El, M., *J. Polym. Sci., Part A: Polym. Chem.* **2010,** *48* (6), 1456-1460.

89. Ponomarenko, S. A.; Kirchmeyer, S.; Elschner, A.; Huisman, B. H.; Karbach, A.; Drechsler, D., *Adv. Funct. Mater.* **2003,** *13* (8), 591-596.

90. Saeki, A.; Ohsaki, S.-i.; Koizumi, Y.; Seki, S.; Tagawa, S., *Synth. Met.* **2009,** *159* (17-18), 1800-1803.

91. Siddiqui, A. S.; Wilson, E. G., *Journal of Physics C: Solid State Physics* **1979,** *12* (20), 4237-4243.

92. Zuppiroli, L.; Bussac, M. N.; Paschen, S.; Chauvet, O.; Forro, L., *Physical Review B* **1994,** *50* (8), 5196-5203.

93. Rakhmanova, S. V.; Conwell, E. M., *Appl. Phys. Lett.* **2000,** *76* (25), 3822-3824.

94. Li, H.; Li, C.; Duan, L.; Qiu, Y., *Isr. J. Chem.* **2014,** *54* (7), 918-926.

95. Malliaras, G.; Friend, R., *Physics Today* **2005,** *58* (5), 53-58.

96. Cheng, H.-L.; Lin, W.-Q.; Wu, F.-C., *Appl. Phys. Lett.* **2009,** *94* (22), 223302.

97. Krebs, F. C.; Nyberg, R. B.; Jørgensen, M., *Chem. Mater.* **2004,** *16* (7), 1313-1318.

98. Mihailetchi, V. D.; Wildeman, J.; Blom, P. W. M., *Phys. Rev. Lett.* **2005,** *94* (12).

99. Bernius, M. T.; Inbasekaran, M.; O'Brien, J.; Wu, W., *Adv. Mater.* **2000,** *12* (23), 1737-1750.

100. Cornil, J.; Beljonne, D.; Calbert, J. P.; Brédas, J. L., *Adv. Mater.* **2001,** *13* (14), 1053-1067.

101. Brédas, J. L.; Calbert, J. P.; da Silva Filho, D. A.; Cornil, J., *Proceedings of the National Academy of Sciences* **2002,** *99* (9), 5804-5809.

102. Kažukauskas, V.; Tzeng, H.; Chen, S. A., *Appl. Phys. Lett.* **2002,** *80* (11), 2017-2019.

103. Smits, E. C. P.; Anthopoulos, T. D.; Setayesh, S.; van Veenendaal, E.; Coehoorn, R.; Blom, P. W. M.; de Boer, B.; de Leeuw, D. M., *Physical Review B* **2006,** *73* (20).

104. Chua, L.-L.; Zaumseil, J.; Chang, J.-F.; Ou, E. C. W.; Ho, P. K. H.; Sirringhaus, H.; Friend, R. H., *Nature* **2005,** *434* (7030), 194-199.

105. Coropceanu, V.; Cornil, J.; da Silva Filho, D. A.; Olivier, Y.; Silbey, R.; Brédas, J.-L., *Chem. Rev.* **2007,** *107* (4), 926-952.

106. Li, G.; Shrotriya, V.; Huang, J.; Yao, Y.; Moriarty, T.; Emery, K.; Yang, Y., *Nat Mater* **2005,** *4* (11), 864-868.

107. Park, Y. D.; Park, J. K.; Seo, J. H.; Yuen, J. D.; Lee, W. H.; Cho, K.; Bazan, G. C., *Adv. Energy Mater.* **2011,** *1* (1), 63-67.

108. Jacobson, M. Z.; Masters, G. M., *Science* **2001,** *293* (5534), 1438.

109. Pacala, S.; Socolow, R., *Science* **2004,** *305* (5686), 968-972.

110. Fthenakis, V.; Mason, J. E.; Zweibel, K., *Energy Policy* **2009,** *37* (2), 387-399.

111. Lewis, N. S.; Crabtree, G.; Nozik, A. J.; Wasielewski, M. R.; Alivisatos, P.; Kung, H.; Tsao, J.; Chandler, E.; Walukiewicz, W.; Spitler, M.; Ellingson, R.; Overend, R.; Mazer, J.; Gress, M.; Horwitz, J.; Ashton, C.; Herndon, B.; Shapard, L.; Nault, R. M. *Basic Research Needs for Solar Energy Utilization. Report of the Basic Energy Sciences Workshop on Solar Energy Utilization, April 18-21, 2005*; 2005; p Medium: ED.

112. Ameri, T.; Dennler, G.; Lungenschmied, C.; Brabec, C. J., *Energy & Environmental Science* **2009,** *2* (4), 347-363.

113. Hung, M.-C.; Liao, J.-L.; Chen, S.-A.; Chen, S.-H.; Su, A.-C., *J. Am. Chem. Soc.* **2005,** *127* (42), 14576-14577.

114. Günes, S.; Neugebauer, H.; Sariciftci, N. S., *Chem. Rev.* **2007,** *107* (4), 1324-1338.

115. Wang, D. H.; Kyaw, A. K. K.; Gupta, V.; Bazan, G. C.; Heeger, A. J., *Adv. Energy Mater.* **2013,** *3* (9), 1161-1165.

116. Yang, T.; Wang, M.; Duan, C.; Hu, X.; Huang, L.; Peng, J.; Huang, F.; Gong, X., *Energy & Environmental Science* **2012,** *5* (8), 8208-8214.

117. He, Z.; Zhong, C.; Su, S.; Xu, M.; Wu, H.; Cao, Y., *Nature Photonics* **2012,** *6* (9), 591-595.

118. Chen, H.-C.; Chen, Y.-H.; Liu, C.-C.; Chien, Y.-C.; Chou, S.-W.; Chou, P.-T., *Chem. Mater.* **2012,** *24* (24), 4766-4772.

119. Green, M. A.; Emery, K.; Hishikawa, Y.; Warta, W.; Dunlop, E. D., *Progress in Photovoltaics: Research and Applications* **2015,** *23* (7), 805-812.

120. Liu, Y.; Zhao, J.; Li, Z.; Mu, C.; Ma, W.; Hu, H.; Jiang, K.; Lin, H.; Ade, H.; Yan, H., *Nat Commun* **2014,** *5*.

121. Chen, J.-D.; Cui, C.; Li, Y.-Q.; Zhou, L.; Ou, Q.-D.; Li, C.; Li, Y.; Tang, J.-X., *Adv. Mater.* **2015,** *27* (6), 1035-1041.

122. Liu, C.; Yi, C.; Wang, K.; Yang, Y.; Bhatta, R. S.; Tsige, M.; Xiao, S.; Gong, X., *ACS Applied Materials & Interfaces* **2015,** *7* (8), 4928-4935.

123. Kearns, D.; Calvin, M., *The Journal of Chemical Physics* **1958,** *29* (4), 950-951.

124. Sloan, G. J., *Molecular Crystals* **1966,** *1* (1), 161-194.

125. Tang, C. W.; Albrecht, A. C., *The Journal of Chemical Physics* **1975,** *63* (2), 953-961.

126. Delacote, G. M.; Fillard, J. P.; Marco, F. J., *Solid State Commun.* **1964,** *2* (12), 373-376.

127. Weinberger, B. R.; Akhtar, M.; Gau, S. C., *Synth. Met.* **1982,** *4* (3), 187-197.

128. Glenis, S.; Tourillon, G.; Garnier, F., *Thin Solid Films* **1986,** *139* (3), 221-231.

129. Karg, S.; Riess, W.; Dyakonov, V.; Schwoerer, M., *Synth. Met.* **1993,** *54* (1–3), 427-433.

130. Marks, R. N.; Halls, J. J. M.; Bradley, D. D. C.; Friend, R. H.; Holmes, A. B., *J. Phys.: Condens. Matter* **1994,** *6* (7), 1379.

131. Antoniadis, H.; Hsieh, B. R.; Abkowitz, M. A.; Jenekhe, S. A.; Stolka, M., *Synth. Met.* **1994,** *62* (3), 265-271.

132. Hoppe, H.; Sariciftci, N. S., *J. Mater. Res.* **2004,** *19* (07), 1924-1945.

133. Heeger, A. J.; Sariciftci, N. S.; Namdas, E. B., *Semiconducting and Metallic Polymers*. OUP Oxford: 2010.

134. Cowan, S. R.; Street, R. A.; Cho, S.; Heeger, A. J., *Physical Review B* **2011,** *83* (3).

135. Gregg, B. A., *J. Phys. Chem. B* **2003,** *107* (20), 4688-4698.

136. Wöhrle, D.; Meissner, D., *Adv. Mater.* **1991,** *3* (3), 129-138.

137. Tang, C. W., *Appl. Phys. Lett.* **1986,** *48* (2), 183-185.

138. Peumans, P.; Yakimov, A.; Forrest, S. R., *J. Appl. Phys.* **2003,** *93* (7), 3693-3723.

139. Halls, J. J. M.; Cornil, J.; dos Santos, D. A.; Silbey, R.; Hwang, D. H.; Holmes, A. B.; Brédas, J. L.; Friend, R. H., *Physical Review B* **1999,** *60* (8), 5721-5727.

140. Halls, J. J. M.; Pichler, K.; Friend, R. H.; Moratti, S. C.; Holmes, A. B., *Appl. Phys. Lett.* **1996,** *68* (22), 3120-3122.

141. Haugeneder, A.; Neges, M.; Kallinger, C.; Spirkl, W.; Lemmer, U.; Feldmann, J.; Scherf, U.; Harth, E.; Gügel, A.; Müllen, K., *Physical Review B* **1999,** *59* (23), 15346-15351.

142. Theander, M.; Yartsev, A.; Zigmantas, D.; Sundström, V.; Mammo, W.; Andersson, M. R.; Inganäs, O., *Physical Review B* **2000,** *61* (19), 12957-12963.

143. Yu, G.; Heeger, A. J., *J. Appl. Phys.* **1995,** *78* (7), 4510-4515.

144. Halls, J. J. M.; Walsh, C. A.; Greenham, N. C.; Marseglia, E. A.; Friend, R. H.; Moratti, S. C.; Holmes, A. B., *Nature* **1995,** *376* (6540), 498-500.

145. Granstrom, M.; Petritsch, K.; Arias, A. C.; Lux, A.; Andersson, M. R.; Friend, R. H., *Nature* **1998,** *395* (6699), 257-260.

146. Groves, C.; Blakesley, J. C.; Greenham, N. C., *Nano Lett.* **2010,** *10* (3), 1063-1069.

147. Pal, S. K.; Kesti, T.; Maiti, M.; Zhang, F.; Inganäs, O.; Hellström, S.; Andersson, M. R.; Oswald, F.; Langa, F.; Österman, T.; Pascher, T.; Yartsev, A.; Sundström, V., *J. Am. Chem. Soc.* **2010,** *132* (35), 12440-12451.

148. Proctor, C. M.; Albrecht, S.; Kuik, M.; Neher, D.; Nguyen, T. Q., *Adv. Energy Mater.* **2014,** *4* (10), n/a-n/a.

149. Sariciftci, N. S.; Smilowitz, L.; Heeger, A. J.; Wudl, F., *Science* **1992,** *258* (5087), 1474-1476.

150. Allemand, P. M.; Koch, A.; Wudl, F.; Rubin, Y.; Diederich, F.; Alvarez, M. M.; Anz, S. J.; Whetten, R. L., *J. Am. Chem. Soc.* **1991,** *113* (3), 1050-1051.

151. Brabec, C. J.; Zerza, G.; Cerullo, G.; De Silvestri, S.; Luzzati, S.; Hummelen, J. C.; Sariciftci, S., *Chem. Phys. Lett.* **2001,** *340* (3–4), 232-236.

152. Neugebauer, H.; Brabec, C. J.; Hummelen, J. C.; Janssen, R. A. J.; Sariciftci, N. S., *Synth. Met.* **1999,** *102* (1–3), 1002-1003.

153. Neugebauer, H.; Brabec, C.; Hummelen, J. C.; Sariciftci, N. S., *Sol. Energy Mater. Sol. Cells* **2000,** *61* (1), 35-42.

154. Singh, T. B.; Marjanović, N.; Matt, G. J.; Günes, S.; Sariciftci, N. S.; Montaigne Ramil, A.; Andreev, A.; Sitter, H.; Schwödiauer, R.; Bauer, S., *Org. Electron.* **2005,** *6* (3), 105-110.

155. Hummelen, J. C.; Knight, B. W.; LePeq, F.; Wudl, F.; Yao, J.; Wilkins, C. L., *J. Org. Chem.* **1995,** *60* (3), 532-538.

156. Richards, J. J.; Rice, A. H.; Nelson, R. D.; Kim, F. S.; Jenekhe, S. A.; Luscombe, C. K.; Pozzo, D. C., *Adv. Funct. Mater.* **2013,** *23* (4), 514-522.

157. Yang, X.; Loos, J., *Macromolecules* **2007,** *40* (5), 1353-1362.

158. van Duren, J. K. J.; Yang, X.; Loos, J.; Bulle-Lieuwma, C. W. T.; Sieval, A. B.; Hummelen, J. C.; Janssen, R. A. J., *Adv. Funct. Mater.* **2004,** *14* (5), 425-434.

159. Jonkheijm, P.; van Duren, J. K. J.; Kemerink, M.; Janssen, R. A. J.; Schenning, A. P. H. J.; Meijer, E. W., *Macromolecules* **2006,** *39* (2), 784-788.

160. Byun, M.; Laskowski, R. L.; He, M.; Qiu, F.; Jeffries-El, M.; Lin, Z., *Soft Matter* **2009,** *5* (8), 1583-1586.

161. Lee, J. K.; Ma, W. L.; Brabec, C. J.; Yuen, J.; Moon, J. S.; Kim, J. Y.; Lee, K.; Bazan, G. C.; Heeger, A. J., *J. Am. Chem. Soc.* **2008,** *130* (11), 3619-3623.

162. Hoven, C. V.; Dang, X.-D.; Coffin, R. C.; Peet, J.; Nguyen, T.-Q.; Bazan, G. C., *Adv. Mater.* **2010,** *22* (8), E63-E66.

163. Peet, J.; Kim, J. Y.; Coates, N. E.; Ma, W. L.; Moses, D.; Heeger, A. J.; Bazan, G. C., *Nat Mater* **2007,** *6* (7), 497-500.

164. Hammer, B. A. G.; Bokel, F. A.; Hayward, R. C.; Emrick, T., *Chem. Mater.* **2011,** *23* (18), 4250-4256.

165. Botiz, I.; Darling, S. B., *Macromolecules* **2009,** *42* (21), 8211-8217.

166. Lindner, S. M.; Hüttner, S.; Chiche, A.; Thelakkat, M.; Krausch, G., *Angew. Chem. Int. Ed.* **2006,** *45* (20), 3364-3368.

167. Al-Dmour, H.; Taylor, D. M.; Cambridge, J. A., *J. Phys. D: Appl. Phys.* **2007,** *40* (17), 5034-5038.

168. Stefopoulos, A. A.; Chochos, C. L.; Prato, M.; Pistolis, G.; Papagelis, K.; Petraki, F.; Kennou, S.; Kallitsis, J. K., *Chemistry – A European Journal* **2008,** *14* (28), 8715-8724.

169. Goodman, M. D.; Xu, J.; Wang, J.; Lin, Z., *Chem. Mater.* **2009,** *21* (5), 934-938.

170. Kim, K.; Liu, J.; Namboothiry, M. A. G.; Carroll, D. L., *Appl. Phys. Lett.* **2007,** *90* (16), 163511.

171. Yang, C.; Lee, J. K.; Heeger, A. J.; Wudl, F., *J. Mater. Chem.* **2009,** *19* (30), 5416-5423.

172. Lee, J. U.; Cirpan, A.; Emrick, T.; Russell, T. P.; Jo, W. H., *J. Mater. Chem.* **2009,** *19* (10), 1483-1489.

173. Lee, J. U.; Jung, J. W.; Emrick, T.; Russell, T. P.; Jo, W. H., *J. Mater. Chem.* **2010,** *20* (16), 3287-3294.

174. Zhou, H.; Yang, L.; Stoneking, S.; You, W., *ACS Applied Materials & Interfaces* **2010,** *2* (5), 1377-1383.

175. Roncali, J., *Chem. Rev.* **1997,** *97* (1), 173-206.

176. Nunzi, J.-M., *Comptes Rendus Physique* **2002,** *3* (4), 523-542.

177. Roncali, J., *Macromol. Rapid Commun.* **2007,** *28* (17), 1761-1775.

178. Ma, H.; Yip, H.-L.; Huang, F.; Jen, A. K. Y., *Adv. Funct. Mater.* **2010,** *20* (9), 1371-1388.

179. Foster, S.; Deledalle, F.; Mitani, A.; Kimura, T.; Kim, K.-B.; Okachi, T.; Kirchartz, T.; Oguma, J.; Miyake, K.; Durrant, J. R.; Doi, S.; Nelson, J., *Adv. Energy Mater.* **2014**, 10.1002/aenm.201400311, n/a-n/a.

180. Scharber, M. C.; Mühlbacher, D.; Koppe, M.; Denk, P.; Waldauf, C.; Heeger, A. J.; Brabec, C. J., *Adv. Mater.* **2006,** *18* (6), 789-794.

181. Cowan, S. R.; Roy, A.; Heeger, A. J., *Physical Review B* **2010,** *82* (24).

182. Dennler, G.; Scharber, M. C.; Brabec, C. J., *Adv. Mater.* **2009,** *21* (13), 1323-1338.

183. Varotto, A.; Treat, N. D.; Jo, J.; Shuttle, C. G.; Batara, N. A.; Brunetti, F. G.; Seo, J. H.; Chabinyc, M. L.; Hawker, C. J.; Heeger, A. J.; Wudl, F., *Angew. Chem. Int. Ed.* **2011,** *50* (22), 5166-5169.

184. Meng, X.; Zhao, G.; Xu, Q.; Tan, Z. a.; Zhang, Z.; Jiang, L.; Shu, C.; Wang, C.; Li, Y., *Adv. Funct. Mater.* **2014,** *24* (1), 158-163.

185. Lenes, M.; Wetzelaer, G.-J. A. H.; Kooistra, F. B.; Veenstra, S. C.; Hummelen, J. C.; Blom, P. W. M., *Adv. Mater.* **2008,** *20* (11), 2116-2119.

186. Kooistra, F. B.; Knol, J.; Kastenberg, F.; Popescu, L. M.; Verhees, W. J. H.; Kroon, J. M.; Hummelen, J. C., *Org. Lett.* **2007,** *9* (4), 551-554.

187. Liang, Y.; Xu, Z.; Xia, J.; Tsai, S.-T.; Wu, Y.; Li, G.; Ray, C.; Yu, L., *Adv. Mater.* **2010,** *22* (20), E135-E138.

188. Liang, Y.; Wu, Y.; Feng, D.; Tsai, S.-T.; Son, H.-J.; Li, G.; Yu, L., *J. Am. Chem. Soc.* **2009,** *131* (1), 56-57.

189. Liang, Y.; Feng, D.; Wu, Y.; Tsai, S.-T.; Li, G.; Ray, C.; Yu, L., *J. Am. Chem. Soc.* **2009,** *131* (22), 7792-7799.

190. Blouin, N.; Michaud, A.; Gendron, D.; Wakim, S.; Blair, E.; Neagu-Plesu, R.; Belletete, M.; Durocher, G.; Tao, Y.; Leclerc, M., *J. Am. Chem. Soc.* **2008,** *130* (2), 732-42.

191. Park, S. H.; Roy, A.; Beaupre, S.; Cho, S.; Coates, N.; Moon, J. S.; Moses, D.; Leclerc, M.; Lee, K.; Heeger, A. J., *Nat Photon* **2009,** *3* (5), 297-302.

192. Qin, R.; Li, W.; Li, C.; Du, C.; Veit, C.; Schleiermacher, H.-F.; Andersson, M.; Bo, Z.; Liu, Z.; Inganäs, O.; Wuerfel, U.; Zhang, F., *J. Am. Chem. Soc.* **2009,** *131* (41), 14612-14613.

193. Beaujuge, P. M.; Pisula, W.; Tsao, H. N.; Ellinger, S.; Müllen, K.; Reynolds, J. R., *J. Am. Chem. Soc.* **2009,** *131* (22), 7514-7515.

194. Chen, H.-Y.; Hou, J.; Hayden, A. E.; Yang, H.; Houk, K. N.; Yang, Y., *Adv. Mater.* **2010,** *22* (3), 371-375.

195. Hou, J.; Chen, H.-Y.; Zhang, S.; Li, G.; Yang, Y., *J. Am. Chem. Soc.* **2008,** *130* (48), 16144-16145.

196. Huo, L.; Chen, H. Y.; Hou, J.; Chen, T. L.; Yang, Y., *Chem Commun (Camb)* **2009**, 10.1039/b910443g (37), 5570-2.

197. Coffin, R. C.; Peet, J.; Rogers, J.; Bazan, G. C., *Nat Chem* **2009,** *1* (8), 657-61.

198. Wang, M.; Hu, X.; Liu, P.; Li, W.; Gong, X.; Huang, F.; Cao, Y., *J. Am. Chem. Soc.* **2011,** *133* (25), 9638-9641.

199. Osaka, I.; Shimawaki, M.; Mori, H.; Doi, I.; Miyazaki, E.; Koganezawa, T.; Takimiya, K., *J. Am. Chem. Soc.* **2012,** *134* (7), 3498-3507.

200. Son, H. J.; Wang, W.; Xu, T.; Liang, Y.; Wu, Y.; Li, G.; Yu, L., *J. Am. Chem. Soc.* **2011,** *133* (6), 1885-1894.

201. Chen, H.-Y.; Hou, J.; Zhang, S.; Liang, Y.; Yang, G.; Yang, Y.; Yu, L.; Wu, Y.; Li, G., *Nat Photon* **2009,** *3* (11), 649-653.

202. Albrecht, S.; Janietz, S.; Schindler, W.; Frisch, J.; Kurpiers, J.; Kniepert, J.; Inal, S.; Pingel, P.; Fostiropoulos, K.; Koch, N.; Neher, D., *J. Am. Chem. Soc.* **2012,** *134* (36), 14932-14944.

203. Carsten, B.; Szarko, J. M.; Son, H. J.; Wang, W.; Lu, L.; He, F.; Rolczynski, B. S.; Lou, S. J.; Chen, L. X.; Yu, L., *J. Am. Chem. Soc.* **2011,** *133* (50), 20468-20475.

204. Carsten, B.; Szarko, J. M.; Lu, L.; Son, H. J.; He, F.; Botros, Y. Y.; Chen, L. X.; Yu, L., *Macromolecules* **2012,** *45* (16), 6390-6395.

205. Intemann, J. J.; Yao, K.; Ding, F.; Xu, Y.; Xin, X.; Li, X.; Jen, A. K. Y., *Adv. Funct. Mater.* **2015,** *25* (30), 4889-4897.

206. Zhou, H.; Yang, L.; Stuart, A. C.; Price, S. C.; Liu, S.; You, W., *Angew. Chem. Int. Ed.* **2011,** *50* (13), 2995-2998.

207. Stuart, A. C.; Tumbleston, J. R.; Zhou, H.; Li, W.; Liu, S.; Ade, H.; You, W., *J. Am. Chem. Soc.* **2013,** *135* (5), 1806-1815.

208. Price, S. C.; Stuart, A. C.; Yang, L.; Zhou, H.; You, W., *J. Am. Chem. Soc.* **2011,** *133* (12), 4625-4631.

209. Zhou, H.; Yang, L.; Xiao, S.; Liu, S.; You, W., *Macromolecules* **2010,** *43* (2), 811-820.

210. Huo, L.; Hou, J.; Zhang, S.; Chen, H.-Y.; Yang, Y., *Angew. Chem. Int. Ed.* **2010,** *49* (8), 1500-1503.

211. Huo, L.; Zhang, S.; Guo, X.; Xu, F.; Li, Y.; Hou, J., *Angew. Chem. Int. Ed. Engl.* **2011,** *50* (41), 9697-702.

212. Dou, L.; Gao, J.; Richard, E.; You, J.; Chen, C.-C.; Cha, K. C.; He, Y.; Li, G.; Yang, Y., *J. Am. Chem. Soc.* **2012,** *134* (24), 10071-10079.

213. He, F.; Wang, W.; Chen, W.; Xu, T.; Darling, S. B.; Strzalka, J.; Liu, Y.; Yu, L., *J. Am. Chem. Soc.* **2011,** *133* (10), 3284-3287.

214. Yiu, A. T.; Beaujuge, P. M.; Lee, O. P.; Woo, C. H.; Toney, M. F.; Frechet, J. M., *J. Am. Chem. Soc.* **2012,** *134* (4), 2180-5.

215. Li, Z.; Tsang, S. W.; Du, X. M.; Scoles, L.; Robertson, G.; Zhang, Y. G.; Toll, F.; Tao, Y.; Lu, J. P.; Ding, J. F., *Adv. Funct. Mater.* **2011,** *21* (17), 3331-3336.

216. Amb, C. M.; Chen, S.; Graham, K. R.; Subbiah, J.; Small, C. E.; So, F.; Reynolds, J. R., *J. Am. Chem. Soc.* **2011,** *133* (26), 10062-10065.

217. Yamaguchi, S.; Tamao, K., *Chem. Lett.* **2005,** *34* (1), 2-7.

218. Yamaguchi, S.; Tamao, K., *J. Chem. Soc., Dalton Trans.* **1998**, 10.1039/A804491K (22), 3693-3702.

219. Kim, M.; Kim, J.-H.; Choi, H. H.; Park, J. H.; Jo, S. B.; Sim, M.; Kim, J. S.; Jinnai, H.; Park, Y. D.; Cho, K., *Adv. Energy Mater.* **2014,** *4* (2), n/a-n/a.

220. McDowell, C.; Abdelsamie, M.; Zhao, K.; Smilgies, D.-M.; Bazan, G. C.; Amassian, A., *Adv. Energy Mater.* **2015**, 10.1002/aenm.201501121, n/a-n/a.

221. Bundgaard, E.; Krebs, F. C., *Sol. Energy Mater. Sol. Cells* **2007,** *91* (11), 954-985.

222. Lou, S. J.; Szarko, J. M.; Xu, T.; Yu, L.; Marks, T. J.; Chen, L. X., *J. Am. Chem. Soc.* **2011,** *133* (51), 20661-20663.

223. Brabec, C. J.; Shaheen, S. E.; Winder, C.; Sariciftci, N. S.; Denk, P., *Appl. Phys. Lett.* **2002,** *80* (7), 1288-1290.

224. Schlatmann, A. R.; Floet, D. W.; Hilberer, A.; Garten, F.; Smulders, P. J. M.; Klapwijk, T. M.; Hadziioannou, G., *Appl. Phys. Lett.* **1996,** *69* (12), 1764-1766.

225. Seo, J. H.; Gutacker, A.; Sun, Y.; Wu, H.; Huang, F.; Cao, Y.; Scherf, U.; Heeger, A. J.; Bazan, G. C., *J. Am. Chem. Soc.* **2011,** *133* (22), 8416-8419.

226. He, Z.; Zhang, C.; Xu, X.; Zhang, L.; Huang, L.; Chen, J.; Wu, H.; Cao, Y., *Adv. Mater.* **2011,** *23* (27), 3086-3089.

227. He, Z.; Zhong, C.; Huang, X.; Wong, W.-Y.; Wu, H.; Chen, L.; Su, S.; Cao, Y., *Adv. Mater.* **2011,** *23* (40), 4636-4643.

228. Yang, R.; Xu, Y.; Dang, X.-D.; Nguyen, T.-Q.; Cao, Y.; Bazan, G. C., *J. Am. Chem. Soc.* **2008,** *130* (11), 3282-3283.

229. Beaupré, S.; Belletête, M.; Durocher, G.; Leclerc, M., *Macromol. Theory Simul.* **2011,** *20* (1), 13-18.

# CHAPTER 2

## HETEROATOM INFLUENCE ON THE ELECTRONIC PROPERTIES OF ARYL[3,4-*c*]PYRROLEDIONE BASED COPOLYMERS.

*Benjamin J. Hale,*[a] *Moneim Elshobaki,*[b] *Ryan Gebhardt,*[b] *David Wheeler,*[c] *Jon Stoffer,*[a] *Aimée Tomlinson,*[c] *Sumit Chaudhary,*[d] *Malika Jeffries-EL*[a*]

[a] Department of Chemistry, Iowa State University, Ames, IA 50011

[b] Department of Materials & Science Engineering, Iowa State University, Ames, IA 50011

[c]Department of Chemistry & Biochemistry, University of North Georgia, Dahlonega, GA 30597

[d] Department of Electrical and Computer Engineering, Iowa State University, Ames, IA 50011

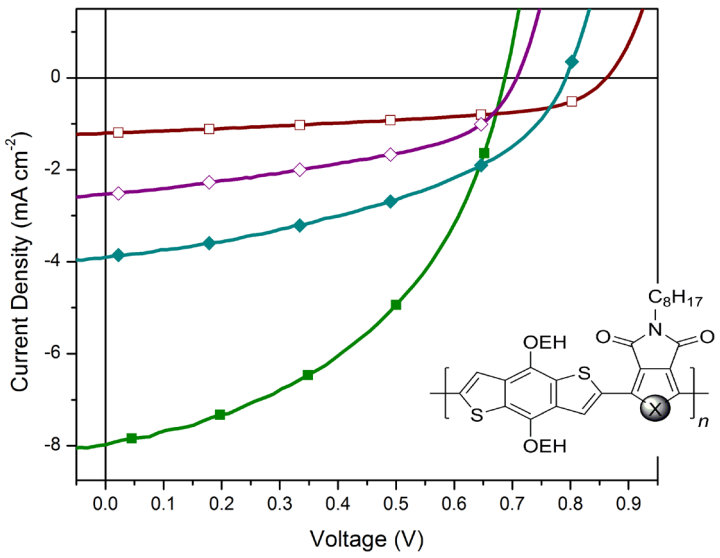

## 2.1 Abstract

A donor-acceptor-type conjugated copolymer (PBDT-PPD) composed of benzodithiophene (BDT) and pyrrolopyrroledione (PPD) was synthesized using the Stille cross-coupling reaction. Using both experimental and theoretical data, the optical, electrochemical, and photovoltaic properties of PBDT-PPD were compared with those of its sulfur analog, PBDT-TPD, which is composed of BDT and thienopyrroledione (TPD). The optical bandgaps of the polymers were determined to be 1.86 and 2.20 eV, respectively. While both materials possessed similar highest occupied molecular orbital (HOMO) levels, the lowest unoccupied molecular orbital (LUMO) level for PBDT-PPD was raised relative to that of PBDT-TPD. Devices incorporating PBDT-PPD had a higher open-circuit voltage and fill factor, yet drastically lower short-circuit current density ($J_{sc}$) than PBDT-TPD leading to a lower power conversion efficiency (PCE). The lack of significant intramolecular charge transfer (ICT) combined with the high LUMO of PBDT-PPD resulted in poor spectral overlap with the solar spectrum, lowering $J_{sc}$. Additionally, there was poor electron injection into PCBM, which also reduced the PCE.

## 2.2 Introduction

Since the discovery of the first semiconducting polymer nearly 40 years ago, research involving conjugated polymers has been on the rise. In particular, studies involving bulk hetero-junction (BHJ) organic photovoltaic solar cells (OPVs), has increased exponentially due to their potential low cost production, and use in lightweight, flexible devices.[1-9] Although improvements in materials and fabrication techniques have led to

dramatic increases in OPV performance, as determined by the power conversion efficiency (PCE), a better understanding of structure-property relationships is still desired.[10-11] The synthesis of conjugated polymers, comprised of alternating π-electron rich and π-electron deficient arylene units, allows for the selective tuning of optical and electronic properties of the material.[12-14] This "donor-acceptor" strategy has given rise to a variety of materials with desirable properties, such as broad optical absorption bands, deep HOMO energy levels, high charge carrier mobilities, and LUMO levels with appropriate alignment to [6,6]-phenyl-$C_{71}$-butyric acid methyl ester ($PC_{71}BM$).[8, 15] In addition, these materials can be further tuned by varying the heteroatoms within the arenes. Indeed, a dramatic impact on the physical, optical, and electronic properties of a material can be achieved through heteroatom substitution.[8, 16] For example, large changes in optical absorption and solubility of many materials have been observed upon replacing of thiophene with the iso-electronic furan or selenophene.[16-19] While substitution within a group (e.g. the group 16 chalcogens) can at often times have predictable effects, the impact of substitution between groups is often less straightforward.[16, 20-21]

The thiophene containing thieno[3,4-*c*]pyrrole-4,6-dione (TPD) unit has been used as an π-electron deficient moiety in a variety of high efficiency donor-acceptor copolymers.[22-24] When polymerized with the π-electron rich benzodithiophene (BDT), BHJ OPV performance as high as 5.5% for 1.0 $cm^2$ devices (PBDT-TPD) has been reported.[22] When the thiophene was replaced with furan (FPD), a widening of the optical bandgap was observed, whereas switching with selenophene (SePD) resulted in a reduction of the optical bandgap, relative to TPD.[25] OPVs fabricated from the SePD based polymer showed a greatly reduced short-circuit current density ($J_{sc}$), which resulted

in a very low PCE of 0.26%.[26] Although an improvement in performance has not been seen with FPD or SePD, exploration outside of the group 16 elements has yet to be researched extensively.

A seldom studied alternative to TPD is the nitrogen analog pyrrolo[3,4-*c*]pyrroledione (PPD), first reported in 1996.[27] While, the additional alkyl chain on the nitrogen atom of PPD can potentially increase solubility, the impact of replacing sulfur with nitrogen is not well understood. Recently, PPD was used in a series of donor-acceptor copolymers with varying results, and there was no direct structural comparison to known high performing TPD based materials.[28] Here, a PPD based copolymer was synthesized, characterized and compared to the structurally analogous PBDT-TPD. In addition to the physical methods, we also evaluated both polymers through density functional theory.

## 2.3 Results and Discussion

### 2.3.1 Synthesis and characterization of monomer and polymers

The PPD monomer **6** was prepared according the synthetic route as illustrated in Scheme 2.1.[27] Diethyl pyrrole-3,4-dicarboxlyate was formed by condensation of diethyl fumarate and *p*-toluenesulfonylmethyl isocyanide followed by saponification to the dicarboxylic acid, **2**. Compound **2** was then converted to the corresponding anhydride by treatment with *N,N'*-dicyclohexylcarbodiimide, which was ring opened with *n*-octylamine, and closed with thionyl chloride to give **4**. The unalkylated **4** was then brominated using NBS in the dark. Compound **5** was then alkylated, in a fashion similar

to its structural isomer diketopyrrolopyrrole, in DMF with potassium carbonate, 1-bromooctane, and 18-crown-6 to give the final PPD monomer, **6**, in moderate yield.

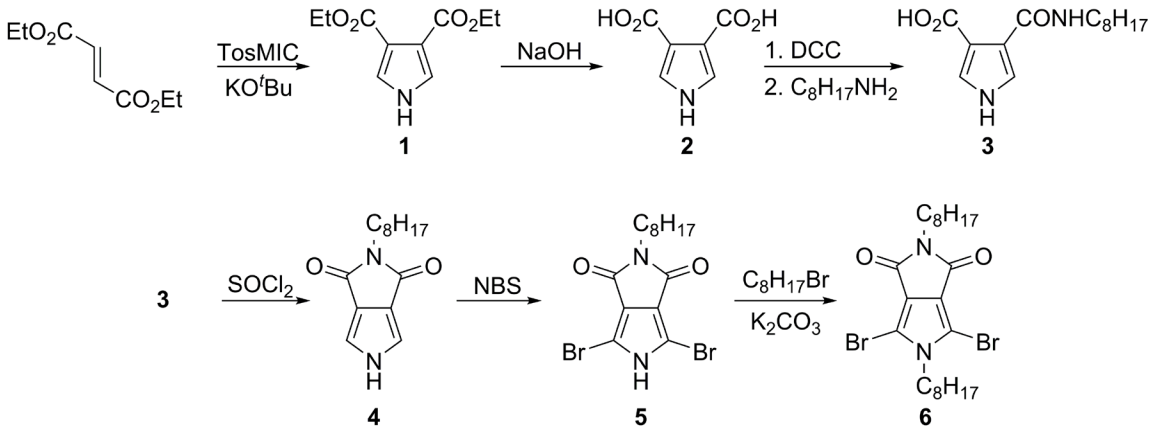


**Scheme 2.1.** Synthesis of PPD monomer **6**.

Alternating copolymers were synthesized by Stille cross-coupling of the diarylhalide monomers (PPD or TPD) and the distannyl BDT monomer in anhydrous toluene, as shown in Scheme 2.2. The molecular weight data for **PBDT-TPD** and **PBDT-PPD** were determined by size exclusion chromatography in chloroform against polystyrene standards. Both materials had reasonable number averaged molecular weights ($M_n$) of 24.9 19.8 kDa for **PBDT-TPD** and **PBDT-PPD**, respectively. The TPD based polymer, **PBDT-TPD**, had poor solubility in organic solvents at room temperature, but was readily dissolved in chlorobenzene and 1,2-dichlorobenzene when heated, as reported by Leclerc et al.[22] The PPD based polymer, **PBDT-PPD**, had greatly improved solubility and was readily dissolved in chloroform, chlorobenzene, and 1,2-dichlorobenzene at room temperature. The increased solubility of **PBDT-PPD** is likely due to the lower degree of polymerization ($DP_n$) and the additional solubilizing alkyl chain on the nitrogen.

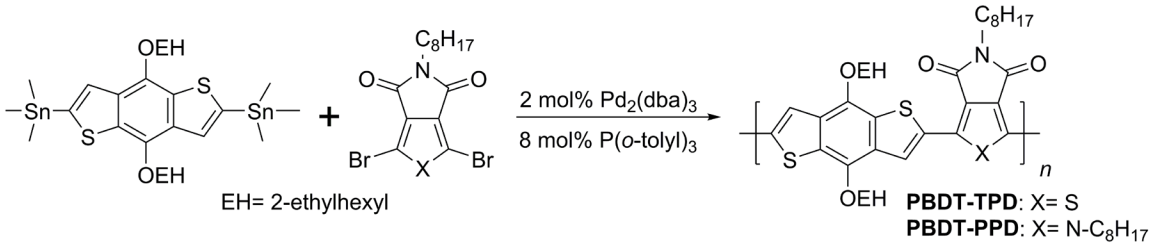


**Scheme 2.2.** Synthesis of donor-acceptor copolymers **PBDT-TPD** and **PBDT-PPD**.

**Table 2.1.** Molecular weight and thermal properties of the synthesized polymers.

| Polymer | Yield[a] (%) | $M_n$[b] (kDa) | $M_w$[b] (kDa) | Đ[c] | $DP_n$ | $T_d5\%$[d] (°C) |
|---|---|---|---|---|---|---|
| PBDT-TPD | 82 | 24.9 | 44.8 | 1.8 | 35.1 | 333.7 |
| PBDT-PPD | 73 | 19.8 | 33.6 | 1.7 | 24.6 | 337.8 |

[a]Isolated yield. [b]Determined by GPC vs polystyrene standards in chloroform. [c]Dispersity: $M_w/M_n$. [d]Temperature at 5% weight loss with a heating rate of 20 °C $min^{-1}$ under nitrogen.

The thermal stabilities of the polymers were evaluated using TGA under air (Figure S2.15, Supporting Information). **PBDT-TPD** and **PBDT-PPD** demonstrated good thermal stability when heated, with a 5% weight loss at 333 and 337 °C, respectively. Differential scanning calorimetry (Figure S2.16, Supporting Information) revealed no phase transitions for **PBDT-PPD** below 250 ° C. The molecular weights and thermal properties of **PBDT-TPD** and **PBDT-PPD** are summarized in Table 2.1.

### 2.3.2 Optical and electrochemical properties

The optical properties of the polymers were investigated using UV-Vis absorption spectroscopy. The normalized absorption spectra of the polymers, both as dilute chloroform solutions and thin films on glass substrates, are shown in Figure 2.1 and 2.2,

respectively. **PBDT-TPD** had a broad absorption from 350 – 650 nm in dilute solution with two peaks of nearly equal intensity at 552 and 627 nm, with a third slightly smaller peak at ~590 nm. The intensities of the broad low energy transition suggests intramolecular charge-transfer (ICT) interaction between the electron-rich BDT and the electron-deficient TPD moieties.[29] In solution **PBDT-PPD** displayed a $\lambda_{max}$ of 526 nm with a narrower and significantly blue shifted absorption range of 350 – 550 nm, relative to **PBDT-TPD**. Strong vibronic coupling can be seen in **PBDT-PPD**, suggesting the formation of aggregates in solution.

As a thin film, **PBDT-TPD** showed very little change in absorption when compared to its solution spectra, with a $\lambda_{max}$ of 624 nm. A slight decrease in the intensity of the higher energy maximum and an increase in the intensity of vibronic coupling was also seen, with the vibronic coupling indicating highly ordered thin films.[30] Interestingly, the thin film of **PBDT-PPD**, had a $\lambda_{max}$ of 533 nm, with a reduction in intensity, and a significant narrowing of the absorption range by a decrease of the $\pi$-$\pi^*$ transitions of the conjugated main chain. A comparison of the absorption profiles of the two polymers shows **PBDT-TPD** has a stronger absorption intensity across nearly all wavelengths and a significantly broader absorption of 350 – 675 nm, versus the 350– 550 nm range of **PBDT-PPD**. The optical bandgaps were determined from the absorption onsets of the polymer films. The measured optical bandgaps for **PBDT-TPD** and **PBDT-PPD** were 1.86 eV and 2.20 eV, respectively. The narrow absorption range of **PBDT-PPD** and the wide bandgap suggest there is little, if any, ICT occurring between the BDT and PPD moieties.[31-33] The optical data is summarized in Table 2.2.

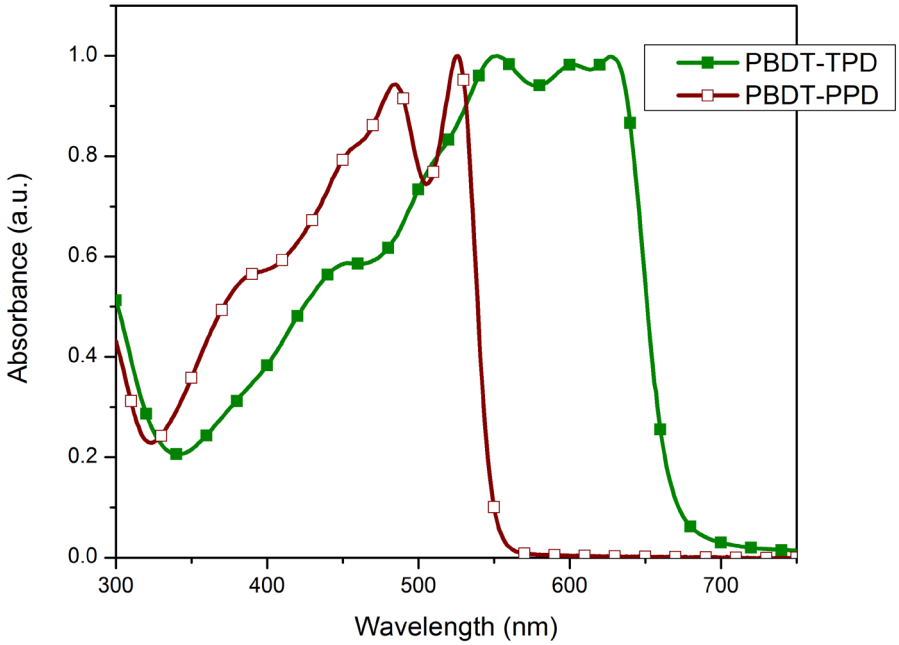


**Figure 2.1.** Normalized UV-vis spectra of **PBDT-TPD** and **PBDT-PPD** in $CHCl_3$.

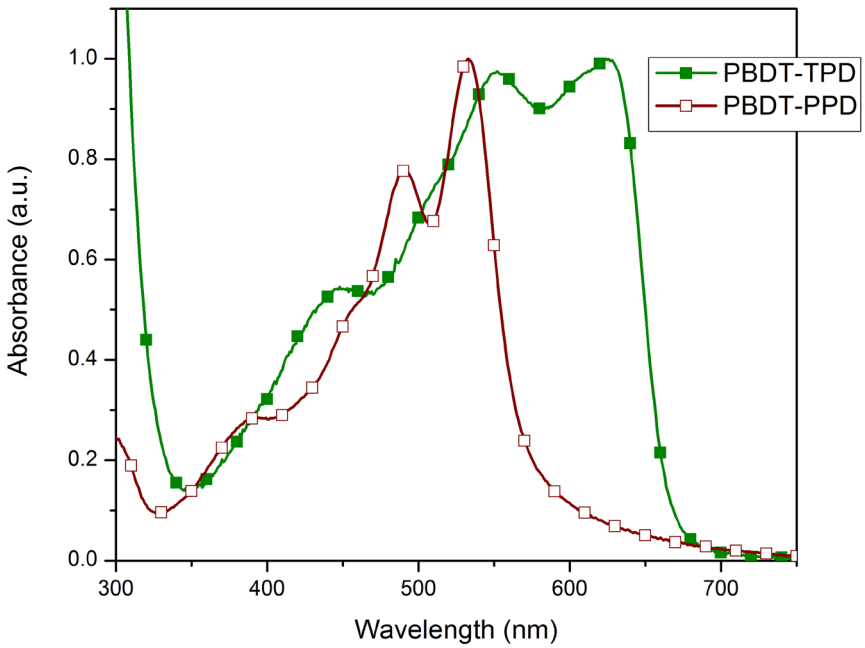


**Figure 2.2.** Normalized UV-vis spectra of **PBDT-TPD** and **PBDT-PPD** thin films.

**Table 2.2.** Optical and electrochemical properties of the synthesized polymers.

| Polymer | $\lambda_{max}^{soln}$ (nm)[a] | $\lambda_{max}^{film}$ (nm) | $E_g^{opt}$ (eV)[b] | $E_{HOMO}$ (eV)[c] | $E_{LUMO}$ (eV)[d] | $E_g^{EC}$ [e] (eV) |
|---|---|---|---|---|---|---|
| PBDT-TPD | 552, 627 | 624 | 1.86 | -5.50 | -3.54 | 1.96 |
| PBDT-PPD | 526 | 533 | 2.20 | -5.50 | -3.10 | 2.40 |

[a]Measured in chloroform. [b]Measured from the optical onset. [c]HOMO = -($E_{onset}^{ox}$ + 4.7)eV; [d]LUMO = -($E_{onset}^{red}$ - 4.7)eV; [e]$E_g^{EC}$ = LUMO – HOMO.

Cyclic voltammetry was used to investigate the redox behavior and to estimate the HOMO energy levels of the polymers. The HOMO and LUMO energy levels were calculated from the oxidation onset using the adjusted energy level of ferrocene/ferrocenium ($Fc/Fc^+$) as -4.7 eV vs vacuum and are summarized in Table 2.2. Both polymers exhibited reversible reduction and irreversible oxidation peaks (Supporting Information). The HOMO energy level for both **PBDT-TPD** and **PBDT-PPD** were found to be -5.50 eV, while the LUMO energy levels were found to be -3.54 eV and -3.10 eV, for **PBDT-TPD** and **PBDT-PPD** respectively. The electrochemical bandgaps of 1.96 eV for **PBDT-TPD** and 2.40 eV for **PBDT-PPD** are in agreement with the optical bandgaps.[34] While both materials had the same HOMO level, the significantly higher LUMO level and narrowing of the optical absorption of PBDT-PPD reinforce the suspicion that little intramolecular charge transfer along the polymer backbone. To further investigate this possibility, DFT calculations were performed.

### 2.3.4 Computational Studies

Density functional theory was used to evaluate the differences in the performance between **PBDT-TPD** and **PBDT-PPD**. Although, the improved performance of OPVs based **PBDT-TPD** can be attributed to the smaller band gap and a lower lying LUMO level relative to **PBDT-PPD**, other factors may be involved. Upon completion of the DFT calculations, the frontier orbitals and electrostatic potential maps were generated (Figure 2.3). For **PBDT-TPD**, the terminal TPD ring is electron deficient in the HOMO and becomes rich in electron density in the LUMO. The opposite trend occurs for the BDT ring, which is electron rich in the HOMO and electron deficient in the LUMO. This trend indicates there may be some donor-acceptor behavior within this system, but it appears to be localized. Whereas in **PBDT-PPD** there is complete delocalization of electron density in the HOMO and again an absence on the BDT ring in the LUMO hence this polymer exhibits less donor-acceptor behavior. Thus, the decrease in ICT in the **PBDT-PPD** is a contributing factor in its poor performance.

**Table 2.3.** Comparison between theoretical and experimental values.

| | HOMO (eV) | | | LUMO (eV) | | | Bandgap (eV) | | |
|---|---|---|---|---|---|---|---|---|---|
| | DFT | Expt | Diff | DFT | Expt | Diff | DFT | Expt | Diff |
| PBDT-TPD | -5.21 | -5.50 | 0.29 | -3.09 | -3.54 | 0.45 | 1.82 | 1.86 | 0.04 |
| PBDT-PPD | -5.15 | -5.50 | 0.35 | -2.38 | -3.10 | 0.72 | 2.42 | 2.20 | 0.22 |

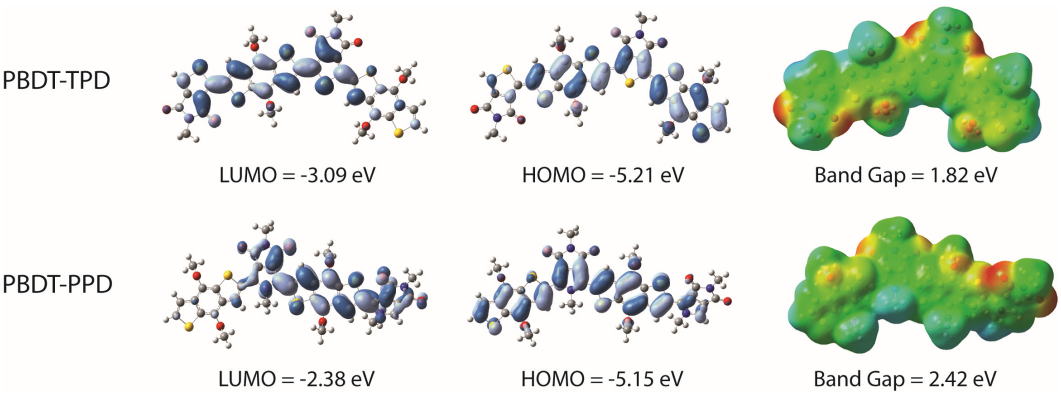


**Figure 2.3.** DFT calculated frontier orbital and electrostatic potential maps.

A comparison between the experimental electrochemical results and the theoretical data is shown in Table 2.3. An absolute difference of 0.35 eV and 0.22 eV was found in the HOMO and band gap respectively, indicating there is good agreement between the two data sets. In order evaluate the potential for charge transfer within these copolymers the reorganization energy for both the hole and the electron was computed and shown in Table 2.4. This energy was generated for both the individual subunits as well as the comonomer in each case. In the case of **PBDT-TPD**, the BDT subunit had a much lower reorganization energy for electron than for the hole indicating it takes less energy for this ring to accept a negative charge than it does for a positive charge. The opposite is true for TPD in which the hole reorganization energy is lower than that of the electron. Putting the two subunits together and making a comonomer shows that the material behaves more favorably as an acceptor than a donor. For the **PBDT-PPD** copolymer, the PPD is more accepting than donating in nature as indicated by the reorganization energy. Like **PBDT-TPD, PBDT-PPD** is an also electron-accepting material. Overall, all of these reorganization energies are quite high and so while trends can be suggested based on their

magnitude it is doubtful either of these copolymers would be able to charge-transfer at a reasonable rate.

**Table 2.4.** Reorganization energies (in eV) for the subunits and their monomers.

| | BDT | PPD | TPD | PBDT-TPD | PBDT-PPD |
|---|---|---|---|---|---|
| $\lambda_h$ [a] | 0.838 | 0.399 | 0.400 | 0.762 | 0.798 |
| $\lambda_e$ [b] | 0.337 | 0.478 | 0.476 | 0.414 | 0.445 |

[a]Hole reorganization: $\lambda_h$. [b]Electron reorganization: $\lambda_e$.

### 2.3.5 Photovoltaic properties

Photovoltaic devices were fabricated with the structure ITO/PEDOT:PSS/donor:$PC_{71}BM$/Ca/Al, where ITO is indium tin oxide and PEDOT:PSS is poly(3,4-ethylenedioxythiophene)-poly(styrenesulfonate). Characteristic *J–V* curves are shown in Figure 2.4 and the resulting data is summarized in Table 2.5. Solutions were cast from a 25 mg $mL^{-1}$ total blend concentration in chlorobenzene using a ratio of 1:2 polymer:$PC_{71}BM$ w/w. Spin-rates ranging from 1000 rpm to 1400 rpm were examined. The best devices of **PBDT-TPD** gave a PCE of 2.5%, with an open-circuit voltage ($V_{OC}$) of 0.68 V, a short-circuit current density ($J_{SC}$) of 7.98 mA $cm^{-2}$, and a fill factor (FF) of 46%, while the best devices of **PBDT-PPD** gave a significantly lower PCE of 0.63%, $V_{OC}$ of 0.87 V, $J_{SC}$ 1.3 mA $cm^{-2}$, and a FF of 57%.

In an effort to further improve the poor performance of **PBDT-PPD**, devices were fabricated with the use of small quantities of the high boiling solvent additives 1-

chloronaphthalene (CN) and 1,8-diiodooctane (DIO) at 5% v/v. In general, devices made from solution with additives had higher PCE in comparison to the ones without additives. Devices fabricated using CN as an additive gave a maximum PCE of 0.83%, an average PCE of 0.72%, $V_{OC}$ of 0.66 V, $J_{SC}$ of 2.5 mA cm$^{-2}$, but a greatly reduced FF of 44%. The devices using DIO gave a significantly higher maximum PCE of 1.34% and an average of 1.23%, $V_{OC}$ of 0.76 V, $J_{SC}$ of 3.9 mA cm$^{-2}$, but also had a low FF of 42%. While improvement was observed using solvent additives, the overall photocurrent remained very low.

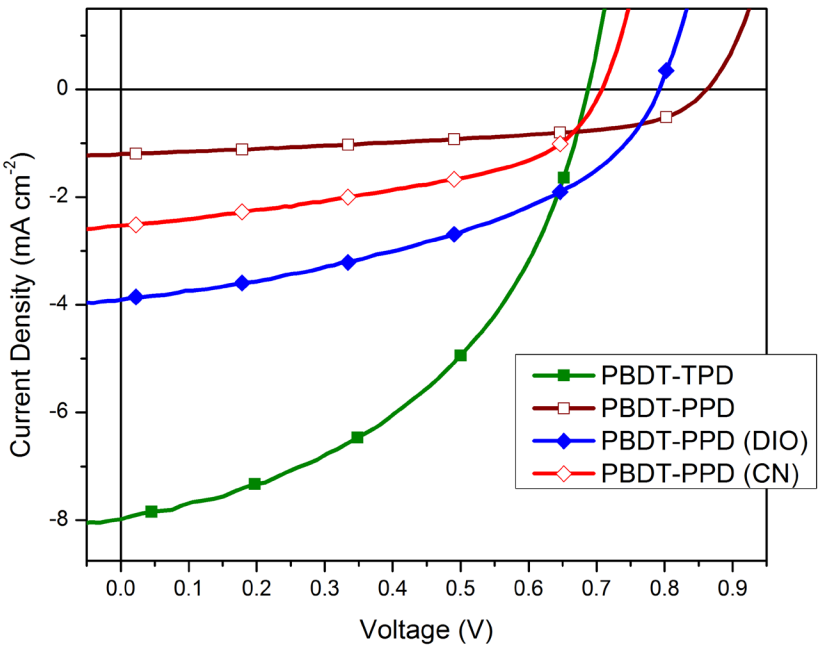


**Figure 2.4.** $J - V$ curves of PBDT-TPD and PBDT-PPD devices.

**Table 2.5.** Summary of the characteristics of photovoltaic devices.

| Polymer[a] | Additive[b] | $J_{SC}$ (mA cm$^{-2}$) | $V_{OC}$ (V) | FF (%) | PCE$_{ave}$[e] (%) | PCE$_{max}$ (%) |
|---|---|---|---|---|---|---|
| PBDT-TPD | -- | 7.8 | 0.69 | 45 | 2.44 | 2.51 |
| PBDT-PPD | -- | 1.3 | 0.87 | 52 | 0.59 | 0.63 |
| | DIO[c] | 3.9 | 0.76 | 42 | 1.23 | 1.34 |
| | CN[d] | 2.5 | 0.66 | 44 | 0.72 | 0.83 |

[a]Fabricated at a 1:1.5 weight ratio of polymer:$PC_{71}BM$ with a total solution concentration of 25 mg mL$^{-1}$. [b]5% *v/v*. [c]1,8-diiodooctane. [d]1-chloronaphthalene. [e]Average of six devices.

The surface roughness and phase distribution of the polymers were studied by atomic force microscopy (AFM) (Fig. 4). The AFM roughness maps of PBDT-TPD:$PC_{70}BM$ and PBDT-PPD:$PC_{70}BM$ neat thin-films show large domain sizes with root-mean square surface roughness (RMS) values of 3.99 and 5.17 nm, respectively. Whereas the AFM height images reveal smooth topography for both polymers with root-mean square (RMS) surface roughness values less than 1.30 nm. The $J_{SC}$ of the **PBDT-PPD** device increased from 1.3 mA cm$^{-2}$ to 3.9 and 2.5 mA cm$^{-2}$ upon using as solvent additives of DIO and CN, respectively. This enhancement in $J_{SC}$ is a result of the reduction in the domain size within the morphology of PBDT-PPD-based thin-films with solvent additives as seen in AFM images (Figure 2.5 and 2.6). The films with additives have small grain sizes with slight variation in the surface roughness ($RMS_{DIO}$ = 5.59 nm, and $RMS_{CN}$ = 4.25 nm). This change morphology is beneficial for suppressing the charge recombination and better charge transport and dissociation is achieved.

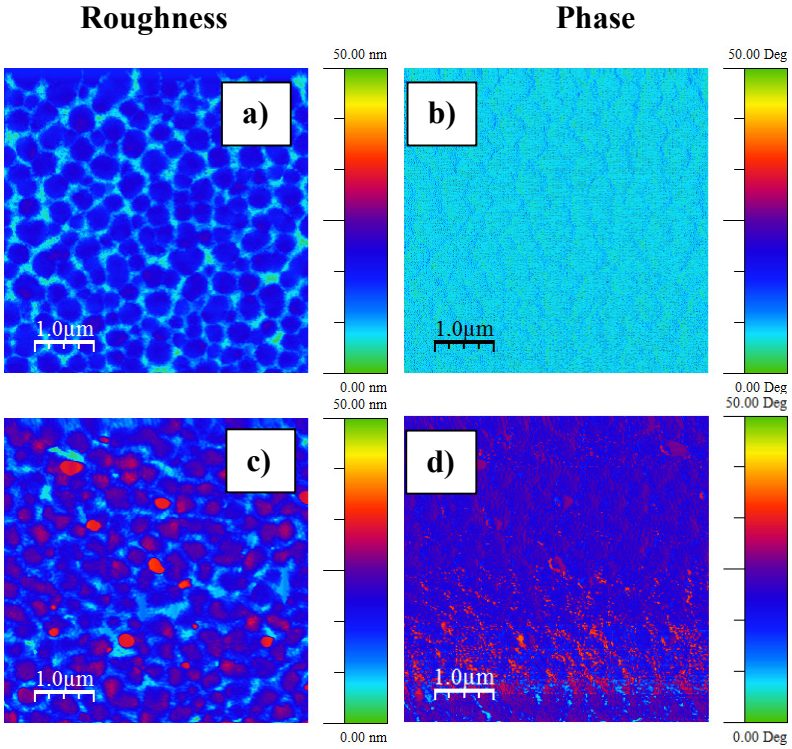


**Figure 2.5.** AFM height (left) and phase (right) images at 5 µm x 5 µm of PBDT-TPD:$PC_{71}BM$ (a-b), PBDT-PPD:$PC_{71}BM$ (c-d) thin-films.

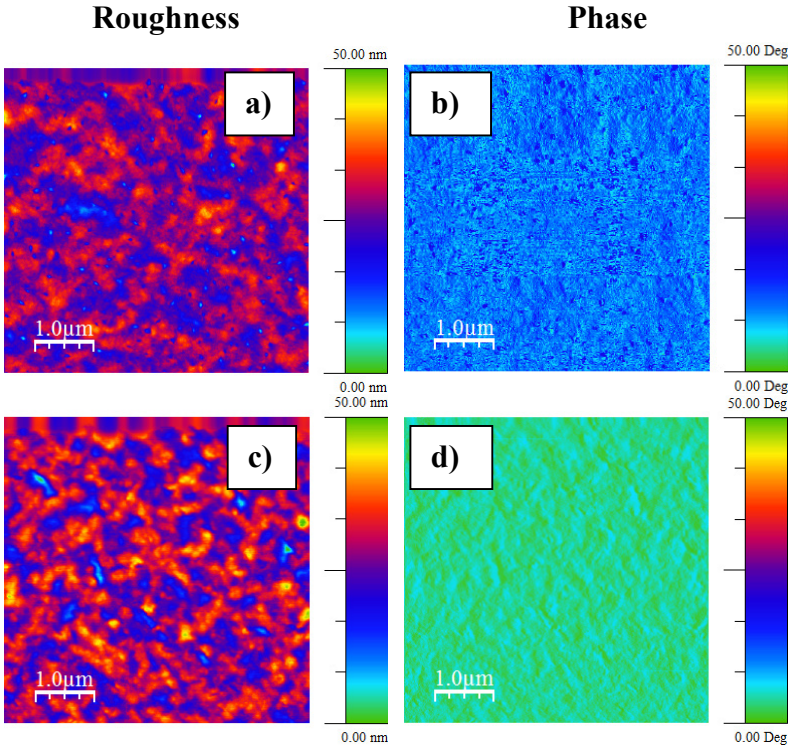


**Figure 2.6.** AFM height (left) and phase (right) images at 5 µm x 5 µm of PBDT-PPD:$PC_{71}BM$ with 5% DIO (a-b) and 5% CN (c-d) solvent additives.

The hole mobility of **PBDT-TPD** and **PBDT-PPD** were examined using the space-charge limited current (SCLC) method with a hole only device structure of ITO/PEDOT:PSS/polymer:$PC_{71}BM$/$MoO_x$/Al. The mobilites were calculated according to the equation:

$$J_{SCLC} = \frac{9}{8}\varepsilon_o \varepsilon_r \mu_h (V^2/L^3), \quad (2.1)$$

where $\varepsilon_o$ is the zero-field mobility, $\varepsilon_r$ is the permittivity of the material, $\mu_h$ is the carrier mobility, $V$ is the effective voltage, and $L$ is the thickness of the active layer. The hole mobilities were determined to be $4.36 \times 10^{-6}$ for **PBDT-TPD** and $1.31 \times 10^{-5}$ $cm^2$ $V^{-1}$ $s^{-1}$ for **PBDT-PPD**. The hole-only current-voltage characteristics are shown in Figure 2.7.

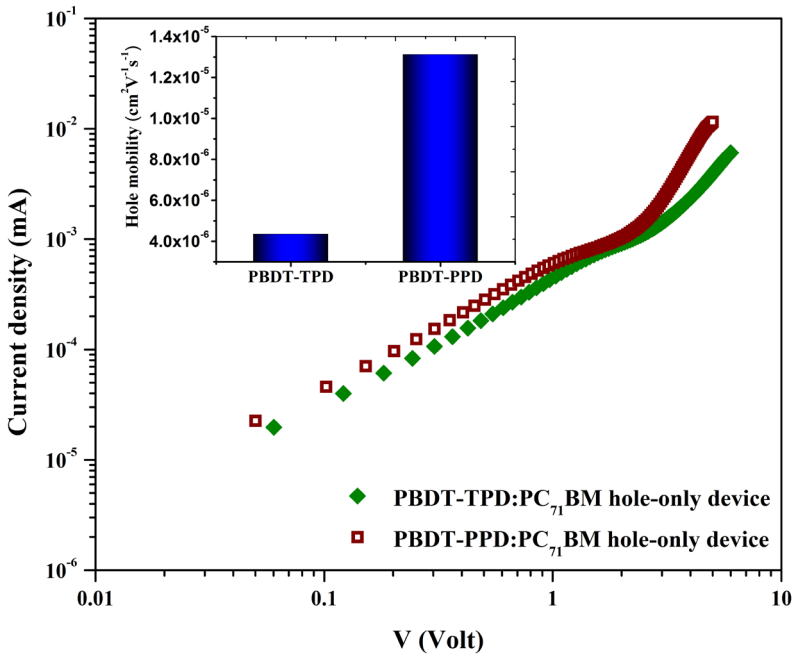


**Figure 2.7.** The current-voltage characteristics of PBDT-TPD:$PC_{71}BM$ and PBDT-PPD:$PC_{71}BM$ photovoltaic devices in dark under ambient conditions.

Since the **PBDT-PPD** blend has a higher mobility and more favorable morphology than the **PBDT-TPD** blend, one of the most likely causes for the low photocurrent of **PBDT-PPD** is the absorption profile of the material having poor overlap with the solar spectrum.[30] Additionally, the high LUMO of **PBDT-PPD** may have too high of an offset with that of $PC_{71}BM$, leading to recombination in the donor due to the poor rate of electron injection into the acceptor.[31]

## 2.4 Conclusions

A novel conjugated polymer, **PBDT-PPD** was synthesized and compared to the well-known sulfur analog **PBDT-TPD**. Both polymers were used in OPVs and it was found that **PBDT-PPD** performed worse than **PBDT-TPD**. Experimental and theoretical studies on the optoelectronic properties of these polymers demonstrated that **PBDT-PPD** had a lower electron affinity and wider optical bandgap than **PBDT-TPD**. Furthermore, the ICT was weaker in **PBDT-PPD** than in **PBDT-TPD**, and neither material was a particularly good donor polymer. Collectively, these results suggest that replacing sulfur with nitrogen in pyrrole dione monomers could be a good strategy for designing efficient OPV materials, however a different electron-donating group should be explored. Research is ongoing in our group to improve upon these results.

## 2.5 Experimental

### 2.5.1 Materials

Air- and moisture- sensitive reactions were performed using standard Schlenk techniques. Solvents used for palladium-catalyzed reactions were deoxygenated prior to use by sparging with argon for 30 minutes. The preparation of compounds **6** and **8** are described in the Supporting Information. (4,8-bis((2-ethylhexyl)oxy)benzo[1,2-*b*:4,5-*b'*]dithiophene-2,6-diyl)bis(trimethylstannane) (BDT)[35] was prepared according to literature procedures. Thiophene-3,4-dicarboxylic acid was purchased from Oakwood Chemicals and recrystallized from water before use. All other chemical reagents were purchased commercially and used without further purification unless otherwise noted.

### 2.5.2 Characterization

Nuclear magnetic resonance (NMR) spectra were collected on Varian VXR-300, Varian MR-400, or Bruker Advance III-600 spectrometers. $^{1}$H NMR spectra were internally referenced to the residual solvent peak. In all spectra, chemical shifts are given in ppm (δ) relative to the solvent. Gel permeation chromatography (GPC) measurements were performed on a Shimadzu Prominence GPC with two 10 μm AM Gel columns connected in series (guard, 10,000 Å, 1,000 Å) in chloroform at 40 °C relative to polystyrene standards. Thermogravimetric analysis (TGA) were performed over an interval of 30 – 850 °C at a heating rate of 20 °C min$^{-1}$ under ambient atmosphere. Differential scanning calorimetry (DSC) was performed using a first scan heating rate of 15 °C min$^{-1}$ to erase thermal history and a second scan to measure transitions between 0 and 330 °C under nitrogen. Cyclic voltammetry (CV) measurements were carried out

using an *e*-DAQ *e*-corder 410 potentiostat with a scanning rate of 100 mV $s^{-1}$. The polymer films were dropcast from 1 – 2 mg $mL^{-1}$ solutions in chlorobenzene onto a platinum working electrode. $Ag/Ag^{+}$ and Pt wire were used as the reference and auxiliary electrodes, respectively. The reported values were referenced to $Fc/Fc^{+}$ (-4.8 versus vacuum). All electrochemical experiments were performed in deoxygenated acetonitrile under an argon atmosphere using 0.1 M tetrabutylammonium hexafluorophosphate as electrolyte. Absorption spectra were obtained on a photodiode-array Agilent 8453 UV-visible spectrophotometer using polymer solutions in $CHCl_3$ and thin films. The films were cast by spin coating 25 x 25 x 1 mm glass slides using solutions of polymer (2.5 – 5.0 mg $mL^{-1}$) in $CHCl_3$/*o*-dichlorobenzene at a spin rate of 1200 rpm on a Headway Research, Inc. PWM32 spin-coater. A Veeco Digital Instruments atomic force microscope was used to capture the surface roughness and phase of PBDTTPD- and PBDTPPD-based thins films . The tapping-mode AFM was carried out using TESPA tip with scan rate of 0.6 μm $sec^{-1}$ and scan size of 5 μm x 5 μm

### 2.5.3 Computational modeling

To elucidate the difference in performance between **PBDT-TPD** and **PBDT-PPD** we performed theoretical calculations using density functional theory (DFT). The geometries of model oligomers (n = 1, 2, 3, and 4) for both copolymers were optimized at the B3LYP/6-31G* level in which the long side chains were truncated to methyl groups in order to save computational expense. The first ten excited states were determined through a time dependent density functional theory treatment using the same level of theory as the

optimization. The HOMO, LUMO, and optical band gaps were produced by fitting the set of oligomers with the Kuhn expression:[36-37]

$$E = E_0\sqrt{1 + 2\frac{k'}{k_0}\cos\frac{\pi}{N+1}} \quad (2)$$

where $E_0$ is the transition energy of a formal double bond, N is the number of double bonds in the oligomer (thought to be identical oscillators), and $k'/k_0$ is an adjustable parameter (indicative of the strength of coupling between the oscillators). In addition, the reorganization energy, which is a measure of charge mobility for both the hole ($\lambda_h$) and electron ($\lambda_e$), was calculated using:[38-41]

$$\lambda = (E_0^* - E_0) + (E_\pm^* - E_\pm) \quad (3)$$

where $E_0$ and $E_\pm$ are the energies of the neutral and charged optimized geometries and the $E_0^*$ and $E_{\pm 0}^*$ are the energies of neutral geometry with charge and the charged geometry set to neutral.

### 2.5.4 Fabrication of photovoltaic devices

All devices were produced via a solution-based, spin-casting fabrication process. All polymers were mixed with $PC_{70}BM$ (1-material) (mixed 1:1.5 with a total solution concentration of 25 mg $mL^{-1}$) dissolved in chlorobenzene (Sigma Aldrich) and stirred overnight at 115 °C at 800 rpm. ITO (sheet resistance: 5 – 15 Ω □$^{-1}$) coated glass slides (Delta Technologies) were cleaned by consecutive 10 minute sonication in (i) Alconox

detergent (dissolved in deionized water), (ii) deionized water, and then (iii) isopropanol. The slides were then dried with $N_2$ and cleaned with air plasma for 10 minutes. Filtered (0.45 μm) PEDOT:PSS (Clevios P$^{TM}$ 4083) was spin-coated onto the prepared substrates (5000 rpm/60 sec) and then annealed at 120 °C for 20 minutes. After cooling, the substrates were transferred to an argon-filled glovebox. The polymer:$PC_{70}BM$ solutions were filtered with 0.2 μm pore filter, and simultaneously dropped onto the PEDOT:PSS-coated substrates and spin-cast at 1400 rpm for 60 seconds. The films were dried under petri-dish for eight hours. For the active layers with solvent additives, 5% (v/v) of either CN or DIO was added to the stock solution, and then deposited at the aforementioned casting conditions. Finally, Ca (20 nm) and Al (100 nm) were thermally evaporated through a shadow mask (area = 0.1256 $cm^{-2}$) under vacuum of $10^{-6}$ mbar to complete the devices. Current-voltage (*J-V*) data were generated by illuminating the devices using an ELH Quartzline halogen lamp at 1 sun. The solar simulator was calibrated using a crystalline silicon photodiode with a KG-5 filter. The hole only devices were prepared following the same procedure, except calcium was replaced with molybdenum suboxide. The hole mobility was extracted from the SCLC measurement using a Keithley 2400 SourceMeter in the dark under ambient conditions.

### 2.5.4 Synthesis

**Synthesis of PBDT-TPD**

BDT (193.0 mg, 0.25 mmol) and compound **8** (105.7 mg, 0.25 mmol) were dissolved in toluene (9 mL) and sparged with argon for 30 min. Tris(dibenzylideneacetone)dipalladium(0) (4.9 mg, 2 mol%) and tri(*o*-tolyl)phosphine

(7.1 mg, 9 mol%) were added and the reaction refluxed for 48 h. The polymer was end-capped by refluxing with trimethyl(phenyl)tin (50 mg) for 4 h, followed by refluxing with iodobenzene (0.1 mL) overnight. After cooling to ambient temperature, the mixture was precipitated into methanol and filtered through a Soxhlet thimble. The polymer was washed with methanol (4 h), acetone (4 h), hexanes (12 h), and extracted with chloroform. The chloroform fraction was then concentrated and the polymer run through a short silica gel plug. The resulting fraction was then concentrated (~5 mL) and precipitated into methanol, filtered, and dried to give the expected polymer as a dark purple solid (145.6 mg, 82%). $M_n$: 24.9 kDa, PDI: 1.8; Not soluble enough in $CDCl_3$ for $^1H$ NMR.

**Synthesis ofPBDT-PPD**

Compound **6** (186.2 mg, 0.36 mmol) and BDT (278.0 mg, 0.36 mmol) were dissolved in toluene (10 mL) and sparged with argon for 30 min. Tris(dibenzylideneacetone)dipalladium(0) (6.6 mg, 2 mol%) and tri(*o*-tolyl)phosphine (9.8 mg, 9 mol%) were added and the reaction refluxed for 48 h. The polymer was end-capped by refluxing with trimethyl(phenyl)tin (50 mg) for 4 h, followed by refluxing with iodobenzene (0.1 mL) overnight. After cooling to ambient temperature, the mixture was precipitated into methanol and filtered through a Soxhlet thimble. The polymer was washed with methanol (4 h), acetone (4 h), hexanes (12 h), and extracted with chloroform. The chloroform fraction was then concentrated and the polymer run through a short silica gel plug. The resulting fraction was then concentrated (~5 mL) and precipitated into methanol, filtered, and dried in vacuo to give the expected polymer as a

dark orange solid (210.8 mg, 73%). $M_n$: 20.1 kDa, PDI: 1.8; $^1$H NMR (600 MHz, $CDCl_3$) δ 8.34 (s, 2H), 4.63 (s, 2H), 4.40 (s, 4H), 3.64 (s, 2H), 2.05 – 0.68 (m, 60H).

## 2.6 Acknowledgements

This work was supported by the 3M Foundation and Iowa State University (ISU) and partially supported by DMR-1410088. We wish to thank Steve Veysey and the ISU Chemical Instrumentation Facility for training and assistance with the thermal analysis. We also thank Dr. Kamel Harrata and the ISU Mass Spectroscopy Laboratory for analysis. The OPVs were fabricated at the ISU Microelectronics Research Center.

## 2.7 Supporting Information

### 2.7.1 Synthesis

**Diethyl 1*H*-pyrrole-3,4-dicarboxylate (1)** A suspension of potassium *tert*-butoxide (11.5 g, 102 mmol) in THF (100 mL) was stirred under argon in a flame dried two neck 500 mL round bottom flask. A solution of diethyl fumarate (8.8 g, 51.5 mmol) and *p*-toluenesulfonylmethyl isocyanide (10.0 g, 51.6 mmol) in THF (50 mL) was slowly added to the suspension and allowed to stir overnight. The reaction was then quenched with a saturated sodium chloride solution, extracted with THF (3 x 200 mL), and dried with anhydrous sodium sulfate. The solvent was removed under reduced pressure and the resulting solid dissolved methanol (50 mL). The solution was then precipitated in water, filtered, and dried to give the expected product as an off-white solid (7.2 g, 67%).

$^{1}$HNMR (600 MHz, DMSO-$d_6$) δ: 7.36 (s, 2H), 4.15 (q, $J$ = 7.0 Hz, 4H), 1.23 (t, $J$ = 7.1 Hz, 6H).; $^{13}$CNMR (150 MHz, DMSO-$d_6$) δ: 163.41, 125.26, 115.03, 59.39, 14.20.

**1*H*-pyrrole-3,4-dicarboxylic acid (2)** Compound **1** (5.30 g, 25 mmol) was added to a solution of NaOH (8.2 g, 205 mmol) in 50% (v/v) aqueous ethanol (50 mL). The reaction was refluxed overnight and diluted with water (50 mL) while still hot. The reaction was acidified with 1M HCl and a white precipitate formed. The precipitate was filtered, washed with water, and dried to give the expected product as a white solid (3.48 g, 89%). $^{1}$HNMR (400 MHz, DMSO-$d_6$) δ: 14.05 (s, 2H), 12.17 (s, 1H), 7.61 (d, $J$ = 2.9 Hz, 2H); $^{13}$CNMR (100 MHz, DMSO-$d_6$) δ: 167.0, 128.9, 109.9

**4-(octylcarbamoyl)-1*H*-pyrrole-3-carboxylic acid (3)** A solution of *N,N'*-dicyclohexylcarbodiimide (3.99 g, 19.4 mmol) in THF (120 mL) was added to a suspension of **2** (2.50 g, 16 mmol) in THF (80 mL) in one portion. The reaction mixture was allowed to reflux for 2 h before cooling to room temperature after which a precipitate formed. The precipitate was filtered off and washed with THF before the filtrate was concentrated (~20 mL). Octylamine (2.31 g, 17.8 mmol) was added slowly and the reaction stirred at room temperature overnight. The solvent was removed and the remaining oil triturated with 1 M HCl, resulting in a thick paste. A solution of 3 M NaOH was added to dissolve the acid and sonicated for 30 min. The excess urea was filtered off and the filtrate neutralized with 1 M HCl forming a white precipitate. The precipitate was filtered and dried to give the expected product as a white solid (3.77 g, 88%) which was used without further purification. $^{1}$H NMR (400 MHz, DMSO-$d_6$) δ 11.88 (s, 1H), 9.03

(s, 1H), 7.66 (s, 1H), 7.50 (s, 1H), 3.24 (q, *J* = 6.9 Hz, 2H), 1.51 (dp, *J* = 4161.9, 7.0 Hz, 2H), 1.33 – 1.19 (m, 10H), 0.85 (t, *J* = 7.2, 6.5 Hz, 3H).

**2-octylpyrrolo[3,4-*c*]pyrrole-1,3(2*H*,5*H*)-dione (4)** Compound **3** (0.36 g, 1.4 mmol) was dissolved in dry DMF (10 mL) and cooled with an ice bath. Thionyl chloride (0.51 g, 4.3 mmol) was added slowly over 10 min. The reaction was allowed to stir at room temperature for 2 h before quenching with water/ice. Saturated NaCl solution was added before extraction with THF (3 x 100 mL). The organic layers were combined, dried with $Na_2SO_4$, and concentrated. The crude material was then purified by silica gel chromatography using 7:3 hexane/THF as eluent to give the expected product as a tacky off-white low melting solid (0.33 g, 97%). $^1$HNMR (400 MHz, $CDCl_3$) δ: 9.49 (s, 1H), 7.08 (d, *J* = 2.5 Hz, 2H), 3.54 (t, *J* = 7.5 Hz, 2H), 1.61 (p, *J* = 7.3 Hz, 2H), 1.36 – 1.15 (m, 10H), 0.86 (t, *J* = 7.1 Hz, 3H); $^{13}$CNMR (100 MHz, $CDCl_3$) δ: 164.99, 121.59, 115.96, 38.18, 31.92, 29.37, 29.33, 28.92, 27.05, 22.77, 14.21.

**4,6-dibromo-2-octylpyrrolo[3,4-*c*]pyrrole-1,3(2*H*,5*H*)-dione (5)** A solution of **4** (1.42 g, 5.7 mmol) in THF (20 mL) was cooled to -78 °C and protected from light. NBS (2.27 g, 12.7 mmol) was added in one portion. The reaction mixture stirred at -78 °C for 30 min followed by stirring at 0 °C for 3.5 h. The reaction was quenched by the addition of $Na_2SO_3{\cdot}5H_2O$ and allowed to stir for 15 min before being decanted. The solvent was removed followed by addition of $CCl_4$ (20 mL) and further stirring. After 15 min, the resulting precipitate was filtered and the filtrate concentrated. The crude material was then purified on a silica gel column using 1:1 hexane/ether as eluent to give the expected

product as an off-white tacky solid (1.84 g, 79%). $^{1}$HNMR (600 MHz, $CDCl_3$) δ: 10.37 (s, 1H), 3.57 (t, $J$ = 7.3 Hz, 2H), 1.61 (p, $J$ = 7.6, 7.2, 6.8 Hz, 2H), 1.26 (br, 10H), 0.85 (t, $J$ = 6.9 Hz, 3H); $^{13}$CNMR (150 MHz, $CDCl_3$) δ: 162.62, 121.66, 98.58, 38.57, 31.91, 29.31, 29.29, 28.72, 26.98, 22.76, 14.21.

**4,6-dibromo-2,5-dioctylpyrrolo[3,4-*c*]pyrrole-1,3(2*H*,5*H*)-dione (7)** Anhydrous $K_2CO_3$ (0.60 g, 4.4 mmol) and 18-crown-6 (14 mg) were added to a solution of compound **5** (0.80 g, 2.0 mmol) dissolved in dry DMF (15 mL) and the reaction stirred at 100 °C for 1 h. The drop wise addition of 1-bromooctane (0.58 g, 3.0 mmol) was followed by stirring at 120 °C for 36 h. The mixture was quenched with a brine solution and extracted with THF (3 x 50 mL). The organic layers were combined, dried with $Na_2SO_4$, and concentrated. The crude product was purified on a silica gel column using 19:1 hexane:THF as eluent to give the expected product as a light orange solid (0.49 g, 48%). mp 124-125.5 °C. $^{1}$HNMR (400 MHz, $CDCl_3$) δ: 4.03 (t, $J$ = 7.8 Hz, 2H), 3.53 (t, $J$ = 7.3 Hz, 2H), 1.72 (p, $J$ = 7.2 Hz, 2H), 1.59 (p, $J$ = 7.8 Hz, 2H), 1.40 – 1.19 (m, 20H), 0.87 (q, $J$ = 7.1, 6.7 Hz, 6H); $^{13}$CNMR (100 MHz, $CDCl_3$) δ: 162.49, 121.59, 100.81, 47.62, 38.28, 31.95, 31.85, 30.47, 29.99, 29.35, 29.30, 29.21, 29.18, 28.75, 26.97, 26.56, 22.78, 22.75, 14.24, 14.22. HRMS (ESI) *m/z*: $[M + Na]^+$ calcd for $C_{22}H_{34}Br_2NaN_2O_2$, 539.0879; found, 539.0868; deviation, 2.18 ppm.

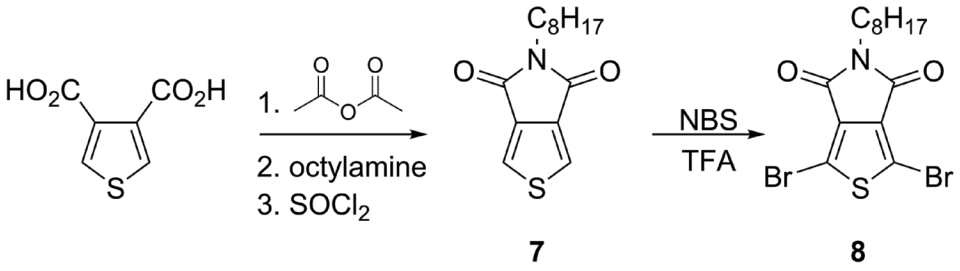


**5-octyl-4*H*-thieno[3,4-*c*]pyrrole-4,6(5*H*)-dione (7)** A suspension of thiophene-3,4-dicarboxylic acid (1.01 g, 5.9 mmol) in acetic anhydride (20 mL) was heated at 140 °C overnight. Upon cooling to ambient temperature, the solvent was removed under high vacuum. The resulting crude solid was dissolved in toluene (15 mL) and *n*-octylamine (1.01 g, 7.8 mmol) was added dropwise. The reaction mixture was refluxed overnight. The solvent was then removed under reduced pressure, and the resulting solid dissolved in thionyl chloride (20 mL) before being refluxed for 4h. After cooling, the solvent was removed and the solid taken up in chloroform before being washed with excess water. The organic layer was dried with anhydrous sodium sulfate and removed under reduced pressure. Purification by silica gel column chromatography using 1:1 hexanes/chloroform as eluent gave the expected product as an off-white solid (1.32 g, 85%). $^1$H NMR (600 MHz, $CDCl_3$) δ 7.80 (s, 2H), 3.61 (t, $J$ = 7.3 Hz, 2H), 1.64 (p, $J$ = 7.9, 7.4, 7.0 Hz, 2H), 1.37 – 1.22 (m, 10H), 0.87 (t, $J$ = 7.1 Hz, 3H).

**1,3-dibromo-5-octyl-4*H*-thieno[3,4-*c*]pyrrole-4,6(5*H*)-dione (8)** Compound **7** (1.42 g, 5.4 mmol) was dissolved in 20 mL trifluoroacetic acid/sulfuric acid (10:3) and protected from light. NBS (3.81 g, 21.6 mmol) was added in three portions and the reaction stirred overnight at ambient temperature. The reaction was extracted with chloroform and washed with dilute aqueous KOH, water, and dried over anhydrous sodium sulfate. After

removal of the solvent, purification by silica gel column chromatography using 1:1 hexanes/chloroform as eluent gave the expected product as an off-white solid (1.19 g, 53%). $^{1}$H NMR (400 MHz, $CDCl_3$) δ 3.59 (t, $J$ = 7.2 Hz, 2H), 1.63 (p, $J$ = 7.4 Hz, 2H), 1.38 – 1.20 (m, 2H), 0.87 (t, $J$ = 7.0 Hz, 2H).

### 2.7.2 NMR Spectra and analytical data

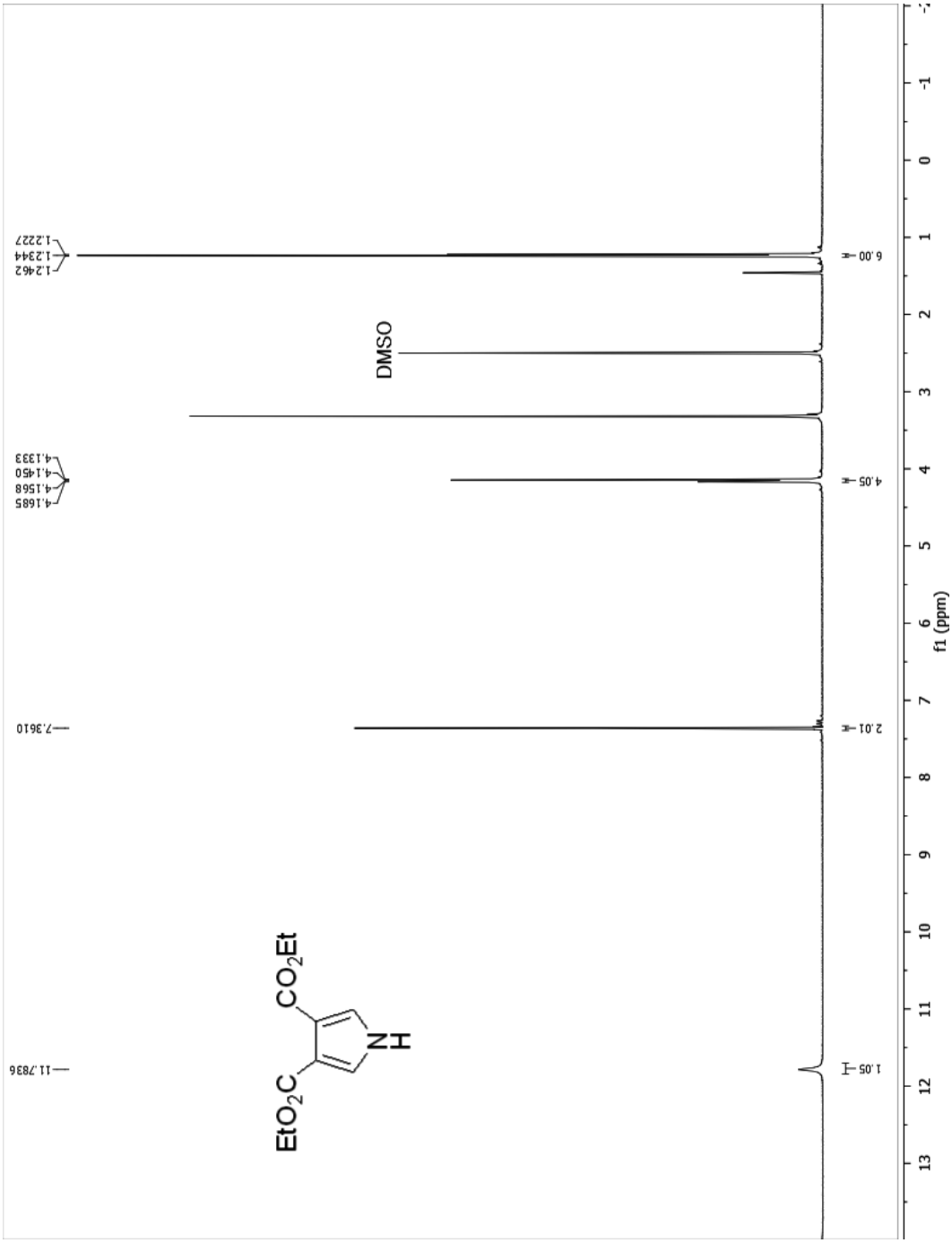


**Figure S2.1.** $^{1}$H NMR of **1**.

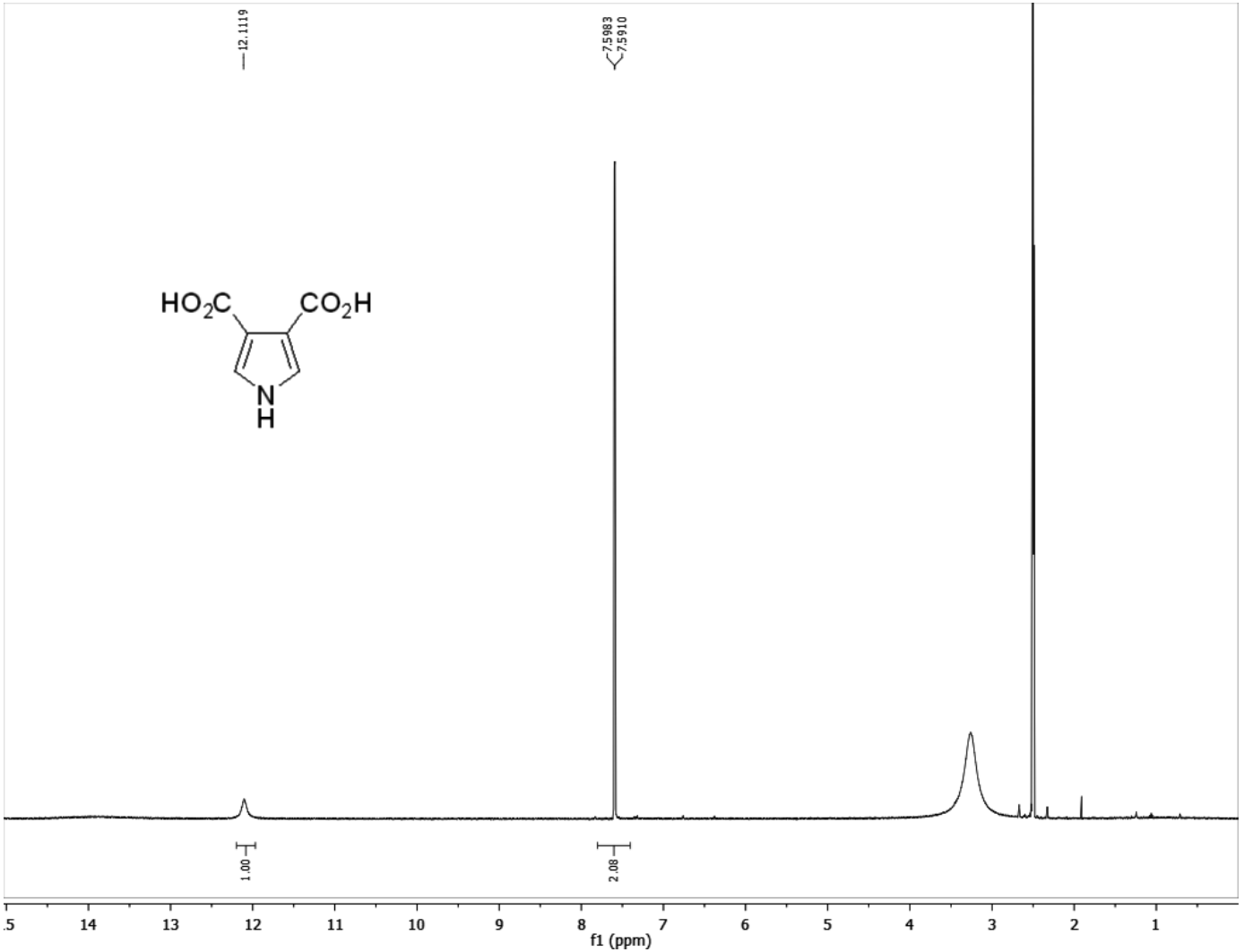


**Figure S2.2.** $^{1}$H NMR of **2**.

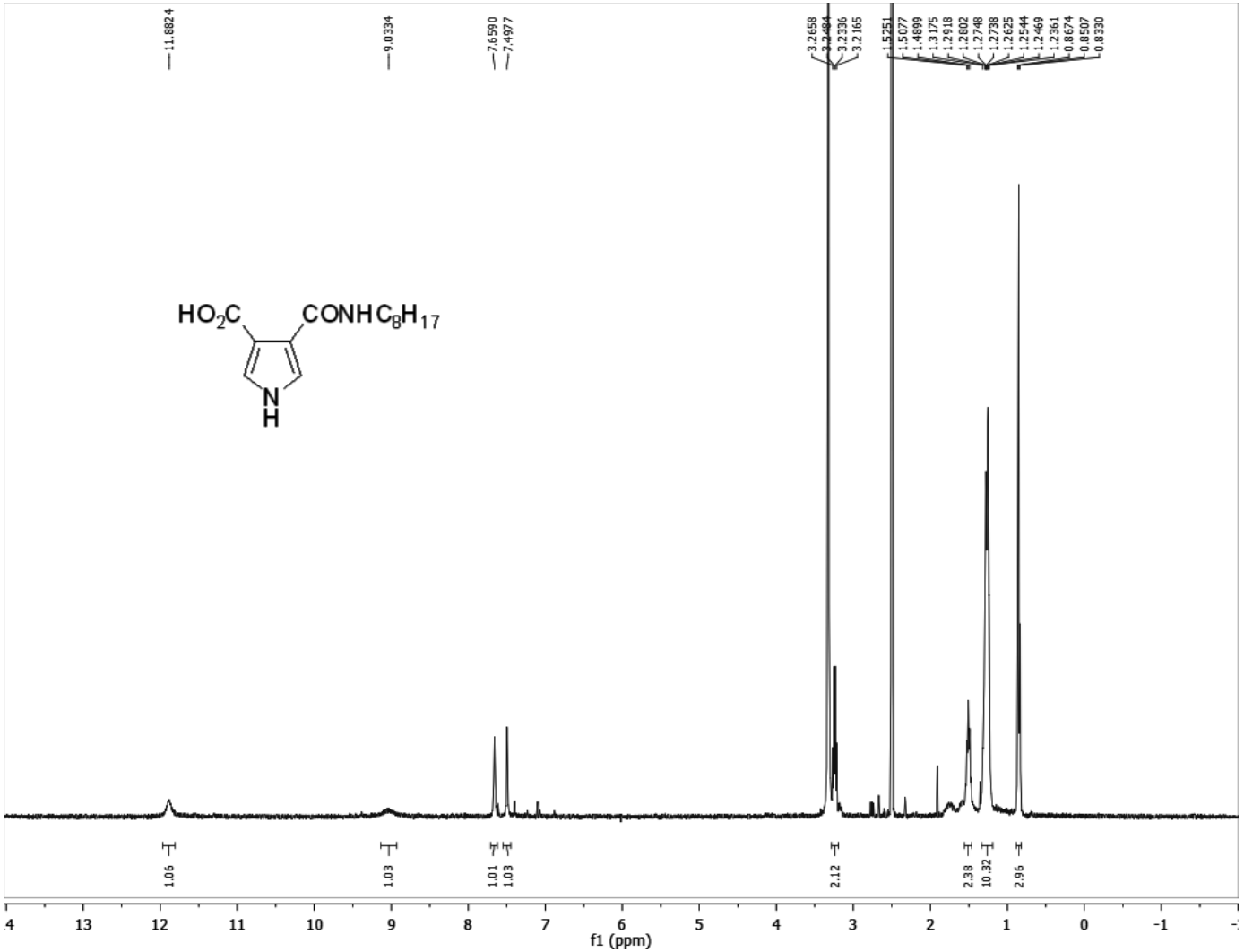


**Figure S2.3.** $^{1}$H NMR of **3**.

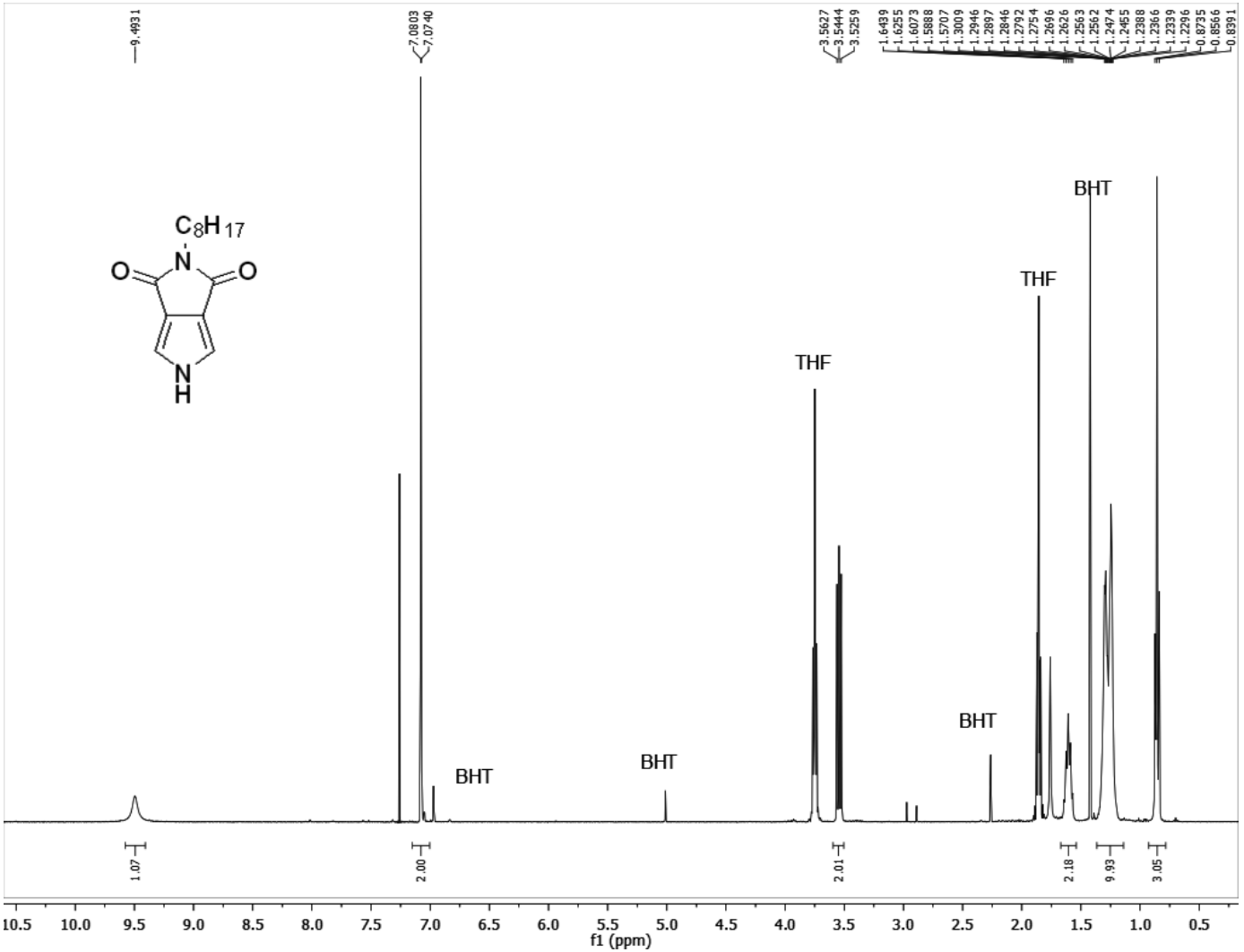


**Figure S2.4.** $^{1}$H NMR of **4**.

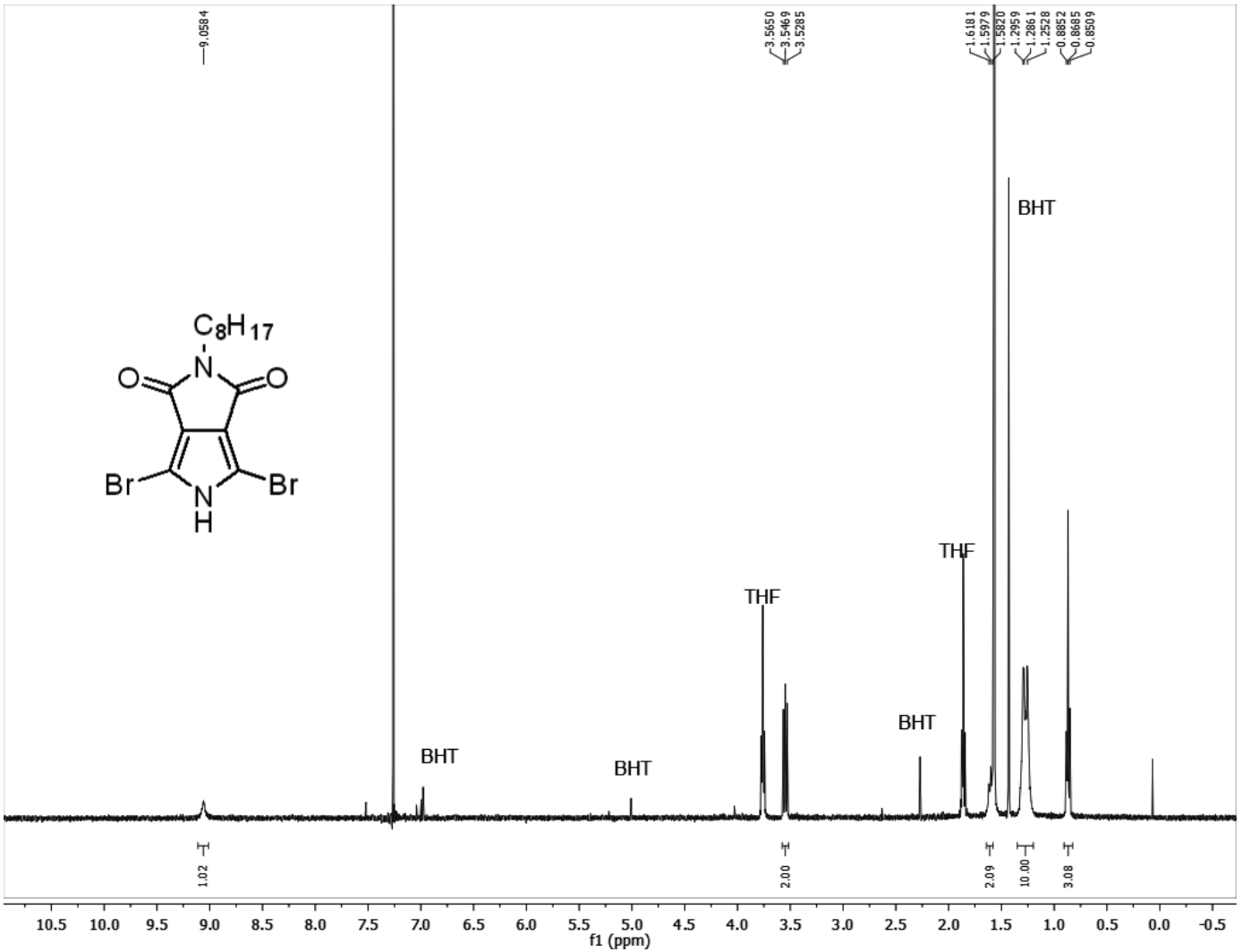


**Figure S2.5.** $^{1}$H NMR of **5**.

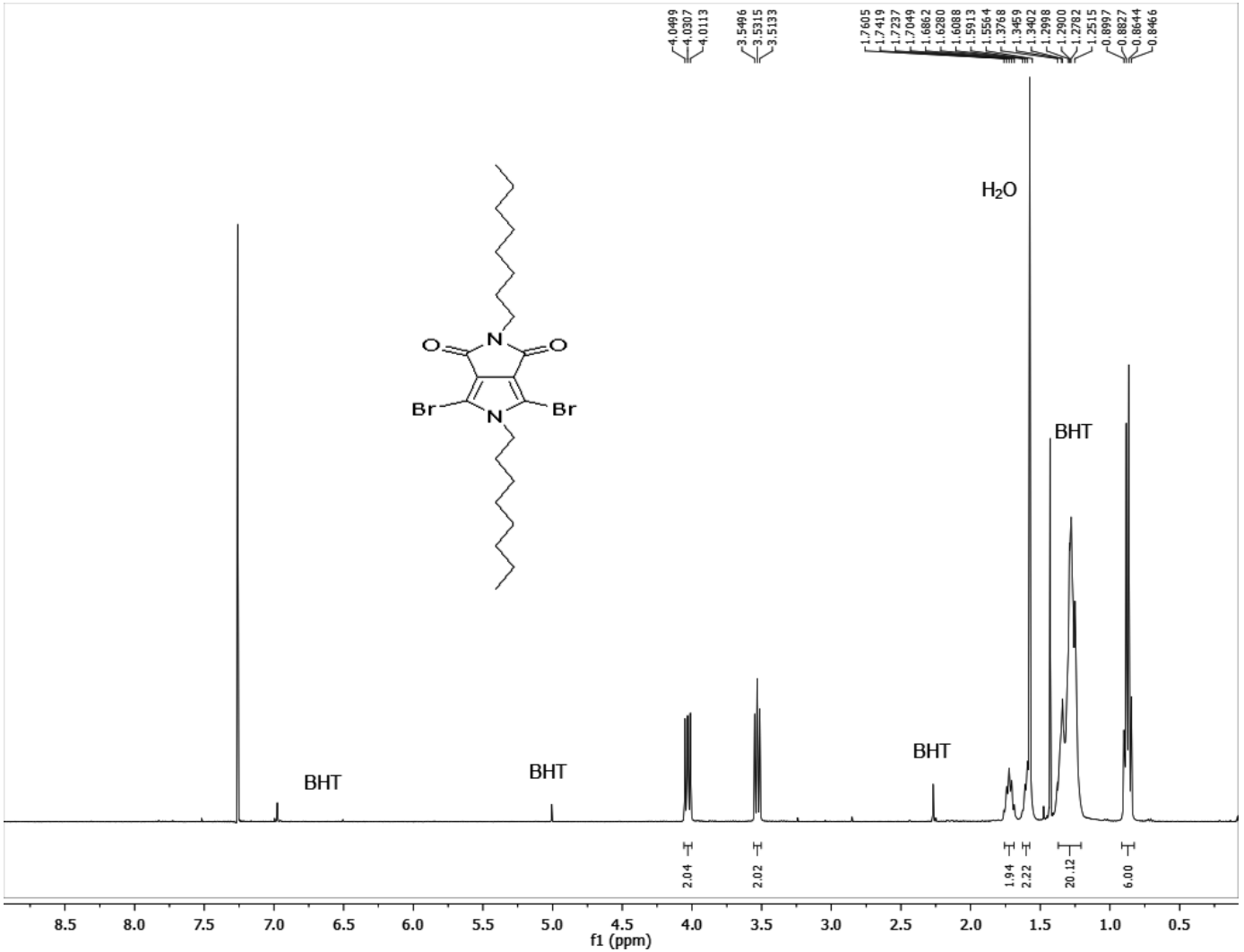


**Figure S2.6.** $^{1}$H NMR of **6**.

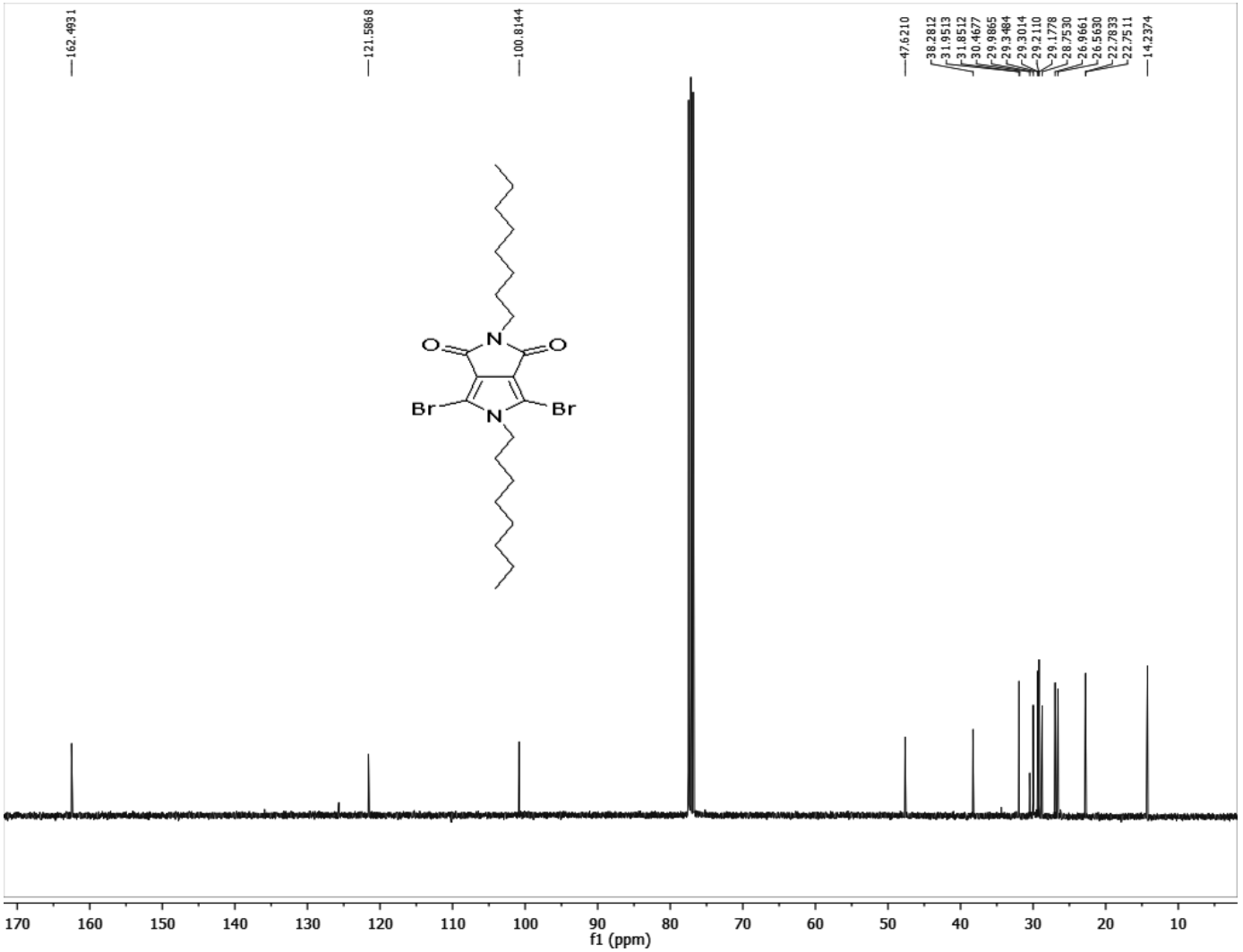


**Figure S2.7.** $^{13}$C NMR of **6**.

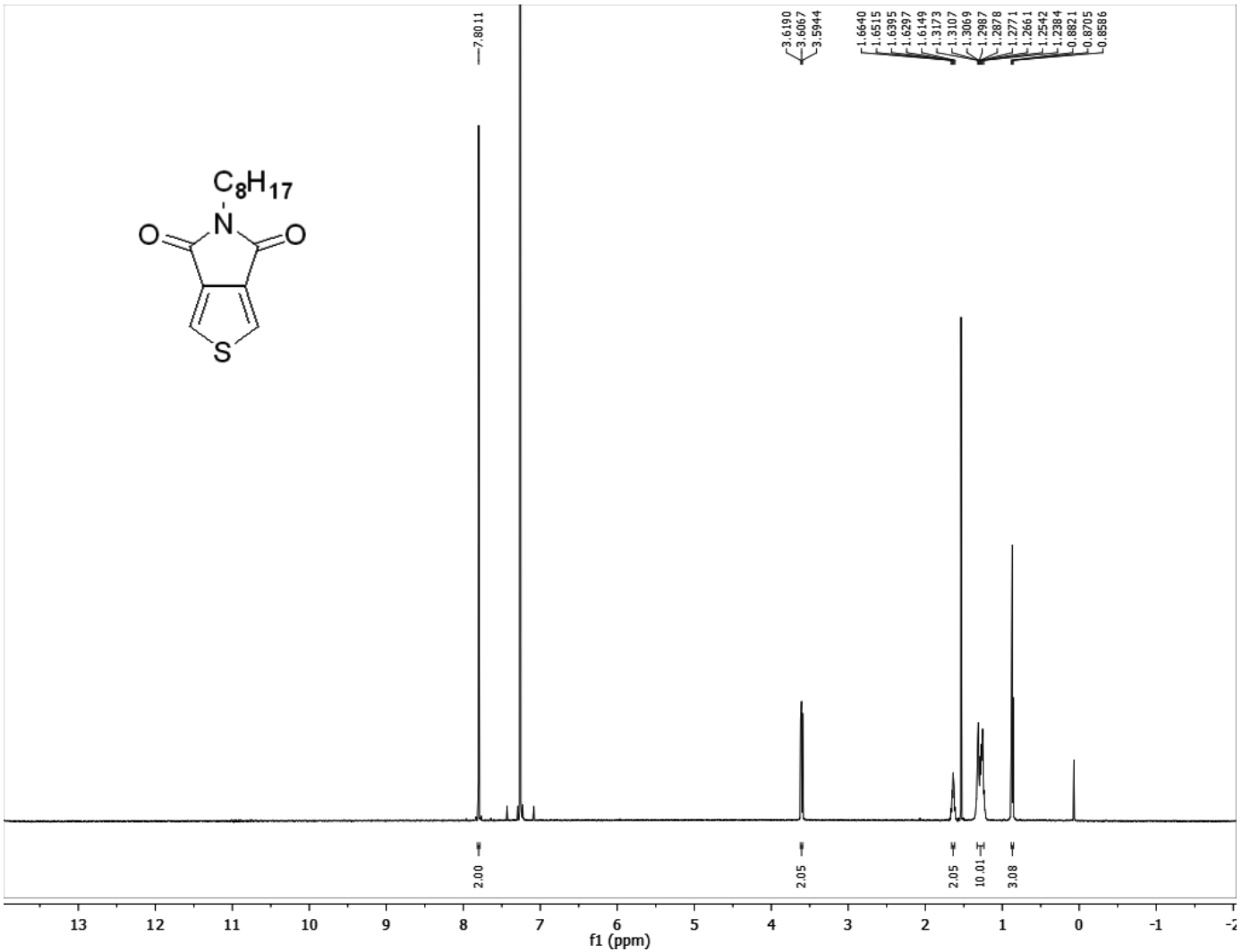


**Figure S2.8.** $^{1}$H NMR of **7**.

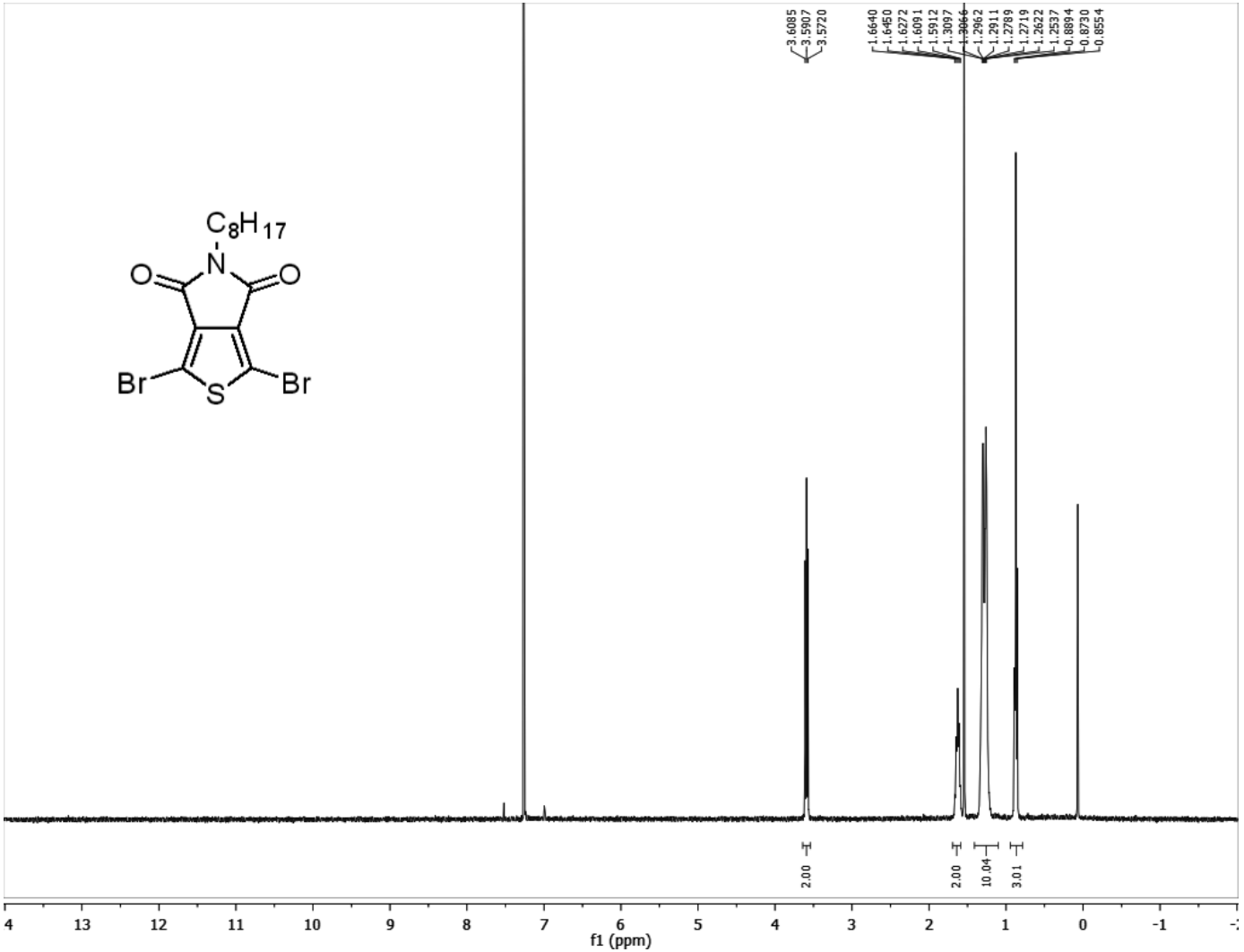


**Figure S2.9.** $^{1}$H NMR of **8**.

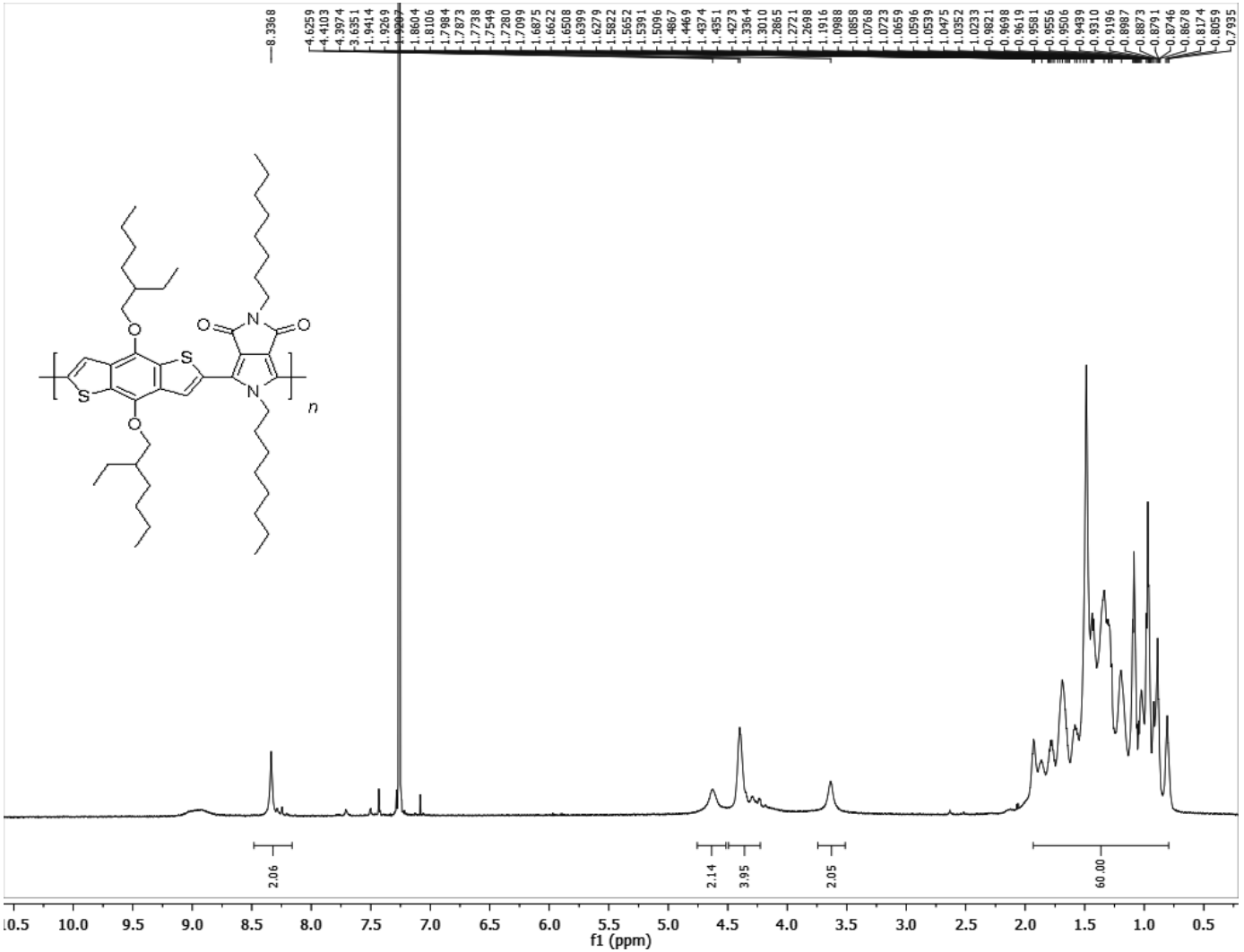


**Figure S2.10.** $^{1}$H NMR of **PBDT-PPD**.

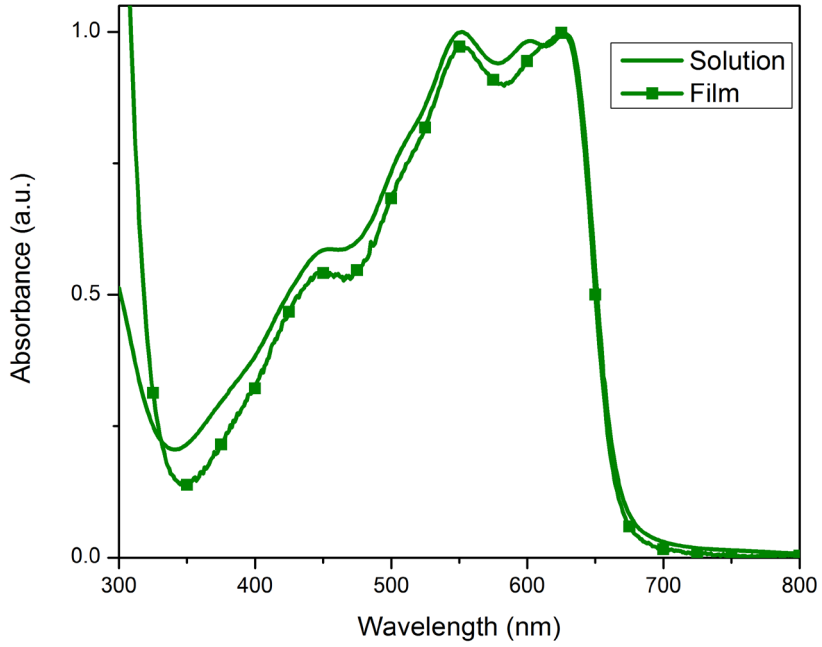


**Figure S2.11.** UV-vis absorption of **PBDT-TPD** in solution and film.

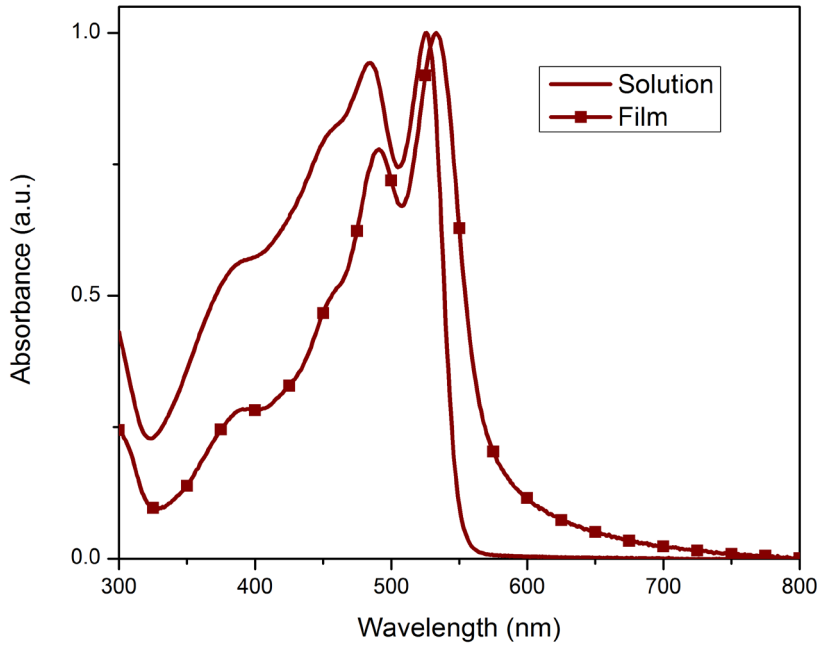


**Figure S2.12.** UV-vis absorption of **PBDT-PPD** in solution and film.

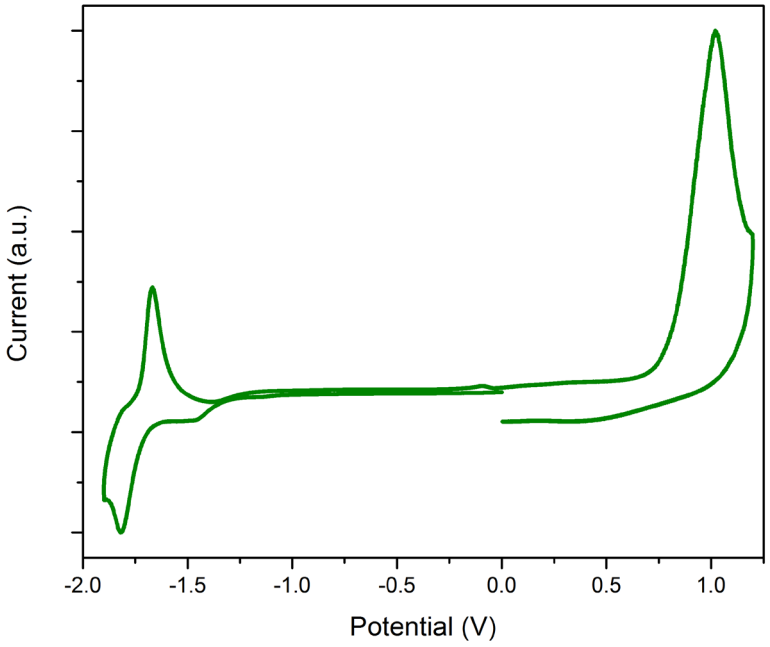


**Figure S2.13.** Cyclic voltammetry trace of **PBDT-TPD**.

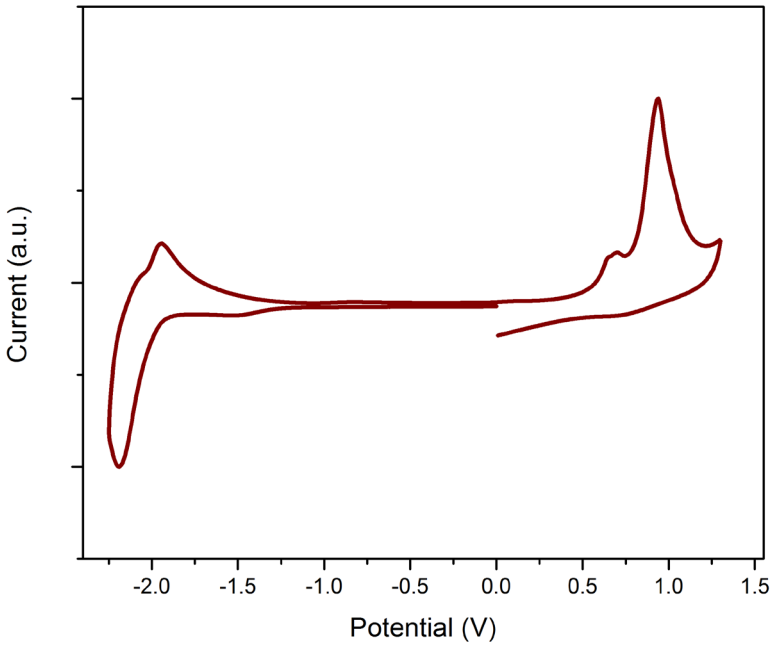


**Figure S2.14.** Cyclic voltammetry trace of **PBDT-PPD**.

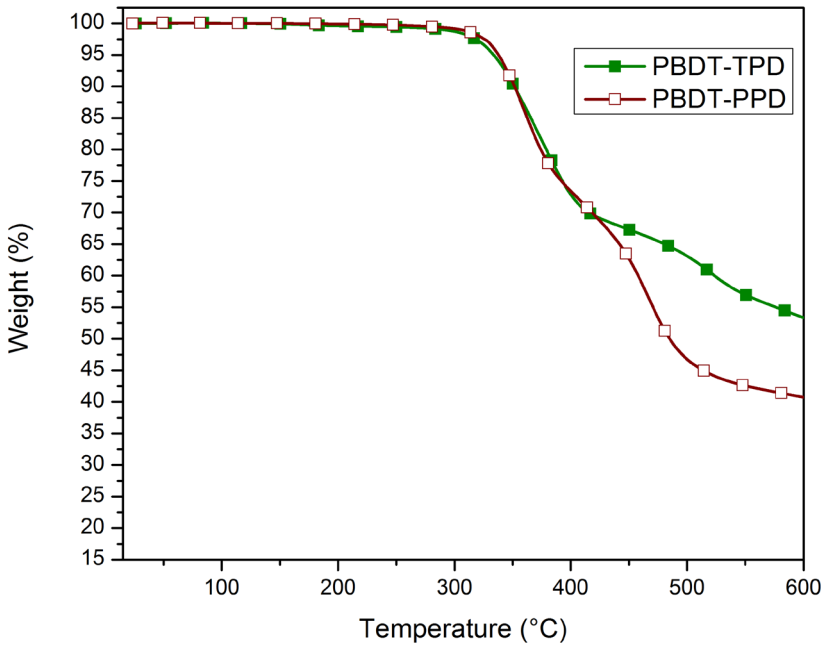


**Figure S2.15.** Thermal gravometric analysis of **PBDT-TPD** and **PBDT-PPD** under air.

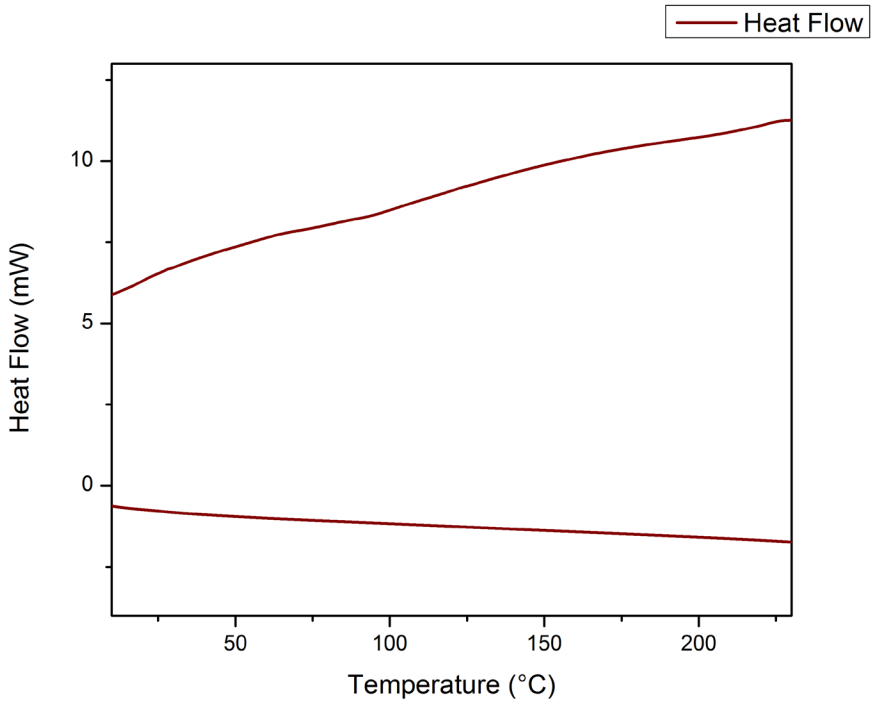


**Figure S2.16.** Differential scanning calorimetry of **PBDT-PPD** under nitrogen.

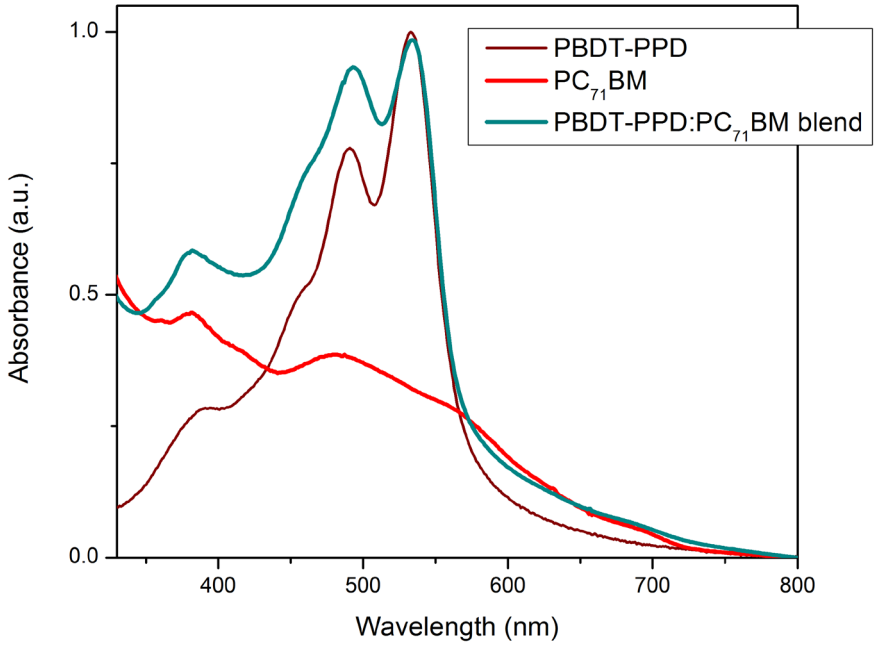


**Figure S2.17.** Absorption of **PBDT-PPD**, $PC_{71}BM$, and **PBDT-PPD**:$PC_{71}BM$ blend.

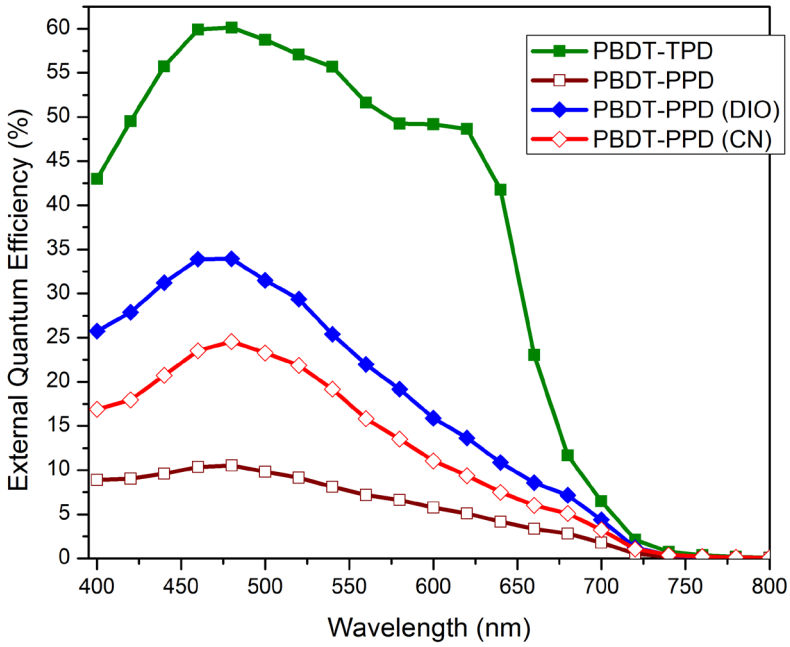


**Figure S2.18.** External quantum efficiencies of **PBDT-TPD** and **PBDT-PPD** devices.

## 2.8 References


1. Shirakawa, H.; Louis, E. J.; Macdiarmid, A. G.; Chiang, C. K.; Heeger, A. J., *J Chem Soc Chem Comm* **1977**, DOI 10.1039/c39770000578 (16), 578-580.

2. Chiang, C. K.; Fincher, C. R.; Park, Y. W.; Heeger, A. J.; Shirakawa, H.; Louis, E. J.; Gau, S. C.; MacDiarmid, A. G., *Phys. Rev. Lett.* **1977,** *39* (17), 1098-1101.

3. Darling, S. B.; You, F., *RSC Advances* **2013,** *3* (39), 17633-17648.

4. Facchetti, A., *Chem. Mater.* **2010,** *23* (3), 733-758.

5. Thompson, B. C.; Fréchet, J. M. J., *Angew. Chem. Int. Ed.* **2008,** *47* (1), 58-77.

6. Yu, G.; Gao, J.; Hummelen, J. C.; Wudl, F.; Heeger, A. J., *Science* **1995,** *270* (5243), 1789-1791.

7. Nelson, J., *Mater. Today* **2011,** *14* (10), 462-470.

8. Cheng, Y.-J.; Yang, S.-H.; Hsu, C.-S., *Chem. Rev.* **2009,** *109* (11), 5868-5923.

9. Günes, S.; Neugebauer, H.; Sariciftci, N. S., *Chem. Rev.* **2007,** *107* (4), 1324-1338.

10. Liu, Y.; Zhao, J.; Li, Z.; Mu, C.; Ma, W.; Hu, H.; Jiang, K.; Lin, H.; Ade, H.; Yan, H., *Nat Commun* **2014,** *5*.

11. Liu, C.; Yi, C.; Wang, K.; Yang, Y.; Bhatta, R. S.; Tsige, M.; Xiao, S.; Gong, X., *ACS Applied Materials & Interfaces* **2015,** *7* (8), 4928-4935.

12. Yamamoto, T.; Zhou, Z.-h.; Kanbara, T.; Shimura, M.; Kizu, K.; Maruyama, T.; Nakamura, Y.; Fukuda, T.; Lee, B.-L.; Ooba, N.; Tomaru, S.; Kurihara, T.; Kaino, T.; Kubota, K.; Sasaki, S., *J. Am. Chem. Soc.* **1996,** *118* (43), 10389-10399.

13. Beaujuge, P. M.; Fréchet, J. M. J., *J. Am. Chem. Soc.* **2011,** *133* (50), 20009-20029.

14. Li, Y., *Acc. Chem. Res.* **2012,** *45* (5), 723-733.

15. Carsten, B.; He, F.; Son, H. J.; Xu, T.; Yu, L., *Chem. Rev.* **2011,** *111* (3), 1493-1528.

16. Jeffries-El, M.; Kobilka, B. M.; Hale, B. J., *Macromolecules* **2014,** *47* (21), 7253-7271.

17. Intemann, J. J.; Yao, K.; Yip, H.-L.; Xu, Y.-X.; Li, Y.-X.; Liang, P.-W.; Ding, F.-Z.; Li, X.; Jen, A. K. Y., *Chem. Mater.* **2013,** *25* (15), 3188-3195.

18. Kobilka, B. M.; Hale, B. J.; Ewan, M. D.; Dubrovskiy, A. V.; Nelson, T. L.; Duzhko, V.; Jeffries-El, M., *Polymer Chemistry* **2013,** *4* (20), 5329.

19. Woo, C. H.; Beaujuge, P. M.; Holcombe, T. W.; Lee, O. P.; Fréchet, J. M. J., *J. Am. Chem. Soc.* **2010,** *132* (44), 15547-15549.

20. Hollinger, J.; Gao, D.; Seferos, D. S., *Isr. J. Chem.* **2014,** *54* (5-6), 440-453.

21. Ohshita, J., *Macromol. Chem. Phys.* **2009,** *210* (17), 1360-1370.

22. Zou, Y.; Najari, A.; Berrouard, P.; Beaupré, S.; Réda Aïch, B.; Tao, Y.; Leclerc, M., *J. Am. Chem. Soc.* **2010,** *132* (15), 5330-5331.

23. Chu, T. Y.; Lu, J.; Beaupre, S.; Zhang, Y.; Pouliot, J. R.; Wakim, S.; Zhou, J.; Leclerc, M.; Li, Z.; Ding, J.; Tao, Y., *J. Am. Chem. Soc.* **2011,** *133* (12), 4250-4253.

24. Amb, C. M.; Chen, S.; Graham, K. R.; Subbiah, J.; Small, C. E.; So, F.; Reynolds, J. R., *J. Am. Chem. Soc.* **2011,** *133* (26), 10062-10065.

25. Beaupré, S.; Pron, A.; Drouin, S. H.; Najari, A.; Mercier, L. G.; Robitaille, A.; Leclerc, M., *Macromolecules* **2012,** *45* (17), 6906-6914.

26. Ikai, T.; Azam, A. K. M. F.; Kuzuba, M.; Kuwabara, T.; Maeda, K.; Takahashi, K.; Kanoh, S., *Synth. Met.* **2012,** *162* (17–18), 1707-1712.

27. Pollack, S. K.; Hijji, Y. M.; Kgobane, B., *Macromolecules* **1997,** *30* (21), 6709-6711.

28. Tamilavan, V.; Song, M.; Agneeswari, R.; Kang, J.-W.; Hwang, D.-H.; Hyun, M. H., *Polymer* **2013,** *54* (22), 6125-6132.

29. Li, Y.; Xu, B.; Li, H.; Cheng, W.; Xue, L.; Chen, F.; Lu, H.; Tian, W., *The Journal of Physical Chemistry C* **2011,** *115* (5), 2386-2397.

30. Ostroverkhova, O.; Shcherbyna, S.; Cooke, D. G.; Egerton, R. F.; Hegmann, F. A.; Tykwinski, R. R.; Parkin, S. R.; Anthony, J. E., *J. Appl. Phys.* **2005,** *98* (3), 033701.

31. Zhu, Y.; Champion, R. D.; Jenekhe, S. A., *Macromolecules* **2006,** *39* (25), 8712-8719.

32. Beaujuge, P. M.; Amb, C. M.; Reynolds, J. R., *Acc. Chem. Res.* **2010,** *43* (11), 1396-1407.

33. Duan, C.; Huang, F.; Cao, Y., *J. Mater. Chem.* **2012,** *22* (21), 10416-10434.

34. Cardona, C. M.; Li, W.; Kaifer, A. E.; Stockdale, D.; Bazan, G. C., *Adv. Mater.* **2011,** *23* (20), 2367-71.

35. Liang, Y.; Feng, D.; Wu, Y.; Tsai, S.-T.; Li, G.; Ray, C.; Yu, L., *J. Am. Chem. Soc.* **2009,** *131* (22), 7792-7799.

36. Milián-Medina, B.; Gierschner, J., *Wiley Interdisciplinary Reviews: Computational Molecular Science* **2012,** *2* (4), 513-524.

37. Mike, J. F.; Nalwa, K.; Makowski, A. J.; Putnam, D.; Tomlinson, A. L.; Chaudhary, S.; Jeffries-El, M., *PCCP* **2011,** *13* (4), 1338-1344.

38. Tai, C.-K.; Hsieh, C.-A.; Hsiao, K.-L.; Wang, B.-C.; Wei, Y., *Org. Electron.* **2015,** *16*, 54-70.

39. Malagoli, M.; Brédas, J. L., *Chem. Phys. Lett.* **2000,** *327* (1-2), 13-17.

40. Chi, W. J.; Li, Z. S., *Phys. Chem. Chem. Phys.* **2015,** *17* (8), 5991-8.

41. Sun, C.; Qi, D.; Li, Y.; Yang, L., *RSC Adv.* **2015,** *5* (24), 18492-18500.

# CHAPTER 3

## INFLUENCE OF D1 AND D2 ON THE PHOTOVOLTAIC PROPERTIES OF FLUOROBENZOTHIADIAZOLE BASED D1-A-D2-A-D2 SMALL MOLECULES.

*Benjamin J. Hale,[a] Ryan Gebhardt,[b] Balaji Ganapathy,[c] Sumit Chaudhary,[d]*

*Malika Jeffries-EL**[a]*

[a] Department of Chemistry, Iowa State University, Ames, IA 50011

[b] Department of Materials Science & Engineering,

Iowa State University, Ames, IA 50011

[c] Microelectronics Research Center, Iowa State University, Ames, IA 50011

[d] Department of Electrical and Computer Engineering,

Iowa State University, Ames, IA 50011

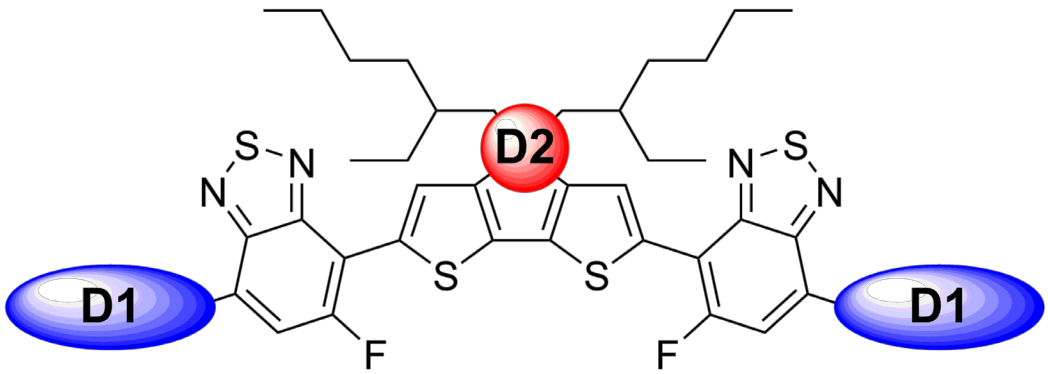

## 3.1 Abstract

A series of four D1-A-D2-A-D1 molecular donors are reported, where D1 is bithiophene or thieno[3,2-*b*]thiophene, A is fluorobenzothiadiazole, and D2 is a 3,3'- bridged bithiophene. The resulting materials have broad absorption with a maximum near 700 nm in thin films. The incorporation of thieno[3,2-*b*]thiophene resulted in a widening of the optical bandgap, relative to the bithiophene; while the use of carbon as the bridging atom resulted in a narrowing of the optical bandgap, relative to the silicon bridged bithiophene. Their initial use in organic solar cells gave mixed results due to poor film formation. The poor films, visible to the naked eye, resulted in low current density, and therefore low power conversion efficiency. Fabrication conditions, focusing on casting spin rate, are currently being optimized. After optimization, a direct relationship between structure, morphology, and efficiency will be established.

## 3.2 Introduction

Since their introduction 20 years ago, organic photovoltaics (OPVs) have gained traction as promising potential alternatives to silicon based photovoltaics, due to being solution-proccesable, low-cost, lightweight, and flexible.[1] In recent years, OPVs based on polymeric and molecular donors have achieved power conversion efficiencies (PCEs) over 10% using bulk heterojunction (BHJ) architectures.[2-8] Small molecule donors, as opposed to polymeric materials, are monodisperse, resulting in little batch to batch variation, and are obtainable in very high purity due to their increased solubility, allowing them to be purified readily by common techniques. The monodisperse nature of small

molecules allows for meaningful structure-property relationships to be assessed, through structural modifications, without any possible complications from varying average molecular weights and polydispersities.[9, 10]

To date, one of the most popular and successful designs for molecular donors has been the D1-A-D2-A-D1 framework.[11] These structures consist of a central π-electron rich core (D2) flanked by two π-electron deficient groups (A) with further π-conjugated side groups (D1), generally comprised of oligiothiophenes, extending out and end capping the system. The use of electron rich bridged bithiophenes for D2, such as dithieno[3,2-*b*:2',3'-*d*]silole (DTS) and cyclopenta[2,1-*b*:3,4-*b'*]dithiophene (CPDT), helps increase the planarity of the system and also enables the incorporation of solubilizing alkyl chains, while also allowing ample electron density for strong donor-acceptor interactions.[12-14] The use of two acceptors with high electron affinity, such as 2,1,3-benzothiadiazole derivatives, allow for deep LUMO energy levels and strong donor-acceptor interactions with D2. Further extension of the π-conjugated system with oligiothiophenes as D1 narrows the bandgap and helps promote self-assembly through the incorporation of an end capping alkyl chain.

The most efficient D1-A-D2-A-D1 molecular donor, to date, is a DTS based material reported by Bazan et al.[15] The use of asymmetric 2,1,3-benzothiadiazole derivatives, allow for a much higher degree of synthetic control due to the selective reactivity in palladium catalyzed cross couplings.[11, 16-18] This material possessed a relatively narrow optical bandgap and broad absorption over the solar spectrum. While various iterations of the corresponding 2,1,3-pyridylthiadiazole have been extensively studied, to date, there have

been no reports on the effect of heterocycle substitution of D1 or bridgehead substitution in D2 in the FBT containing material.[17, 19-21]

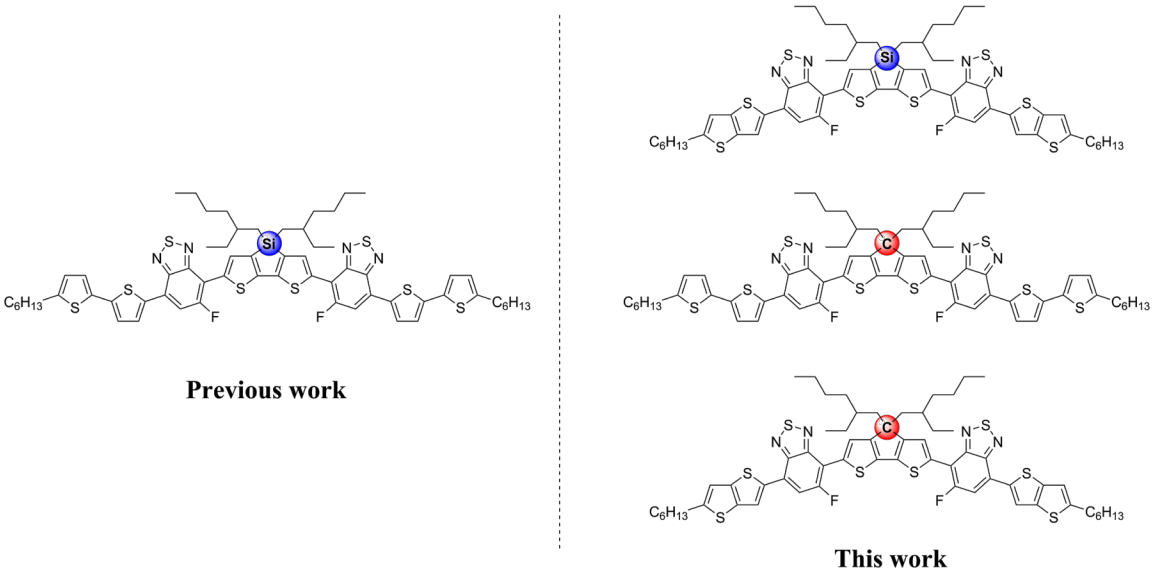


**Figure 3.1.** Work reported by Bazan et al.[15] and this work.

Herein, we report three new molecular donors utilizing the D1-A-D2-A-D1 framework, where D1 is and alkylated 2,2'-bithiophene (BT) or thieno[3,2-*b*]thiophene (TT); A is 5-fluoro-2,1,3-benzothiadiazole (FBT); and D2 is either DTS or CPDT, as shown in Figure 3.1. The use of CPDT causes a small red-shift in the maximum absorption of ~12 nm and a narrowing of the optical bandgap, relative to DTS. The incorporation of TT is seen to cause a blue-shift of over 20 nm and a wider bandgap than the BT analogues. Unoptimized OPV cells show the DTS containing materials with higher current densities than the CPDT analogues. The device fabrication, which is notoriously sensitive to processing conditions, is still being optimized.[18, 20] After optimization, general conclusions over the photovoltaic performance of the materials and the role of heterocycle substitution will be drawn.

## 3.3 Results and Discussion

### 3.3.1 Synthesis and Characterization

The synthesis of the side groups is shown in Scheme 3.1. The side groups were prepared by the regioselective Stille cross-coupling between 4,7-dibromo-5-fluoro-2,1,3-benzothiadiazole (**6**) and 5'-hexyl-2,2'-bithophene-5-trimethylstannane (**2**) or (5-hexylthieno[3,2-*b*]thiophen-2-yl)trimethylstannane (**4**), to give **FBT-BT** and **FBT-TT**, respectively, using methods similar to those used by Bazan et al. and, reported during the preparation of this article, Jen et al.[15, 22] The correct regioisomers of **FBT-BT** and **FBT-TT** were confirmed via 2D $^{1}$H-$^{1}$H NOESY (Figure S3.9 and S3.12, Supporting Information). Synthetic procedures for the side groups are described in the Supporting Information.

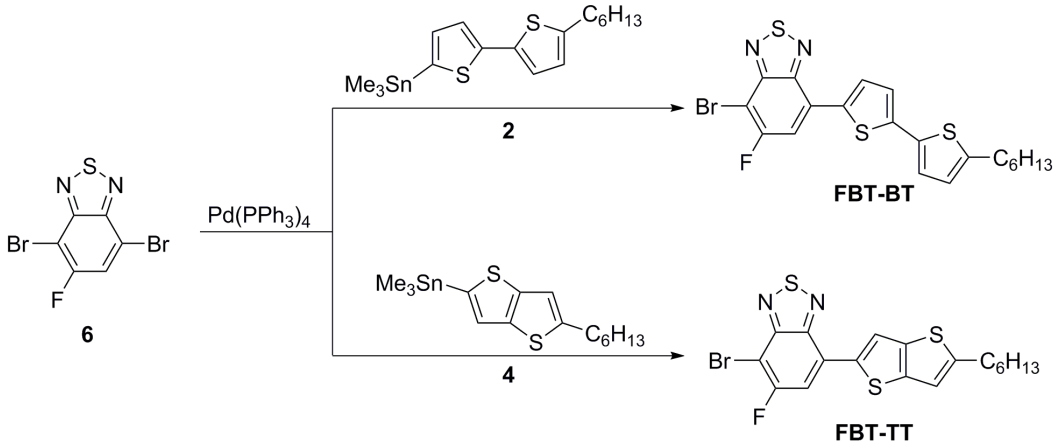


**Scheme 3.1.** Synthesis of D1-A side groups **FBT-BT** and **FBT-TT**.

The Stille cross-coupling of compounds **FBT-BT** and **FBT-TT** with DTS or CPDT to give the small molecules **DTS-FBT-BT**, **DTS-FBT-TT**, **CPDT-FBT-BT**, and **CPDT-FBT-TT** is shown in Scheme 3.2. All of the products were isolated in moderate

yield after extensive purification and were soluble in chlorobenzene and dichlorobenzene at room temperature, while only slightly soluble in chloroform.

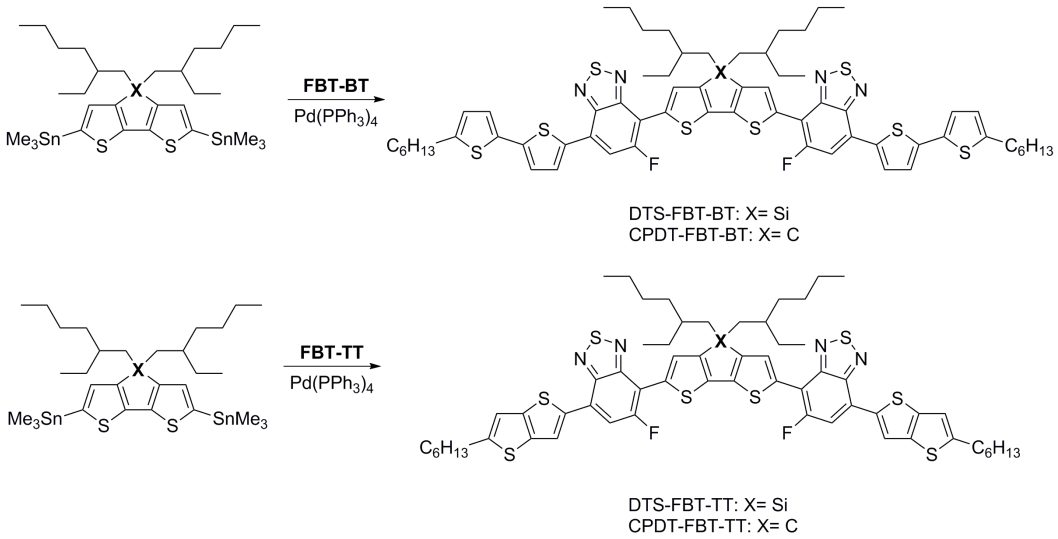


**Scheme 3.2.** Synthesis of the D1-A-D2-A-D1 small molecules DTS-FBT-BT, CPDT-FBT-BT, DTS-FBT-TT, and CPDT-FBT-TT.

The solution and thin film optical properties of the small molecules, given in Table 3.2, were investigated using UV-vis absorption spectroscopy. Absorption spectra in dilute chloroform solution are shown in Figure 3.1 and thin films cast from chlorobenzene are shown in Figure 3.2. All four materials displayed similar broad low-energy transitions with $\lambda_{max}$ between 579 nm and 610 nm. In an effort to gauge chromophore strength, absorption coefficients were measured (Table S3.1, Supporting information) and plotted versus wavelength in Figure 3.1. Both **DTS-FBT-BT** and **CPDT-FBT-BT** showed stronger absorption and a slight red shift of 5 and 8 nm, respectively, when compared to **DTS-FBT-TT** and **CPDT-FBT-TT**. When comparing D2, another increase in absorption can be seen when going from DTS to CPDT with both the BT and TT containing side groups, as well as slightly larger red shifts of 26 and 23 nm, respectively.

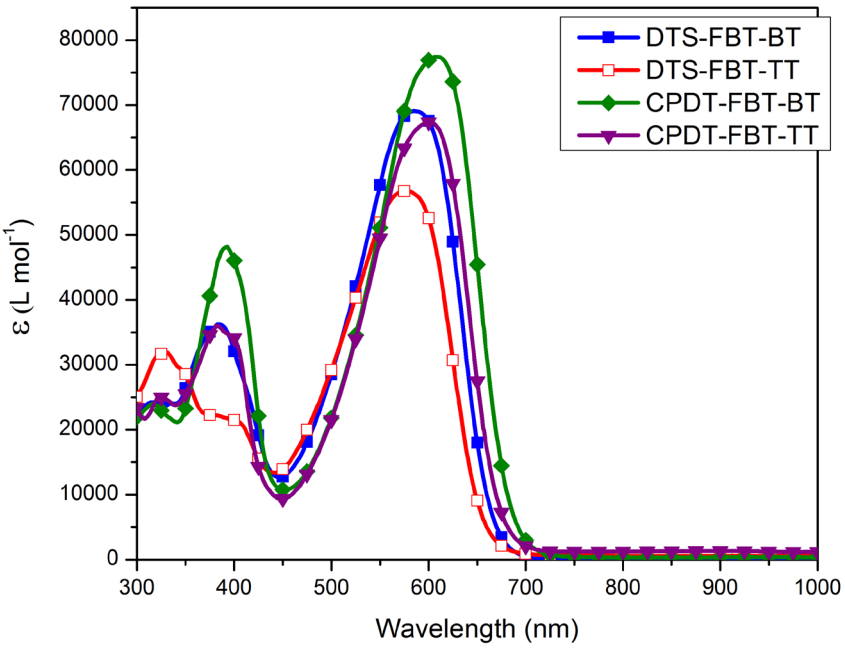


**Figure 3.2.** UV-vis of D1-A-D2-A-D1 small molecules in $CHCl_3$.

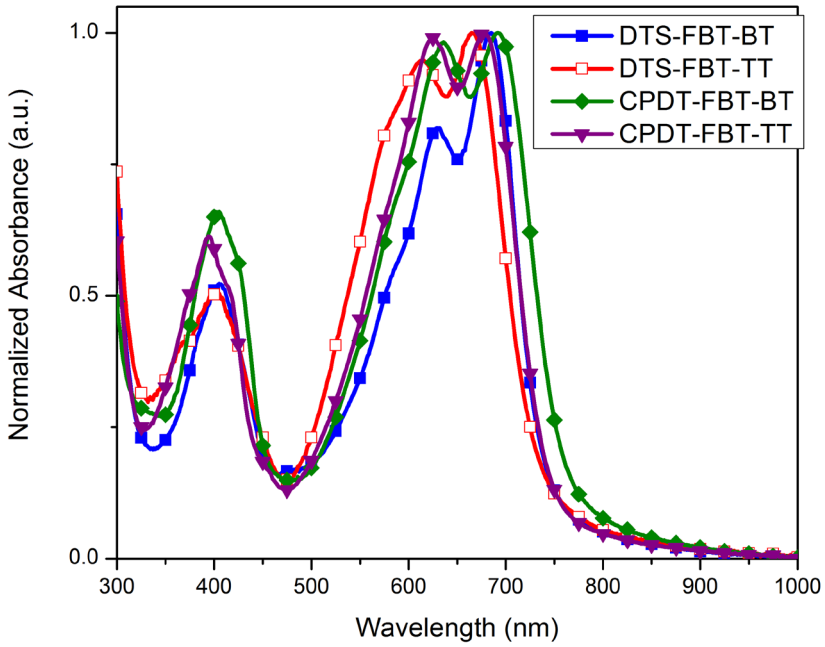


**Figure 3.3.** UV-vis of D1-A-D2-A-D1 small molecule thin films.

Thin film absorption measurements, showed large red-shifts in $\lambda_{max}$, compared to solution, for **DTS-FBT-BT**, **DTS-FBT-TT**, **CPDT-FBT-BT**, and **CPDT-FBT-TT** of 101, 86, 82, and 76 nm, respectively. The absorption spectra are shown in Figure 3.3. All materials displayed a red-shift in the optical onset between film and solution in the range of 71 – 77 nm, suggesting a similar order of π-stacking. Vibronic structure can be seen in all four materials, indicative of highly ordered films.[13, 23] The optical bandgap measured from the thin films follows the same trend as in solution, with **DTS-FBT-TT** > **DTS-FBT-BT** > **CPDT-FBT-TT** > **CPDT-FBT-BT**.

**Table 3.1.** Optical and electrochemical properties of D1-A-D2-A-D1 small molecules.

| SM | $\lambda_{max}^{soln}$ (nm)[a] | $E_g^{soln}$ (eV)[b] | $\lambda_{max}^{film}$ (nm) | $E_g^{film}$ (eV)[c] | $E_{HOMO}$ (eV)[d] | $E_{LUMO}$ (eV)[e] |
|---|---|---|---|---|---|---|
| DTS-FBT-BT | 584 | 1.86 | 685 | 1.68 | -4.97 | -3.29 |
| DTS-FBT-TT | 579 | 1.89 | 665 | 1.70 | -5.04 | -3.34 |
| CPDT-FBT-BT | 610 | 1.82 | 692 | 1.63 | -5.01 | -3.38 |
| CPDT-FBT-TT | 602 | 1.85 | 678 | 1.67 | -4.95 | -3.28 |

[a]Taken in dilute chloroform solution. [b]Calculated from the absorption onset of the solution spectra. [c]Calculated from the absorption onset of the film spectra. [d]Calculated from the reduction and oxidation onsets using the equation $E_{HOMO}$ = -4.8 - $E_{redox}$. [e]Calculated from the HOMO energy level and optical band-gap.

The electrochemical properties of the molecules were measured using solution cyclic voltammetry. All four of the materials showed reversible oxidation and reduction cycles (Figure S3.32 – S3.35, Supporting Information). The highest occupied molecular orbital (HOMO) was estimated from the oxidation onset and lowest unoccupied molecular orbital (LUMO) was calculated using the HOMO energy level and the optical band-gap. All

of the compounds have very similar HOMO levels of -4.97, -5.04, -5.01, and -4.95 eV for **DTS-FBT-BT**, **DTS-FBT-TT**, **CPDT-FBT-BT**, and **CPDT-FBT-TT**, respectively, which are all well within the error associated with cyclic voltammetry.[24]

### 3.3.2 Photovoltaic Devices

Photovoltaic devices were fabricated with the structure ITO/PEDOT:PSS/ donor:$PC_{71}BM$/Ca/Al, where ITO is indium tin oxide and PEDOT:PSS is poly(3,4-ethylenedioxythiophene) polystyrene sulfonate, and $PC_{71}BM$ is [6,6]-phenyl-$C_{71}$-butyric acid methyl ester. The resulting *J–V* curves of the unoptimized devices are shown in Figure 3.4, and the results summarized in Table 3.2. Devices based on all four materials had reasonable open-circuit voltages ($V_{OC}$), with the lowest being 0.74 V from the **CPDT-FBT-BT** device. The poor efficiencies are primarily due to the low short-circuit current density ($J_{SC}$) and low fill-factors (FF). The low $J_{SC}$ and FF are likely due to the poor film quality and uniformity. The lack of uniformity in the thin films is visible by eye, as seen in Figure S3.36 – S3.38 (Supporting Information).

**Table 3.2.** Characteristics of the unoptimized photovoltaic devices.

| Material[a] | $J_{SC}$ (mA cm$^{-2}$) | $V_{OC}$ (V) | FF | $PCE_{ave}$ (%) | $PCE_{max}$ (%) |
|---|---|---|---|---|---|
| DTS-FBT-BT | 6.0 | 0.78 | 0.36 | 1.68 | 1.81 |
| DTS-FBT-TT | 6.0 | 0.85 | 0.43 | 2.21 | 2.30 |
| CPDT-FBT-BT | 4.6 | 0.74 | 0.52 | 1.80 | 1.82 |
| CPDT-FBT-TT | 4.0 | 0.86 | 0.42 | 1.45 | 1.46 |

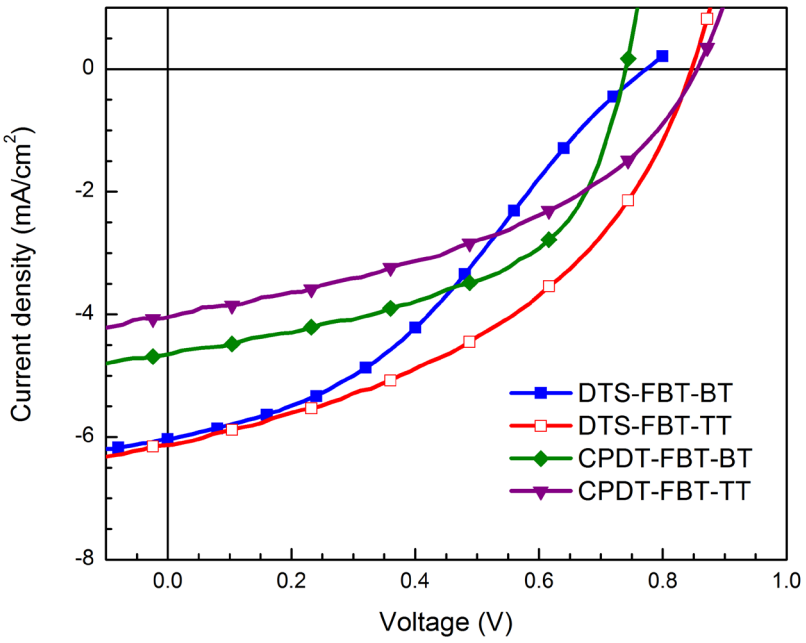


**Figure 3.4.** Characteristic current density–voltage (*J–V*) curves of unoptimized BHJ solar cells under AM 1.5G, 100 mW cm$^{-2}$ illumination.

The poor film quality is likely caused by too high of an initial spin rate when casting films (2000 rpm). In an attempt to alleviate this issue, devices are currently being fabricated at with a spin rate of 800 rpm and 1200 rpm with a ramp of 200 rpm/s. Even with the issue of film quality, it appears that the DTS based materials have much higher $J_{SC}$ than the CPDT based materials. This is a somewhat common occurrence within BHJ devices incorporating DTS or CPDT. This effect has been previously attributed to the enhanced structural order of DTS due to longer covalent bonds and orbital interactions of Si between molecules.[14, 25-26] Once film uniformity is accomplished, a more direct comparison between all of the structures and device performance can be firmly established, as well as collection of external quantum efficiencies and charge mobilities through the space-charge limited current method.

## 3.4 Conclusions

We have reported the synthesis of three new D1-A-D2-A-D1 molecular donors comprising various oligiothiophenes as D1 and DTS or CPDT as D2. All three materials show broad light absorption around 700 nm. The CPDT based materials display higher molar absorptivity and narrower optical bandgaps than their respective DTS analogs. Initial use of the materials in OPVs has given low overall efficiencies, most likely due to unoptimized device fabrication conditions, particularly in terms of poor film uniformity. Optimization of the photovoltaic devices is currently ongoing, after which, conclusions based on material performance can be firmly established.

## 3.5. Experimental

### 3.5.1 Materials

Air- and moisture-sensitive reactions were performed using standard Schlenk techniques. Solvents used for palladium-catalyzed reactions were deoxygenated prior to use by sparging with argon for 30 minutes. 4,4-bis(2-ethylhexyl)-2,6-bis(trimethylstannyl)-4*H*-cyclopenta[2,1-*b*:3,4-*b'*]dithiophene (CPDT)[27], 2,2'-bithiophene[28], thieno[3,2-*b*]thiophene[29], and 3,3',5-5'-tetrabromobithiophene[28] were prepared according to literature procedure. The CPDT stannane was purified by preparative HPLC using the same conditions as for DTS. The preparation of FBT-BT, FBT-TT, DTS, and all corresponding precursors are described in the Supporting Information section. All other chemical reagents were purchased commercially and used without further purification unless otherwise noted.

### 3.5.2 Characterization

Nuclear magnetic resonance (NMR) spectra were collected on Varian VXR-300, Varian MR-400, or Bruker Avance III-600 spectrometers. $^{1}$H NMR spectra were internally referenced to the residual solvent peak. In all spectra, chemical shifts are given in ppm (δ) relative to the solvent. Preparative HPLC was done on an Agilent 1100 series HPLC using a Phenomenex Luna 21.2 mm X 250 mm C18 (TMS endcapped, 5 μm particle size) AXIA column, using 40% acetonitrile 60% acetone at 10 mL/min as eluent and detected at 340 nm. Cyclic voltammetry (CV) measurements were carried out using an *e*-DAQ *e*-corder 410 potentiostat with a scanning rate of 50 mV $s^{-1}$. A platinum button electrode was used with $Ag/Ag^{+}$ and Pt wire used as the reference and auxiliary electrodes, respectively. The reported values were referenced to $Fc/Fc^{+}$ (-4.8 versus vacuum). All electrochemical experiments were performed in deoxygenated dichloromethane under an argon atmosphere using 0.1 M tetrabutylammonium hexafluorophosphate as electrolyte at a small molecule concentration of ≈1 mg $mL^{-1}$. Absorption spectra were obtained on a photodiode-array Agilent 8453 UV-visible spectrophotometer using polymer solutions in $CHCl_3$ and thin films. The thin films were spin coated from chlorobenzene at a concentration of 3 mg $mL^{-1}$ on to glass slides at a spin rate of 1200 rpm on a Headway Research, Inc. PWM32 spin-coater.

### 3.5.3 Photovoltaic Device Fabrication

Devices were fabricated on ITO coated glass substrates (5-15 Ω/□) from Delta Technologies. The substrates were ultrasonicated consecutively in detergent (alconox), deionized water and 2-propanol for 10 minutes. The substrates were blown dry with nitro-

gen and kept on a hot plate at 100 °C for 10 minutes. These were treated with air plasma and then PEDOT:PSS (VP 4083) was spin coated on top of them at 5000 rpm for 30 seconds as the hole transport layer (HTL) of the device, and finally annealed at 150 °C for 10 minutes before transferring the substrates inside the glove box. The active layer solutions were prepared inside the glove box. Donor and $PC_{70}BM$ from 1-materials Inc. were dissolved in chlorobenzene (CB) from Sigma-Aldrich with a total concentration of 35mg/ml donor:$PC_{70}BM$ (3:2 by weight). 0.4% by volume DIO was added to the solution. These solutions were stirred at 300 rpm at 60 °C on a hot plate for more than 12 hours and filtered using a 0.22 μm PTFE filter (Sigma-Aldrich). Solutions were heated to 90 °C for 15 minutes before spin coating on the HTL coated ITO slides. Films were spin coated at 2000 rpm for 40 seconds. The spin coated films were solvent annealed for 10 minutes and thermal annealed at 80 °C for 10 minutes. Finally, 20 nm of Ca and 100 nm of Al were deposited sequentially on top of the active-layers as the electrode. Ca and Al were deposited using a thermal evaporator in $10^{-6}$ mbar vacuum at a rate slower than 0.5 and 5 Å/s, respectively.

### 3.5.4 Synthesis

**General procedure for the Stille coupling of 1 and DTS or CPDT:** In a two neck round-bottom flask, DTS or CPDT (0.2 mmol) and **1** (194.8 mg, 0.4 mmol) were dissolved in toluene (12 mL) and sparged with argon for 45 min. Tetrakis(tripheylphosphine)palladium(0) (19.5 mg, 8 mol %) was added and the reaction mixture was refluxed for 48 h before cooling to ambient temperature. The reaction mix-

ture was taken up in chloroform and loaded onto silica gel followed by washing with methanol and purification by silica gel chromatography using a hexanes/chloroform gradient *in triplicate*. The collected fractions were concentrated, precipitated into methanol, filtered, washed with acetone, and dried *in vacuo*.

**DTS-FBT-BT:** The product was recovered as a metallic purple solid (147.3 mg, 60%). $^1$H NMR (400 MHz, $CDCl_3$) δ 8.34 (t, *J* = 4.8 Hz, 2H), 8.04 (d, *J* = 3.9 Hz, 2H), 7.74 (d, *J* = 13.2 Hz, 2H), 7.19 (d, *J* = 3.9 Hz, 2H), 7.12 (d, *J* = 3.5 Hz, 2H), 6.73 (d, *J* = 3.6 Hz, 2H), 2.82 (t, *J* = 7.6 Hz, 4H), 1.77 – 1.64 (m, 4H), 1.58 – 1.54 (m, 2H), 1.45 – 1.17 (m, 28H), 1.17 – 1.02 (m, 4H), 0.97 – 0.87 (m, 6H), 0.87 – 0.78 (m, 12H).

**CPDT-FBT-BT:** The product was recovered as a metallic purple solid (105.1 mg, 44%). $^1$H NMR (400 MHz, $CDCl_3$) δ 8.24 (t, *J* = 5.9 Hz, 2H), 8.01 (dt, *J* = 3.6, 1.7 Hz, 2H), 7.72 (dd, *J* = 13.3, 1.1 Hz, 2H), 7.17 (d, *J* = 3.9 Hz, 2H), 7.12 (d, *J* = 3.5 Hz, 2H), 6.73 (d, *J* = 3.5 Hz, 2H), 2.82 (t, *J* = 7.6 Hz, 4H), 2.14 – 2.01 (m, 4H), 1.71 (p, *J* = 7.5 Hz, 4H), 1.46 – 1.37 (m, 4H), 1.37 – 1.29 (m, 8H), 1.13 – 0.94 (m, 16H), 0.95 – 0.87 (m, 6H), 0.84 (q, *J* = 5.4 Hz, 2H), 0.70 – 0.61 (m, 12H).

**General procedure for the Stille coupling of 2 and DTS or CPDT:** In a two neck round-bottom flask, DTS or CPDT (0.2 mmol) and **2** (181.3 mg, 0.4 mmol) were dissolved in toluene (12 mL) and sparged with argon for 45 min. Tetrakis(tripheylphosphine)palladium(0) (19.5 mg, 8 mol %) was added and the reaction mixture was refluxed for 48 h before cooling to ambient temperature. The reaction mix-

ture was taken up in chloroform and loaded onto silica gel followed by washing with methanol and purification by silica gel chromatography using a hexanes/chloroform gradient *in triplicate*. The collected fractions were concentrated, precipitated into methanol, filtered, and dried *in vacuo*.

**DTS-FBT-TT:** The product was recovered as a metallic purple solid (103.0 mg, 43%). $^1$H NMR (400 MHz, $CDCl_3$) δ 8.38 (s, 2H), 8.34 (t, $J$ = 4.6 Hz, 2H), 7.67 (d, $J$ = 13.2 Hz, 2H), 6.98 (s, 2H), 2.91 (t, $J$ = 7.7 Hz, 4H), 1.81 – 1.69 (m, 4H), 1.62 – 1.52 (m, 2H), 1.47 – 1.20 (m, 28H), 1.18 – 1.04 (m, 4H), 0.96 – 0.88 (m, 6H), 0.88 – 0.81 (m, 12H).

**CPDT-FBT-TT:** The product was recovered as a metallic purple solid (59.1 mg, 26%). $^1$H NMR (400 MHz, $CDCl_3$) δ 8.42 (s, 2H), 8.24 (t, $J$ = 5.7 Hz, 2H), 7.73 (d, $J$ = 13.5 Hz, 2H), 7.00 (s, 2H), 2.92 (t, $J$ = 7.6 Hz, 4H), 2.08 (s, 4H), 1.75 (p, $J$ = 7.6 Hz, 4H), 1.47 – 1.37 (m, 4H), 1.37 – 1.29 (m, 8H), 1.25 (s, 2H), 1.09 – 0.93 (m, 14H), 0.94 – 0.86 (m, 6H), 0.86 – 0.77 (m, 2H), 0.72 – 0.60 (m, 12H).

## 3.6 Acknowledgements

We thank Iowa State University (ISU) for support of this work. We wish to thank Dr. Sarah Cady and the ISU NMR Laboratory for training and assistance with the 2-dimensional NMR experiments. We also wish to thank Dr. Kamel Harrata and the ISU Mass Spectrometry Laboratory for analysis. The OPVs were fabricated at the ISU Microelectronics Research Center.

## 3.7 Supporting Information

### 3.7.1 Synthesis

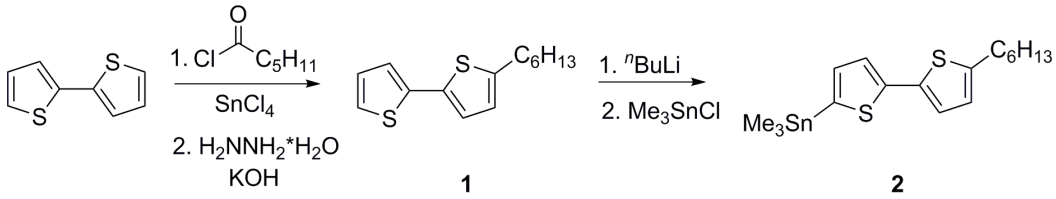


1 2

**5-hexyl-2,2'bithiophene (1)** A solution of 2,2'-bithiophene (3.17 g, 19 mmol) and hexanoyl chloride (2.8 mL, 20 mmol) in anhydrous benzene (20 mL) was cooled to 0 °C with an ice-bath. Anhydrous tin(IV) chloride (2.4 mL, 20.5 mmol) was added dropwise, and the solution allowed to stir for 1h at 0 °C. The reaction was then quenched with ice and diluted with dichloromethane (50 mL). The reaction mixture was then washed with water, saturated sodium bicarbonate solution, and then dried over anhydrous sodium sulfate. The solvent was removed, and the crude material was suspended in ethylene glycol (30 mL). Solid potassium hydroxide pellets (4.37 g, 78 mmol) were added, followed by the dropwise addition of hydrazine monohydrate (7.5 mL, 155 mmol). The reaction mixture was then heated at 180 °C overnight. After cooling to ambient temperature, the reaction was neutralized with dilute HCl solution and extracted with diethyl ether. The ether layer was washed with water, brine, and dried over anhydrous sodium sulfate. Purification using column chromatography on silica gel with hexanes as eluent gave the expected product as a colorless oil (3.51 g, 74%). $^1$H NMR (400 MHz, $CDCl_3$) δ 7.16 (dd, $J$ = 5.1, 1.0 Hz, 1H), 7.10 (dd, $J$ = 3.6, 1.1 Hz, 1H), 6.99 (d, $J$ = 3.7 Hz, 1H), 6.98 (d, $J$ = 3.5 Hz, 1H),

6.68 (d, $J$ = 3.5 Hz, 1H), 2.79 (t, $J$ = 7.5 Hz, 2H), 1.68 (p, $J$ = 7.4 Hz, 2H), 1.45 – 1.25 (m, 6H), 0.89 (t, $J$ = 6.9 Hz, 3H).

**5'-hexyl-5-(trimethylstannyl)-2,2'-bithiophene (2)** Compound **1** (0.71 g, 2.8 mmol) was dissolved in THF (20 mL) and cooled to -78 °C. After the dropwise addition of *n*-butyllithium (1.4 mL, 2.5 M in hexanes), the reaction was allowed to stir at -78 °C for 30 min before being warmed to 0 °C for an hour. The reaction was then cooled back to -78 °C and trimethyltin chloride (3.4 mL, 1.0 M in THF) was added dropwise. The reaction was allowed to stir at room temperature overnight before being quenched with saturated ammonium chloride solution. The crude product was extracted with ether and dried. After removal of the solvent, the crude material was purified by vacuum distillation to give the expected product as a colorless oil (0.98 g, 84%). $^1$H NMR (600 MHz, $CDCl_3$) δ 7.20 (d, $J$ = 3.3 Hz, 1H), 7.06 (d, $J$ = 3.4 Hz, 1H), 6.97 (d, $J$ = 3.6 Hz, 1H), 6.67 (d, $J$ = 3.8 Hz, 1H), 2.78 (t, $J$ = 7.5 Hz, 2H), 1.68 (p, $J$ = 7.5 Hz, 2H), 1.43 – 1.35 (m, 2H), 1.35 – 1.26 (m, 4H), 0.89 (t, $J$ = 6.3 Hz, 3H), 0.38 (s, 9H).

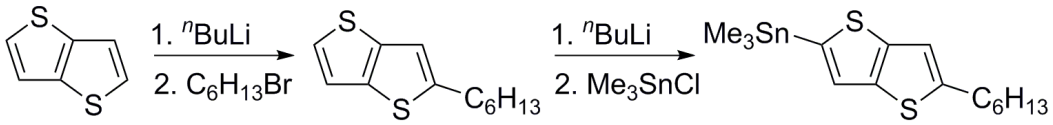


**3** **4**

**2-hexylthieno[3,2-*b*]thiophene (3)** A solution of thieno[3,2-*b*]thiophene (0.25 g, 1.8 mmol) in THF (10 mL) was cooled to -78 °C before the dropwise addition of *n*-butyllithium (0.67 mL, 2.5 M in hexanes). The reaction was stirred at temperature 1h be-

fore the very slow addition of 1-bromohexane (0.37 g, 2.2 mmol). The reaction was allowed to slowly warm to ambient temperature and stirred overnight. The mixture was then poured into water and extracted with dichloromethane. The organic layer was dried over anhydrous sodium sulfate and the solvent removed under reduced pressure. The crude material was purified by vacuum distillation to give the expected product as a colorless oil (0.24 g, 65%). $^1$H NMR (400 MHz, $CDCl_3$) δ 7.27 (d, $J$ = 5.2 Hz, 1H), 7.18 (d, $J$ = 5.2 Hz, 1H), 6.96 (s, 1H), 2.88 (t, $J$ = 7.6 Hz, 2H), 1.71 (p, $J$ = 7.5 Hz, 2H), 1.45 – 1.34 (m, 2H), 1.36 – 1.27 (m, 4H), 0.89 (t, $J$ = 6.9 Hz, 3H).

**5-hexyl-2-(trimethylstannyl)thieno[3,2-*b*]thiophene (4)** Compound **3** (0.61 g, 2.7 mmol) was dissolved in THF (20 mL) and cooled to -78 °C. After the dropwise addition of *n*-butyllithium (1.2 mL, 2.5 M in hexanes), the reaction was allowed to stir at -78 °C for 30 min before being warmed to 0 °C for an hour. The reaction was then cooled back to -78 °C and trimethyltin chloride (4.0 mL, 1.0 M in THF) was added dropwise. The reaction was allowed to stir at room temperature overnight before being quenched with saturated ammonium chloride solution. The crude product was extracted with ether and dried. After removal of the solvent, the crude material was purified by vacuum distillation to give the expected product as a colorless oil (0.81 g, 77%). $^1$H NMR (400 MHz, $CDCl_3$) δ 7.21 (s, 1H), 6.94 (s, 1H), 2.86 (t, $J$ = 7.4 Hz, 2H), 1.70 (p, $J$ = 7.6 Hz, 2H), 1.42 – 1.35 (m, 2H), 1.34 – 1.27 (m, 4H), 0.88 (t, $J$ = 7.0 Hz, 3H), 0.38 (s, 9H).

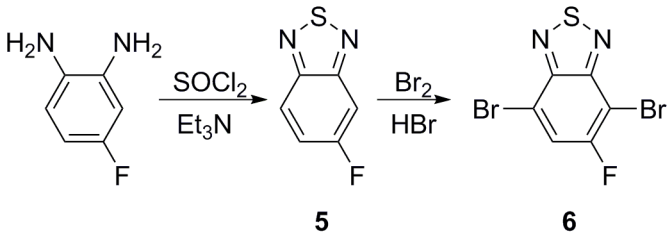


**5** **6**

**5-fluoro-2,1,3-benzothiadiazole (5)** A solution of 4-fluoro-1,2-diaminobenzene (4.05 g, 32.1 mmol) and triethylamine (14 mL, 190 mmol) were dissolved in chloroform (60 mL) was cooled to 0 °C with an ice bath. Thionyl chloride (4.6 mL, 63.3 mmol) was added dropwise, and the reaction was refluxed overnight. After cooling to ambient temperature, the reaction was washed with water to remove excess amine. The crude material was run through a short chloroform plug. The material was further purified by silica gel column chromatography using 1:3 hexanes/dichloromethane as eluent to give the expected product as an off white solid (4.71 g, 95%). $^1$H NMR (600 MHz, $CDCl_3$) δ 7.99 (dd, $J$ = 9.5, 5.2 Hz, 1H), 7.62 (dd, $J$ = 8.8, 2.5 Hz, 1H), 7.44 (ddd, $J$ = 9.5, 8.5, 2.5 Hz, 1H).

**4,7-dibromo-5-fluoro-2,1,3-benzothiadiazole (6)** Compound **5** (4.42 g, 28.7 mmol) was dissolved in 48% HBr (50 mL). Bromine (15.7 mL, 312 mmol) in HBr (50 mL) was added very slowly over 2h. After the complete addition of bromine, the reaction was refluxed for 72h before being diluted with water. The reaction mixture was extracted with chloroform, and the organic layer was washed with dilute sodium hydroxide solution, followed by excess water, dried over anhydrous sodium sulfate, and the solvent removed. Purification of the crude material with silica gel column chromatography using 1:1 hexanes/chloroform as eluent gave the expected product as a white solid (6.52 g, 96%). $^1$H NMR (600 MHz, $CDCl_3$) δ 7.79 (d, $J$ = 8.3 Hz, 1H).

**4-bromo-5-fluoro-7-(5'-hexyl-[2,2'-bithiophene]-5-yl)-2,1,3-benzothiadiazole (FBT-BT)** In a two neck round-bottom flask, **2** (308.9 mg, 1.00 mmol) and **6** (412.8 mg, 1.00 mmol) were dissolved in toluene (12 mL) and sparged with argon for 45 min. Tetrakis(tripheylphosphine)palladium(0) (126.7 mg, 8 mol %) was added and the reaction mixture was refluxed for 48 h before cooling to ambient temperature. The solvent was removed and the reaction mixture taken up in chloroform followed by being run through a short silica gel plug. The resulting fraction was then concentrated to give a dark red solid. The crude product was then recrystallized from ethanol to give a light red powder (272.4 mg, 57%). $^1$H NMR (600 MHz, $CDCl_3$) δ 8.04 (q, $J$ = 3.8, 3.2 Hz, 1H), 7.68 (d, $J$ = 9.4 Hz, 1H), 7.19 (d, $J$ = 3.8 Hz, 1H), 7.12 (d, $J$ = 3.5 Hz, 1H), 6.73 (d, $J$ = 3.5 Hz, 1H), 2.82 (t, $J$ = 7.6 Hz, 2H), 1.70 (p, $J$ = 7.8 Hz, 2H), 1.46 – 1.37 (m, 2H), 1.36 – 1.28 (m, 4H), 0.90 (t, $J$ = 6.1 Hz, 3H).

**4-bromo-5-fluoro-7-(5-hexylthieno[3,2-*b*]thiophen-2-yl)-2,1,3-benzothiadiazole (FBT-TT)** In a two neck round-bottom flask, **4** (808.6 mg, 2.08 mmol) and **6** (646.6 mg, 2.08 mmol) were dissolved in toluene (12 mL) and sparged with argon for 45 min. Tetrakis(tripheylphosphine)palladium(0) (195.9 mg, 8 mol %) was added and the reaction mixture was refluxed for 48 h before cooling to ambient temperature. The solvent was removed and the reaction mixture taken up in chloroform followed by being run through a short silica gel plug. The resulting fraction was then concentrated to give a dark orange solid. The crude product was then recrystallized from ethanol to give bright orange crystals (559.8 mg, 59%). $^1$H NMR (600 MHz, $CDCl_3$) δ 8.46 (s, 1H), 7.70 (d, $J$ = 10.1 Hz, 1H), 7.03 (s, 1H), 2.95 (t, $J$ = 8.1 Hz, 2H), 1.78 (p, $J$ = 7.6 Hz, 2H), 1.50 – 1.41 (m, 2H),

1.39 – 1.34 (m, 4H), 0.94 (t, $J$ = 6.9 Hz, 3H); $^{13}$C NMR (151 MHz, $CDCl_3$) δ 160.76 (d, $J$ = 251.4 Hz), 154.37 (d, $J$ = 7.3 Hz), 151.45 , 148.93 , 140.30 , 138.56 , 137.06 (d, $J$ = 2.6 Hz), 128.20 (d, $J$ = 10.2 Hz), 122.41, 116.46, 115.56 (d, $J$ = 30.8 Hz), 95.78 (d, $J$ = 24.8 Hz), 31.56, 31.44, 31.36, 28.76, 22.58, 14.08; HRMS (ESI, *m/z*): calcd. For $C_{18}H_{15}BrFN_2S_3$ $[M-H]^-$ 452.9565; found 452.9554; Diff (ppm) 2.38.

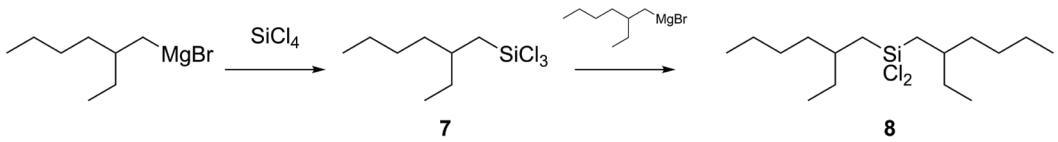


7 8

**(2-ethylhexyl)trichlorosilane (7)** A solution of silicon tetrachloride (14 mL, 122.2 mmol) in THF (40 mL) was cooled to -10 °C with an acetone/ice bath. 2-ethylhexylmagnesium bromide solution (60 mL, 1.0 M in ether, Aldrich) was added dropwise and the reaction allowed to stir overnight at room temperature. The reaction was poured into hexanes and filtered to remove inorganic salts. The solution was concentrated, and the crude material purified by fractional distillation to give the expected product as a clear oil (13.4 g, 90%). $^1$H NMR (400 MHz, $CDCl_3$) δ 1.78 (p, $J$ = 12.5, 6.2 Hz, 1H), 1.49 – 1.35 (m, 6H), 1.35 – 1.23 (m, 4H), 0.90 (t, $J$ = 7.1 Hz, 3H), 0.87 (t, $J$ = 7.9 Hz, 3H).

**bis(2-ethylhexyl)dichlorosilane (8)** A solution of compound **7** (13.4 g, 54 mmol) in THF (75 mL) was cooled to 0 °C with an ice bath. 2-ethylhexylmagnesium bromide solution (39 mL, 1.0 M in ether, Aldrich) was added dropwise and the reaction allowed to stir overnight at room temperature, followed by removal of the solvent. After dilution of the

crude material in hexanes, a precipitate formed. The solid was filtered and the filtrate concentrated. The resulting oil was purified by fractional distillation under high vacuum, giving the expected product as a colorless oil (10.2 g, 80%). $^1$H NMR (400 MHz, $CDCl_3$) δ 1.70 (p, $J$ = 12.4, 6.1 Hz, 2H), 1.44 – 1.20 (m, 16H), 1.11 (d, $J$ = 6.7 Hz, 4H), 0.90 (t, $J$ = 6.6 Hz, 6H), 0.86 (t, $J$ = 7.4 Hz, 6H).

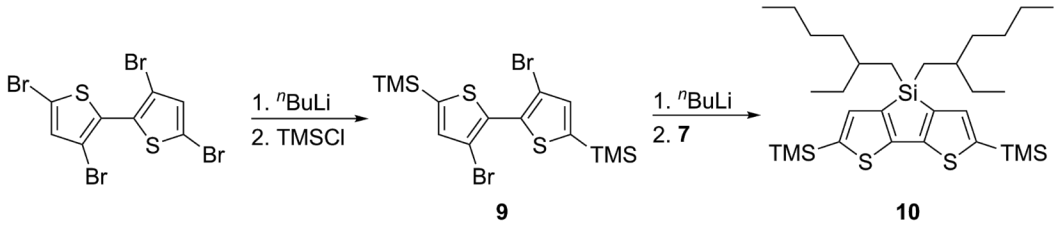


**3,3'-dibromo-5,5'-(trimethylsilyl)-2,2'bithiophene (9)** A solution of 3,3'-5,5'-tetrabromo-2,2'-bithiophene (30.1 g, 62 mmol) in THF (300 mL) was cooled to -78 °C. *n*-butyllithium solution (53 mL, 2.5 M in hexanes) was added dropwise and the reaction stirred for 4h at temperature. Trimethylsilyl chloride (21 mL, 165 mmol) was added dropwise and the reaction stirred for 15 min at -78 °C before being allowed to stir at ambient temperature overnight. The reaction was diluted with ether (400 mL) and washed with water and dried. Purification by silica gel column chromatography using hexanes as eluent, followed by recrystallization from ethanol gave the expected product as a light yellow solid (18.2 g, 62%). $^1$H NMR (400 MHz, $CDCl_3$) δ 7.15 (s, 2H), 0.34 (s, 18H).

**4,4-bis(2-ethylhexyl)-2,6-bis(trimethylsilyl)-dithieno[3,2-*b*:2',3'-*d*]silole (10)** A solution of **9** (11.78 g, 25 mmol) in THF (200 mL) was cooled to -78 °C. *n*-butyllithium solution (21.5 mL, 2.5 M in hexanes) was added dropwise and the reaction stirred for 2h at

temperature. Compound **8** (9.42 g, 30 mmol) was added dropwise and the reaction stirred at ambient temperature overnight. The reaction was poured into water and the crude material extracted with ether, dried with anhydrous sodium sulfate, and the solvent removed. Purification by silica gel column chromatography using hexanes as eluent gave the expected product as a light yellow oil (11.54 g, 82%). $^1$H NMR (400 MHz, $CDCl_3$) δ 7.11 (s, 2H), 1.39 (p, *J* = 6.8, 5.9, 5.7 Hz, 2H), 1.33 – 1.20 (m, 4H), 1.20 – 1.10 (m, 12H), 1.01 – 0.82 (m, 4H), 0.82 (t, *J* = 6.4 Hz, 6H), 0.76 (t, *J* = 7.3 Hz, 6H), 0.32 (s, 18H).

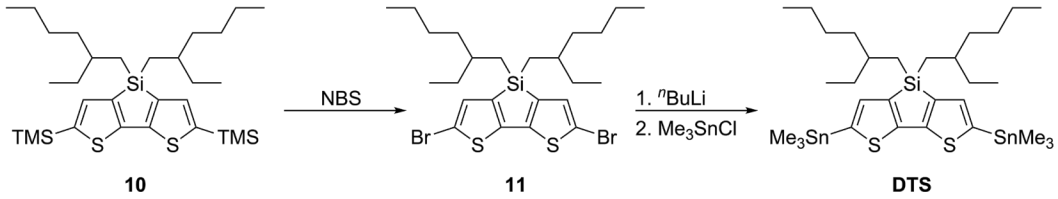


**10** **11** **DTS**

**4,4-bis(2-ethylhexyl)-2,6-dibromo-dithieno[3,2-*b*:2',3'-*d*]silole (11)** Compound **10** (1.14 g, 2 mmol) was dissolved in THF (25 mL) and protected from light. NBS (0.73 g, 4.1 mmol) was added in two portions. The reaction was allowed to stir for 2h before being extracted with ether, washed with water, dried over anhydrous sodium sulfate, and concentrated. Purification by silica gel column chromatography using hexanes as eluent gave the expected product as a yellow oil (1.12 g, 96%). $^1$H NMR (400 MHz, $CDCl_3$) δ 6.98 (s, 2H), 1.37 (p, *J* = 6.2 Hz, 2H), 1.30 – 1.08 (m, 16H), 0.91 (dd, *J* = 6.7, 4.6 Hz, 4H), 0.84 (t, *J* = 6.8 Hz, 6H), 0.77 (t, *J* = 7.4 Hz, 6H).

**4,4-bis(2-ethylhexyl)-2,6-bis(trimethylstannyl)-dithieno[3,2-*b*:2',3'-*d*]silole (DTS)** A solution of **11** (1.12 g, 1.9 mmol) in THF (30 mL) was cooled to -78 °C. A solution of

$^{n}$BuLi (5.25 mmol, 2.5 M in hexanes) was added dropwise and the reaction allowed to stir for two hours at -78 °C. Trimethyl tin chloride solution (6.25 mmol, 1 M in THF) was added dropwise. The reaction was slowly allowed to warm to room temperature and stirred overnight. The reaction mixture was poured into water and the crude product extracted with hexanes and dried over anhydrous $Na_2SO_4$. After removal of the solvent, the crude product was heated under high vacuum at 40 °C overnight. The crude material was purified by preparative HPLC to give the expected product as a tacky light yellow oil (0.97 g, 67%). $^1$H NMR (600 MHz, $CDCl_3$) δ 7.07 (s, 2H), 1.45 – 1.37 (m, 2H), 1.32 – 1.07 (m, 16H), 0.99 – 0.92 (m, 4H), 0.92 – 0.86 (m, 4H), 0.82 (t, $J$ = 6.6 Hz, 6H), 0.77 (t, $J$ = 7.3 Hz, 6H), 0.37 (s, 18H).

### 3.7.2 NMR Spectra and analytical data

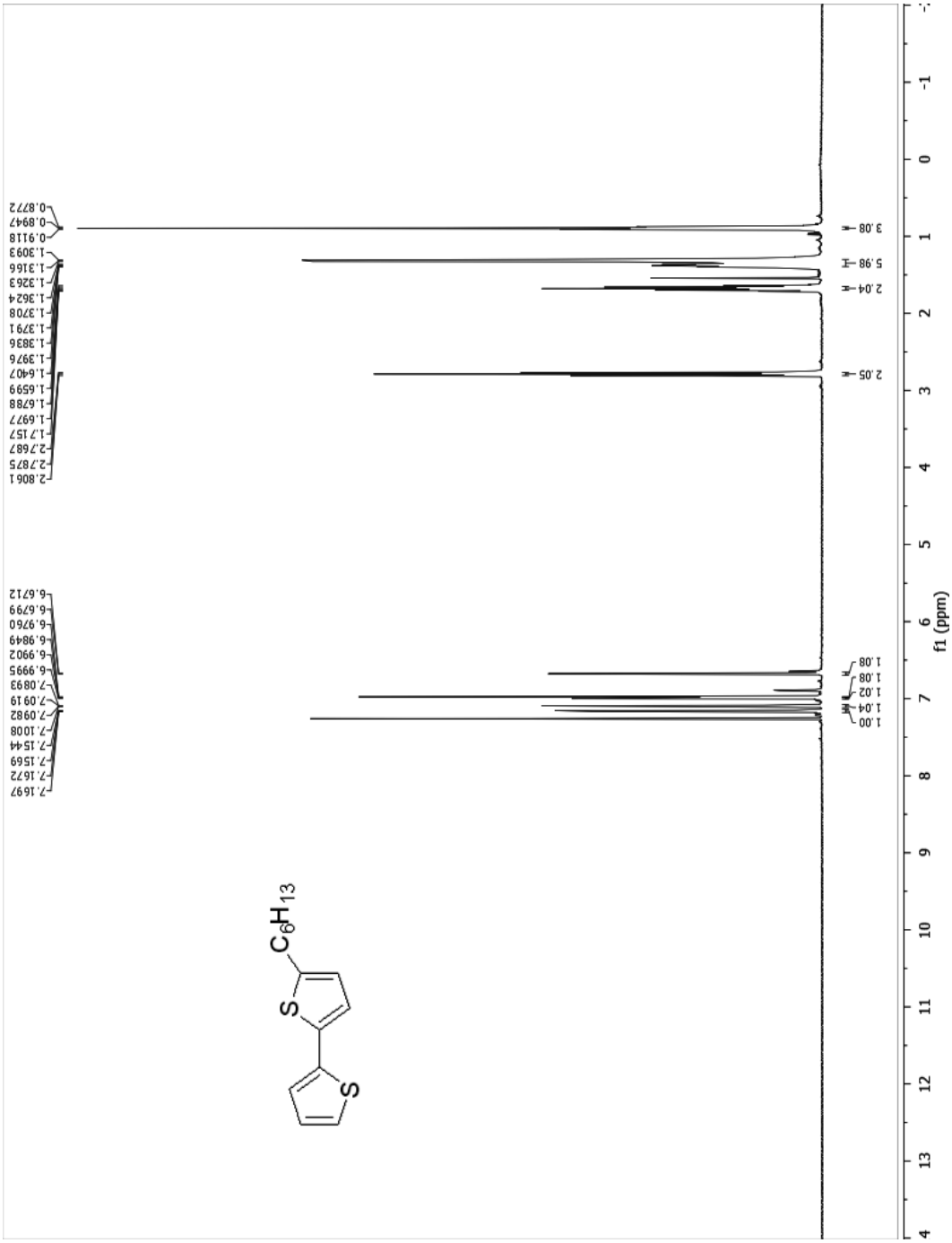


**Figure S3.1.** $^{1}H$ NMR of **1**.

-

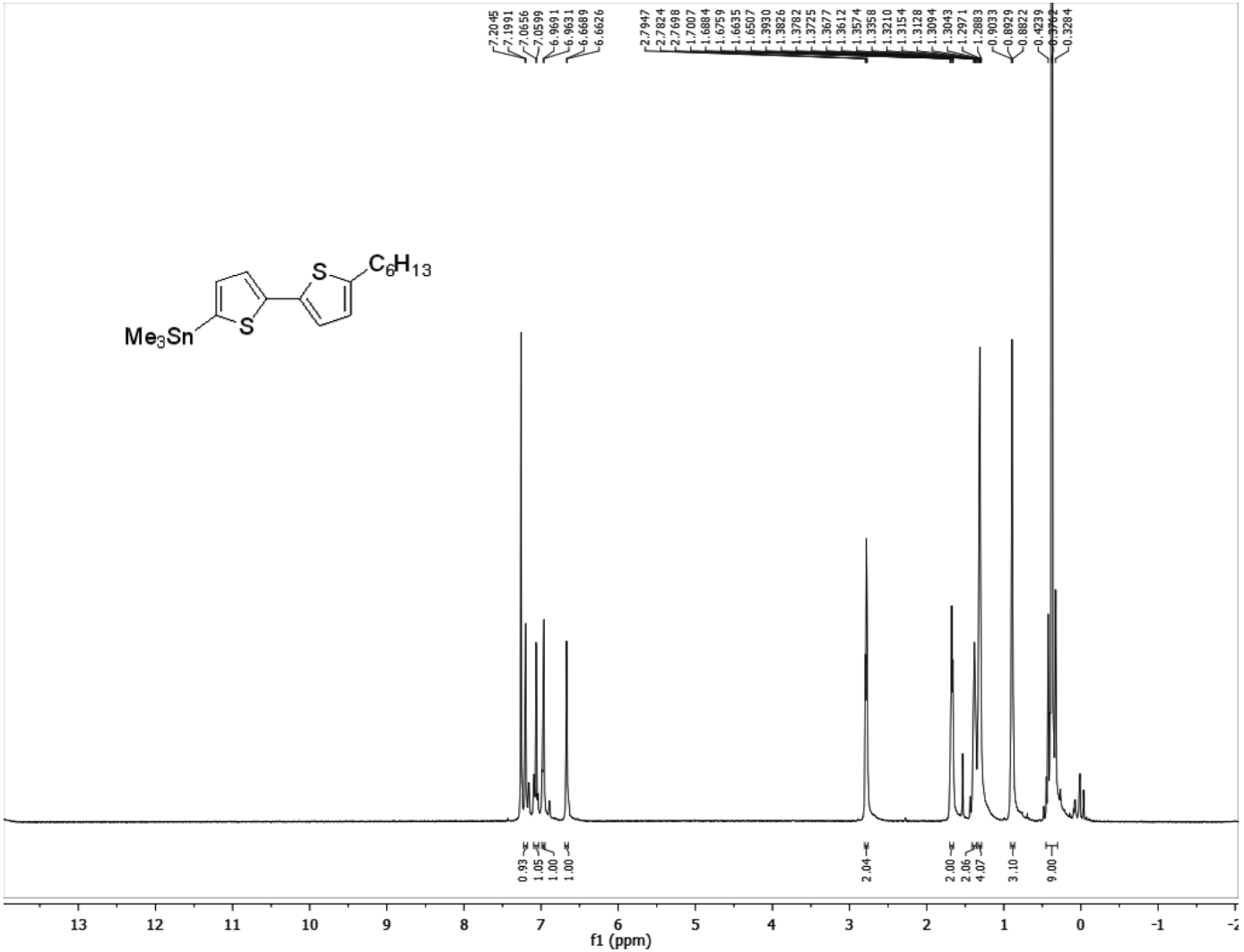


**Figure S3.2.** $^{1}$H NMR of **2**.

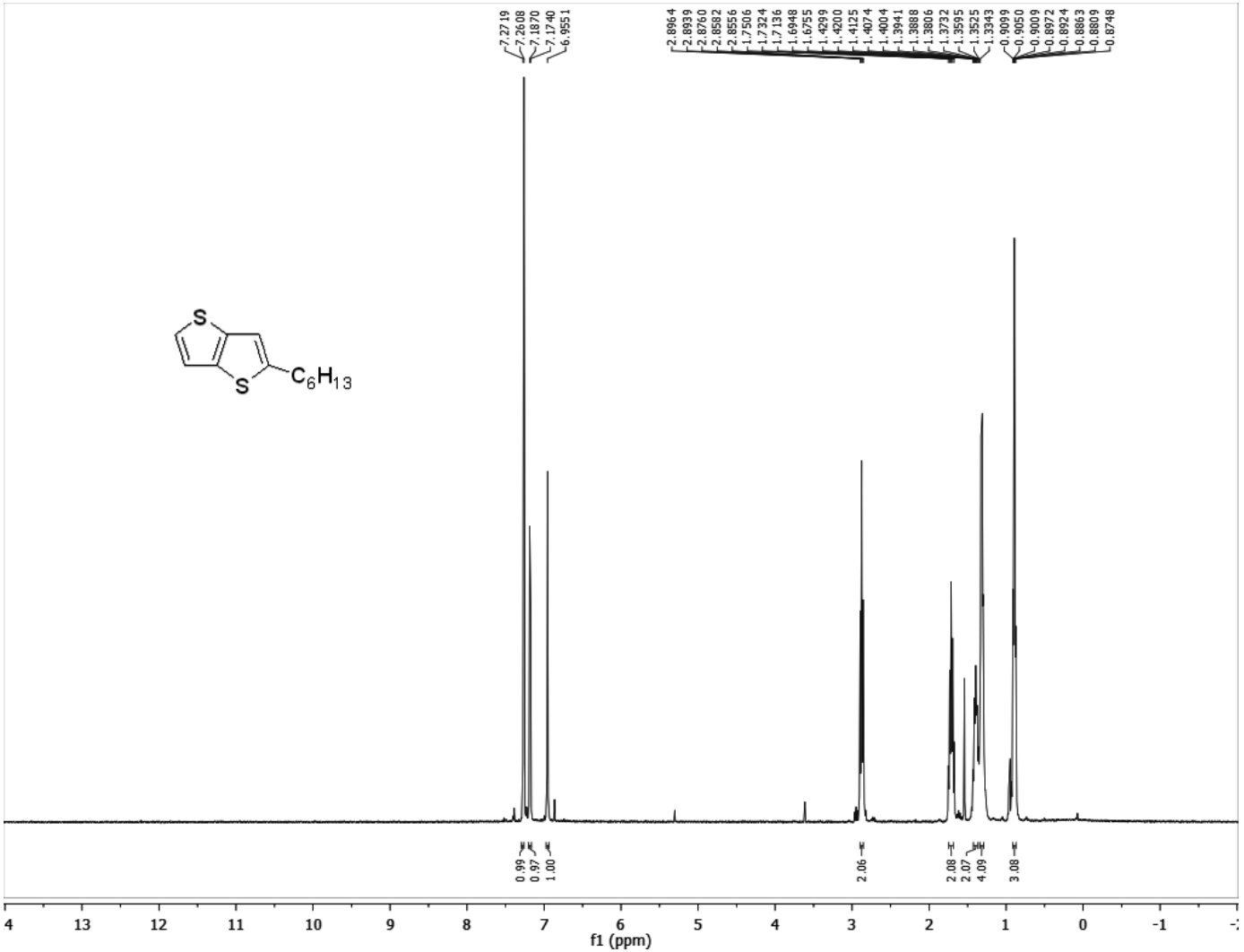


**Figure S3.3.** $^{1}$H NMR of **3**.

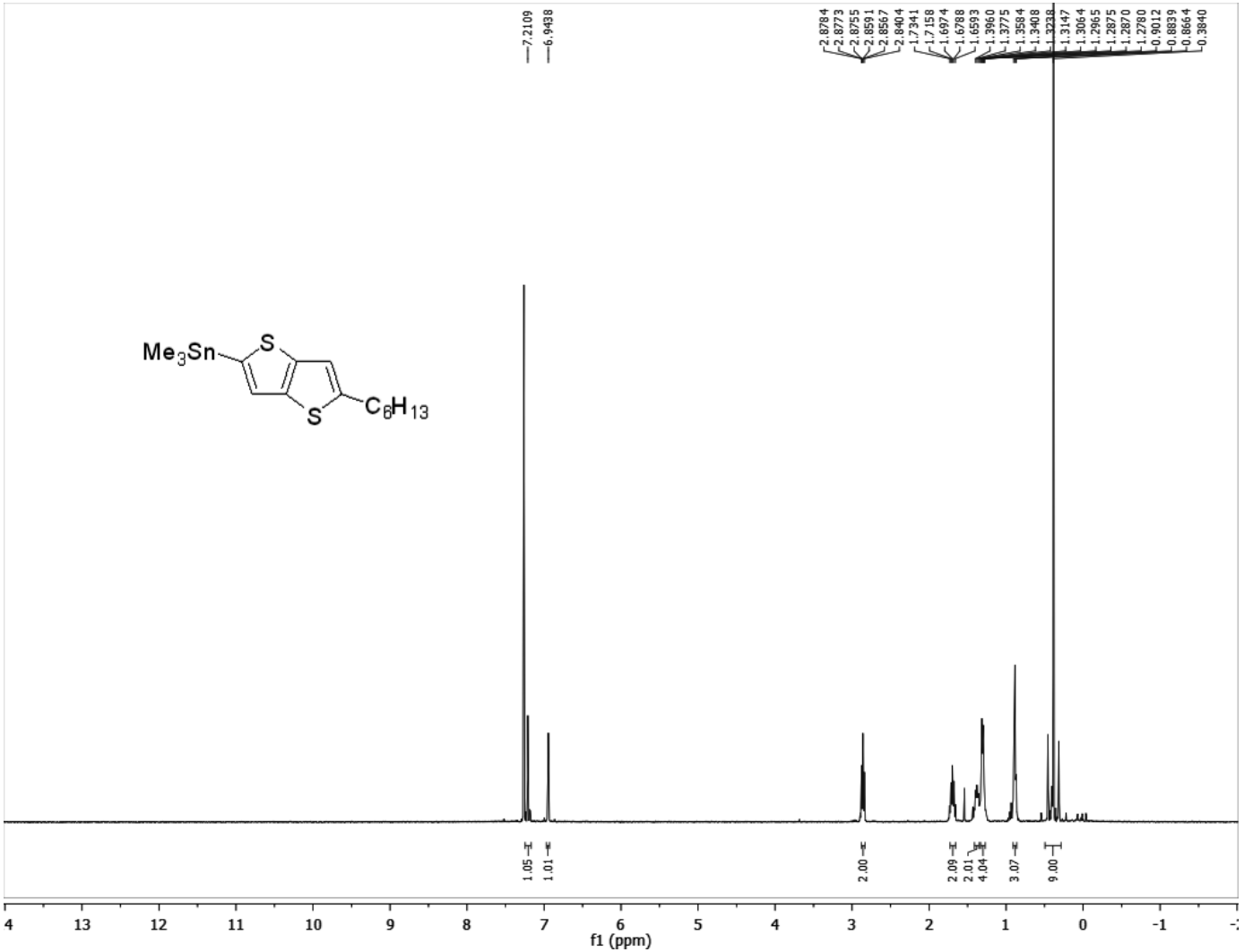


**Figure S3.4.** $^{1}$H NMR of **4**.

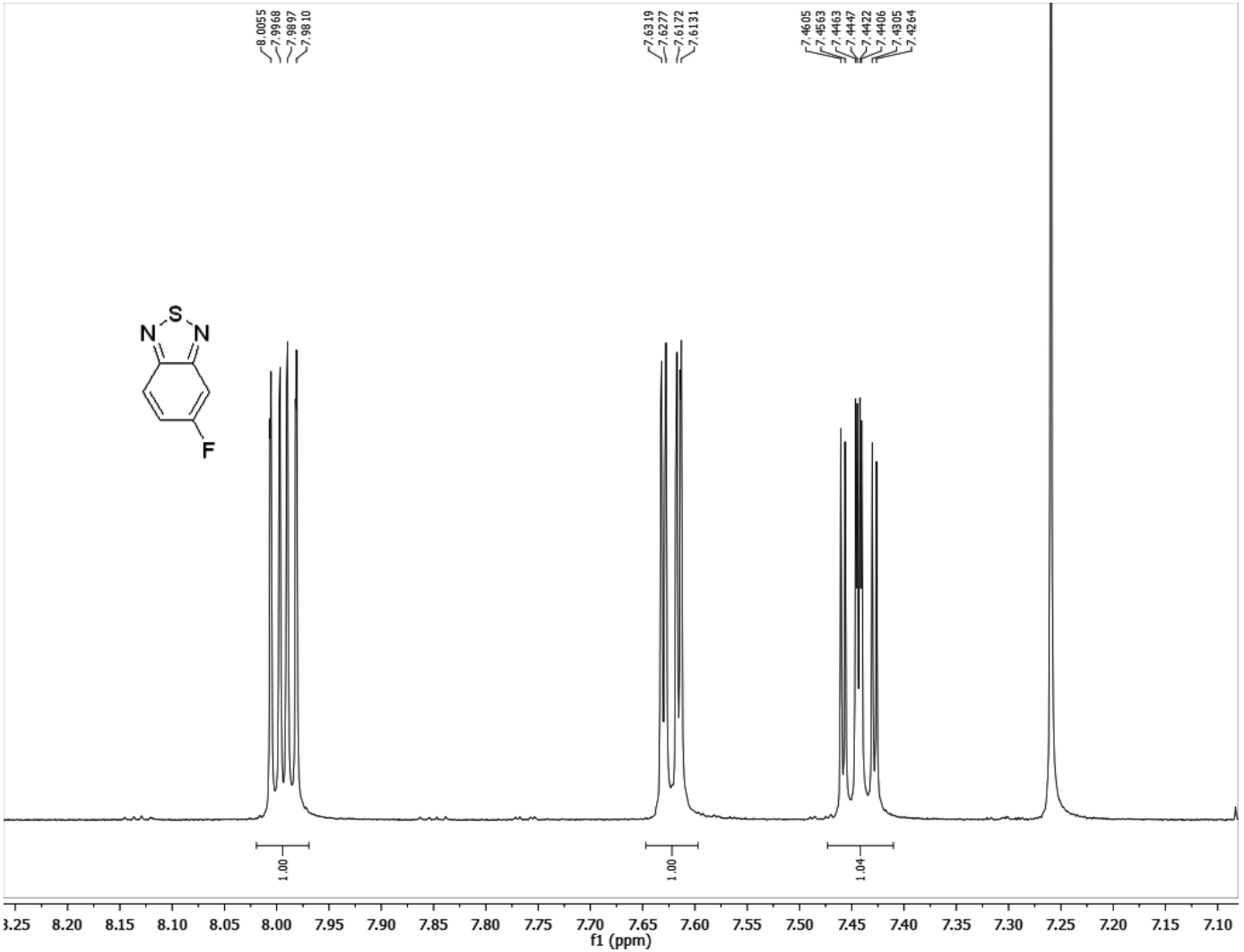


**Figure S3.5.** $^{1}$H NMR of **5**.

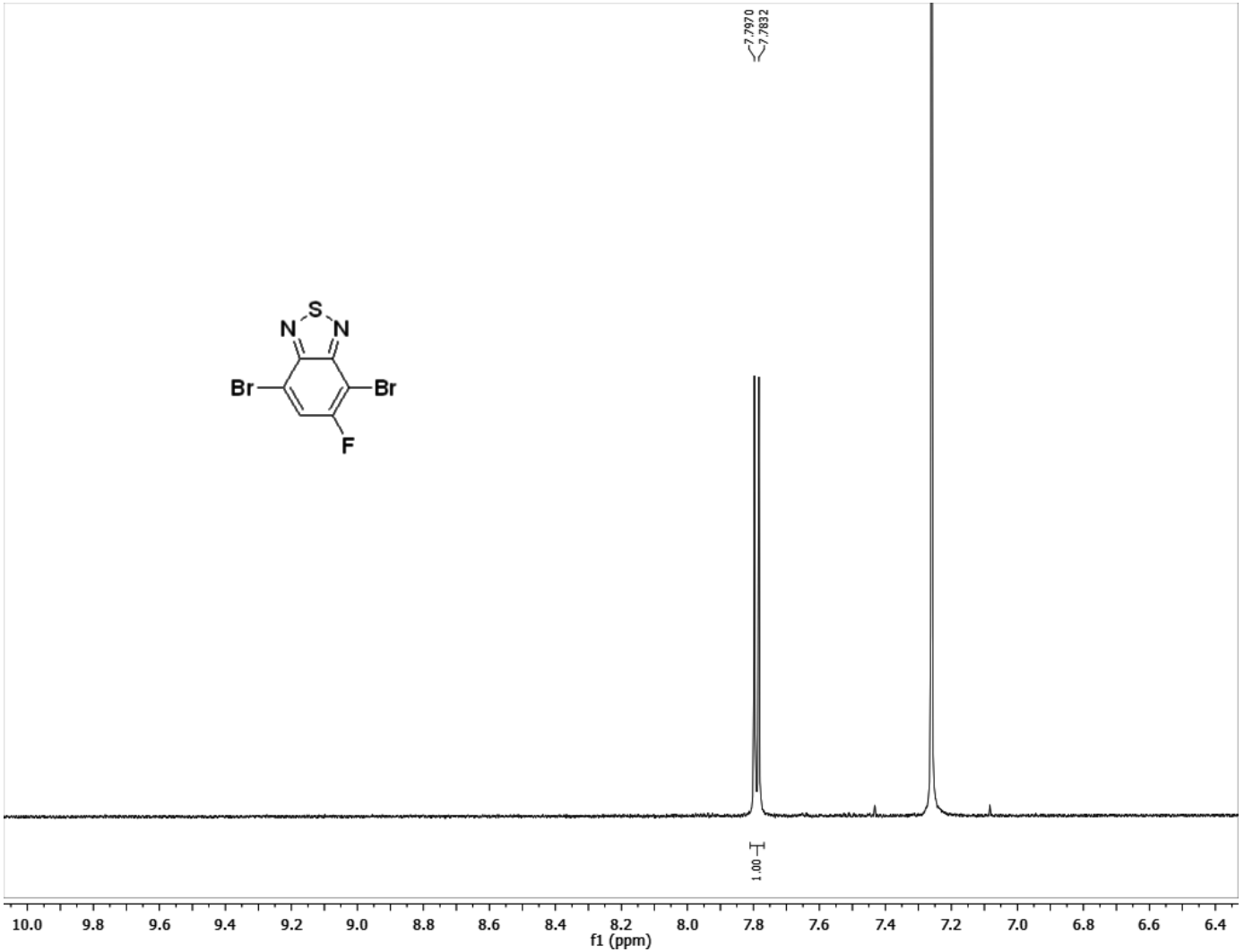


**Figure S3.6.** $^{1}$H NMR of **6**.

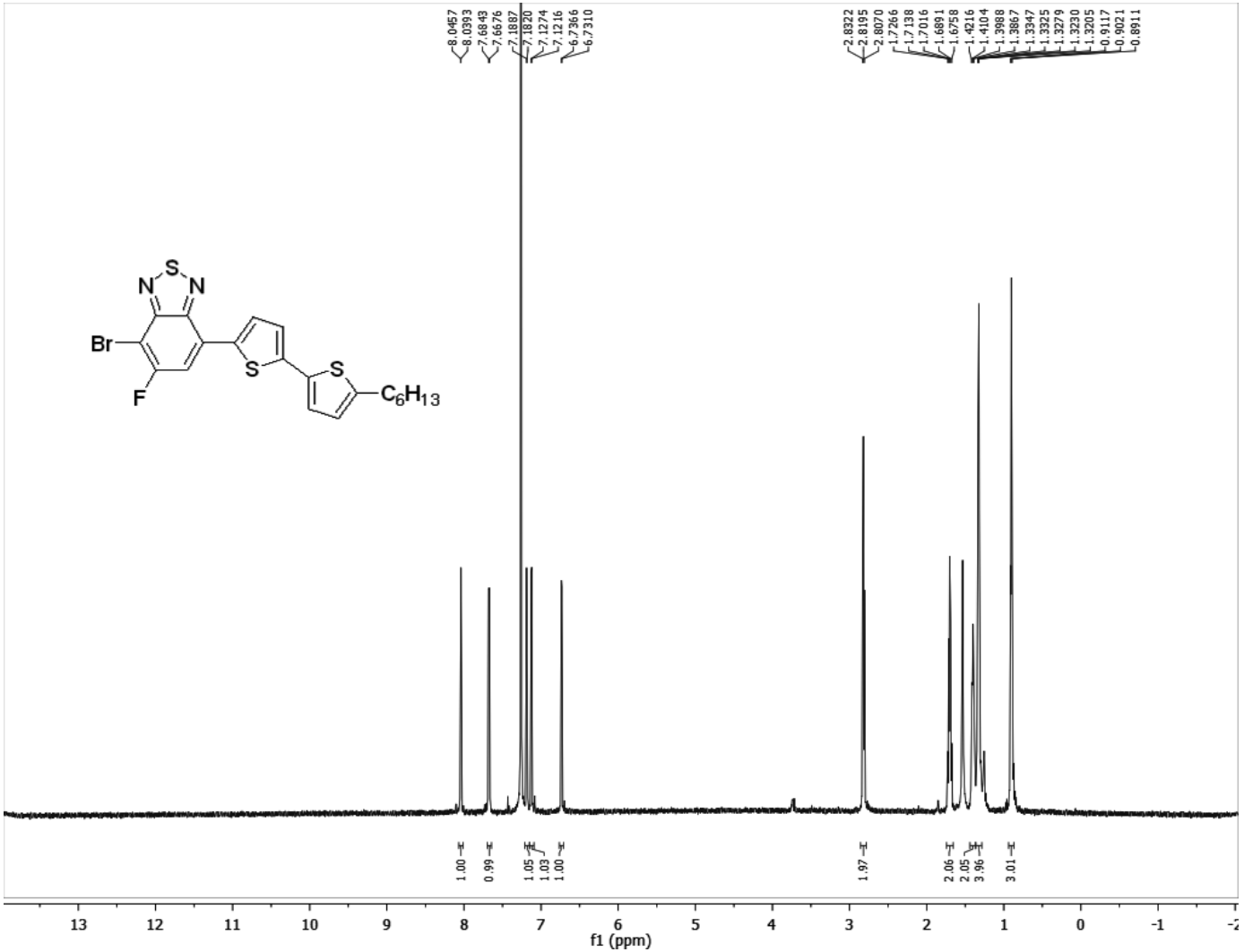


**Figure S3.7.** $^{1}$H NMR of **FBT-BT**.

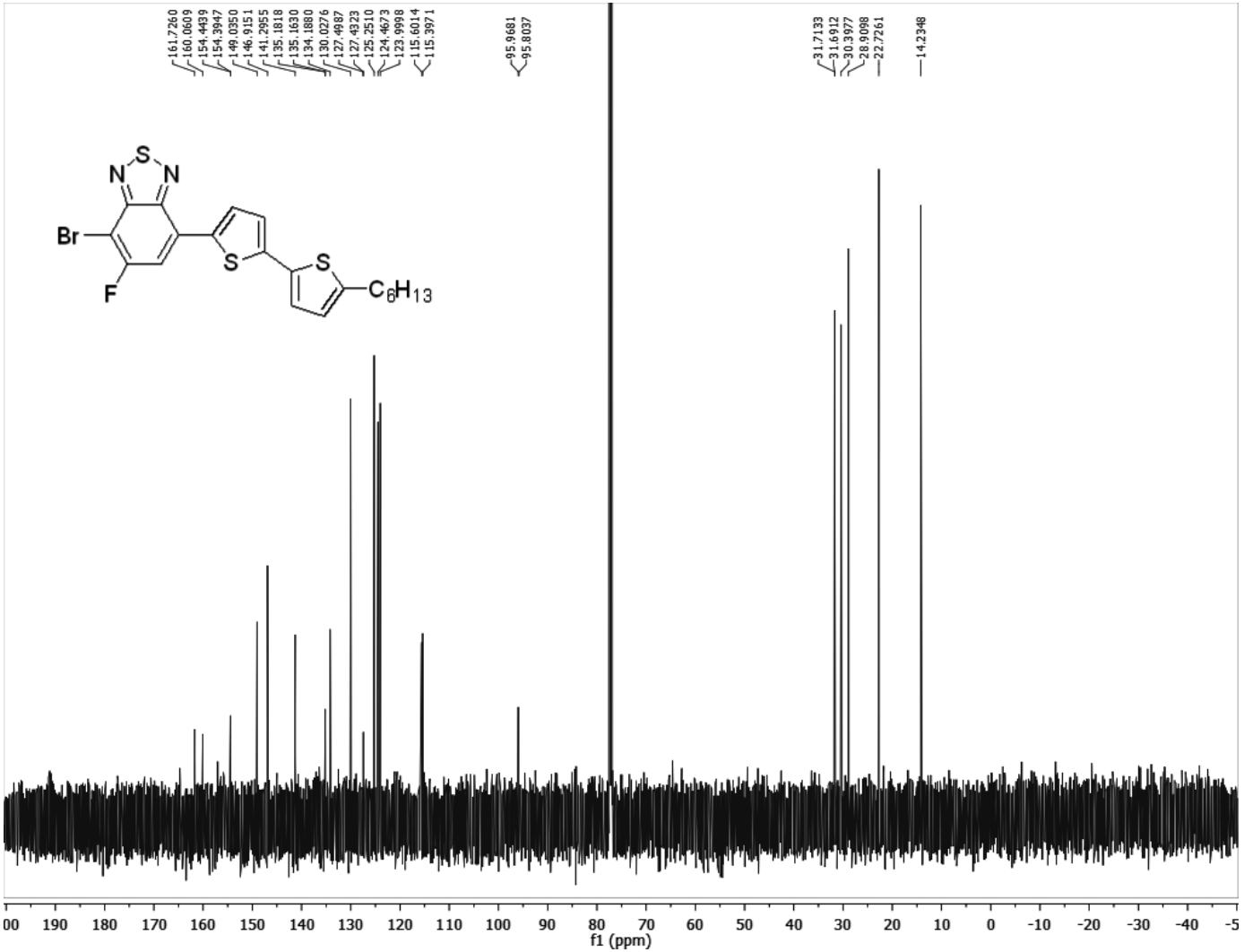


**Figure S3.8.** $^{13}$C NMR of **FBT-BT**.

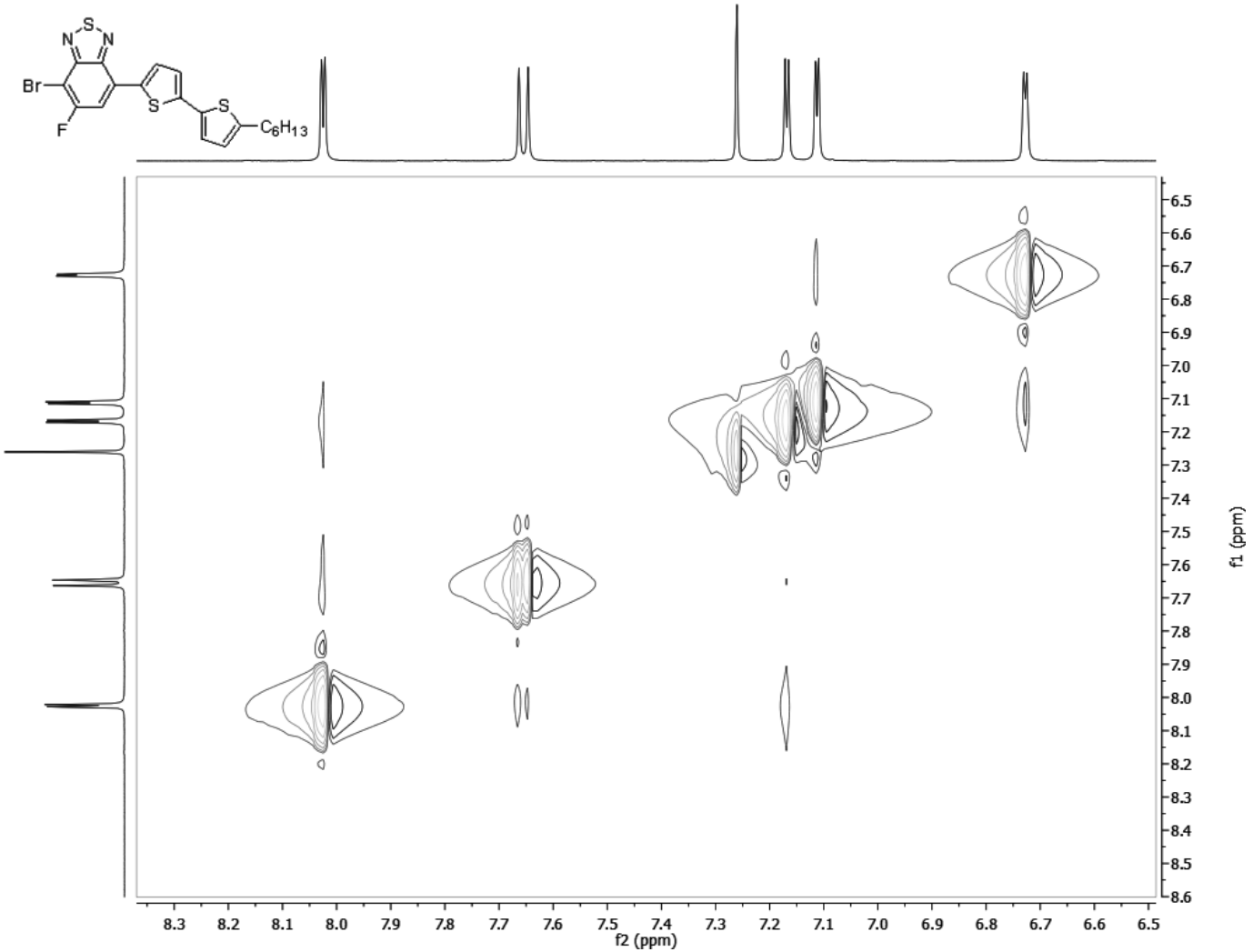


**Figure S3.9.** $^{1}$H-$^{1}$H NOESY expanded in aromatic region of **FBT-BT**.

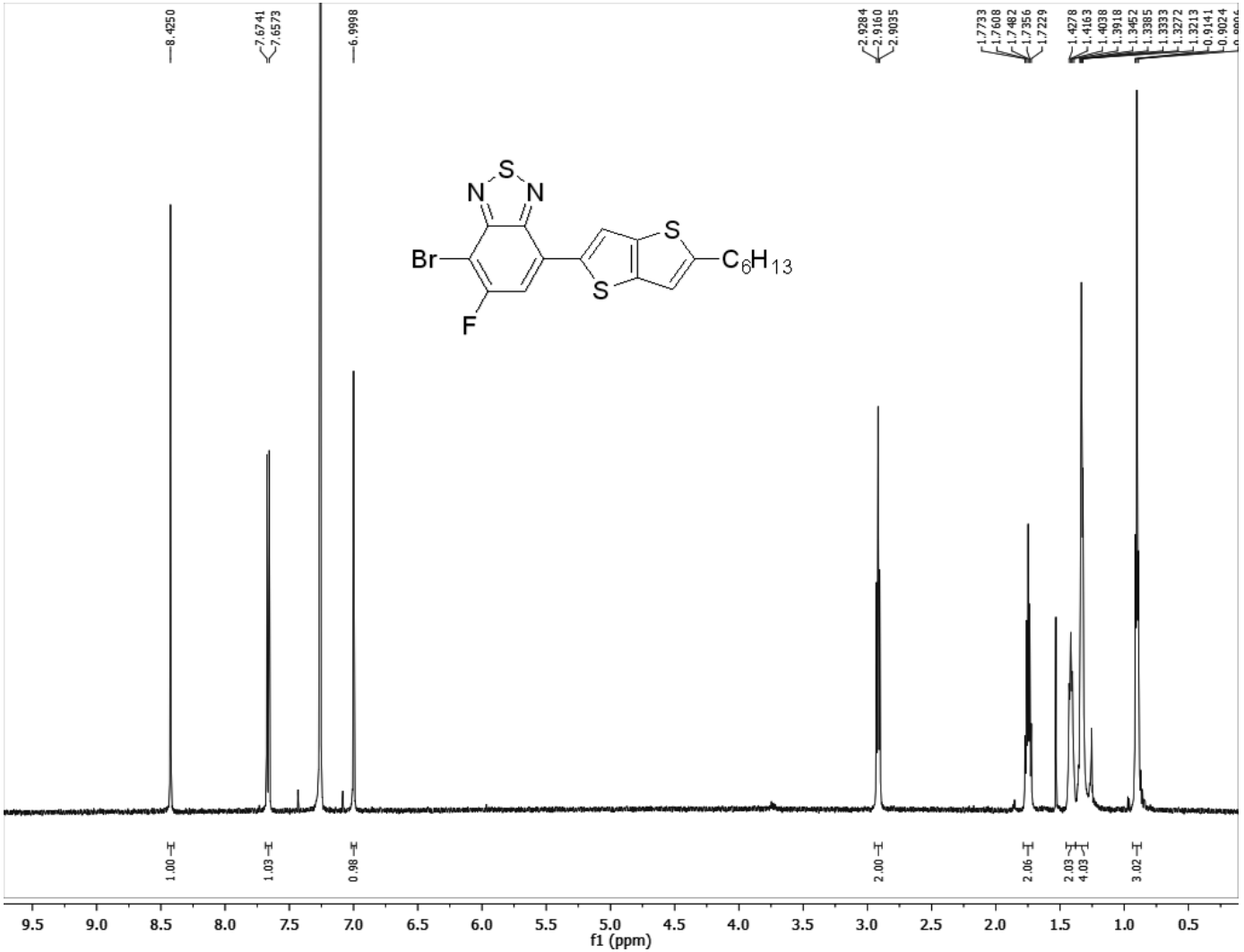


**Figure S3.10.** $^{1}$H NMR of **FBT-TT.**

-

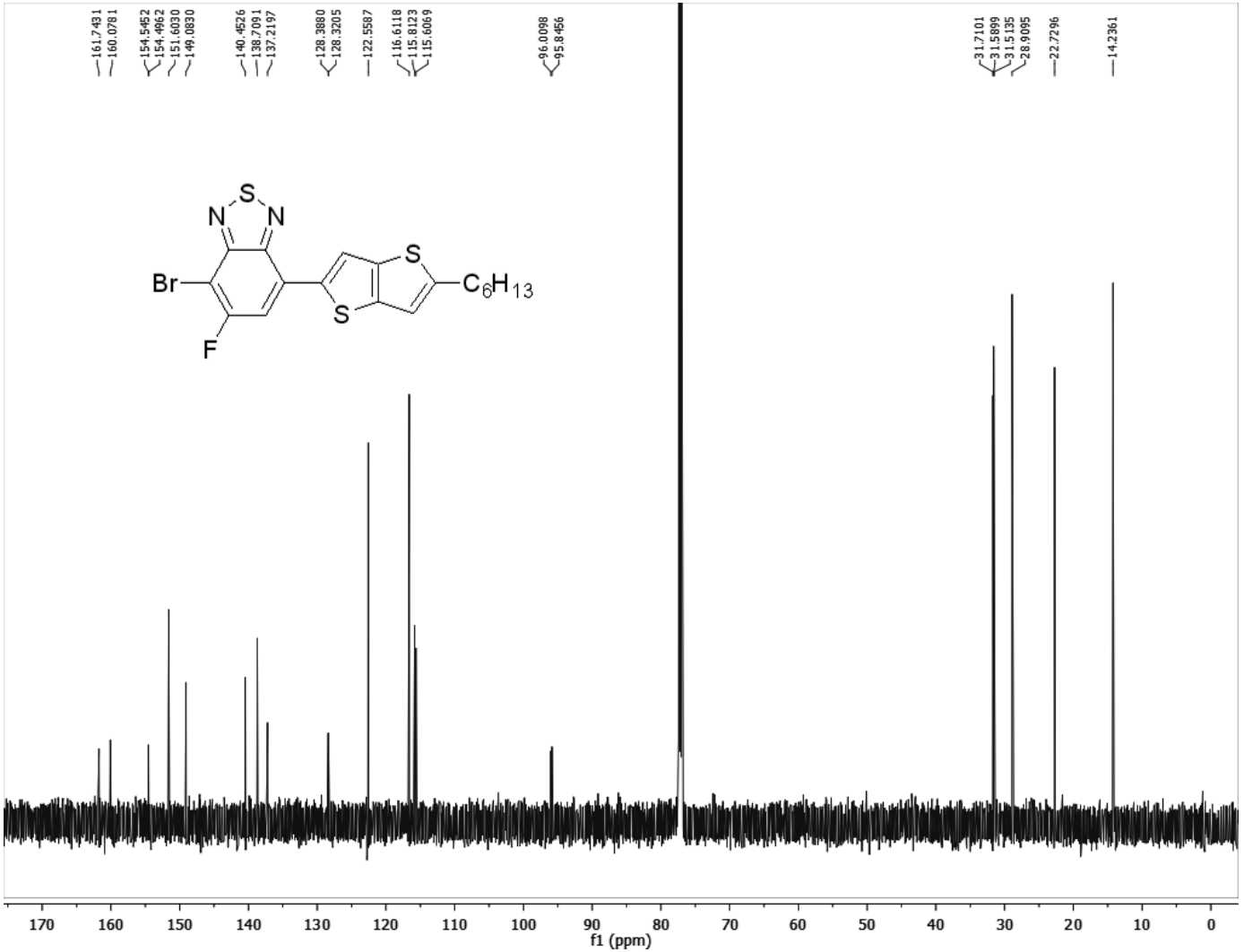


**Figure S3.11.** $^{13}$C NMR of **FBT-TT**.

-

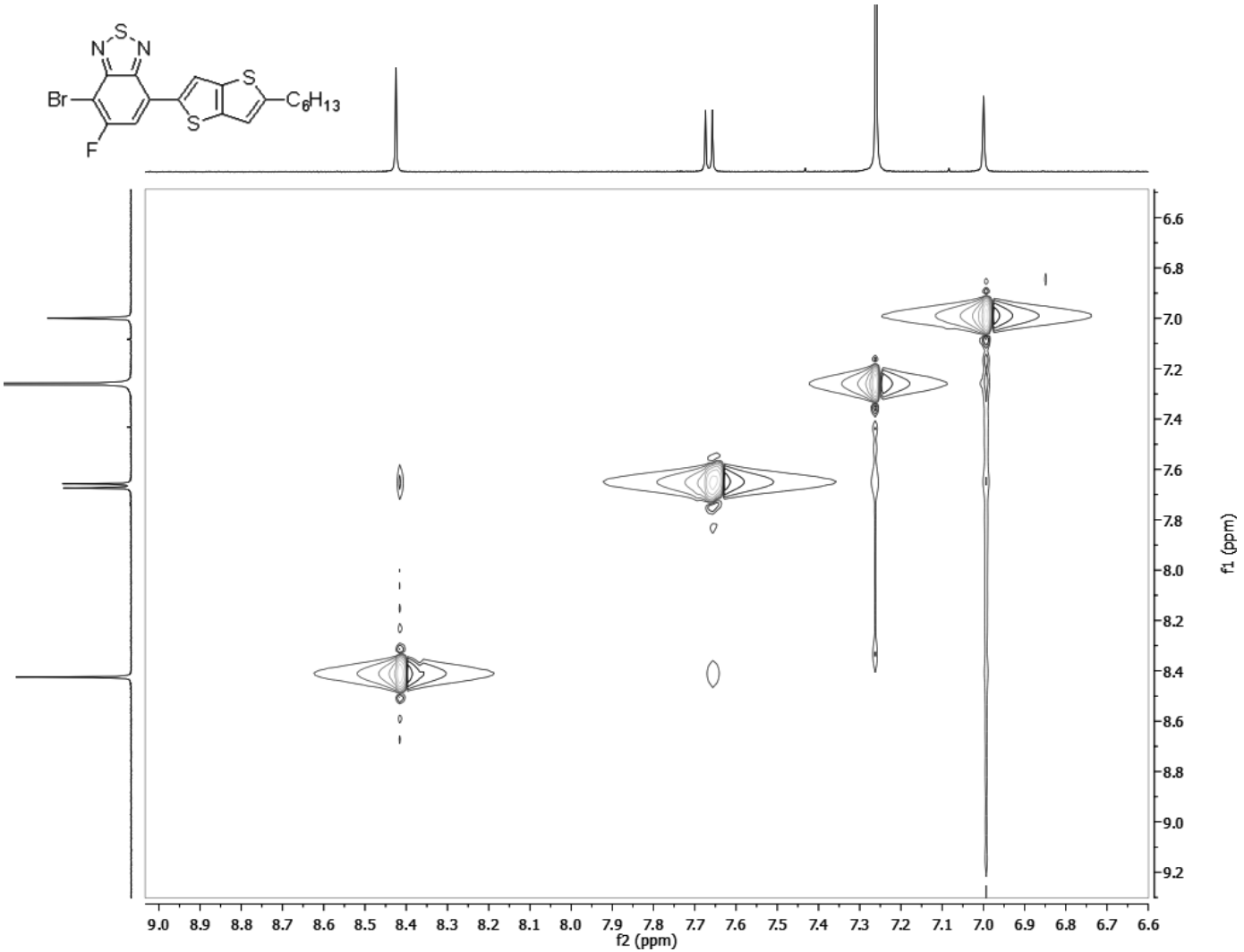


**Figure S3.12.** $^{1}$H-$^{1}$H NOESY expanded in aromatic region of **FBT-TT**.

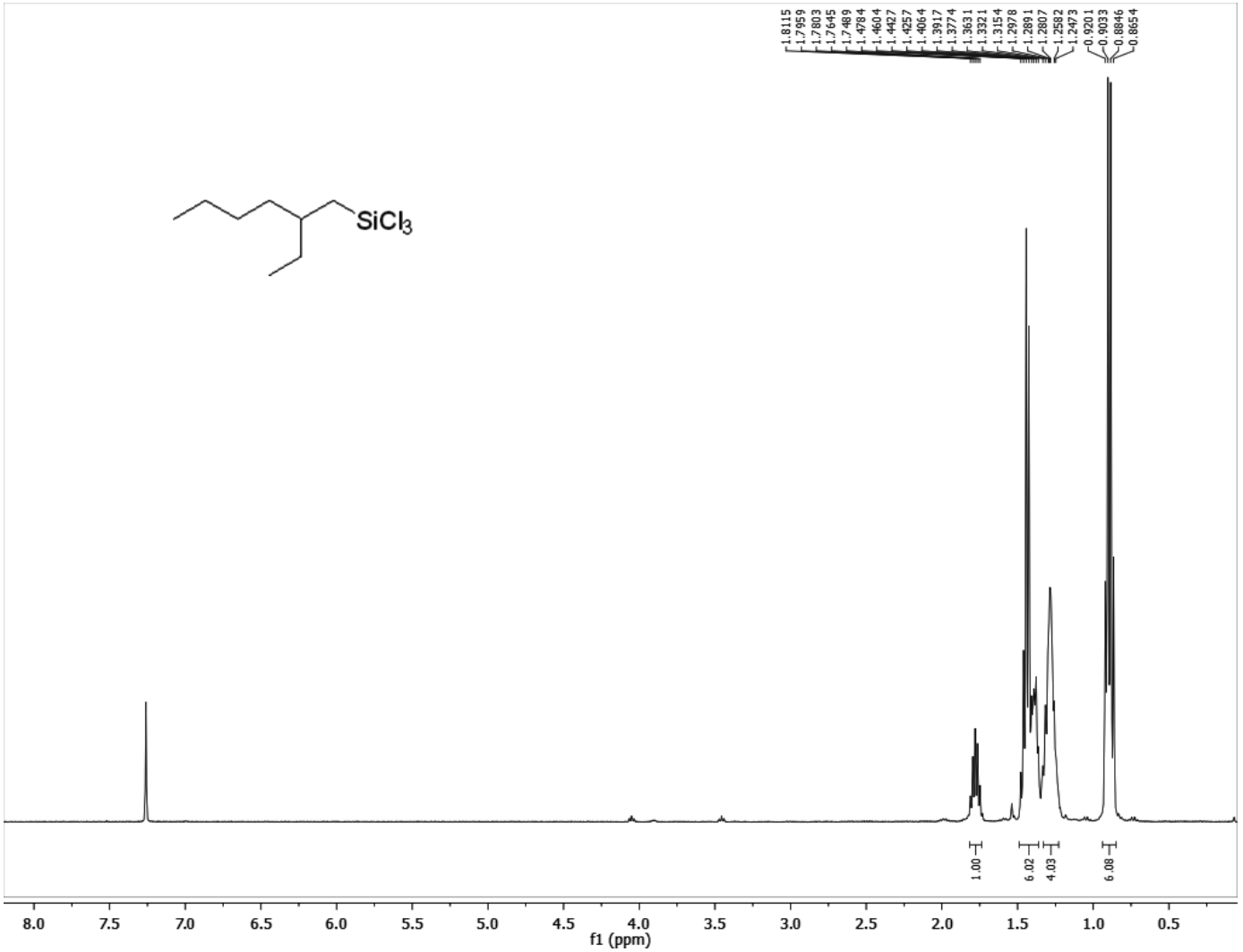


**Figure S3.13.** $^{1}$H NMR of **7**.

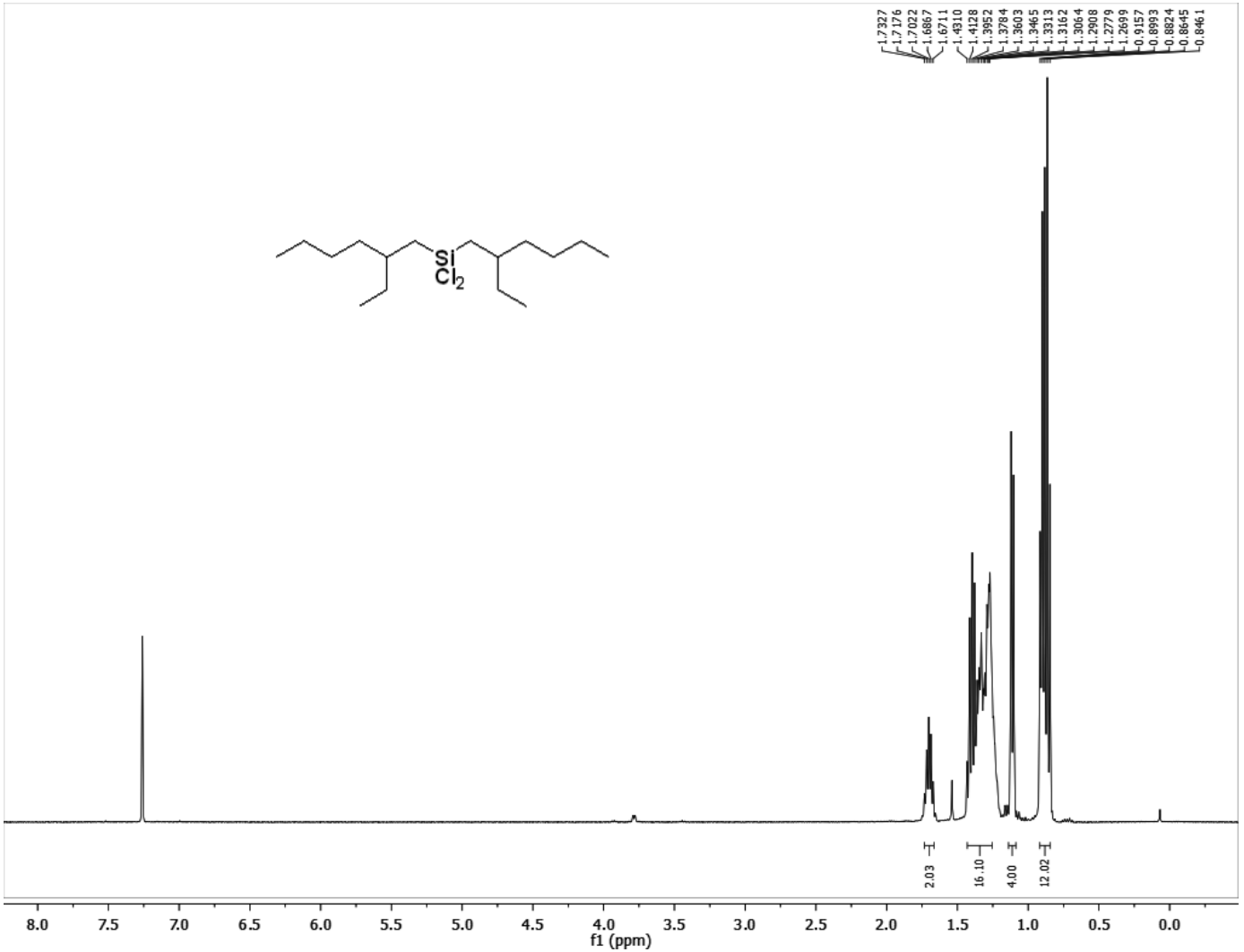


**Figure S3.14.** $^{1}$H NMR of **8**.

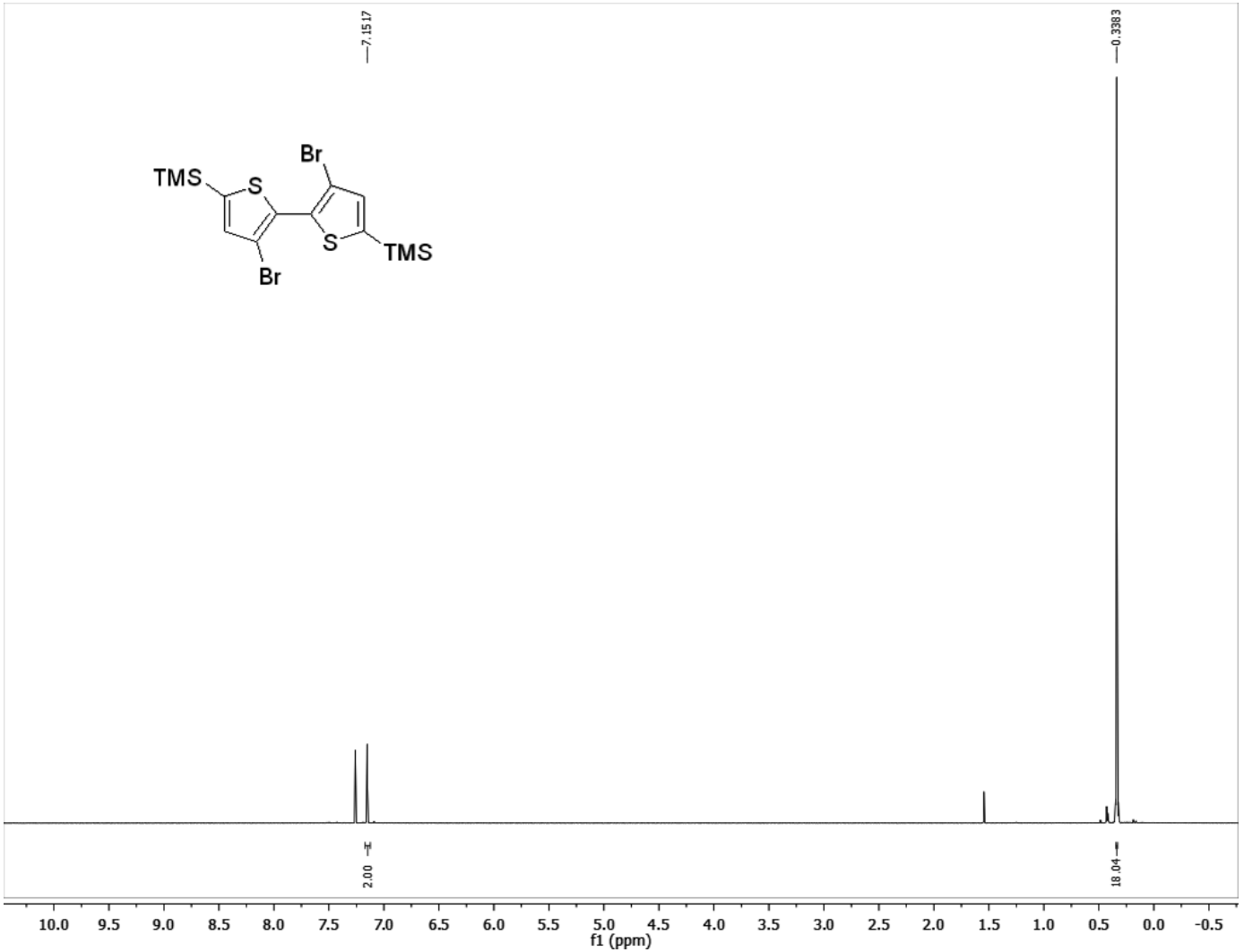


**Figure S3.15.** $^{1}$H NMR of **9**.

-

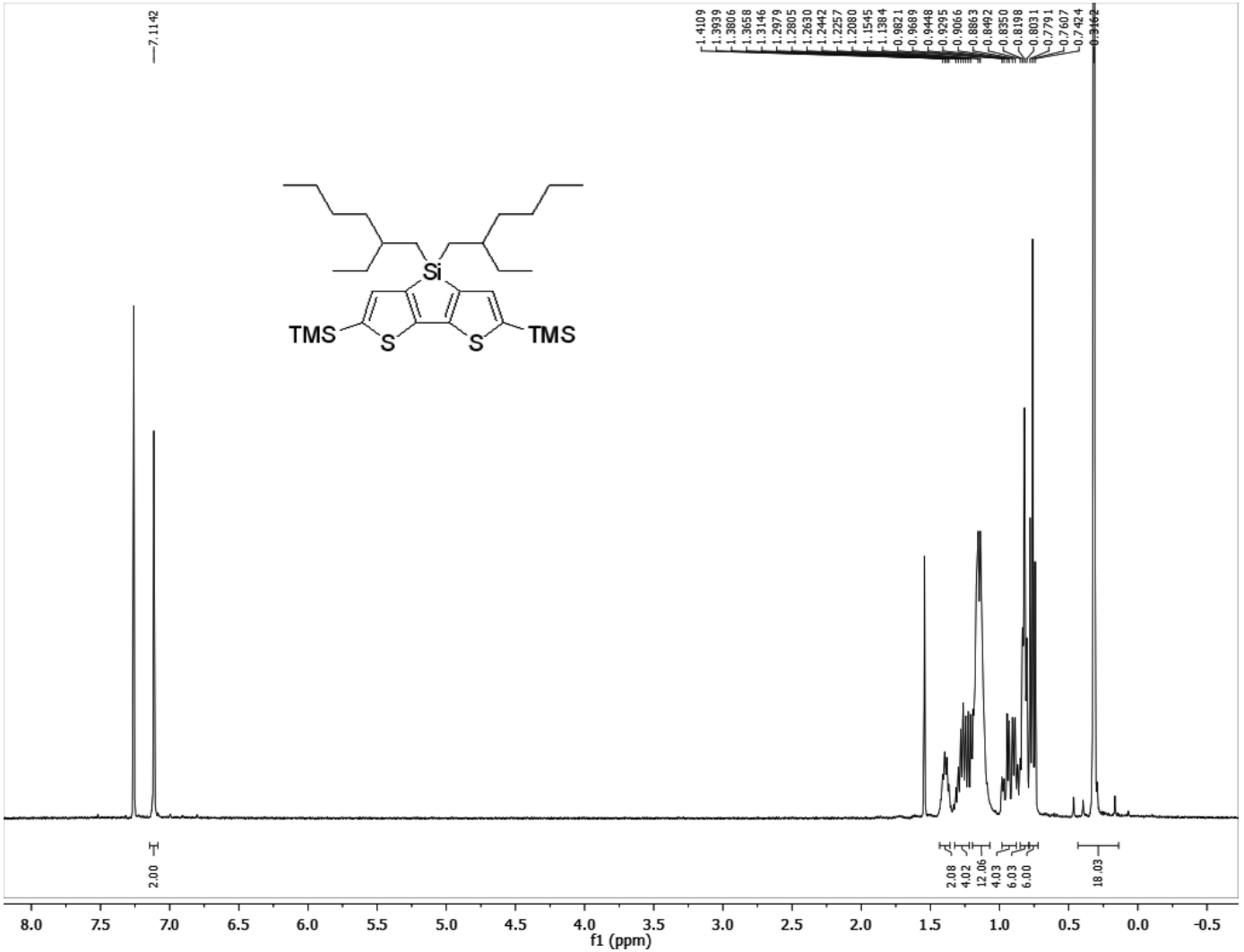


**Figure S3.16.** $^{1}$H NMR of **10**.

-

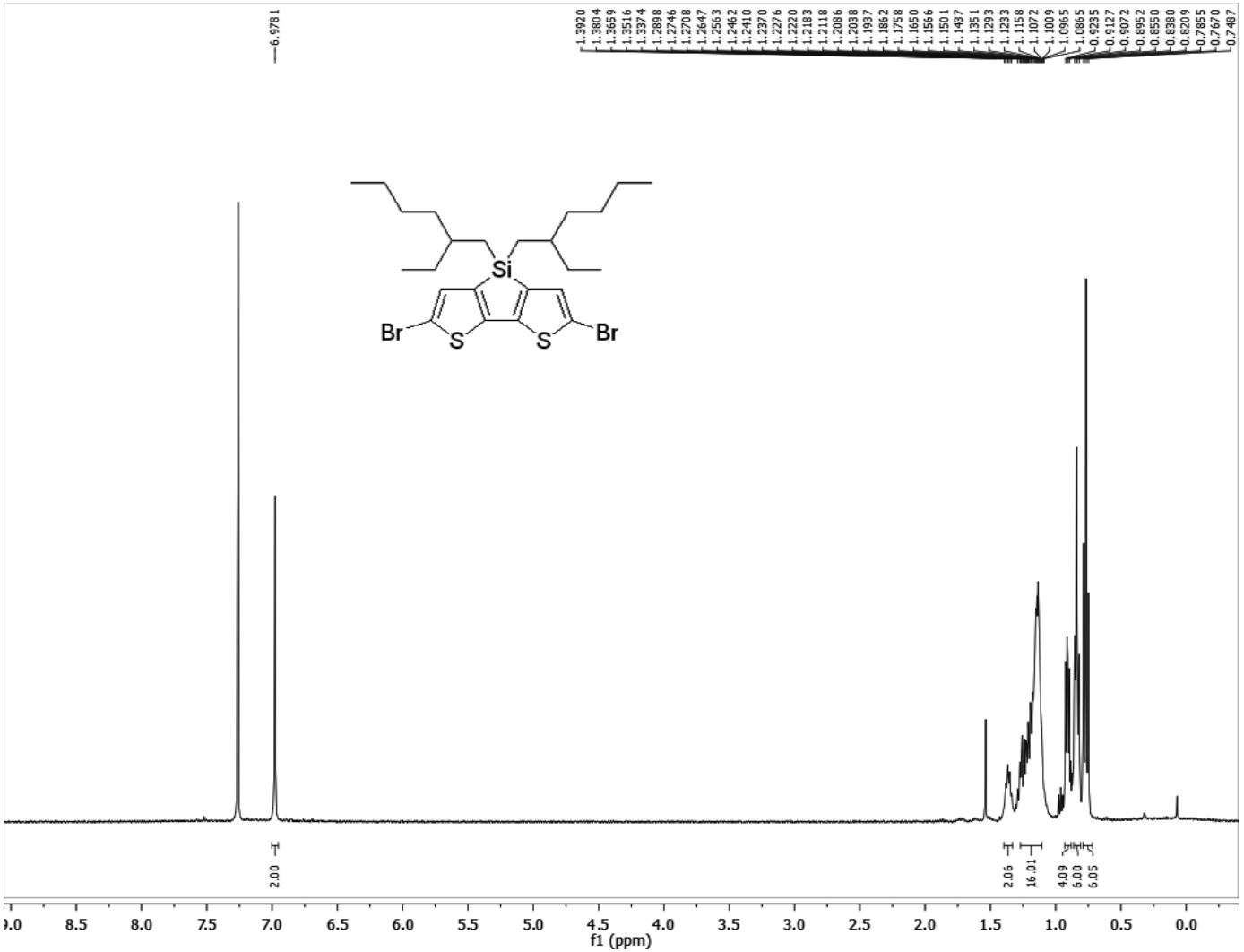


**Figure S3.17.** $^{1}$H NMR of **11**.

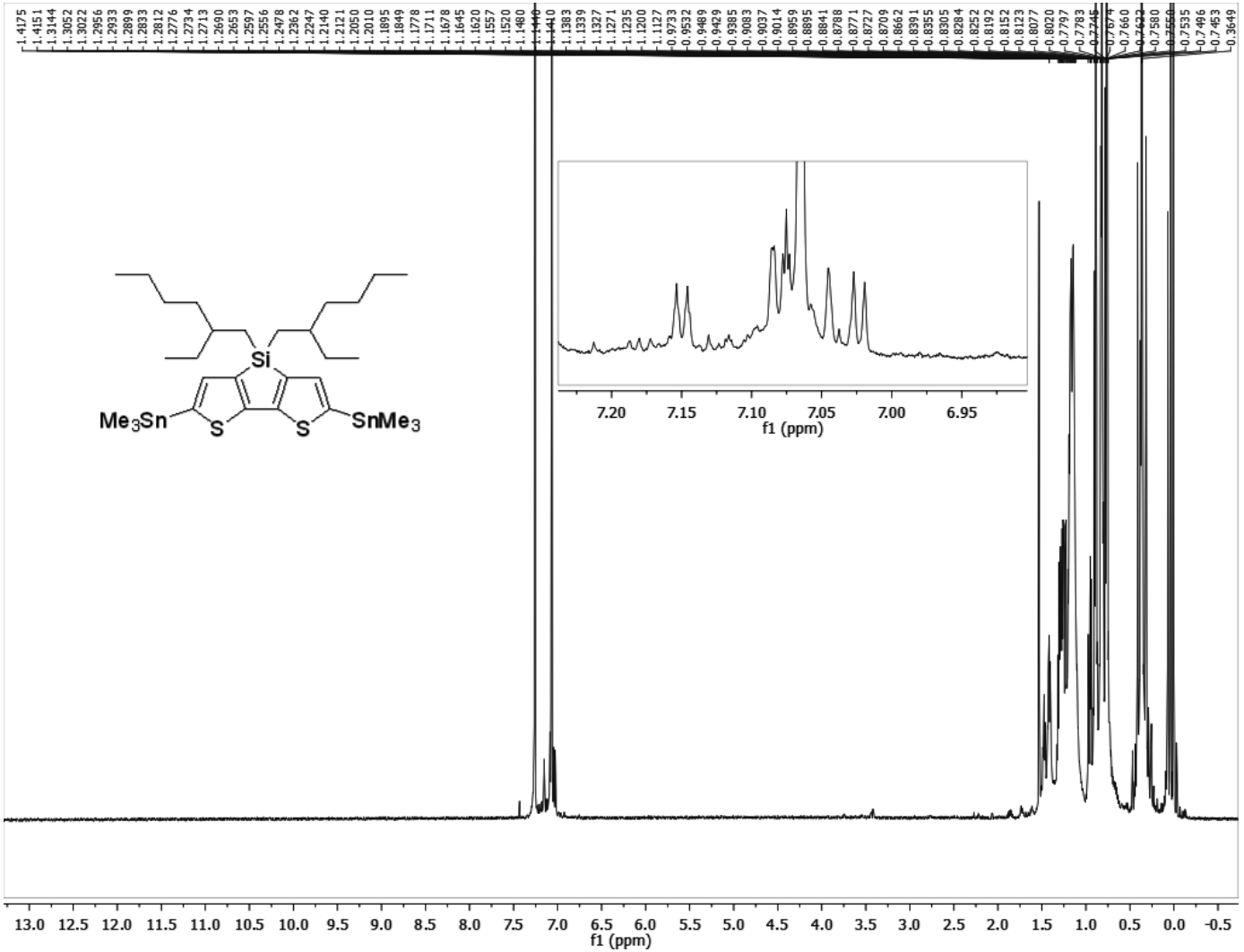


**Figure S3.18.** $^{1}$H NMR of **DTS** (crude) with inset of aromatic region.

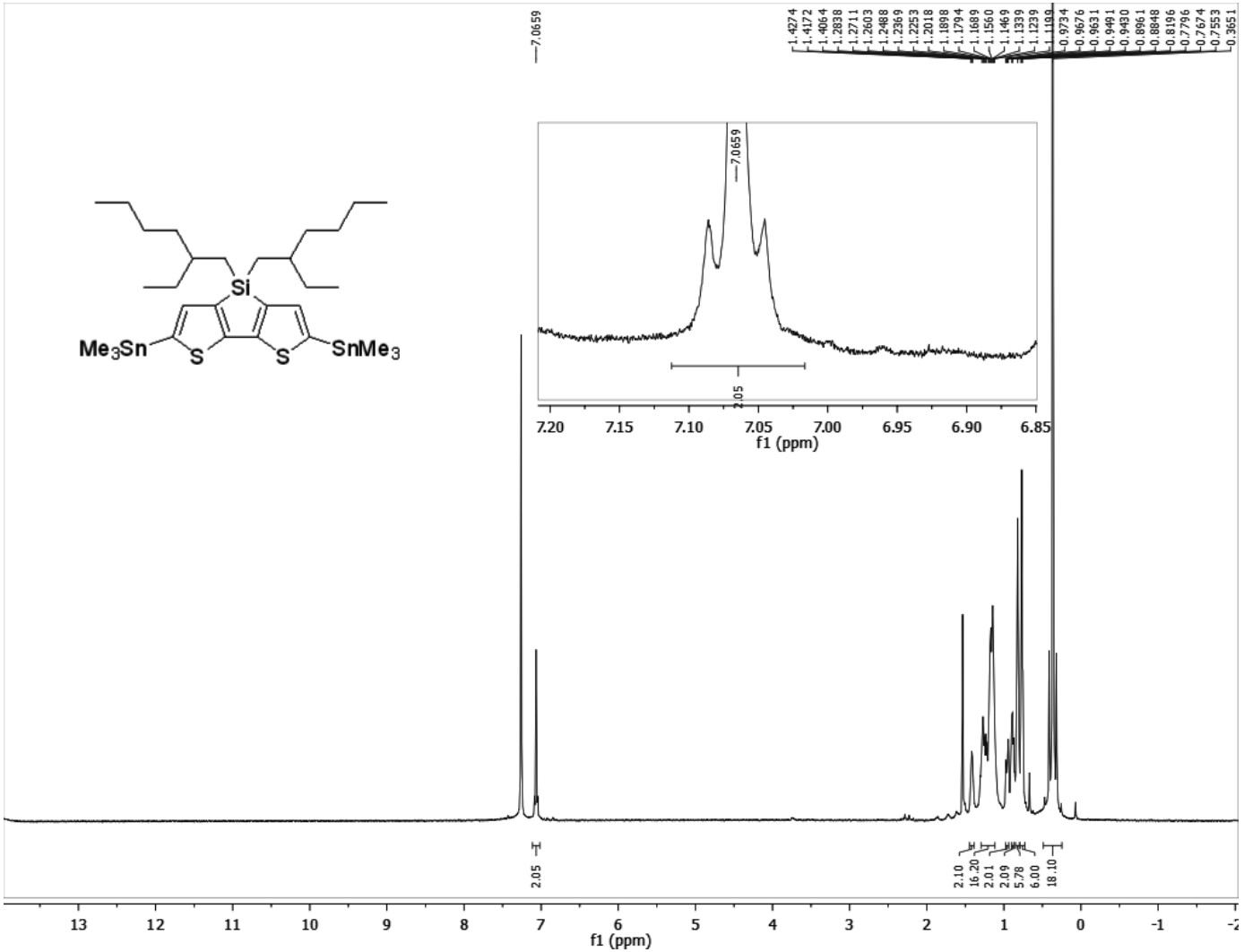


**Figure S3.19.** $^{1}$H NMR of **DTS** (HPLC purified) with inset of aromatic region.

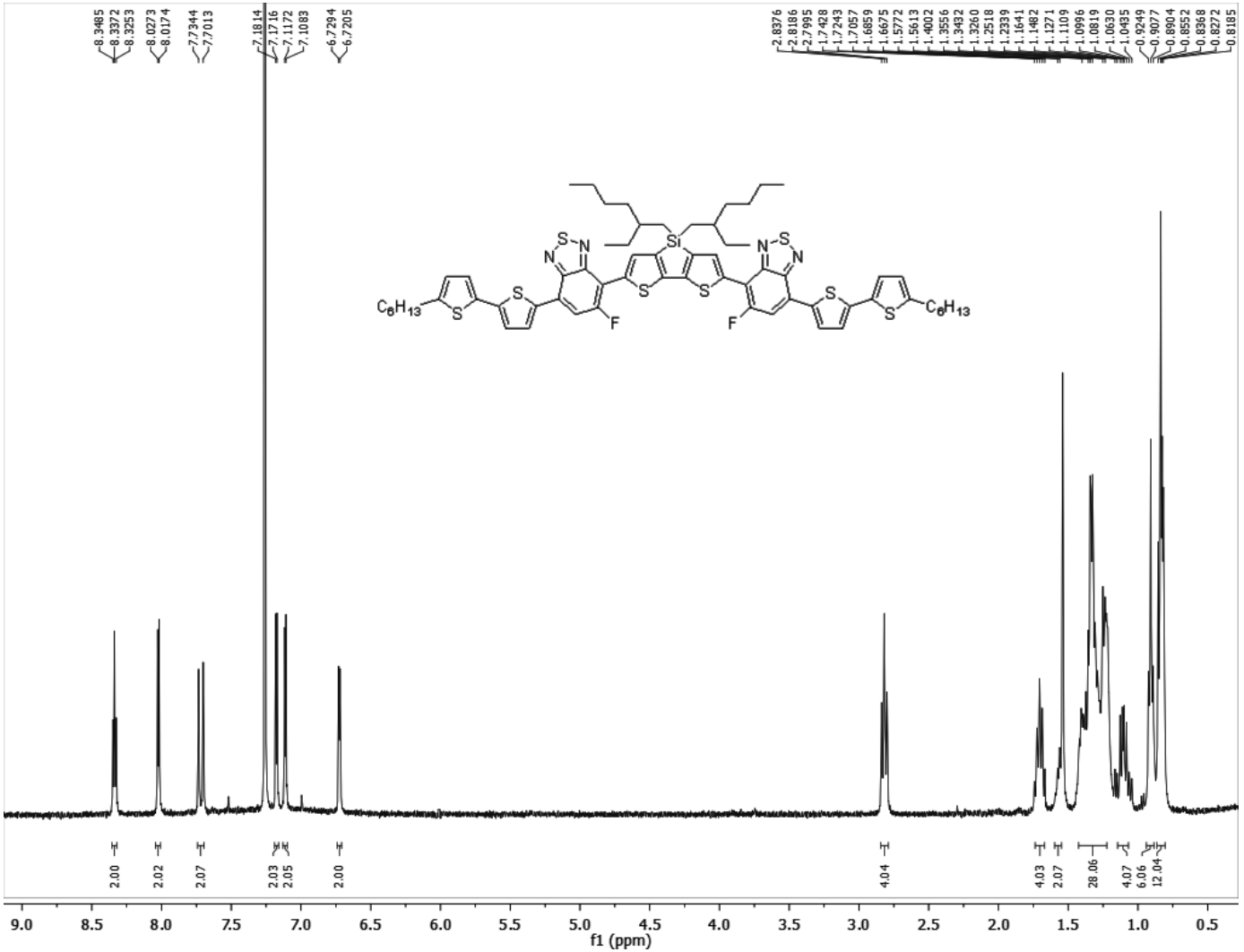


**Figure S3.20.** $^{1}$H NMR of **DTS-FBT-BT**.

-

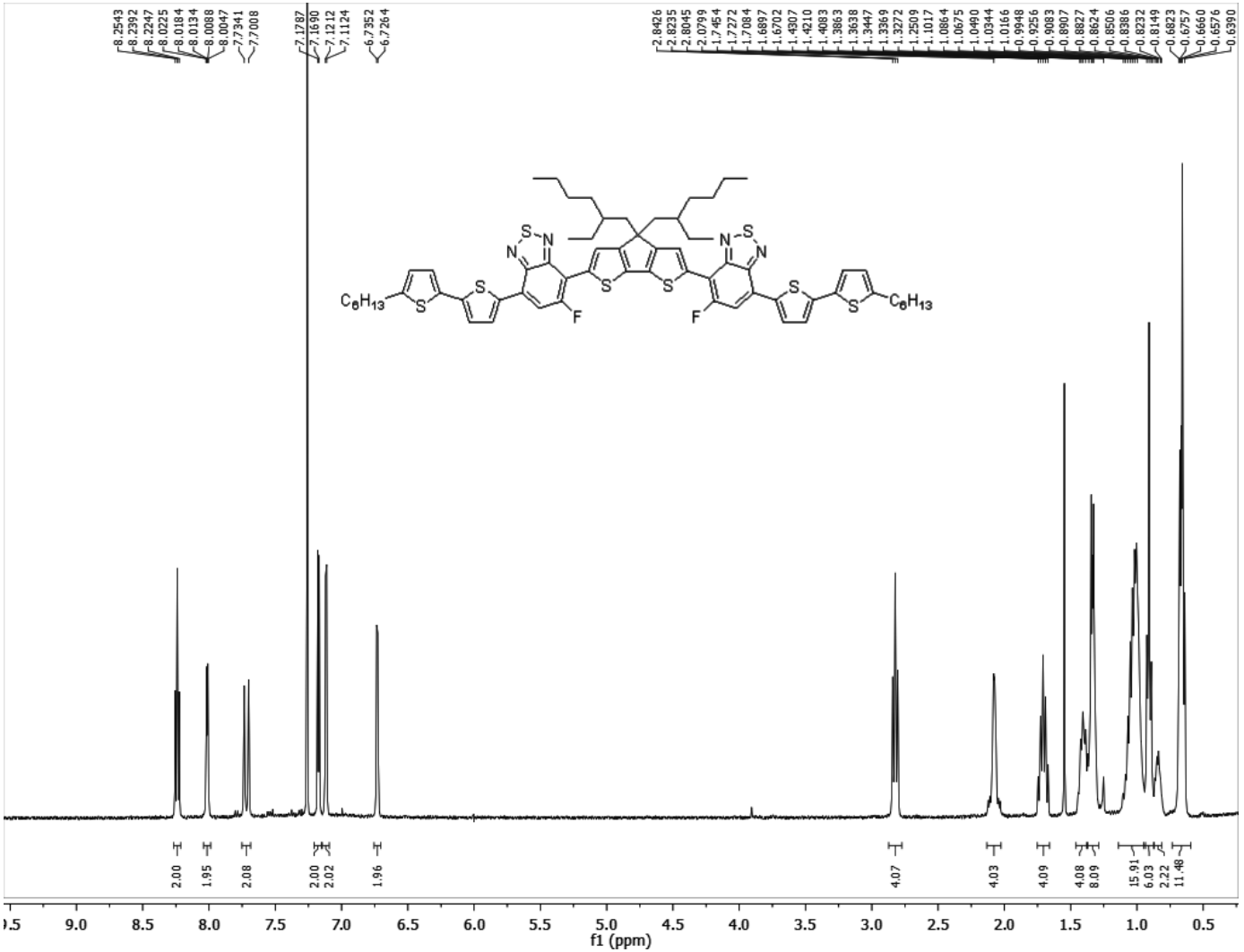


**Figure S3.21.** $^{1}$H NMR of **CPDT-FBT-BT**.

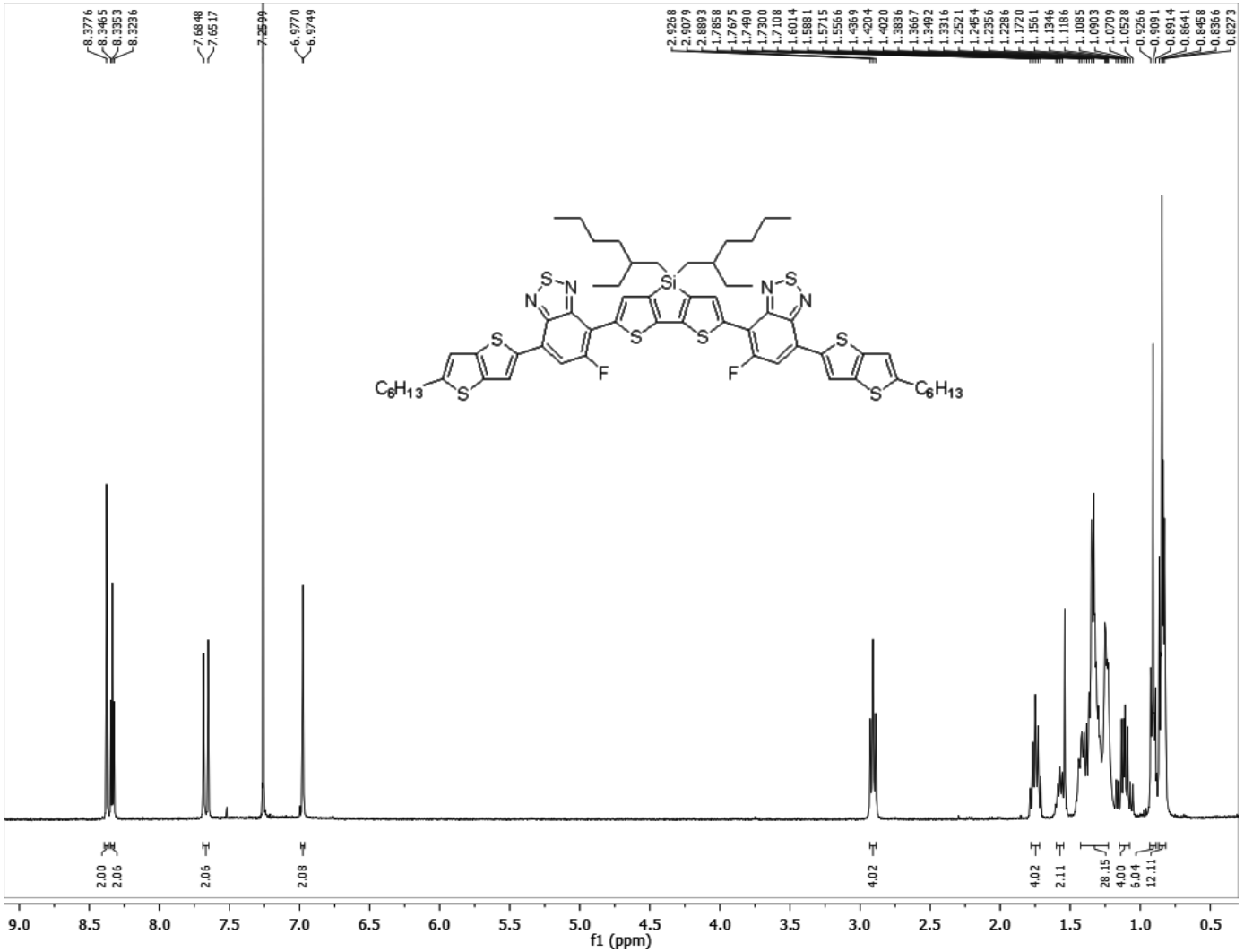


**Figure S3.22.** $^{1}$H NMR of **DTS-FBT-TT**.

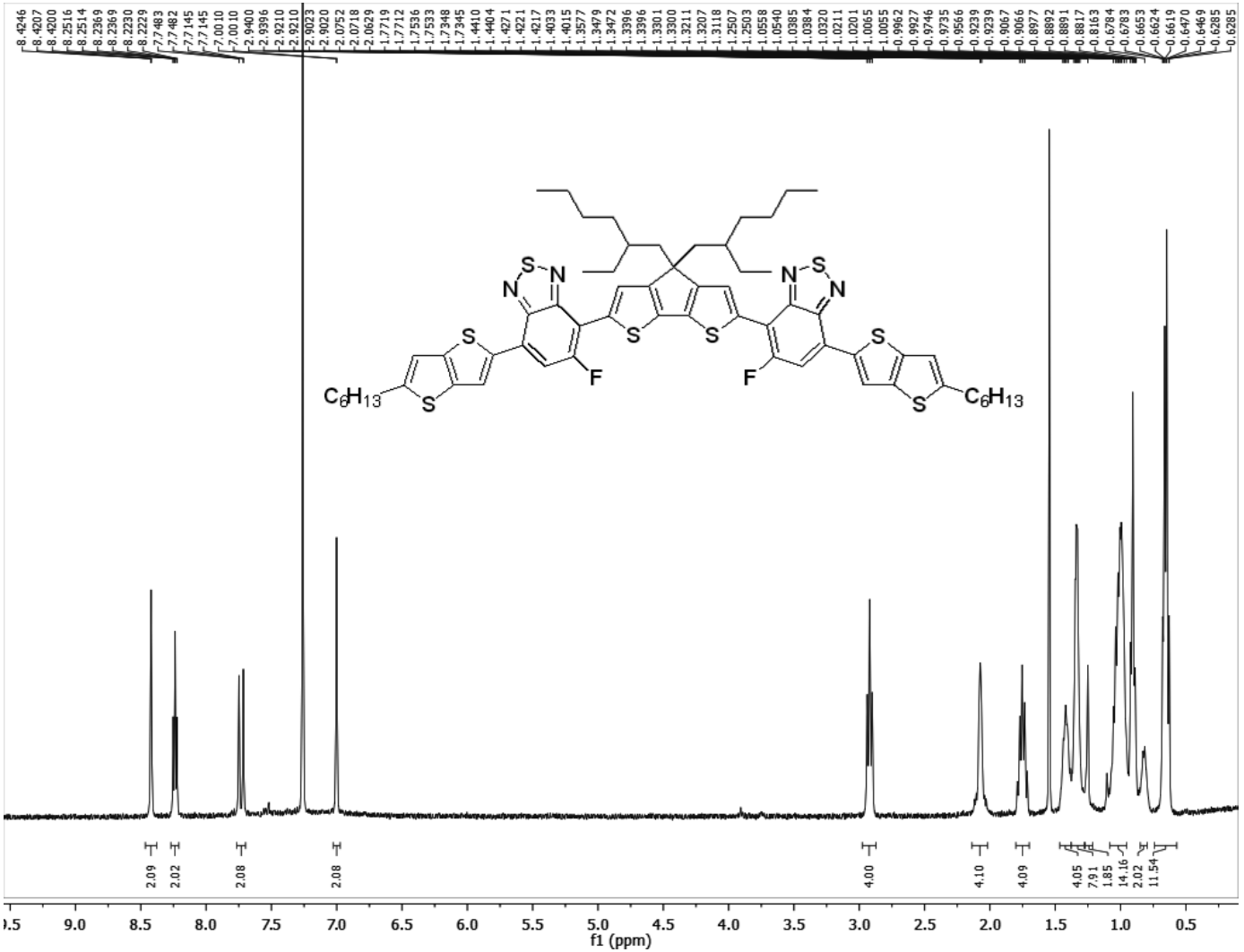


**Figure S3.23.** $^{1}$H NMR of **CPDT-FBT-TT**.

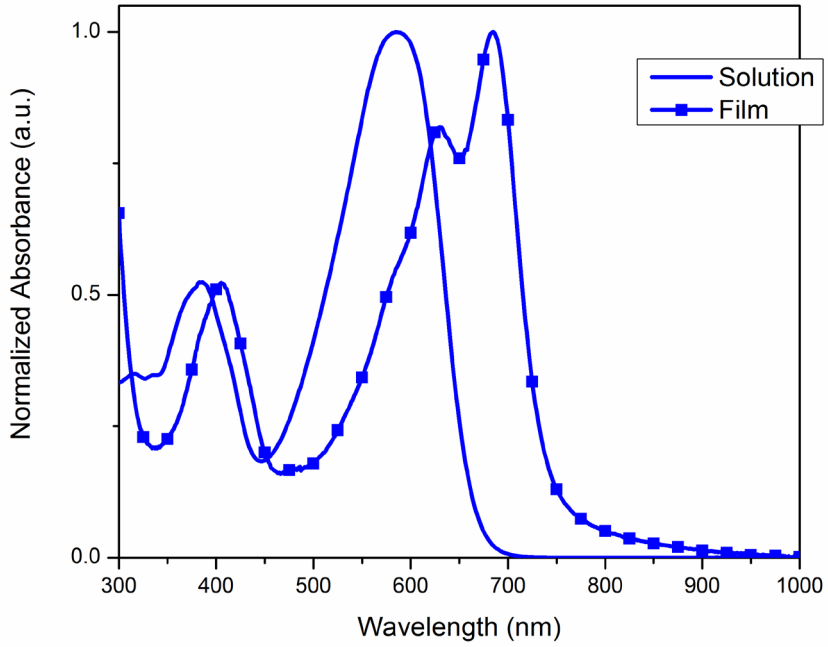


**Figure S3.24.** UV-vis absorption of DTS-FBT-BT in $CHCl_3$ and thin film.

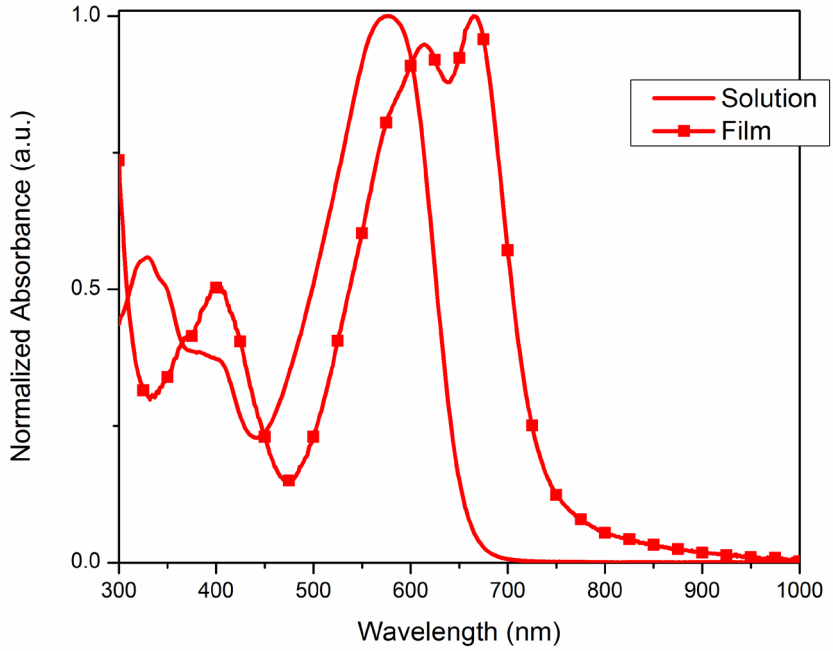


**Figure S3.25.** UV-vis absorption of DTS-FBT-TT in $CHCl_3$ and thin film.

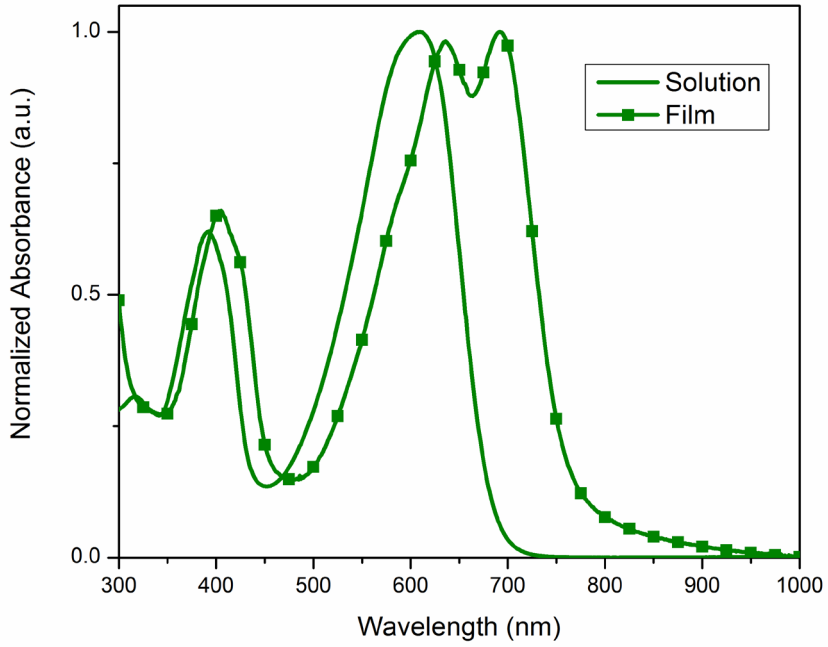


**Figure S3.26.** UV-vis absorption of CPDT-FBT-BT in $CHCl_3$ and thin film.

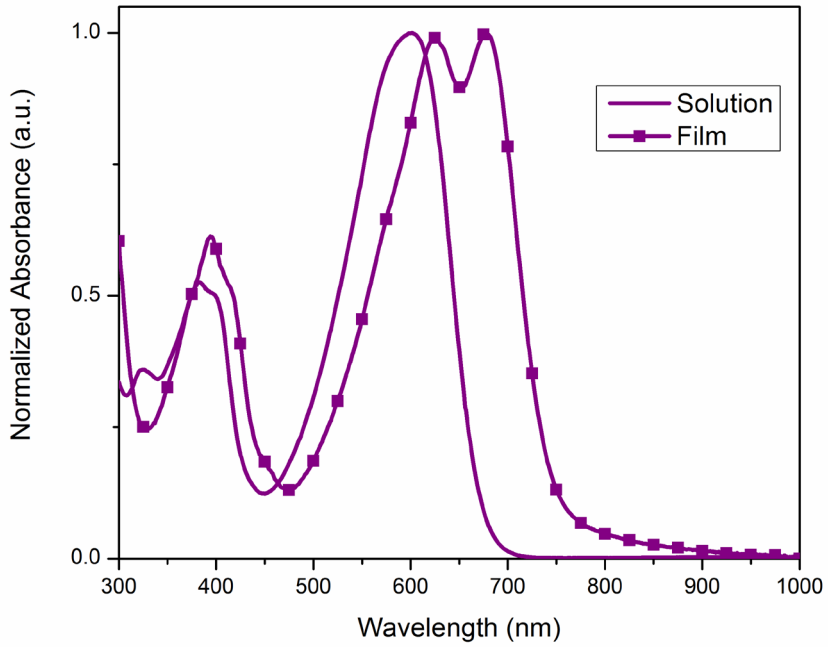


**Figure S3.27.** UV-vis absorption of CPDT-FBT-TT in $CHCl_3$ and thin film.

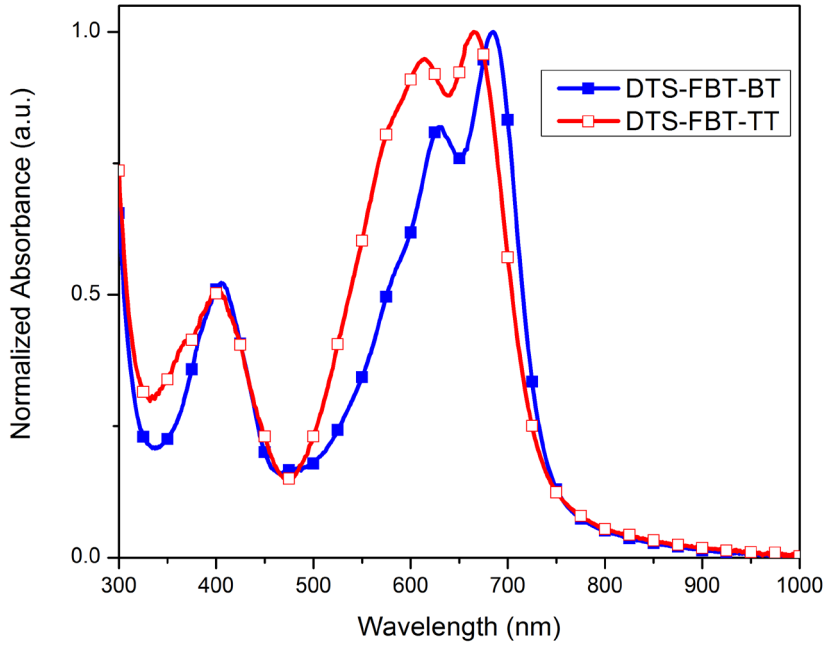


**Figure S3.28.** Thin film UV-vis comparison of D1 with DTS core.

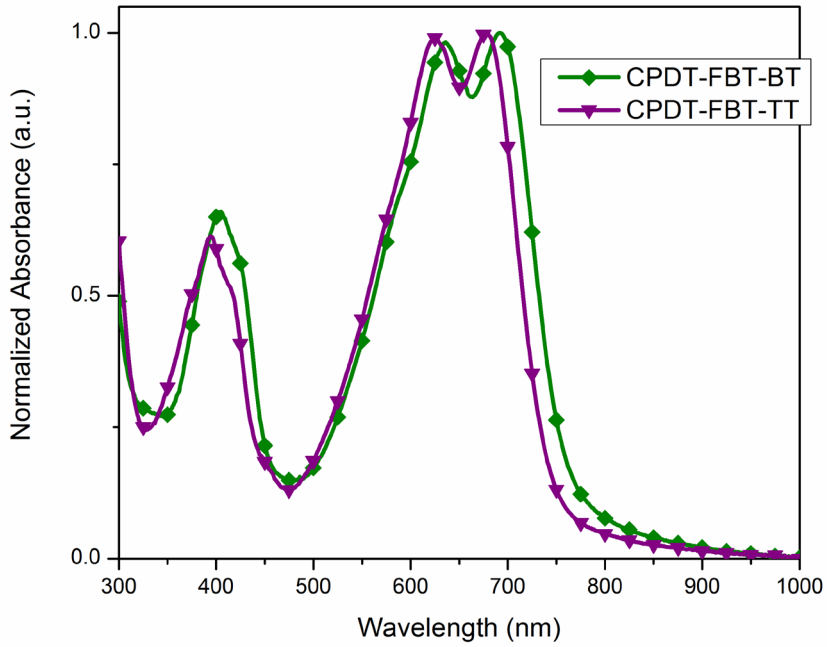


**Figure S3.29.** Thin film UV-vis comparison of D1 with CPDT core.

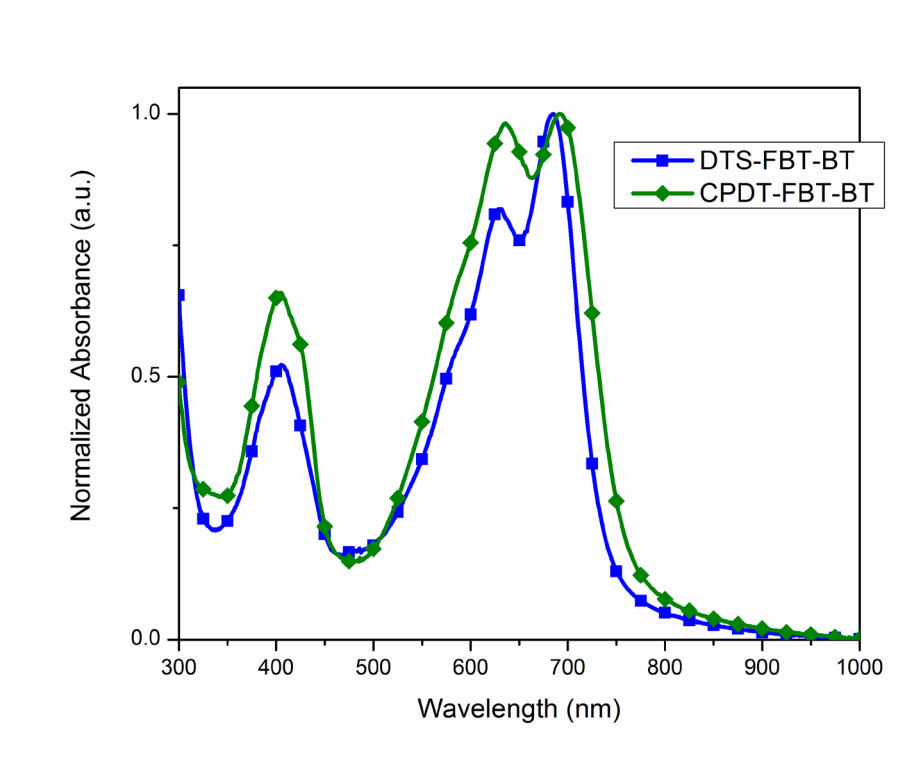


**Figure S3.30.** Thin film UV-vis comparison of D2 with FBT-BT side group.

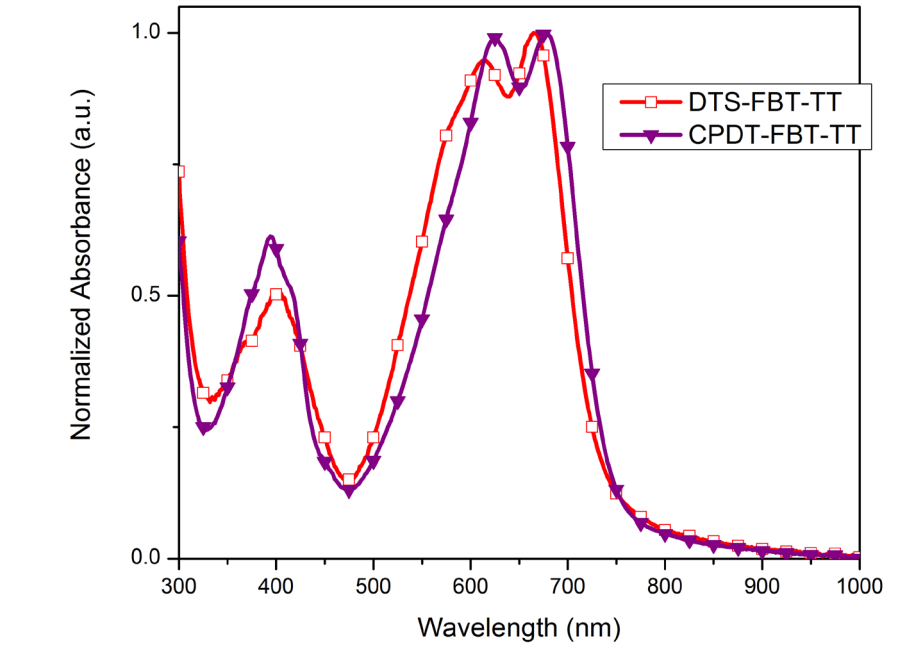


**Figure S3.31.** Thin film UV-vis comparison of D2 with FBT-TT side group.

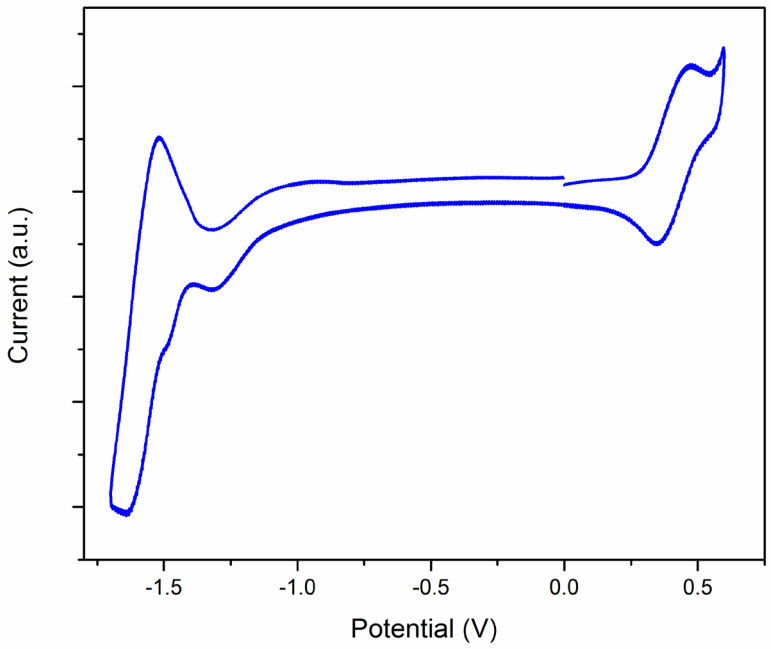


**Figure S3.32.** Cyclic voltammetry trace of DTS-FBT-BT in $CH_2Cl_2$ (~ 1mg $mL^{-1}$).

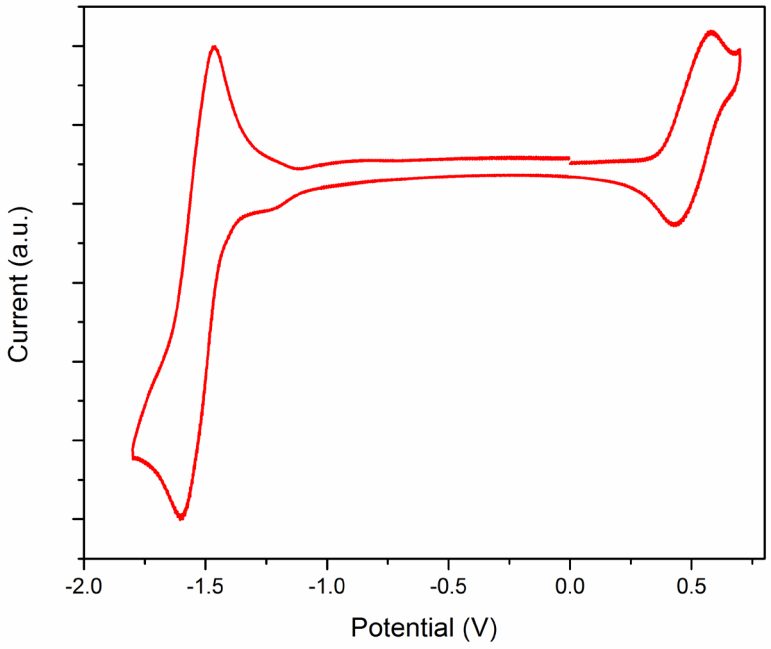


**Figure S3.33.** Cyclic voltammetry trace of DTS-FBT-TT in $CH_2Cl_2$ (~ 1mg $mL^{-1}$).

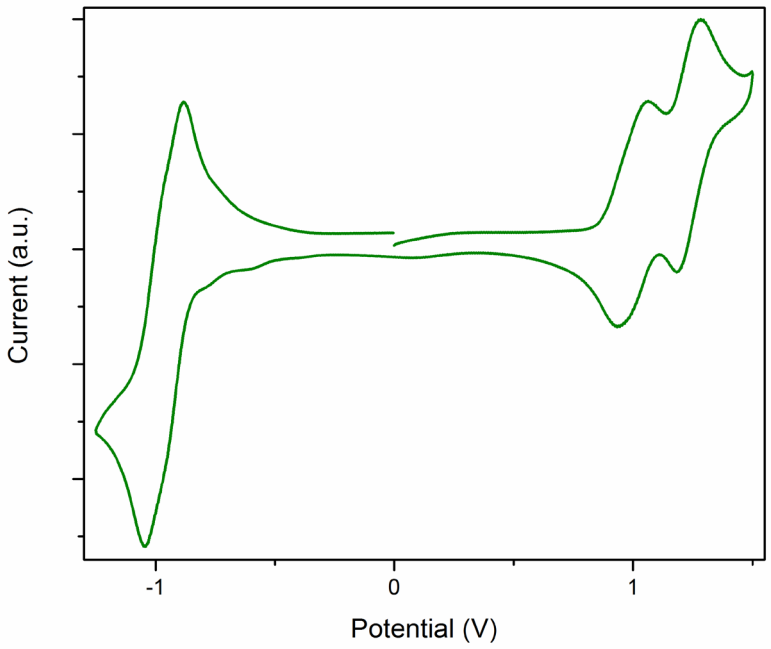


**Figure S3.34.** Cyclic voltammetry trace of CPDT-FBT-BT in $CH_2Cl_2$ (~ 1mg $mL^{-1}$).

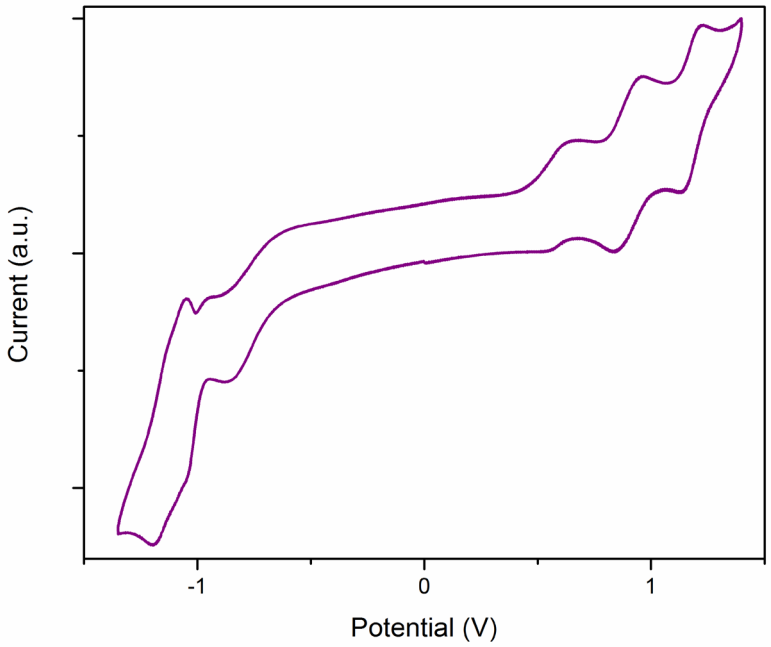


**Figure S3.35.** Cyclic voltammetry trace of CPDT-FBT-TT in $CH_2Cl_2$ (~ 1mg $mL^{-1}$).

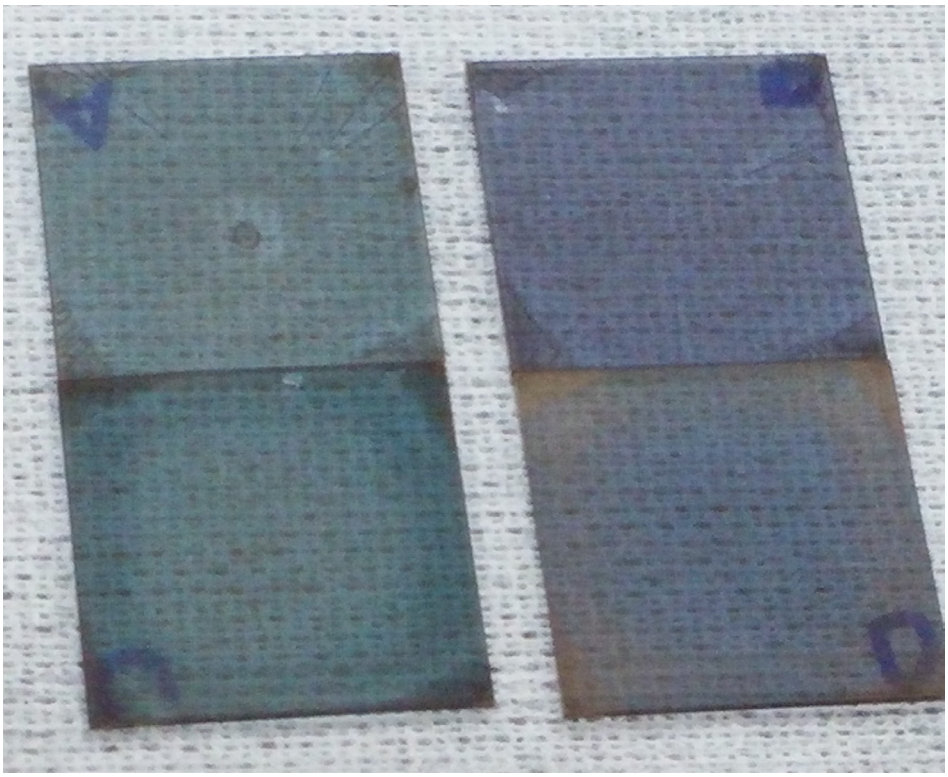

**Figure S3.36.** Image of ITO substrates after casting of the active layer.

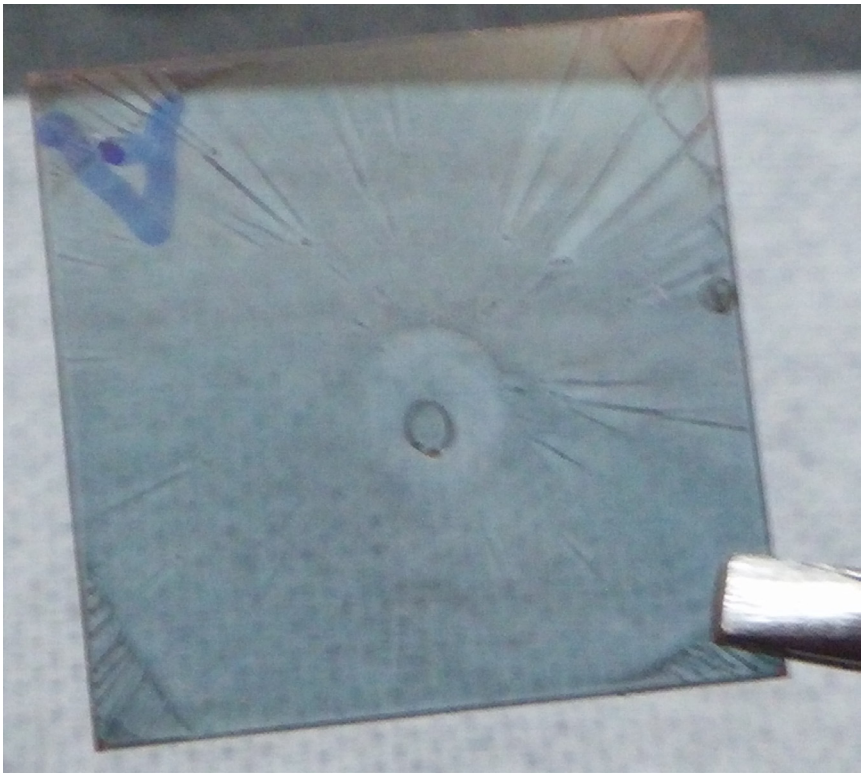

**Figure S3.37.** Image of poor film uniformity of a DTS-FBT-BT coated substrate.

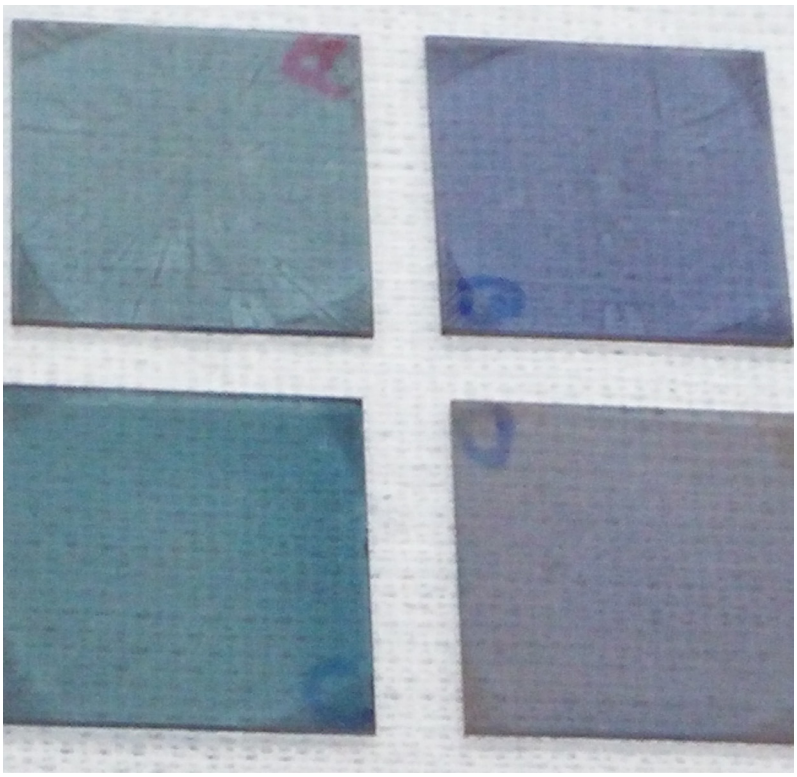

**Figure S3.38.** Image of ITO substrates after casting of the active layer on other.

**Table S3.1.** Molar absorptivity of D1-A-D2-A-D1 small molecules

| material | $\lambda_{max}^{soln}$ (nm)[a] | $\varepsilon^{b}$ (L mol$^{-1}$) |
|---|---|---|
| DTS-FBT-BT | 584 | 69,100 |
| DTS-FBT-TT | 579 | 56,200 |
| CPDT-FBT-BT | 610 | 76,400 |
| CPDT-FBT-TT | 602 | 65,800 |

[a]Taken in dilute chloroform solution. [b]Measured at $\lambda_{max.}$

## 3.8 References


1. Service, R. F., *Science* **2011,** *332* (6027), 293.

2. You, J.; Dou, L.; Yoshimura, K.; Kato, T.; Ohya, K.; Moriarty, T.; Emery, K.; Chen, C.-C.; Gao, J.; Li, G.; Yang, Y., *Nat Commun* **2013,** *4*, 1446.

3. Chen, J.-D.; Cui, C.; Li, Y.-Q.; Zhou, L.; Ou, Q.-D.; Li, C.; Li, Y.; Tang, J.-X., *Adv. Mater.* **2015,** *27* (6), 1035-1041.

4. Kang, H.; Kee, S.; Yu, K.; Lee, J.; Kim, G.; Kim, J.; Kim, J.-R.; Kong, J.; Lee, K., *Adv. Mater.* **2015,** *27* (8), 1408-1413.

5. Kan, B.; Li, M.; Zhang, Q.; Liu, F.; Wan, X.; Wang, Y.; Ni, W.; Long, G.; Yang, X.; Feng, H.; Zuo, Y.; Zhang, M.; Huang, F.; Cao, Y.; Russell, T. P.; Chen, Y., *J. Am. Chem. Soc.* **2015,** *137* (11), 3886-3893.

6. Liu, Y.; Zhao, J.; Li, Z.; Mu, C.; Ma, W.; Hu, H.; Jiang, K.; Lin, H.; Ade, H.; Yan, H., *Nat Commun* **2014,** *5*.

7. Chen, C.-C.; Chang, W.-H.; Yoshimura, K.; Ohya, K.; You, J.; Gao, J.; Hong, Z.; Yang, Y., *Adv. Mater.* **2014,** *26* (32), 5670-5677.

8. Kan, B.; Zhang, Q.; Li, M.; Wan, X.; Ni, W.; Long, G.; Wang, Y.; Yang, X.; Feng, H.; Chen, Y., *J. Am. Chem. Soc.* **2014,** *136* (44), 15529-15532.

9. Coffin, R. C.; Peet, J.; Rogers, J.; Bazan, G. C., *Nat Chem* **2009,** *1* (8), 657-61.

10. Tong, M.; Cho, S.; Rogers, J. T.; Schmidt, K.; Hsu, B. B. Y.; Moses, D.; Coffin, R. C.; Kramer, E. J.; Bazan, G. C.; Heeger, A. J., *Adv. Funct. Mater.* **2010,** *20* (22), 3959-3965.

11. Welch, G. C.; Perez, L. A.; Hoven, C. V.; Zhang, Y.; Dang, X.-D.; Sharenko, A.; Toney, M. F.; Kramer, E. J.; Nguyen, T.-Q.; Bazan, G. C., *J. Mater. Chem.* **2011,** *21* (34), 12700-12709.

12. Ohshita, J., *Macromol. Chem. Phys.* **2009,** *210* (17), 1360-1370.

13. Gierschner, J.; Ehni, M.; Egelhaaf, H. J.; Milian Medina, B.; Beljonne, D.; Benmansour, H.; Bazan, G. C., *J. Chem. Phys.* **2005,** *123* (14), 144914.

14. Chen, H.-Y.; Hou, J.; Hayden, A. E.; Yang, H.; Houk, K. N.; Yang, Y., *Adv. Mater.* **2010,** *22* (3), 371-375.

15. van der Poll, T. S.; Love, J. A.; Nguyen, T.-Q.; Bazan, G. C., *Adv. Mater.* **2012,** *24* (27), 3646-3649.

16. Sharif, M.; Zeeshan, M.; Reimann, S.; Villinger, A.; Langer, P., *Tetrahedron Lett.* **2010,** *51* (21), 2810-2812.

17. Henson, Z. B.; Welch, G. C.; van der Poll, T.; Bazan, G. C., *J. Am. Chem. Soc.* **2012,** *134* (8), 3766-3779.

18. Coughlin, J. E.; Henson, Z. B.; Welch, G. C.; Bazan, G. C., *Acc. Chem. Res.* **2013,** *47* (1), 257-270.

19. Sun, Y.; Welch, G. C.; Leong, W. L.; Takacs, C. J.; Bazan, G. C.; Heeger, A. J., *Nat Mater* **2012,** *11* (1), 44-48.

20. Leong, W. L.; Welch, G. C.; Kaake, L. G.; Takacs, C. J.; Sun, Y.; Bazan, G. C.; Heeger, A. J., *Chemical Science* **2012,** *3* (6), 2103-2109.

21. Takacs, C. J.; Sun, Y.; Welch, G. C.; Perez, L. A.; Liu, X.; Wen, W.; Bazan, G. C.; Heeger, A. J., *J. Am. Chem. Soc.* **2012,** *134* (40), 16597-16606.

22. Intemann, J. J.; Yao, K.; Ding, F.; Xu, Y.; Xin, X.; Li, X.; Jen, A. K. Y., *Adv. Funct. Mater.* **2015,** *25* (30), 4889-4897.

23. Ostroverkhova, O.; Shcherbyna, S.; Cooke, D. G.; Egerton, R. F.; Hegmann, F. A.; Tykwinski, R. R.; Parkin, S. R.; Anthony, J. E., *J. Appl. Phys.* **2005,** *98* (3), 033701.

24. Cardona, C. M.; Li, W.; Kaifer, A. E.; Stockdale, D.; Bazan, G. C., *Adv. Mater.* **2011,** *23* (20), 2367-71.

25. Amb, C. M.; Chen, S.; Graham, K. R.; Subbiah, J.; Small, C. E.; So, F.; Reynolds, J. R., *J. Am. Chem. Soc.* **2011,** *133* (26), 10062-10065.

26. Chu, T. Y.; Lu, J.; Beaupre, S.; Zhang, Y.; Pouliot, J. R.; Wakim, S.; Zhou, J.; Leclerc, M.; Li, Z.; Ding, J.; Tao, Y., *J. Am. Chem. Soc.* **2011,** *133* (12), 4250-4253.

27. Helgesen, M.; Krebs, F. C., *Macromolecules* **2010,** *43* (3), 1253-1260.

28. Khor, E.; Choon Ng, S.; Chze Li, H.; Chai, S., *Heterocycles* **1991,** *32* (9), 1805.

29. S. Fuller, L.; Iddon, B.; A. Smith, K., *J. Chem. Soc., Perkin Trans. 1* **1997**, 10.1039/A701877K (22), 3465-3470.

# CHAPTER 4

## IMPACT OF ENERGY LEVEL OPTIMIZATION AND SIDE CHAIN VARIATION OF LOW BANDGAP DIKETOPYRROLOPYRROLE-DITHIENOSILOLE POLYMERS IN ORGANIC PHOTOVOLTAICS.

*Benjamin J. Hale,[a] Ian Pelse,[b] Brandon M. Kobilka,[a] Achala Bhuwalka,[a]*

*John R. Reynolds,[b] Malika Jeffries-EL*[a]*

[a] Department of Chemistry, Iowa State University, Ames, IA 50011

[b] School of Chemistry and Biochemistry, School of Materials Science and Engineering, Center for Organic Photonics and Electronics, Georgia Institute of Technology, Atlanta

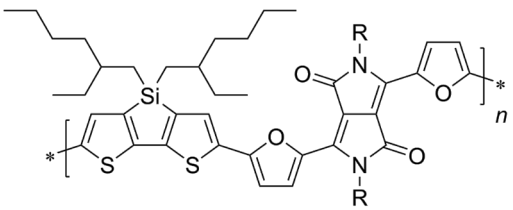


**P1:** R= 2-ethylhexyl
**P2:** R= *n*-decyl
**P3:** R= *n*-dodecyl
**P4:** R= *n*-tetradecyl

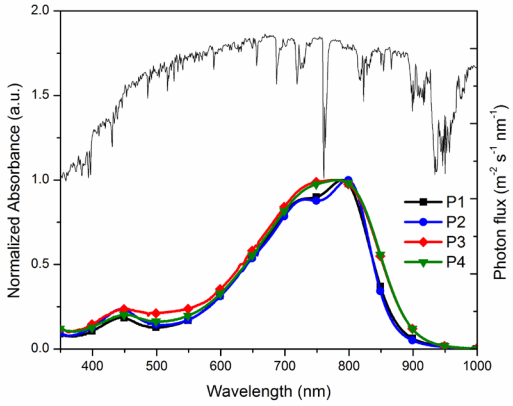

## 4.1 Abstract

We report the synthesis of four narrow bandgap donor-acceptor copolymers based on dithienosilole and furan-flanked diketopyrrolopyrrole. The alkyl chains on the diketo-pyrrolopyrrole were varied to investigate their impact on thin film morphology in the solid state. Incorporation of furan into the polymer allowed for the fine tuning of the energy levels. The furan stabilized the HOMO, allowing for a higher open-circuit voltage when used in photovoltaics. The polymers all exhibit a strong broad low-energy absorption band ranging from 550 – 900 nm and narrow bandgaps of 1.4 eV. Alkyl chain variation on the diketopyrrolopyrrole had negligible effects on the optical and electrochemical properties of the polymers. Their use in organic photovoltaic cells is currently being investigated.

## 4.2 Introduction

Since bulk heterojunction (BHJ) solar cells, comprised of a blend of an electron rich material and an electron deficient fullerene, were first reported 20 years ago, interest in developing narrow bandgap polymeric materials for use in organic photovoltaic (OPV) devices has exploded.[1-11] There are many advantages of OPVs over traditional inorganic based devices, such as the fabrication of light weight and flexible devices, the potential to produce large-area films by low cost solution based techniques, and the ability to tune the properties of the photoactive material through structural modifications.[12-14] An effective route to fine-tuning the optical and electronic properties of these material is to take advantage of the charge transfer characteristics of π-conjugated "donor-acceptor" copoly-

mers comprised of alternating π-electron rich (donor) and π-electron deficient (acceptor) arylene units.[15] Through this approach, and careful optimization of processing conditions, device efficiencies for BHJ OPVs have exceeded 10%.[16-17]

Recently, there has been an increased interest on the role heteroatom substitution plays on the electronic and physical properties of donor-acceptor polymers. This is generally accomplished by replacing the commonly used thiophene for either furan or selenophene. The inclusion of oxygen and selenium can have dramatic effects on the performance of a given material through the widening or narrowing of absorption bands, raising or lowering of energy levels, increasing or decreasing solubility which impacts the ability of the material to be processed resulting in changes to morphology of the thin film. [18,19] Often times, the incorporation of furan and selenophene can have predictable effects relative to the thiophene-based material, such as with the electron deficient diketopyrrolopyrrole (DPP). Donor-acceptor polymers containing the furanyl-DPP unit have been shown to have significantly higher solubility and only a slightly wider optical bandgap ($E_g^{opt}$), while polymers containing the selenophene-DPP have slightly reduced bandgaps and decreased solubility.[18, 20-22] This trend allows for selective tuning of thiophene-based DPP materials that may have had unfavorable solubility or energy levels for efficient OPVs.

Donor-acceptor polymers comprised of the electron-donating dithienosilole (DTS) unit and thiophenyl-DPP were reported by two groups in 2009, with the only variation being the solubilizing alkyl chains on the DTS and DPP units.[23-24] Devices fabricated from the polymers with 2-ethylhexyl chains on both the DTS and DPP suffered from a very low open circuit voltage ($V_{OC}$), yet still gave a power conversion efficiency (PCE) of

2.10%. The low $V_{OC}$, which is primarily determined by the gap between the highest occupied molecular orbital (HOMO) of the donor polymer and lowest unoccupied molecular orbital (LUMO) of the fullerene acceptor, was likely due to the relatively high HOMO of -5.04 eV.[4, 24-25] The substitution of furan for thiophene on the DPP allows for a reduction of the HOMO while still maintaining a broad UV-Vis absorption and narrow bandgap. The morphology of the polymer:fullerene blend can be adjusted by varying the alkyl chain length and branching on the DPP, which has the potential to further increase the PCE.[26]

In an attempt to evaluate the role of heteroatom substitution on DPP containing materials, we have synthesized a series of furan based low bandgap DTS-DPP polymers. To further optimize the materials, the alkyl side chains on the DPP unit were varied, with the 2-ethylhexyl derivative giving us a direct comparison to the previously reported thiophene based DTS-DPP polymer. The synthesized furan series all had similar thermal, optical, and electrochemical properties, as expected due to the consistent polymer backbone. The furan based DTS-DPP polymers had deeper HOMO levels relative to the thiophene based material and a slightly wider optical bandgap. To make a true comparison, OPV devices were fabricated and are reported.

## 4.3 Results and Discussion

### 4.3.1 Synthesis and physical characterization

The synthetic route to the DPP monomers and PDTSDPP polymers are shown in Scheme 4.1 and Scheme 4.2, respectively. In an effort to test the influence of alkyl side-chains on the efficiency of PDTSDPP OPVs, DPP derivatives were synthesized with 2-

ethylhexyl (**M1**), *n*-decyl (**M2**), *n*-dodecyl (**M3**), and *n*-tetradecyl (**M4**) side-chains (see Supporting Information). The Stille cross-coupling polymerization of **DTS** and **M1**-**M4** gave the expected polymers **P1**-**P4** in moderate to good yields (57 – 88%) after purification. All polymers, particularly **P2**, have low solubility in chloroform at room temperature, but were soluble in both chlorobenzene and 1,2-dichlorobenzene.

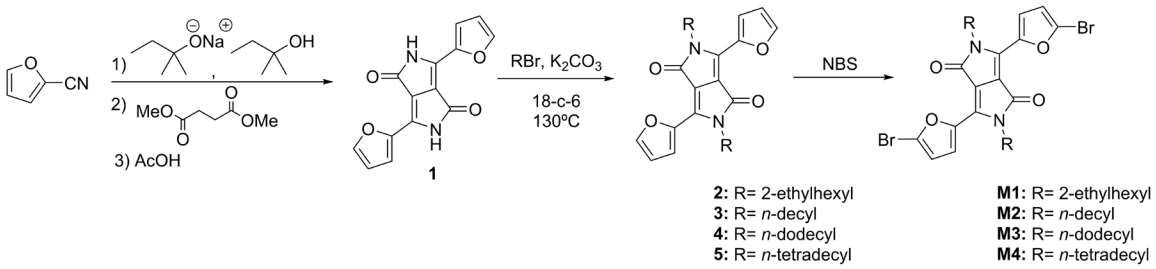


**Scheme 4.1.** Synthesis of DPP monomers **M1**–**M4**.

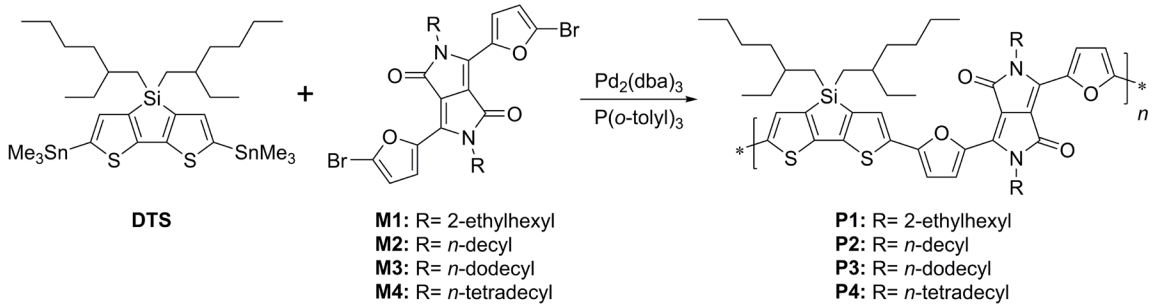


**Scheme 4.2.** Synthesis of PDTSDPP polymers **P1**-**P4**.

Due to the low solubility in chloroform (<1 mg $mL^{-1}$), $^1H$ NMR spectra were unable to be collected. Molecular weights were estimated by gel permeation chromatography (GPC) against polystyrene standards, using chloroform at 40 °C as eluent, and are described in Table 4.1. All four polymers had moderate number averaged molecular weights ($M_n$) ranging from 20.2 – 28.0 kDa, with dispersities (Đ) from 1.5 – 2.4. The

lower $M_n$ and degree of polymerization ($DP_n$) of **P4** was likely due to the poor solubility of **M4** at the concentration required, slowing down the rate of polymerization. While present in **P1-4**, even in very dilute solution, **P2** showed heavy aggregation. The similar $DP_n$ of **P1**, **P2**, and **P3** should allow for reasonable comparisons of the role of side chains on device performance.

**Table 4.1.** Physical and thermal properties of PDTSDPP polymers.

| Polymer | Yield (%) | $M_n$ (kDa)[a] | Đ[b] | $DP_n$ | $T_d5\%$[c] (°C) |
|---|---|---|---|---|---|
| P1 | 84 | 23.1 | 2.4 | 25.5 | 394.4 |
| P2 | 69 | 22.2 | 1.5 | 23.0 | 383.5 |
| P3 | 57 | 28.0 | 1.8 | 27.4 | 354.6 |
| P4 | 88 | 20.2 | 1.7 | 18.8 | 388.3 |

[a]Determined by GPC against polystyrene standards in $CHCl_3$ at 40 °C. [b]Dispersity: $M_w/M_n$. [c]Temperature at 5% weight loss with a heating rate of 20 °C $min^{-1}$ under air.

The thermal properties of the polymers (Figure S4.24, Supporting Information) were investigated using thermogravimetric analysis and are summarized in Table 4.1. All polymers showed good thermal stability with 5% weight loss between 354.6 and 394.4 °C under air, well below the operating temperature of photovoltaic devices.

### 4.3.2 Optical and electrochemical properties

The normalized UV-Vis absorbance spectra of **P1-P4** in dilute chloroform solution and thin films are shown in Figure 4.1 and 4.2, respectively and the data is summarized in Table 4.2. All four polymers possessed similar absorbance spectra with a relatively weak

high-energy band, which can be attributed to localized π-π* transitions, and a strong, broad low-energy band corresponding to intramolecular charge-transfer (ICT) between the electron-donating DTS and electron-accepting DPP units.[27] While **P1**, **P3**, and **P4** all have a single broad low-energy transition, vibrational splitting, common in solids, can be seen in **P2**.[28-30] All polymers exhibit a relatively small shift in absorption from solution to thin film, indicating the polymers are likely aggregated in solution.

The thin film optical properties of all four polymers are very similar. Polymer **P1** displayed the most dramatic change between solution and film with a bathochromic shift in $\lambda_{max}$ of 33 nm, while **P2**, **P3**, and **P4** showed hypsochromic shifts of 9 nm, 20 nm, and 6 nm, respectively. Optical bandgaps, measured from the optical onset, were similar and ranged from 1.38 – 1.43 eV. The similarity in absorbance and optical bandgap between **P1**-**P4** is expected due to possessing the same backbone. While **P4** had a lower $DP_n$ than **P1**, **P2**, and **P3**, the similar optical properties suggest the effective conjugation length of the polymer was reached.[31] The slight variance in the thin film measurements is likely due to the difference in alkyl chains on the DPP unit.[26]

**Table 4.2.** Optical and electrochemical properties of PDTSDPP polymers.

| Polymer | $\lambda_{max}^{soln}$ (nm)[a] | $\lambda_{max}^{film}$ (nm) | $E_g^{opt}$ (eV)[b] | $E_{HOMO}$ (eV)[c] | $E_{LUMO}$ (eV)[c] | $E_g^{ec}$ (eV) |
|---|---|---|---|---|---|---|
| P1 | 756 | 789 | 1.42 | -5.30 | -3.39 | 1.91 |
| P2 | 806 | 797 | 1.43 | -5.36 | -3.40 | 1.96 |
| P3 | 794 | 774 | 1.38 | -5.27 | -3.40 | 1.87 |
| P4 | 789 | 783 | 1.38 | -5.27 | -3.42 | 1.85 |

[a]Measured in chloroform. [b]Calculated from the absorption onset of the film spectra; [c]Calculated from the reduction and oxidation onsets using the equation $E_{HOMO/LUMO}$ = -4.8 - $E_{redox}$.

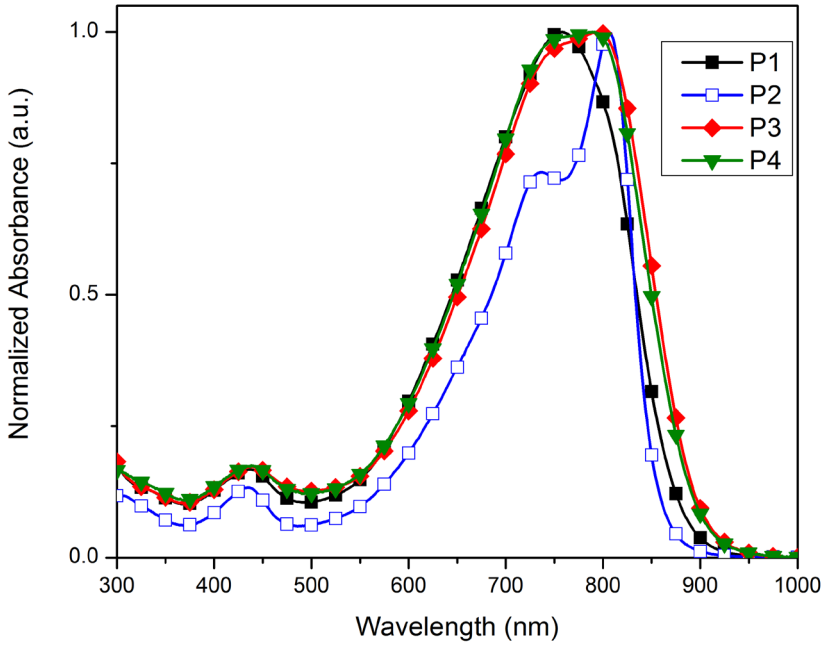


**Figure 4.1.** UV-vis absorption of P1-P4 in $CHCl_3$.

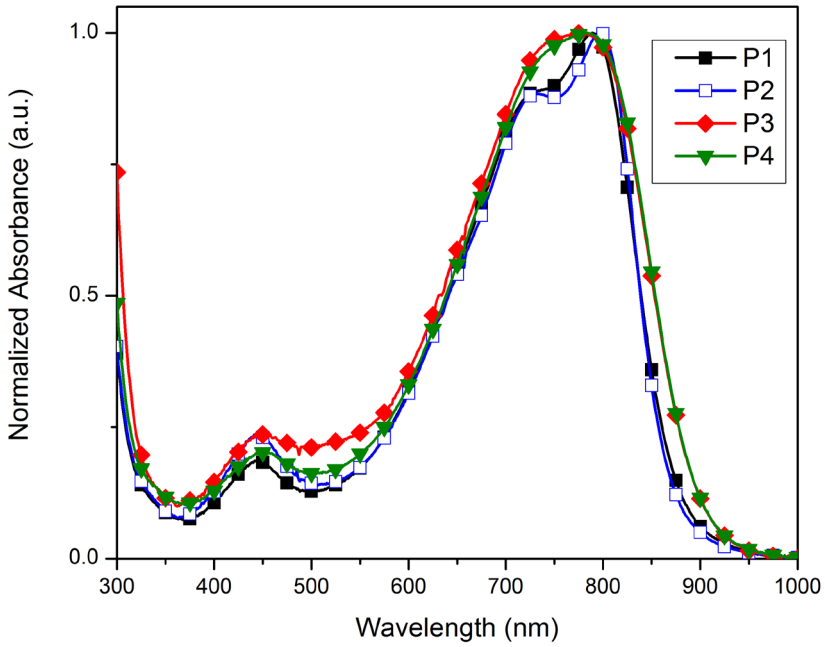


**Figure 4.2.** UV-vis absorption of P1-P4 in thin film.

The oxidation and reduction potentials of the polymers were determined electrochemically by cyclic voltammetry (CV). The highest occupied molecular orbital (HOMO) and lowest occupied molecular orbital (LUMO) of each polymer was estimated from the oxidation onset and reduction onset, respectively, using the absolute energy level of ferrocene/ferrocenium ($Fc/Fc^+$) as -4.8 eV vs vacuum and are summarized in Table 4.2. All four polymers showed reversible oxidation and reduction peaks (Figure S4.20 – S4.23, Supporting Information). The estimated HOMO energy levels for **P1**-**P4** were between -5.3 and -5.4 eV, all below the air oxidation threshold of -5.2 eV.[32] The LUMO levels were approximately -3.4 eV, giving an average electrochemical bandgap of 1.90 ± 0.05 eV. The HOMO, LUMO, and electrochemical bandgaps of each polymer all fall well within the error associated with electrochemical measurements, which is expected since they possess the same polymer backbone.[33]

### 2.3.3 Photovoltaic devices

Photovoltaic devices are currently being fabricated by the Reynolds group at the Georgia Institute of Technology as of the writing of this manuscript.

## 4.4 Conclusions

A series of four copolymers based on dithienosilole and furan containing diketopyrrolopyrrole with various alkyl chains were synthesized. Incorporation of furan stabilized the HOMO of the polymer relative to the previously reported thiophene analog, while still maintaining a low lying LUMO and narrow bandgap of 1.4 eV. The polymers all exhibit a strong broad low-energy absorption band ranging from 550 – 900 nm. Alkyl

chain variation on the diketopyrrolopyrrole had negligible effects on the optical and electrochemical properties of the polymers. The polymers are currently being tested in organic photovoltaic cells as of the writing of this manuscript, where the role of alkyl chain substitution on the photovoltaic performance will be investigated.

## 4.5 Experimental

### 4.5.1 Materials

Air- and moisture-sensitive reactions were performed using standard Schlenk techniques. Solvents used for palladium-catalyzed reactions were deoxygenated prior to use by sparging with argon for 30 minutes. 3,3',5-5'-tetrabromobithiophene[34] and 2-furancarbonitrile[35] were prepared using literature procedures. 2-ethylhexylmagnesium bromide (1.0 M in ether) was purchased from Sigma-Aldrich. The preparation of DTS and the DPP monomers M1, M2, M3, and M4 are described in the Supporting Information. All other chemicals were purchased commercially and used without further purification.

### 4.5.2 Characterization

Nuclear magnetic resonance (NMR) spectra were collected on Varian VXR-300, Varian MR-400, or Bruker Avance III-600 spectrometers. $^1$H NMR spectra were internally referenced to the residual solvent peak. In all spectra, chemical shifts are given in ppm (δ) relative to the solvent. Gel permeation chromatography (GPC) measurements were performed on a Shimadzu Prominence GPC with two 10 μm AM Gel columns connected in series (guard, 10,000 Å, 1,000 Å) in chloroform at 40 °C relative to polystyrene stand-

ards. Preparative HPLC was done on an Agilent 1100 series HPLC using a Phenomenex Luna 21.2 mm X 250 mm C18 (TMS endcapped, 5 μm particle size) AXIA column, using 40% acetonitrile 60% acetone at 10 mL/min as eluent and detected at 340 nm. Thermogravimetric analysis (TGA) was performed over an interval of 30 – 900 °C at a heating rate of 20 °C $min^{-1}$ under ambient atmosphere. Cyclic voltammetry (CV) measurements were carried out using an *e*-DAQ *e*-corder 410 potentiostat with a scanning rate of 100 mV $s^{-1}$. The polymer films were dropcast from 1 – 2 mg $mL^{-1}$ solutions in chlorobenzene onto a platinum working electrode. $Ag/Ag^{+}$ and Pt wire were used as the reference and auxiliary electrodes, respectively. The reported values were referenced to $Fc/Fc^{+}$ (-4.8 versus vacuum). All electrochemical experiments were performed in deoxygenated acetonitrile under an argon atmosphere using 0.1 M tetrabutylammonium hexafluorophosphate as electrolyte. Absorption spectra were obtained on a photodiode-array Agilent 8453 UV-visible spectrophotometer using polymer solutions in $CHCl_3$ and thin films. The films were cast by spin coating 25 x 25 x 1 mm glass slides using solutions of polymer (2.5 – 5.0 mg $mL^{-1}$) in chlorobenzene at a spin rate of 1200 rpm on a Headway Research, Inc. PWM32 spin-coater.

### 4.5.3 Synthesis

**General procedure for the polymerization of P1-P4:** DTS (78.2 mg, 0.11 mmol) and **M1**, **M2**, **M3**, or **M4** (0.10 mmol) were dissolved in deoxygenated chlorobenzene (4 mL) and sparged with argon for an additional 30 min. Tris(dibenzylideneacetone)dipalladium(0) (1.8 mg, 2 mol%) and tri(*o*-tolyl)phosphine (2.4 mg, 8 mol%) were added and the reaction heated at 130 °C for 36 h. The polymer

was end-capped by heating with trimethyl(phenyl)tin (15 mg) for 4 h, followed by heating with iodobenzene (0.05 mL) overnight. After cooling to ambient temperature, the mixture was precipitated into methanol and filtered through a Soxhlet thimble. The polymer was washed with methanol (4 h), acetone (4 h), hexanes (12 h), and extracted with chlorobenzene. The chlorobenzene fraction was then concentrated and the polymer run through a short silica gel plug with chlorobenzene as eluent. The resulting fraction was then concentrated (~5 mL) and precipitated into methanol, filtered, and dried *in vacuo* to yield the desired polymer.

**Synthesis of P1.** Synthesis of **P1** afforded a dark solid (76.8 mg, 84%). GPC ($CHCl_3$, 40 °C): $M_n$ = 23.1 kDa, $M_w$ = 54.6 kDa, Đ = 2.4, $DP_n$ = 25.5. $T_d5\%$ = 394.4 °C

**Synthesis of P2.** Synthesis of **P2** afforded a dark solid (66.9 mg, 69%). GPC ($CHCl_3$, 40 °C): $M_n$ = 22.2 kDa, $M_w$ = 34.2 kDa, Đ = 1.5, $DP_n$ = 23.0. $T_d5\%$ = 383.5 °C.

**Synthesis of P3.** Synthesis of **P3** afforded a dark solid (58.9 mg, 57%). GPC ($CHCl_3$, 40 °C): $M_n$ = 28.0 kDa, $M_w$ = 51.6 kDa, Đ = 1.8, $DP_n$ = 27.4. $T_d5\%$ = 354.6 °C.

**Synthesis of P4.** Synthesis of **P4** afforded a dark solid (94.0 mg, 88%). GPC ($CHCl_3$, 40 °C): $M_n$ = 20.2 kDa, $M_w$ = 35.3 kDa, Đ = 1.7, $DP_n$ = 18.8. $T_d5\%$ = 388.3 °C.

## 4.6 Acknowledgements

We thank the National Science Foundation (DMR-1410088), Iowa State University (ISU), and ISU EPSCOR for support of this work. We wish to thank Steve Veysey and the ISU Chemical Instrumentation Facility for training and assistance with the thermal analysis. The OPVs were fabricated at the ISU Microelectronics Research Center.

## 4.7 Supporting Information

### 4.7.1 Synthesis

**3,6-Di(furan-2-yl)pyrrolo[3,4-*c*]pyrrole-1,4(2H,5H)-dione (1).** Sodium metal (4.94 g, 211 mmol) was added to *tert*-amyl alcohol (120 mL) and the solution refluxed overnight. 2-furancarbonitrile (25.0 g, 269 mmol) was added in one portion to the hot alkoxide solution followed by the dropwise addition of dimethyl succinate (13.09 g, 90 mmol) in *tert*-amyl alcohol (80 mL). After complete addition of the dimethyl succinate solution, the mixture was allowed to stir at reflux overnight. The reaction mixture was then allowed to cool to 60 °C, quenched with 40 mL of acetic acid, and allowed to stir at reflux for 1 h. The resulting suspension was then filtered and the solid washed with hot methanol and water three times and dried under vacuum affording **1** as a dark solid (21.80 g, 91%). Compound **1** was used without further purification.

**General procedure for the preparation of 2,5-dialkyl-3,6-di(furan-2-yl)pyrrolo[3,4-*c*]pyrrole-1,4(2*H*,5*H*)-dione 2, 3, 4, & 5** Compound **1** , potassium carbonate (4.3 equi), and 18-crown-6 (14 mg) were added to dry DMF (35 mL) and heated at 100 °C for 1 h.

Alkyl bromide (3.4 equi) was added dropwise and the reaction was allowed to stir at 130 °C for 48 h. The reaction mixture was allowed to cool and poured into water (100 mL). The crude mixture was then extracted with chloroform (3 x 250 mL). The combined organic layers were washed with copious amounts of water, dried with $Na_2SO_4$, and concentrated to afford dark crude solid.

**2,5-bis(2-ethylhexyl)-3,6-di(furan-2-yl)pyrrolo[3,4-*c*]pyrrole-1,4(2*H*,5*H*)-dione (2):** The crude **2** was purified by silica gel chromatography with chloroform as eluent to afford the expected compound as a shiny red solid (4.60 g, 60 %). $^1$H NMR (400 MHz, $CDCl_3$) δ: 8.33 (dd, *J* = 3.6, 0.7 Hz, 2H), 7.61 (dd, *J* = 1.7, 0.7 Hz, 2H), 6.69 (dd, *J* = 3.7, 1.7 Hz, 2H), 4.04 (dd, *J* = 7.4, 1.1 Hz, 4H), 1.83 – 1.67 (m, 2H), 1.42 – 1.19 (m, 16H), 0.98 – 0.78 (m, 6H).

**2,5-didecyl-3,6-di(furan-2-yl)pyrrolo[3,4-*c*]pyrrole-1,4(2*H*,5*H*)-dione (3)** The crude **3** was purified by silica gel chromatography using 1:2 hexanes/chloroform as eluent to give the expected product as a shiny purple solid (1.39 g, 63 %). $^1$H NMR (300 MHz, $CDCl_3$) δ 8.31 (d, *J* = 3.8 Hz, 2H), 7.64 (d, *J* = 1.5 Hz, 2H), 6.70 (q, *J* = 1.8 Hz, 2H), 4.11 (t, *J* = 7.6 Hz, 4H), 1.68 (d, *J* = 7.6 Hz, 4H), 1.42 – 1.15 (m, 28H), 0.86 (t, *J* = 6.8 Hz, 6H).

**2,5-didodecyl-3,6-di(furan-2-yl)pyrrolo[3,4-*c*]pyrrole-1,4(2*H*,5*H*)-dione (4)** The crude **4** was purified by silica gel chromatography using 1:1 hexanes/chloroform as eluent to give the expected product as a shiny purple solid (1.63 g, 66 %). $^1$H NMR (600 MHz, $CDCl_3$) δ 8.30 (dd, *J* = 3.6, 0.7 Hz, 2H), 7.63 (dd, *J* = 1.7, 0.7 Hz, 2H), 6.69 (dd, *J* = 3.7,

1.7 Hz, 2H), 4.11 (t, *J* = 7.5 Hz, 4H), 1.73 – 1.67 (m, 4H), 1.43 – 1.21 (m, 36H), 0.88 (t, *J* = 7.0 Hz, 6H).

**3,6-di(furan-2-yl)-2,5-ditetradecylpyrrolo[3,4-*c*]pyrrole-1,4(2*H*,5*H*)-dione (5)** The crude **5** was purified by silica gel chromatography using 1:1 hexanes/chloroform as eluent to give the expected product as a shiny purple solid (1.94 g, 73 %). $^1$H NMR (600 MHz, $CDCl_3$) δ 8.31 (dd, *J* = 3.7, 0.7 Hz, 2H), 7.63 (dd, *J* = 1.7, 0.7 Hz, 2H), 6.70 (dd, *J* = 3.7, 1.7 Hz, 2H), 4.13 – 4.08 (m, 4H), 1.83 – 1.58 (m, 4H), 1.43 – 1.18 (m, 44H), 0.88 (t, *J* = 7.1 Hz, 6H).

**General procedure for the preparation of 3,6-bis(5-bromofuran-2-yl)-2,5-dialkylpyrrolo[3,4-*c*]pyrrole-1,4(2*H*,5*H*)-dione M1, M2, M3, & M4** Compounds **2**, **3**, **4**, and **5** were dissolved in chloroform (250 mL) and protected from light. The solution was cooled to 0 °C and NBS (2.2 equi) added in two portions over 10 min. The reaction was stirred at room temperature for 48 h before quenching with methanol (20 mL). The reaction mixture was diluted with chloroform (400 mL) and washed with water (3 x 500 mL), dried with $Na_2SO_4$, and concentrated to give dark crude solids.

**3,6-bis(5-bromofuran-2-yl)-2,5-bis(2-ethylhexyl)pyrrolo[3,4-*c*]pyrrole-1,4(2*H*,5*H*)-dione (M1)** The crude **M1** was purified by silica gel chromatography using 1:1 chloroform:hexane as eluent to give the expected product as a shiny red solid (1.30 g, 60 %). $^1$HNMR (600 MHz, $CDCl_3$) δ: 8.33 (d, *J* = 3.7 Hz, 2H), 6.65 (d, *J* = 3.7 Hz, 2H), 4.02 (d,

*J* = 7.5 Hz, 4H), 1.82 (p, *J* = 6.0, 5.5 Hz, 2H), 1.45 – 1.20 (m, 32H), 0.90 (tt, *J* = 12.0, 7.1 Hz, 12H).

**3,6-bis(5-bromofuran-2-yl)-2,5-didecyl-pyrrolo[3,4-*c*]pyrrole-1,4(2*H*,5*H*)-dione (M2)** The crude **M2** was purified by silica gel chromatography using 2:3 hexanes/chloroform as eluent to give the expected product as a shiny purple solid (0.78 g, 44 %). $^1$H NMR (400 MHz, $CDCl_3$) δ 8.25 (d, *J* = 3.7 Hz, 2H), 6.63 (d, *J* = 3.7 Hz, 2H), 4.05 (t, *J* = 7.7 Hz, 4H), 1.76 – 1.62 (m, 4H), 1.47 – 1.17 (m, 28H), 0.87 (t, *J* = 6.8 Hz, 6H).

**3,6-bis(5-bromofuran-2-yl)-2,5-didodecyl-pyrrolo[3,4-*c*]pyrrole-1,4(2*H*,5*H*)-dione (M3)** The crude **M3** was purified by silica gel chromatography using 1:1 hexanes/chloroform as eluent to give the expected product as a shiny purple solid (1.01 g, 49 %). $^1$H NMR (400 MHz, $CDCl_3$) δ 8.25 (d, *J* = 3.8 Hz, 2H), 6.63 (d, *J* = 3.7 Hz, 2H), 4.05 (t, *J* = 7.4 Hz, 4H), 1.75 – 1.65 (m, 4H), 1.45 – 1.20 (m, 36), 0.87 (t, *J* = 7.1 Hz, 6H).

**3,6-bis(5-bromofuran-2-yl)-2,5-ditetradecyl-pyrrolo[3,4-*c*]pyrrole-1,4(2*H*,5*H*)-dione (M4)** The crude **M4** was purified by silica gel chromatography using 1:1 hexanes/chloroform as eluent to give the expected product as a shiny purple solid (1.15 g, 48 %). $^1$H NMR (400 MHz, $CDCl_3$) δ 8.26 (d, *J* = 3.6 Hz, 2H), 6.63 (d, *J* = 3.7 Hz, 2H), 4.05 (t, 4H), 1.74 – 1.64 (m, 4H), 1.46 – 1.15 (m, 44H), 0.88 (t, *J* = 6.7 Hz, 6H).

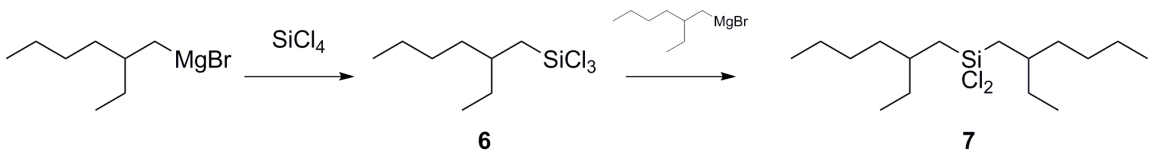


6 7

**(2-ethylhexyl)trichlorosilane (6)** A solution of silicon tetrachloride (14 mL, 122.2 mmol) in THF (40 mL) was cooled to -10 °C with an acetone/ice bath. 2-ethylhexylmagnesium bromide solution (60 mL, 1.0 M in ether, Aldrich) was added dropwise and the reaction allowed to stir overnight at room temperature. The reaction was poured into hexanes and filtered to remove inorganic salts. The solution was concentrated, and the crude material purified by fractional distillation to give the expected product as a clear oil (13.4 g, 90%). $^1$H NMR (400 MHz, $CDCl_3$) δ 1.78 (p, $J$ = 12.5, 6.2 Hz, 1H), 1.49 – 1.35 (m, 6H), 1.35 – 1.23 (m, 4H), 0.90 (t, $J$ = 7.1 Hz, 3H), 0.87 (t, $J$ = 7.9 Hz, 3H).

**bis(2-ethylhexyl)dichlorosilane (7)** A solution of compound **6** (13.4 g, 54 mmol) in THF (75 mL) was cooled to 0 °C with an ice bath. 2-ethylhexylmagnesium bromide solution (39 mL, 1.0 M in ether, Aldrich) was added dropwise and the reaction allowed to stir overnight at room temperature, followed by removal of the solvent. After dilution of the crude material in hexanes, a precipitate formed. The solid was filtered and the filtrate concentrated. The resulting oil was purified by fractional distillation under high vacuum, giving the expected product as a colorless oil (10.2 g, 80%). $^1$H NMR (400 MHz, $CDCl_3$) δ 1.70 (p, $J$ = 12.4, 6.1 Hz, 2H), 1.44 – 1.20 (m, 16H), 1.11 (d, $J$ = 6.7 Hz, 4H), 0.90 (t, $J$ = 6.6 Hz, 6H), 0.86 (t, $J$ = 7.4 Hz, 6H).

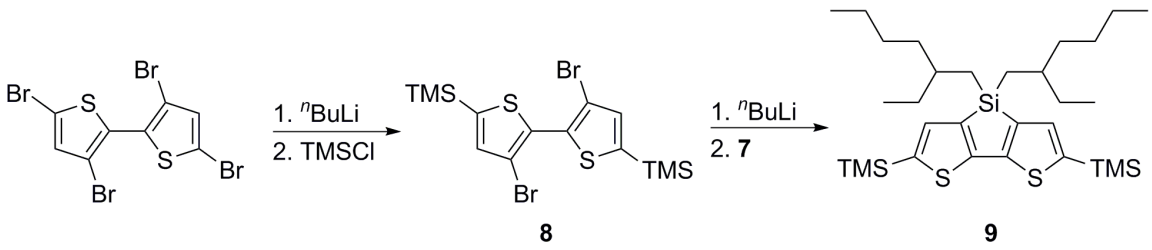


**3,3'-dibromo-5,5'-(trimethylsilyl)-2,2'bithiophene (8)** A solution of 3,3'-5,5'-tetrabromo-2,2'-bithiophene (30.1 g, 62 mmol) in THF (300 mL) was cooled to -78 °C. *n*-butyllithium solution (53 mL, 2.5 M in hexanes) was added dropwise and the reaction stirred for 4h at temperature. Trimethylsilyl chloride (21 mL, 165 mmol) was added dropwise and the reaction stirred for 15 min at -78 °C before being allowed to stir at ambient temperature overnight. The reaction was diluted with ether (400 mL) and washed with water and dried. Purification by silica gel column chromatography using hexanes as eluent, followed by recrystallization from ethanol gave the expected product as a light yellow solid (18.2 g, 62%). $^1$H NMR (400 MHz, $CDCl_3$) δ 7.15 (s, 2H), 0.34 (s, 18H).

**4,4-bis(2-ethylhexyl)-2,6-bis(trimethylsilyl)-dithieno[3,2-*b*:2',3'-*d*]silole (9)** A solution of **8** (11.78 g, 25 mmol) in THF (200 mL) was cooled to -78 °C. *n*-butyllithium solution (21.5 mL, 2.5 M in hexanes) was added dropwise and the reaction stirred for 2h at temperature. Compound **7** (9.42 g, 30 mmol) was added dropwise and the reaction stirred at ambient temperature overnight. The reaction was poured into water and the crude material extracted with ether, dried with anhydrous sodium sulfate, and the solvent removed. Purification by silica gel column chromatography using hexanes as eluent gave the expected product as a light yellow oil (11.54 g, 82%). $^1$H NMR (400 MHz, $CDCl_3$) δ 7.11

(s, 2H), 1.39 (p, $J$ = 6.8, 5.9, 5.7 Hz, 2H), 1.33 – 1.20 (m, 4H), 1.20 – 1.10 (m, 12H), 1.01 – 0.82 (m, 4H), 0.82 (t, $J$ = 6.4 Hz, 6H), 0.76 (t, $J$ = 7.3 Hz, 6H), 0.32 (s, 18H).

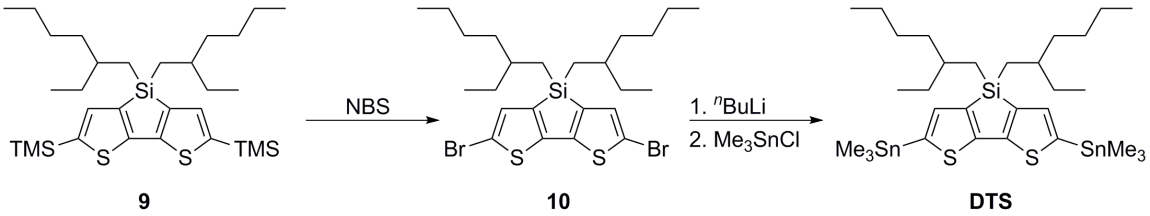


9 10 DTS

**4,4-bis(2-ethylhexyl)-2,6-dibromo-dithieno[3,2-*b*:2',3'-*d*]silole (10)** Compound **9** (1.14 g, 2 mmol) was dissolved in THF (25 mL) and protected from light. NBS (0.73 g, 4.1 mmol) was added in two portions. The reaction was allowed to stir for 2h before being extracted with ether, washed with water, dried over anhydrous sodium sulfate, and concentrated. Purification by silica gel column chromatography using hexanes as eluent gave the expected product as a yellow oil (1.12 g, 96%). $^1$H NMR (400 MHz, $CDCl_3$) δ 6.98 (s, 2H), 1.37 (p, $J$ = 6.2 Hz, 2H), 1.30 – 1.08 (m, 16H), 0.91 (dd, $J$ = 6.7, 4.6 Hz, 4H), 0.84 (t, $J$ = 6.8 Hz, 6H), 0.77 (t, $J$ = 7.4 Hz, 6H).

**4,4-bis(2-ethylhexyl)-2,6-bis(trimethylstannyl)-dithieno[3,2-*b*:2',3'-*d*]silole (DTS)** A solution of **10** (1.12 g, 1.9 mmol) in THF (30 mL) was cooled to -78 °C. A solution of $^n$BuLi (5.25 mmol, 2.5 M in hexanes) was added dropwise and the reaction allowed to stir for two hours at -78 °C. Trimethyl tin chloride solution (6.25 mmol, 1 M in THF) was added dropwise. The reaction was slowly allowed to warm to room temperature and stirred overnight. The reaction mixture was poured into water and the crude product extracted with hexanes and dried over anhydrous $Na_2SO_4$. After removal of the solvent, the

crude product was heated under high vacuum at 40 °C overnight. The crude material was purified by preparative HPLC to give the expected product as a tacky light yellow oil (0.97 g, 67%). $^{1}$H NMR (600 MHz, $CDCl_3$) δ 7.07 (s, 2H), 1.45 – 1.37 (m, 2H), 1.32 – 1.07 (m, 16H), 0.99 – 0.92 (m, 4H), 0.92 – 0.86 (m, 4H), 0.82 (t, $J$ = 6.6 Hz, 6H), 0.77 (t, $J$ = 7.3 Hz, 6H), 0.37 (s, 18H).

### 4.7.2 NMR Spectra and analytical data

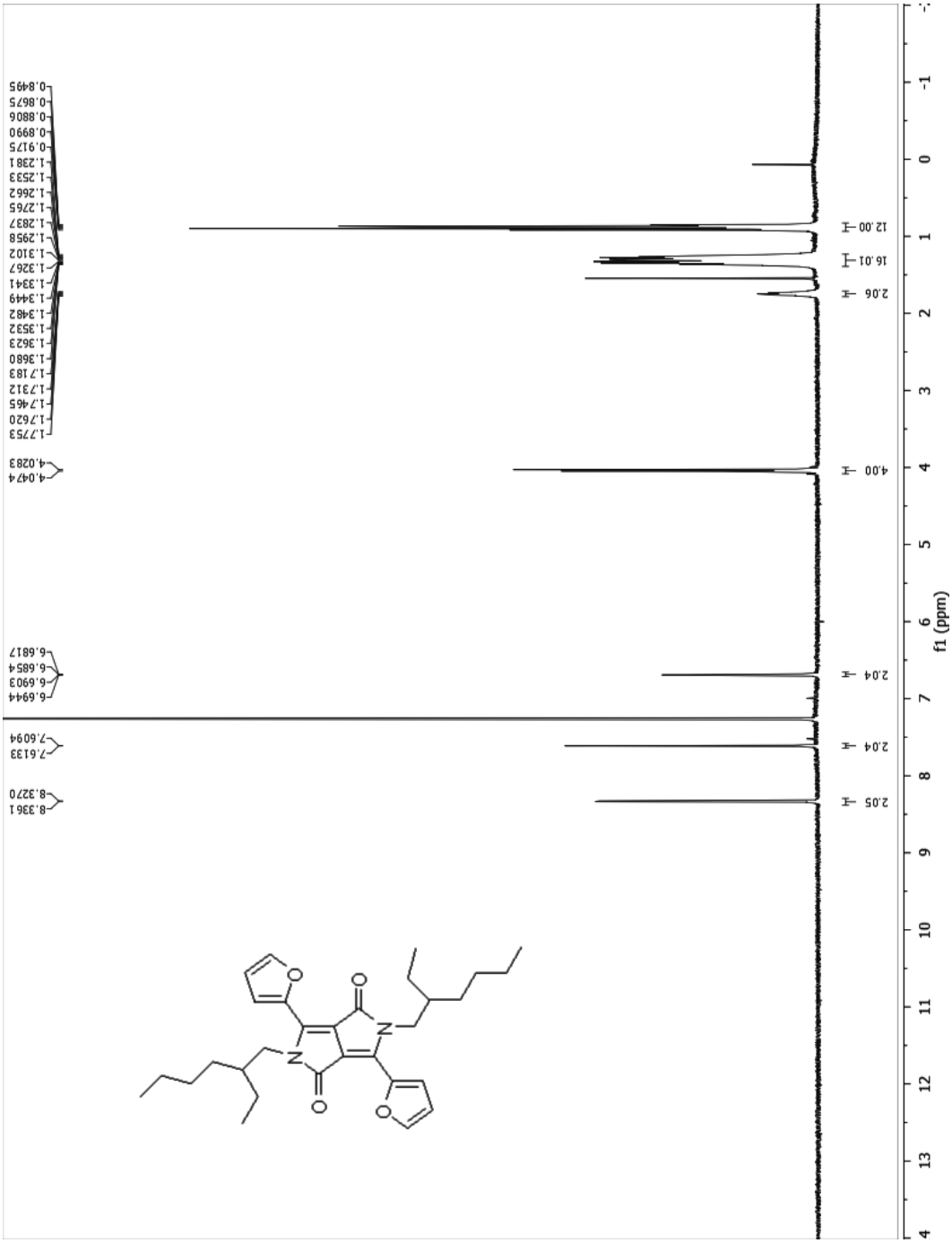


**Figure S4.1.** $^{1}$H NMR of **2**.

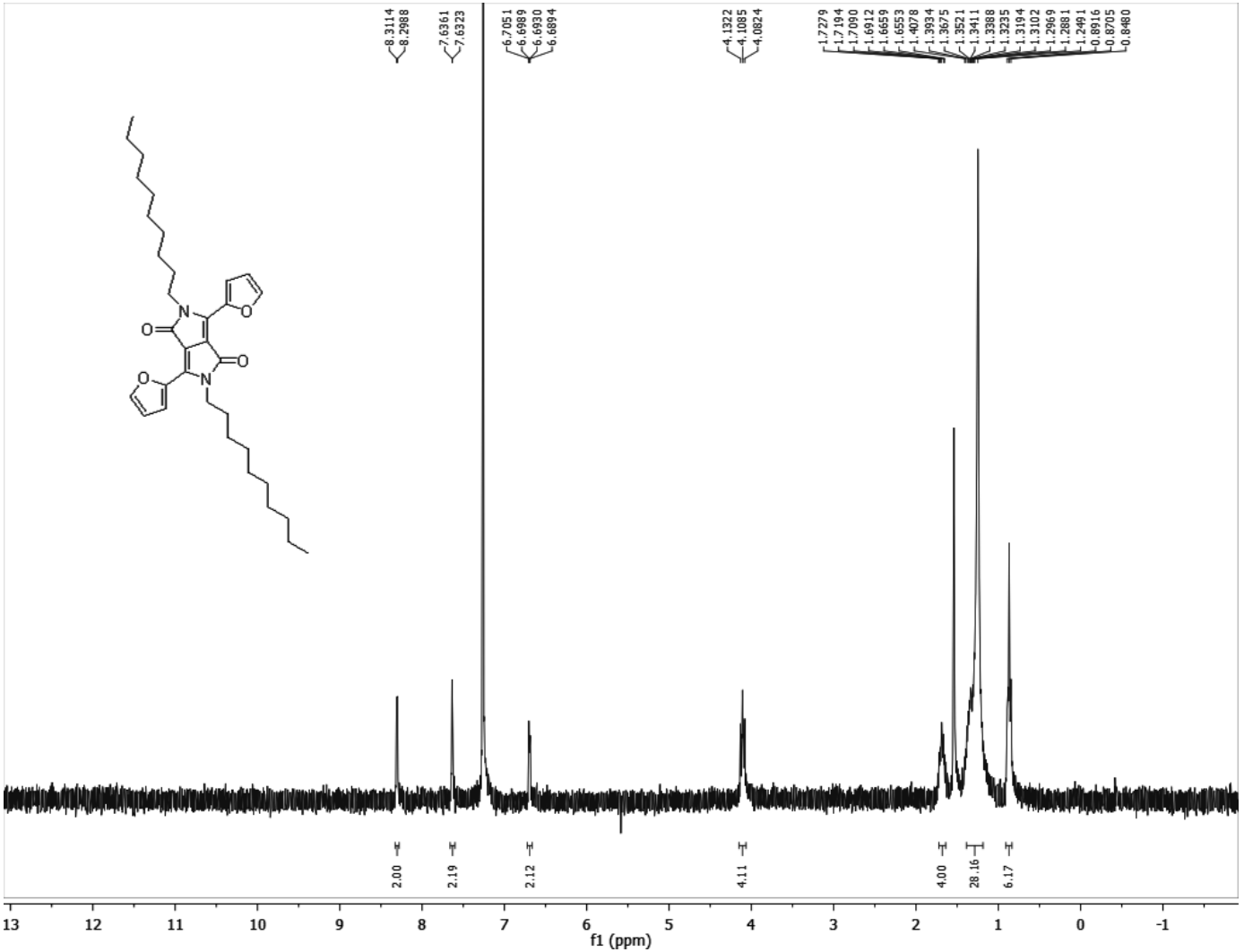


**Figure S4.2.** $^{1}$H NMR of **3**.

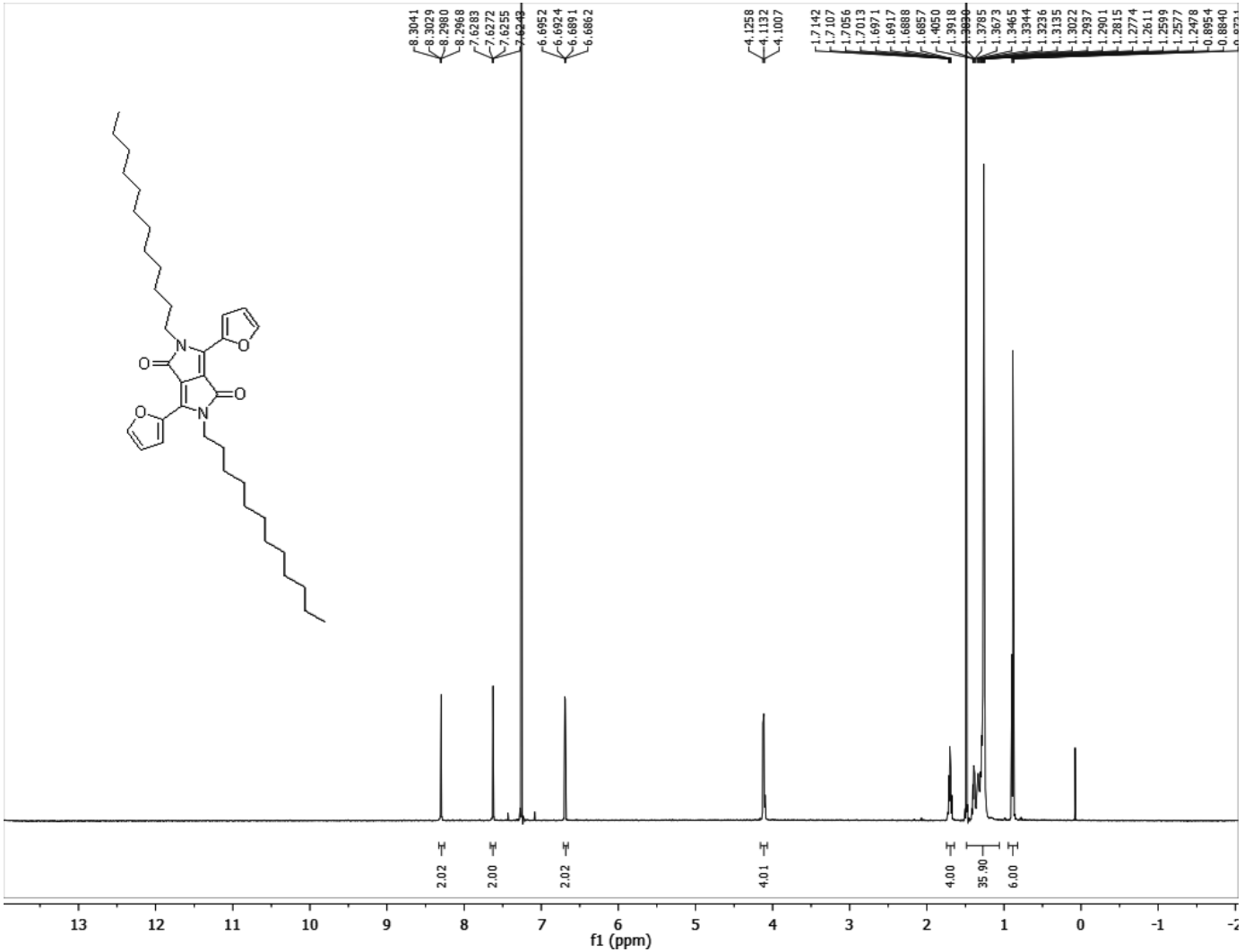


**Figure S4.3.** $^{1}$H NMR of **4**.

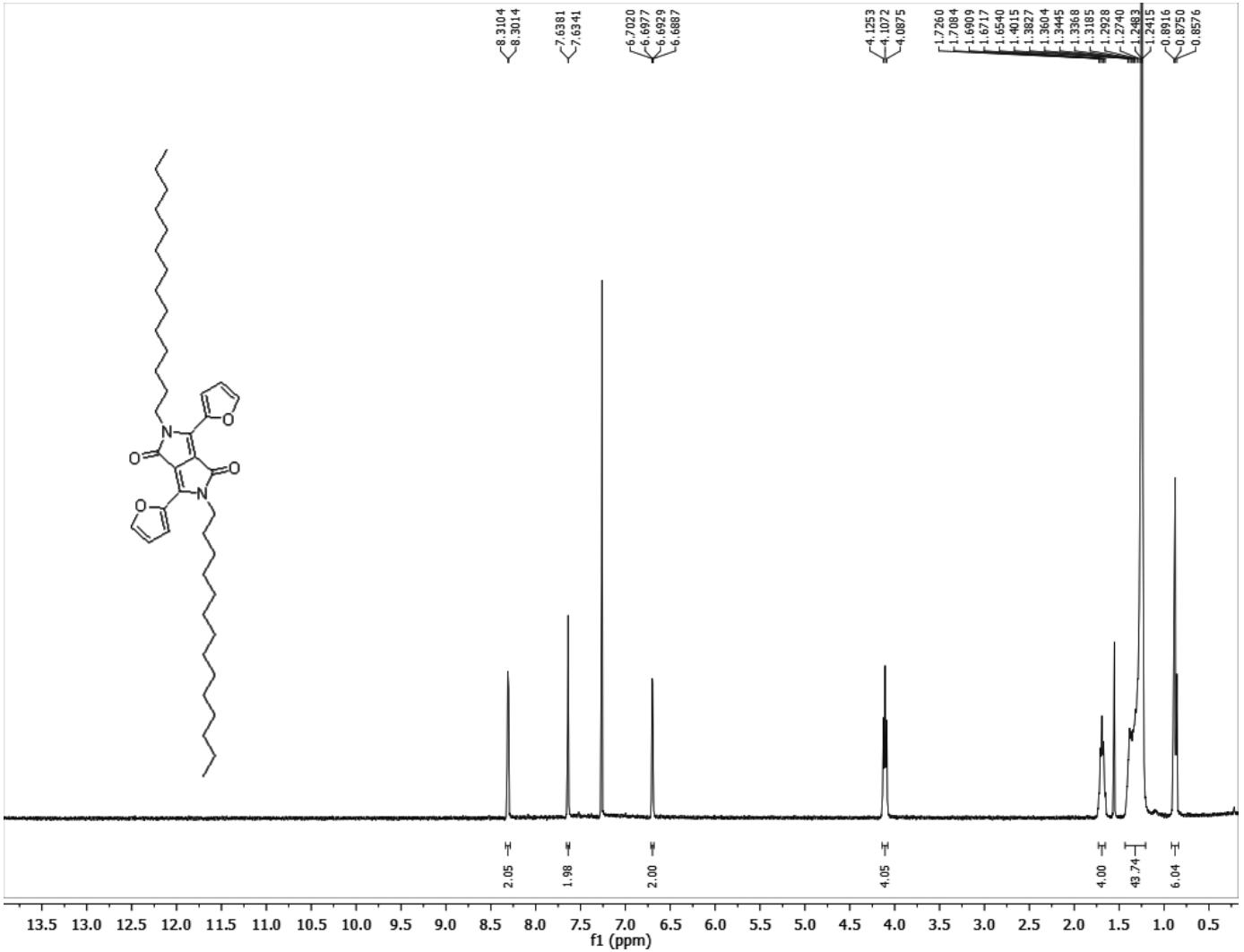


**Figure S4.4.** $^{1}$H NMR of **5**.

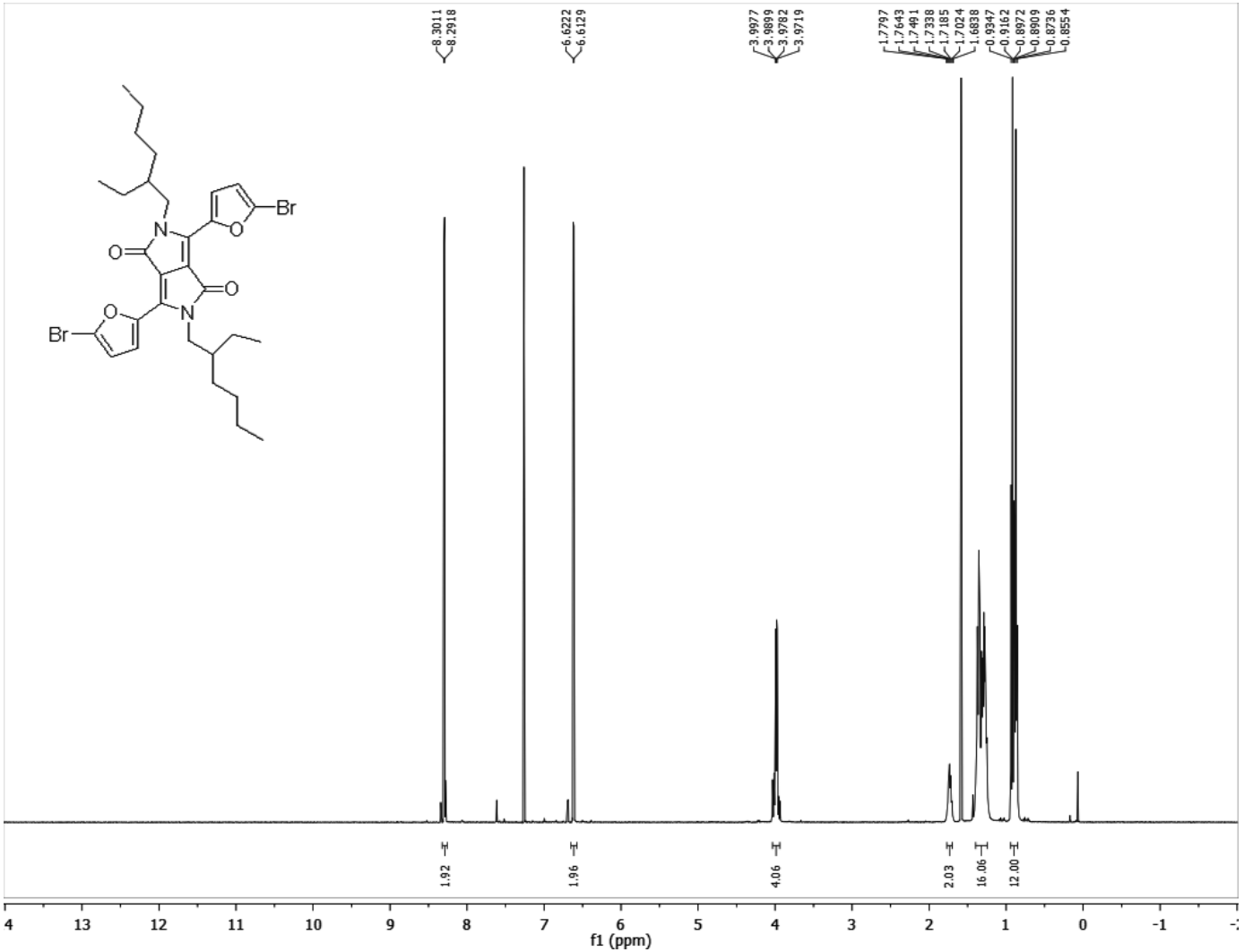


**Figure S4.5.** $^{1}$H NMR of **M1**.

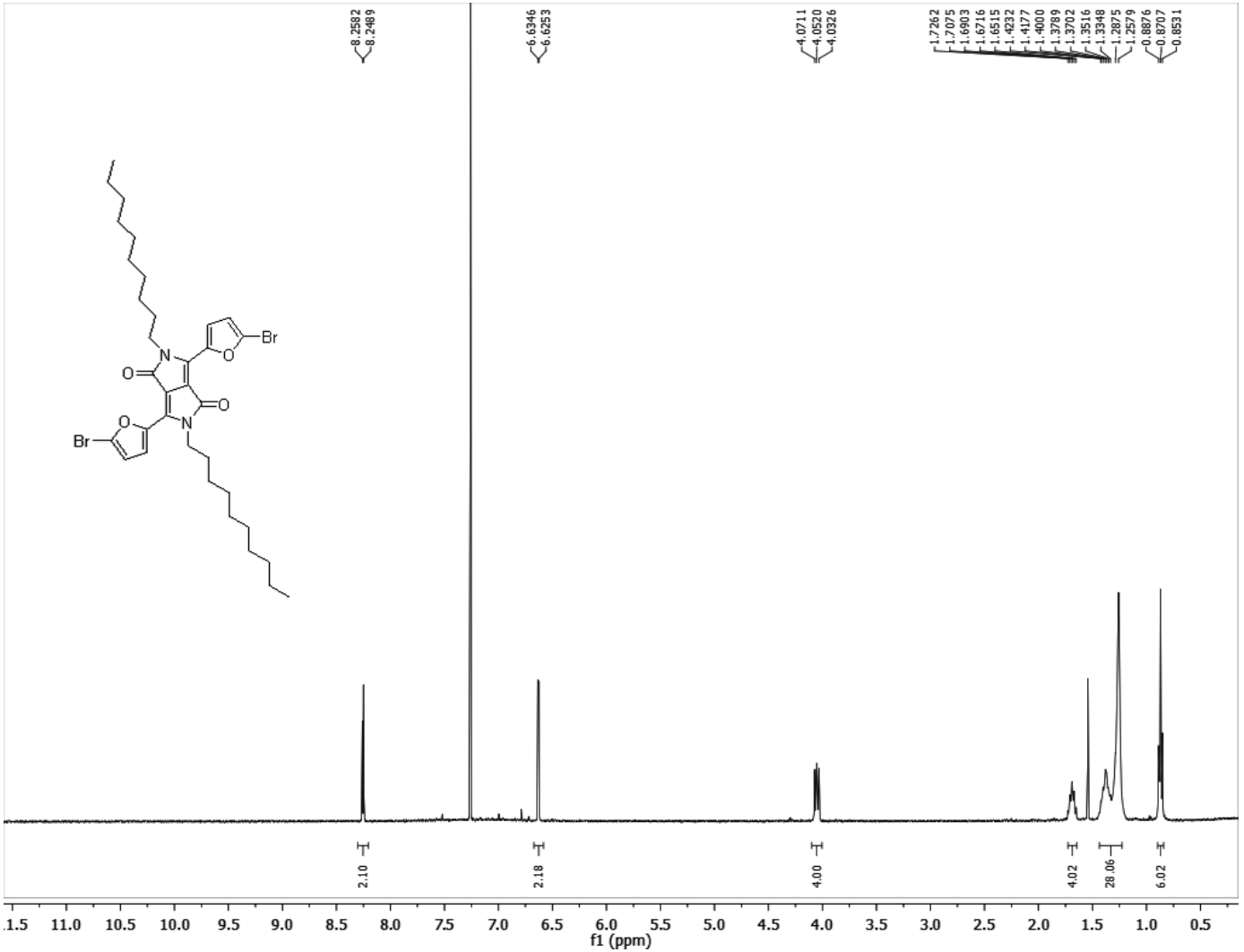


**Figure S4.6.** $^{1}$H NMR of **M2**.

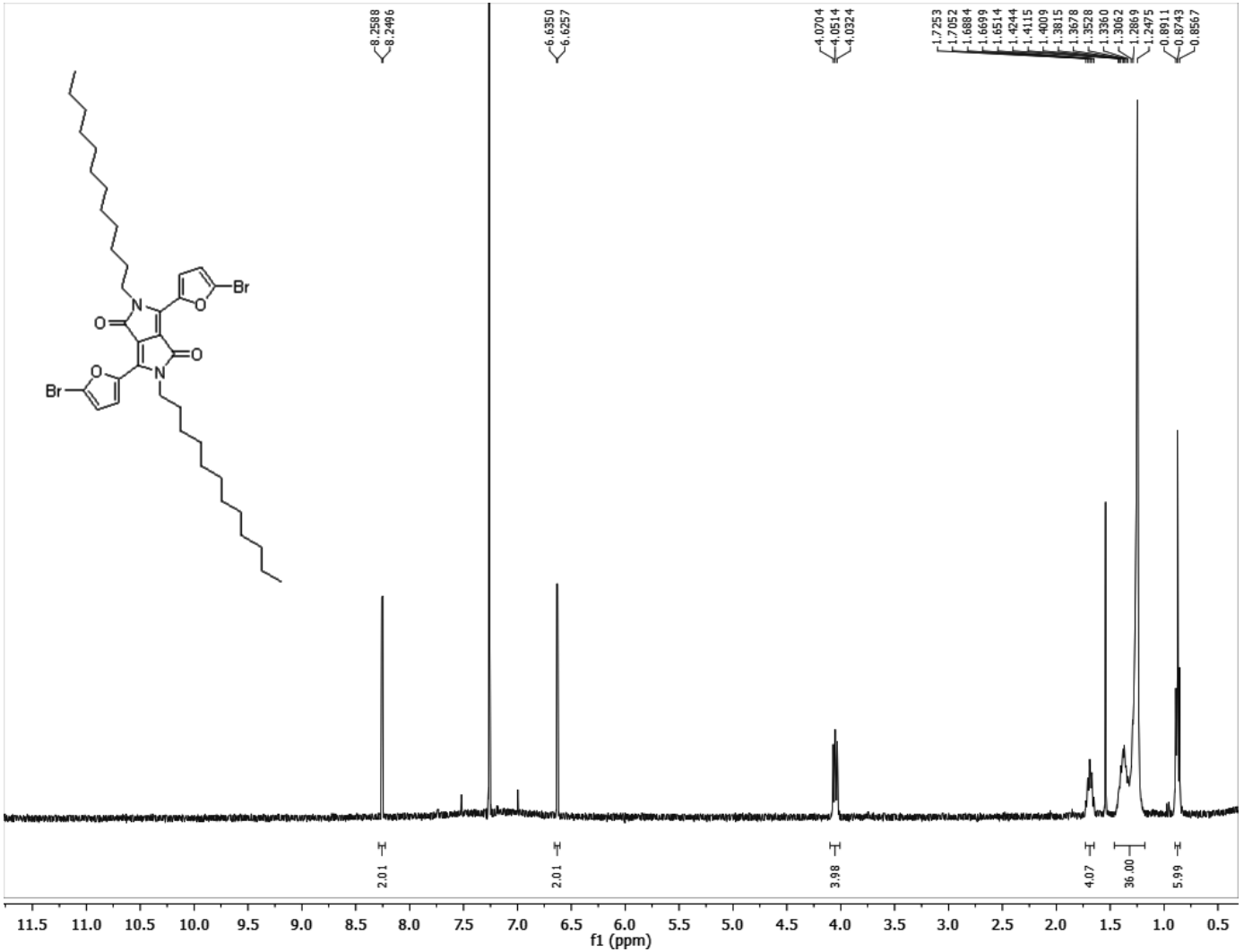


**Figure S4.7.** $^{1}$H NMR of **M3**.

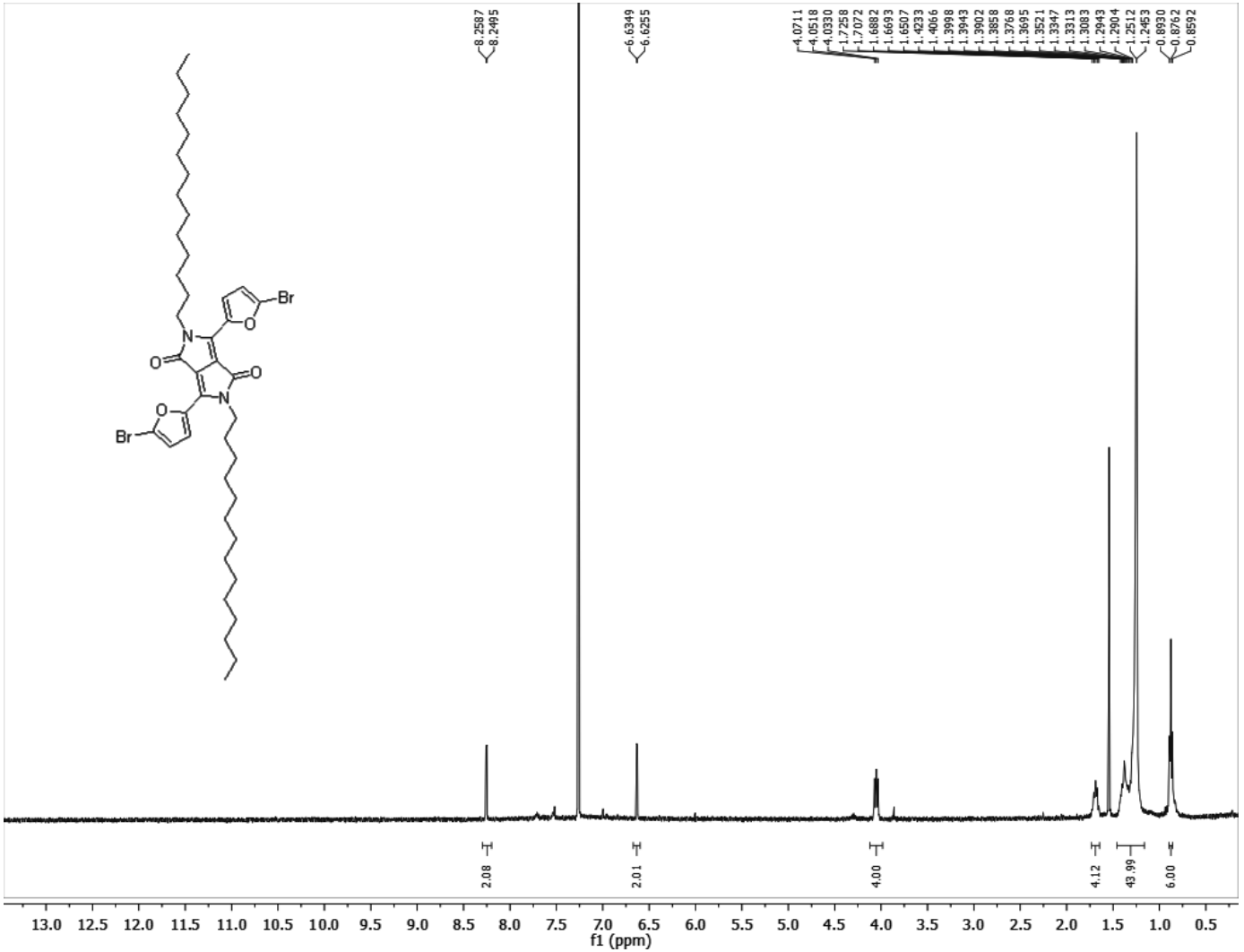


**Figure S4.8.** $^{1}$H NMR of **M4**.

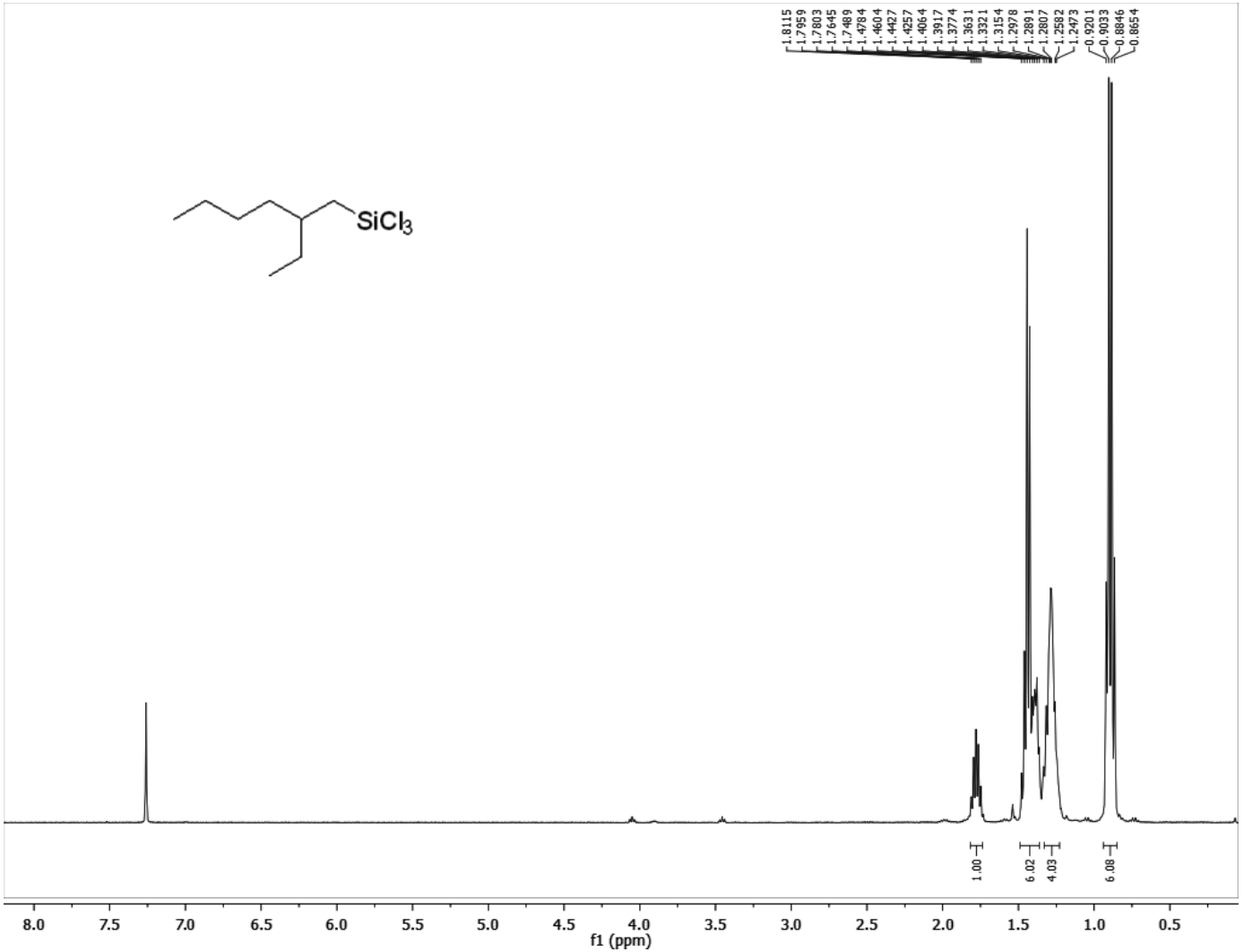


**Figure S4.9.** $^{1}$H NMR of **6**.

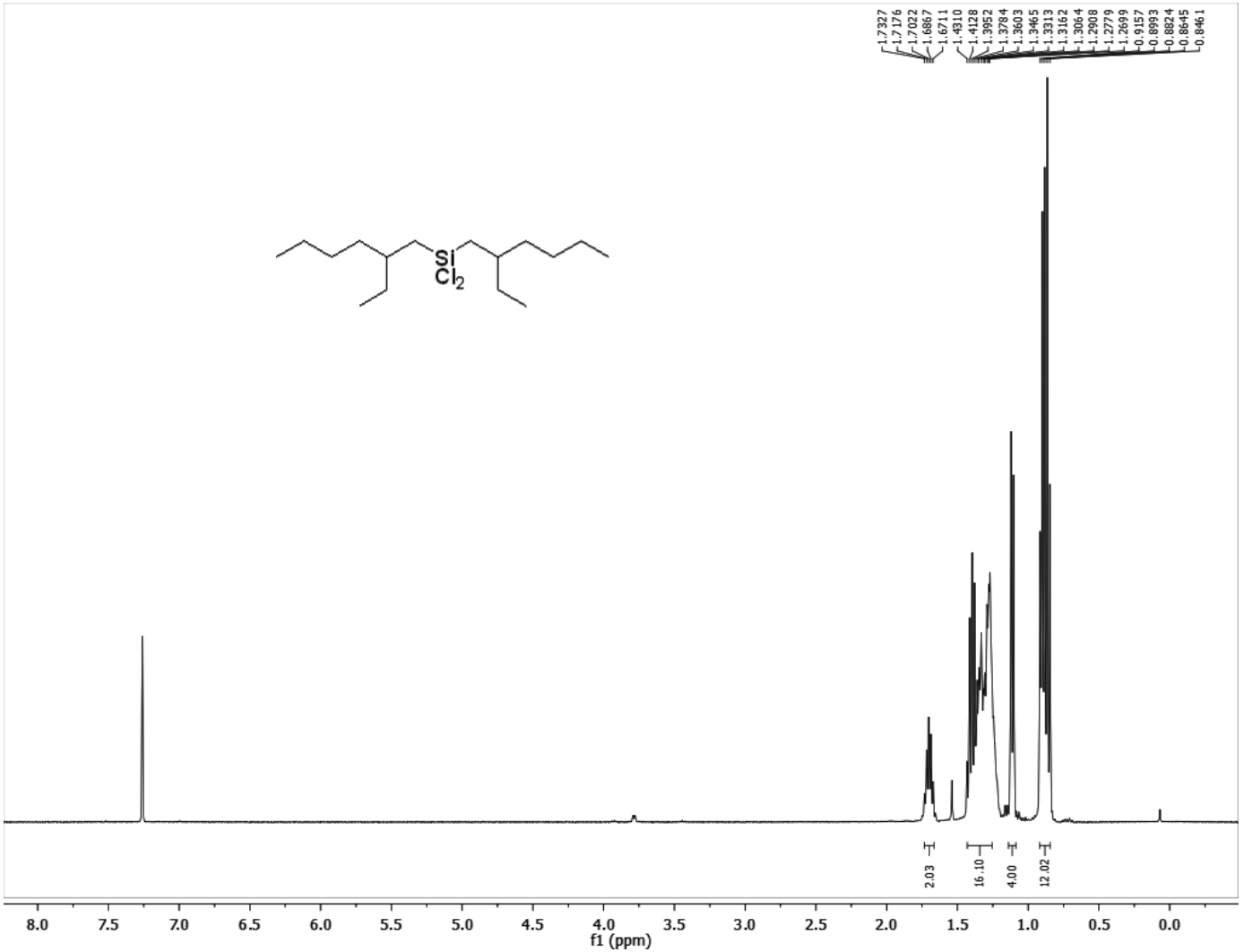


**Figure S4.10.** $^{1}$H NMR of **7**.

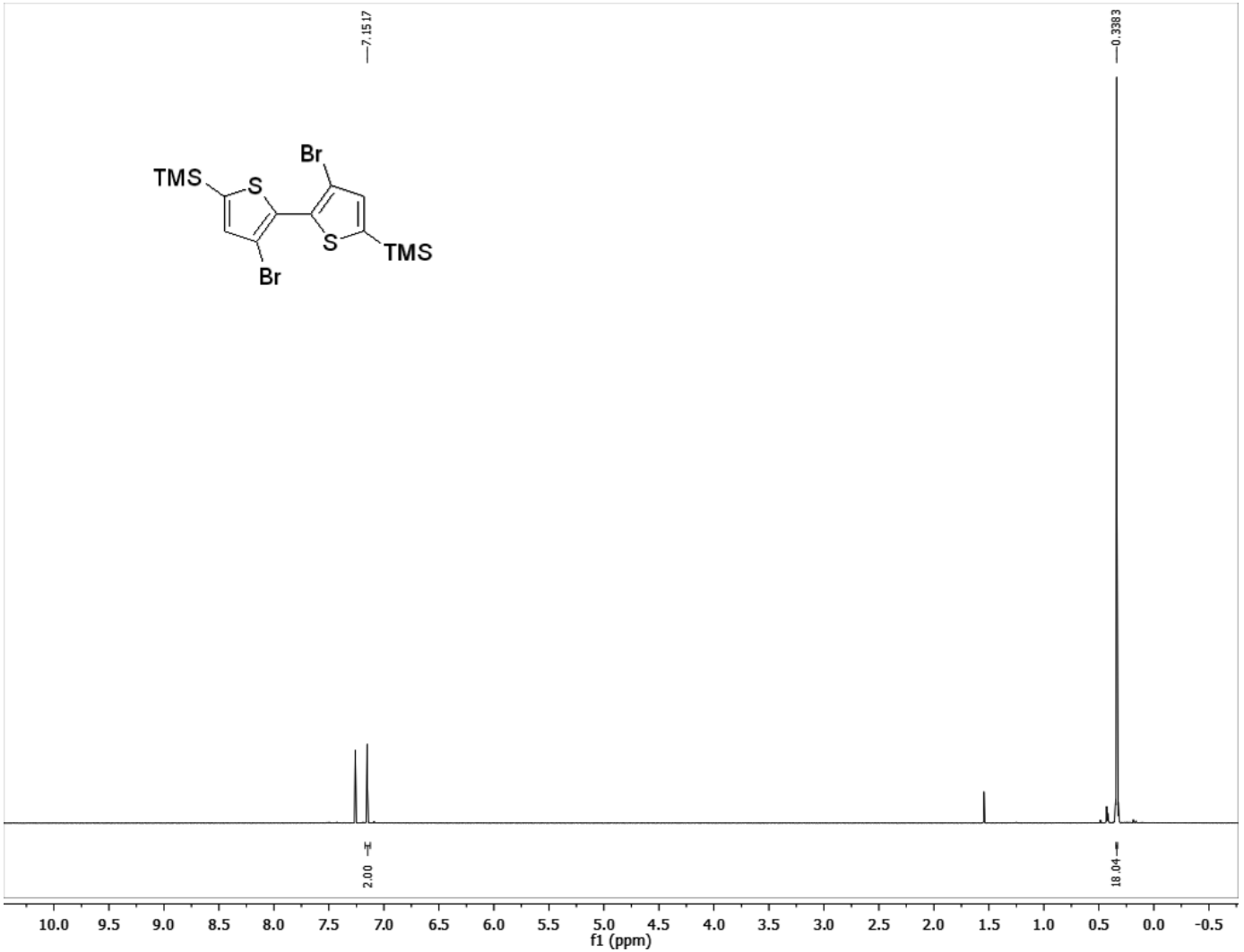


**Figure S4.11.** $^{1}$H NMR of **8**.

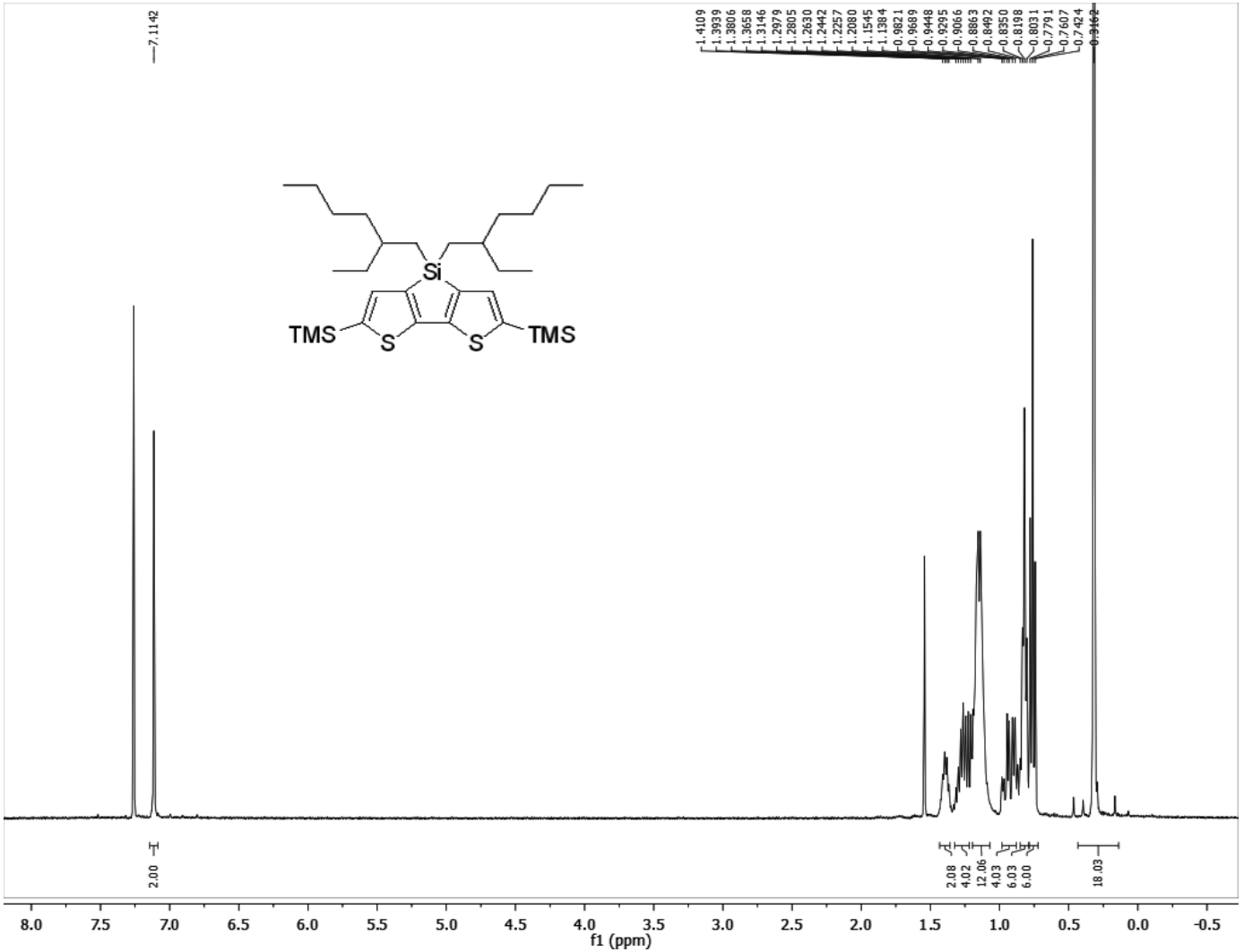


**Figure S4.12.** $^{1}$H NMR of **9**.

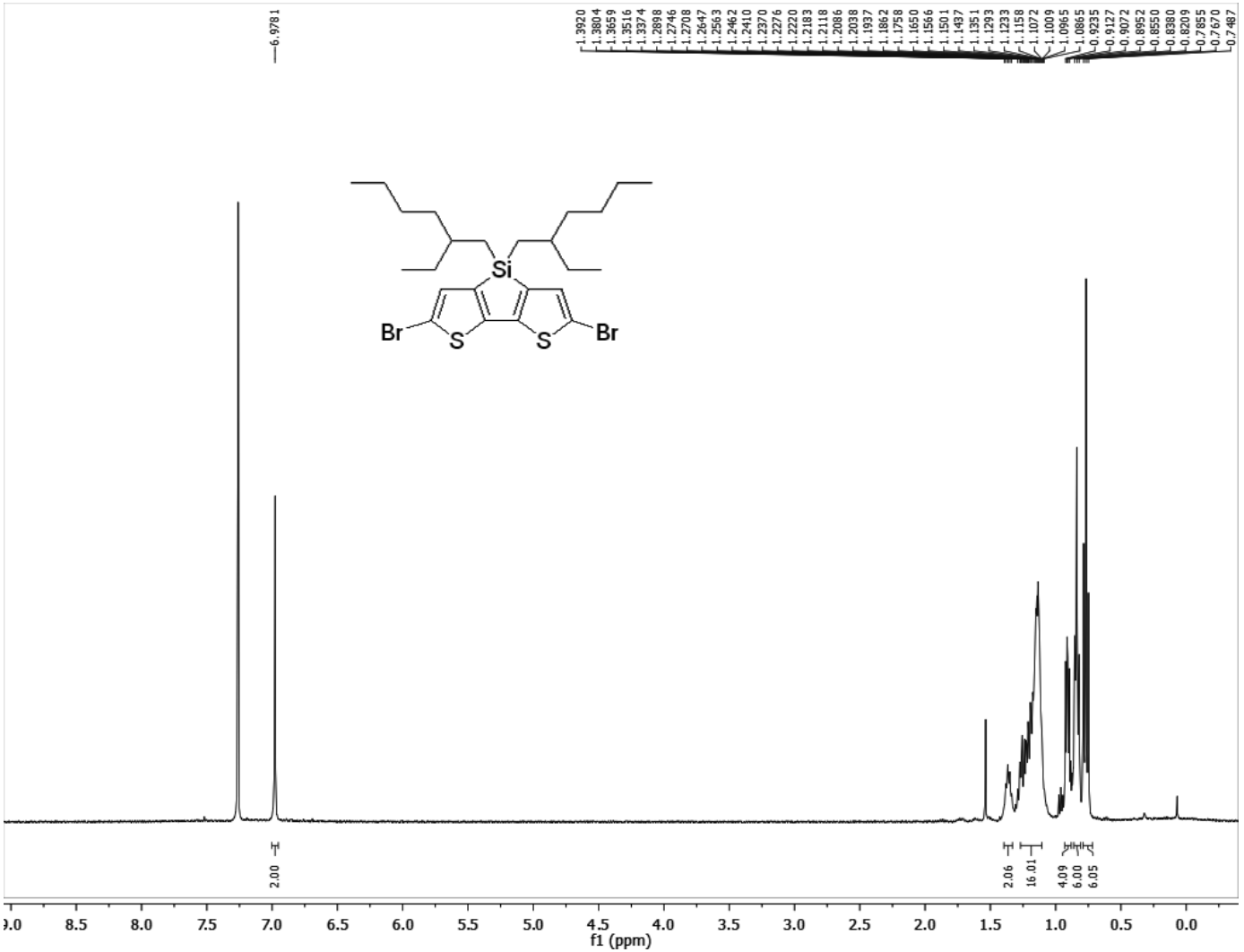


**Figure S4.13.** $^{1}$H NMR of **10**.

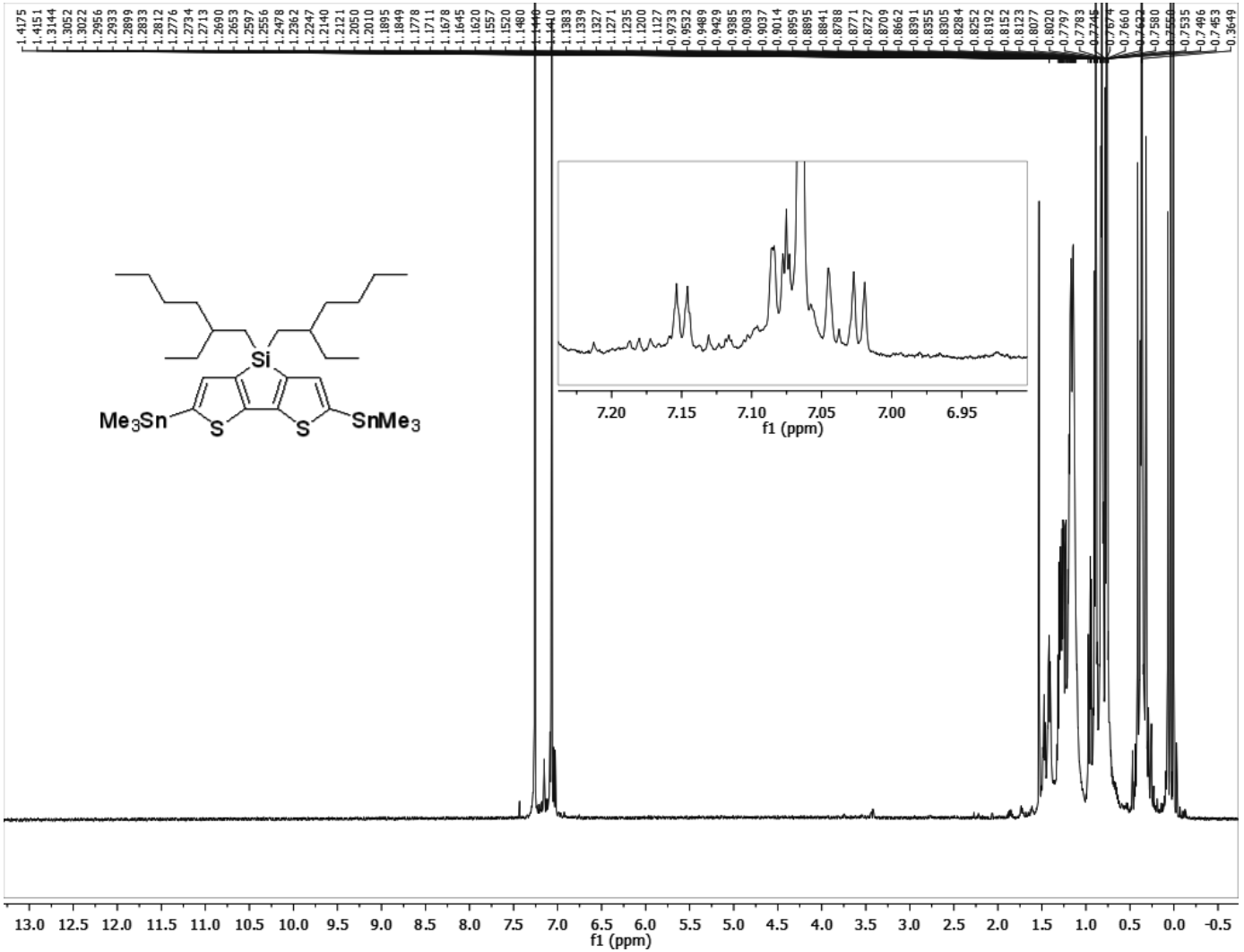


**Figure S4.14.** $^{1}$H NMR of **DTS** (crude) with inset of aromatic region.

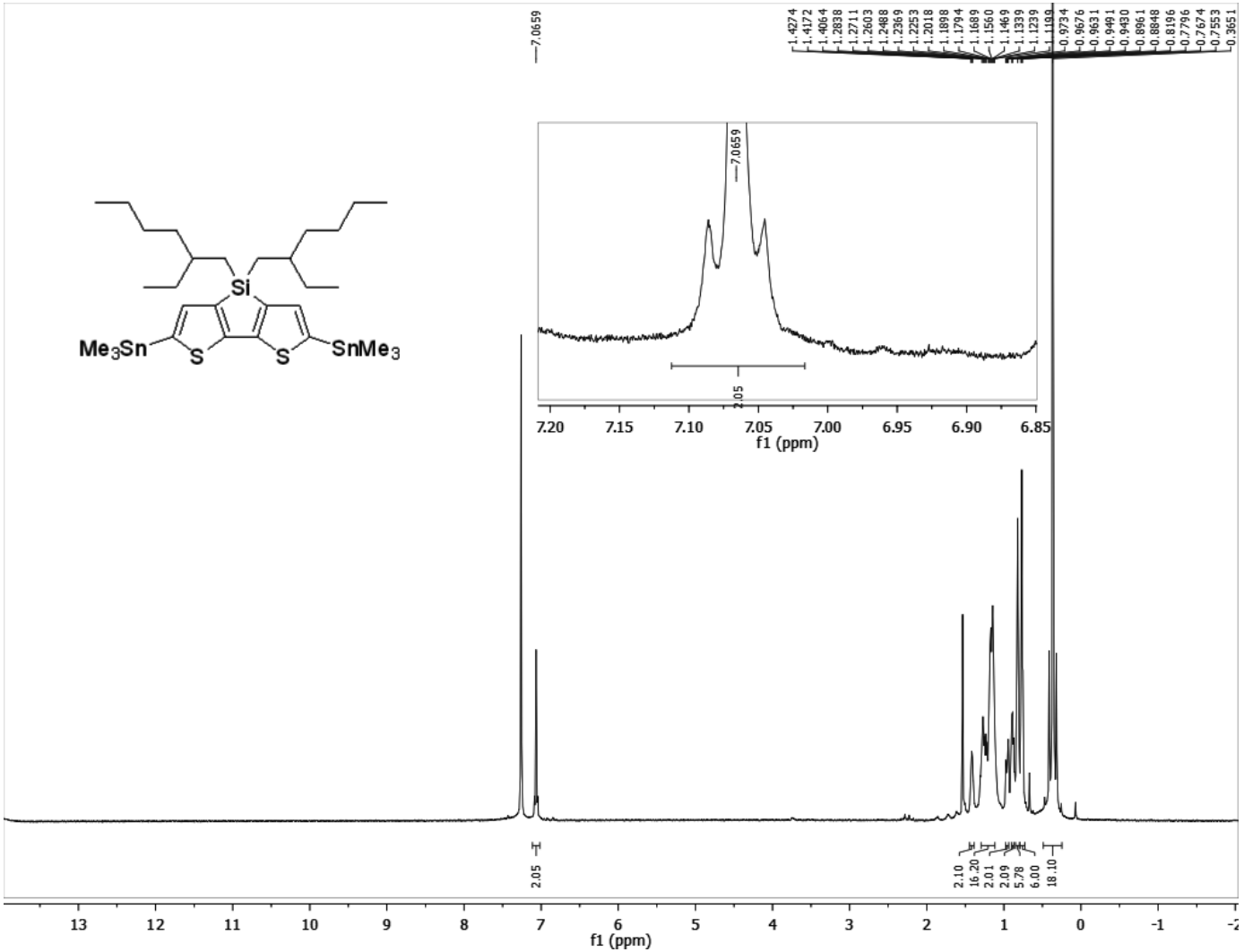


**Figure S4.15.** $^{1}$H NMR of **DTS** (HPLC purified) with inset of aromatic region.

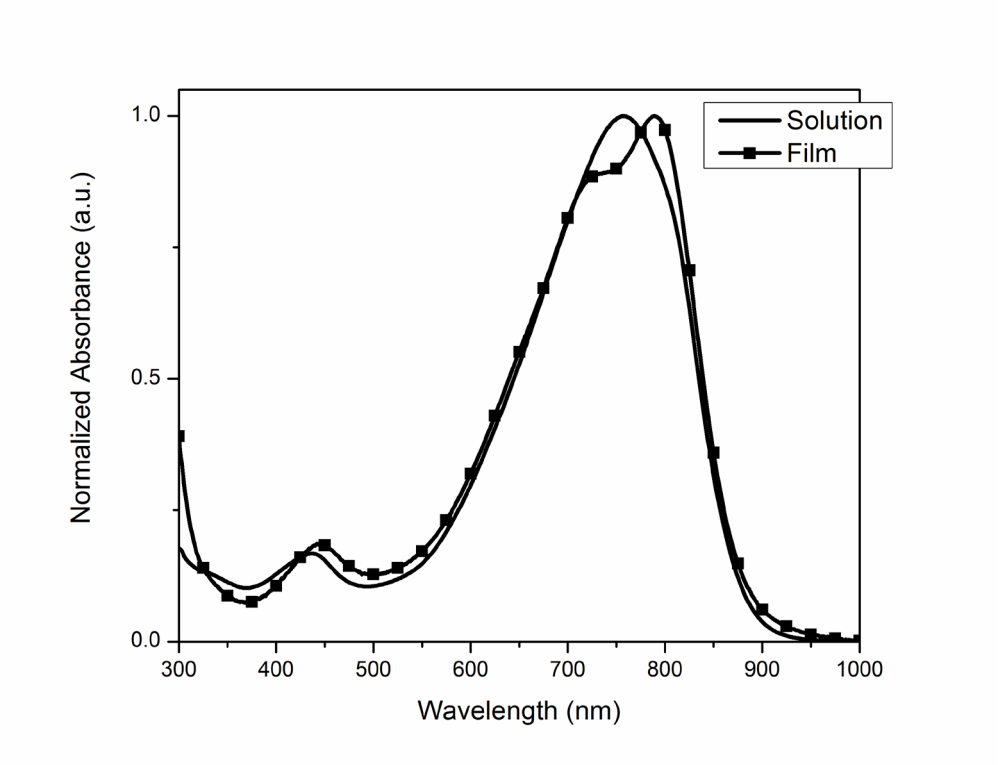


**Figure S4.16.** UV-vis absorption of **P1** in $CHCl_3$ and thin film.

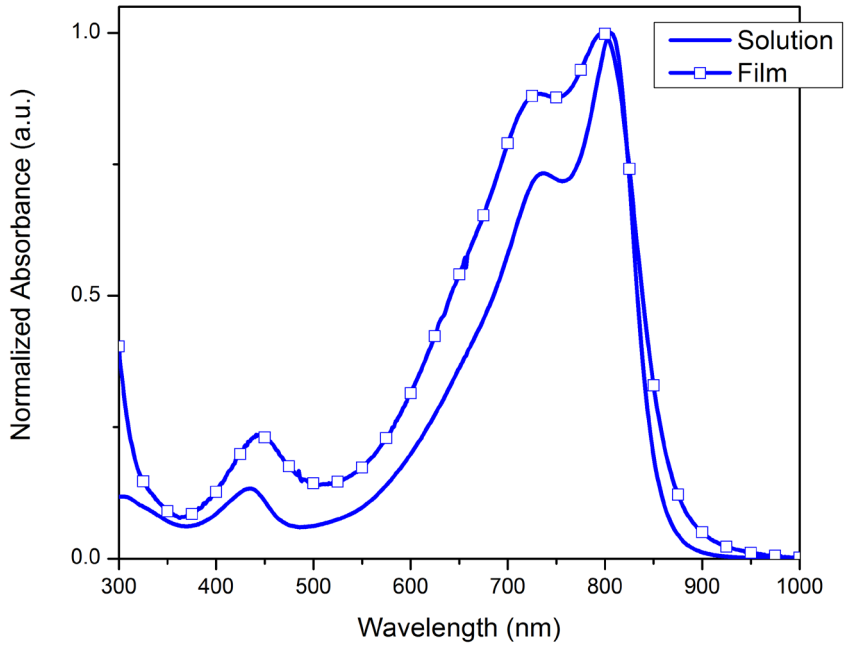


**Figure S4.17.** UV-vis absorption of **P2** in $CHCl_3$ and thin film.

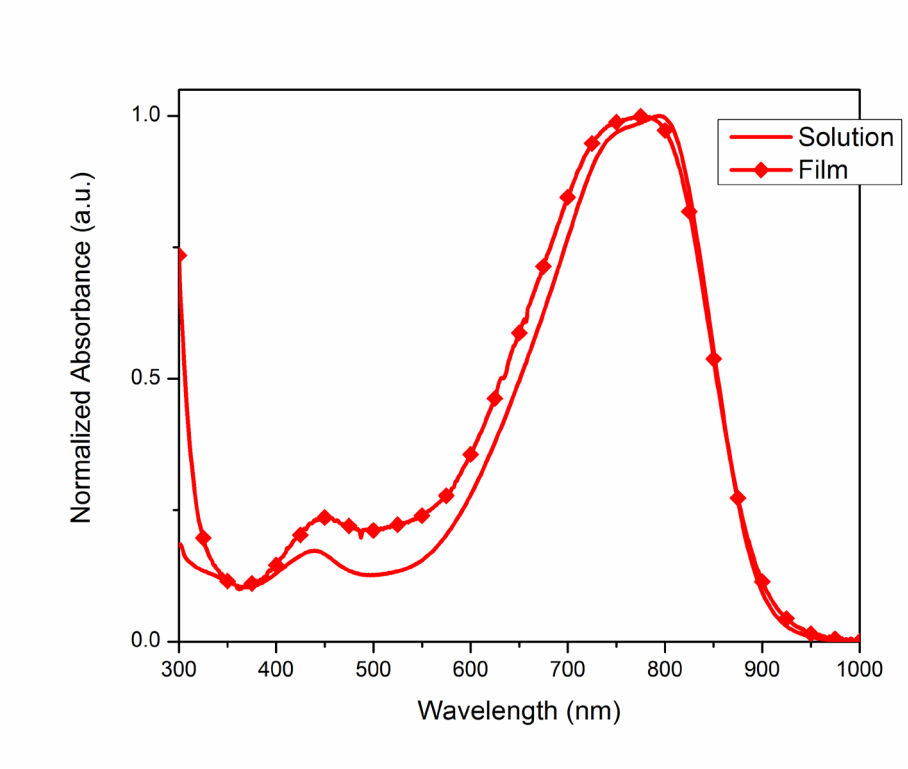


**Figure S4.18.** UV-vis absorption of **P3** in $CHCl_3$ and thin film.

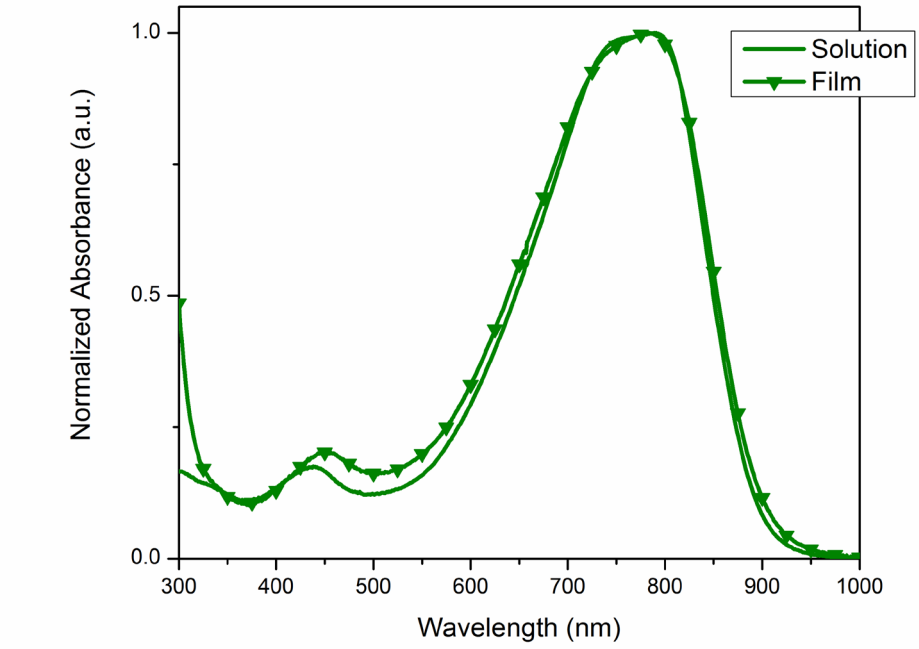


**Figure S4.19.** UV-vis absorption of **P4** in $CHCl_3$ and thin film.

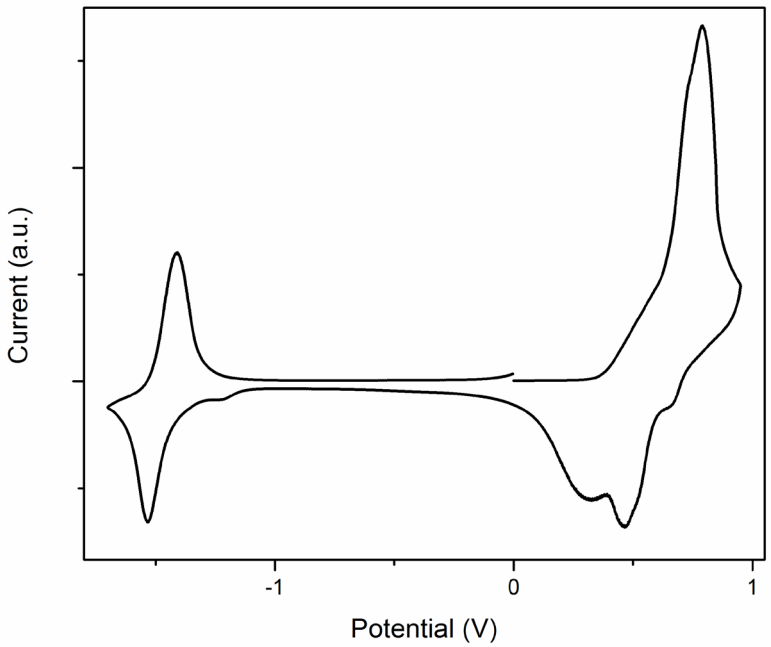


**Figure S4.20.** Cyclic voltammetry trace of **P1**.

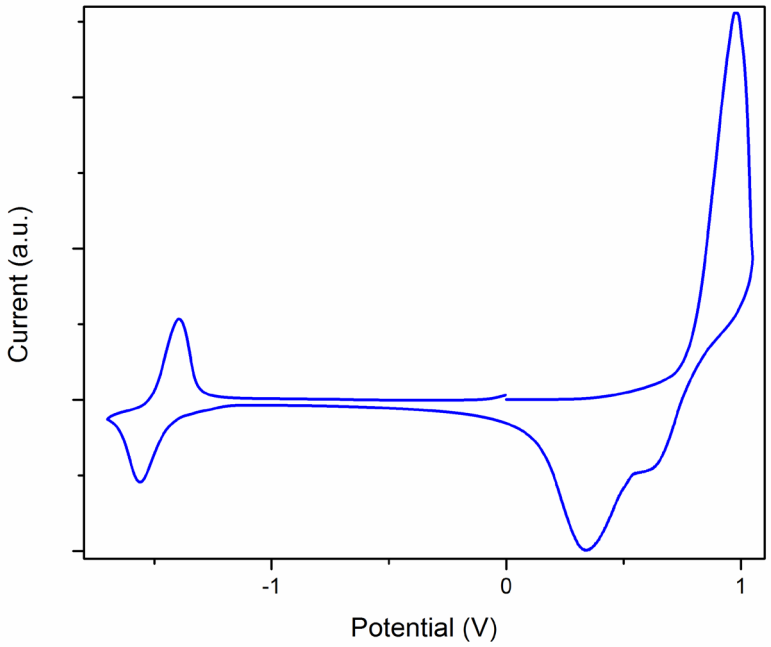


**Figure S4.21.** Cyclic voltammetry trace of **P2**.

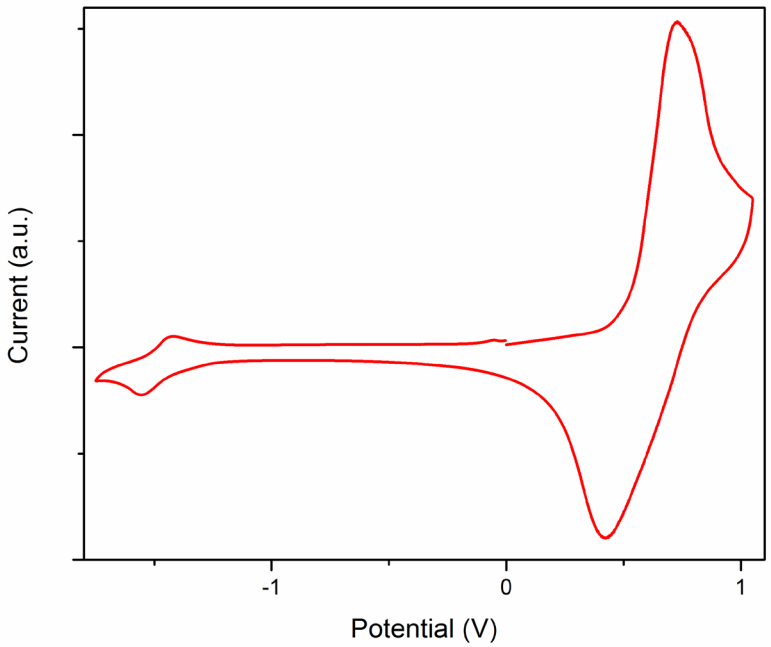


**Figure S4.22.** Cyclic voltammetry trace of **P3**.

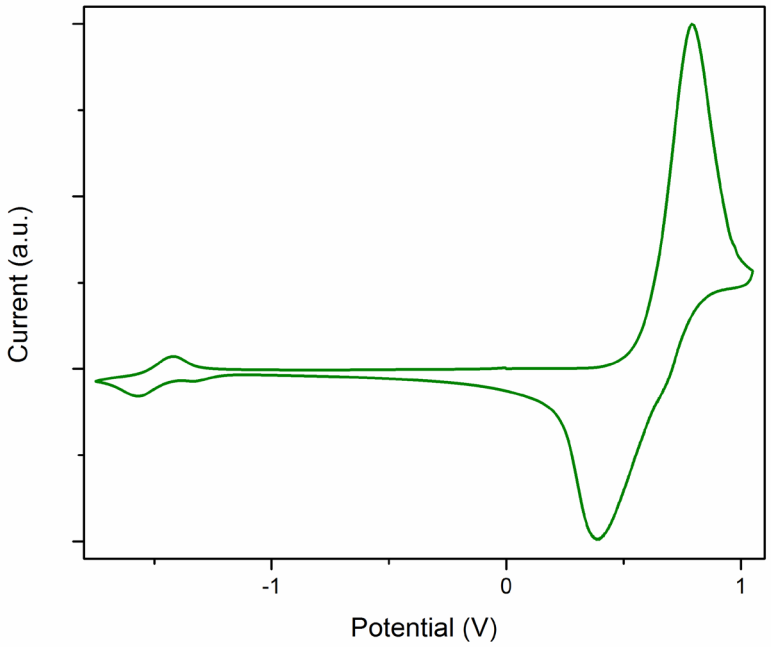


**Figure S4.23.** Cyclic voltammetry trace of **P4**.

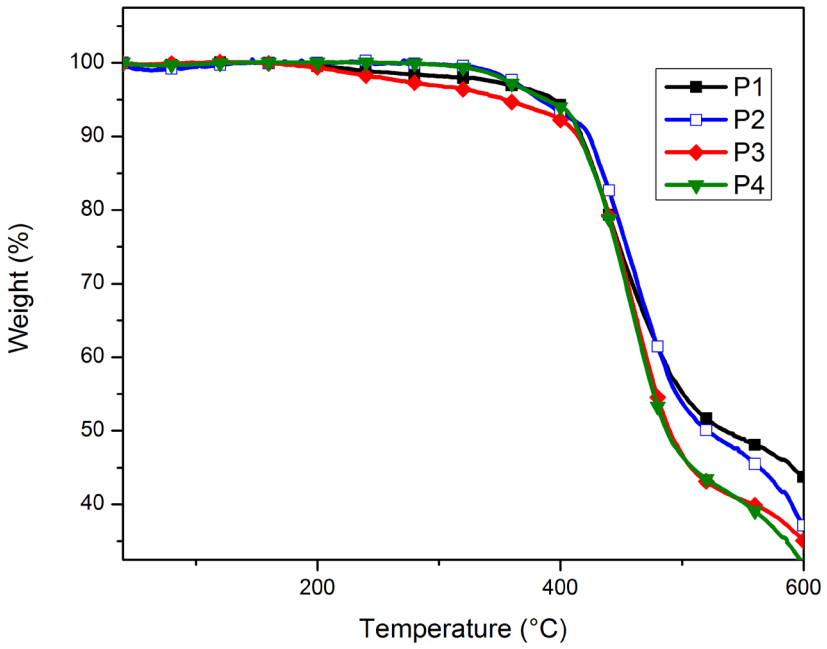


**Figure S4.24.** Thermal gravometric analysis of **P1**-**P4**.

## 4.8 References


1. Yu, G.; Gao, J.; Hummelen, J. C.; Wudl, F.; Heeger, A. J., *Science* **1995,** *270* (5243), 1789-1791.

2. Yu, G.; Heeger, A. J., *J. Appl. Phys.* **1995,** *78* (7), 4510-4515.

3. Thompson, B. C.; Fréchet, J. M. J., *Angew. Chem. Int. Ed.* **2008,** *47* (1), 58-77.

4. Scharber, M. C.; Mühlbacher, D.; Koppe, M.; Denk, P.; Waldauf, C.; Heeger, A. J.; Brabec, C. J., *Adv. Mater.* **2006,** *18* (6), 789-794.

5. Boudreault, P.-L. T.; Najari, A.; Leclerc, M., *Chem. Mater.* **2010,** *23* (3), 456-469.

6. Bundgaard, E.; Krebs, F. C., *Sol. Energy Mater. Sol. Cells* **2007,** *91* (11), 954-985.

7. Günes, S.; Neugebauer, H.; Sariciftci, N. S., *Chem. Rev.* **2007,** *107* (4), 1324-1338.

8. Cheng, Y.-J.; Yang, S.-H.; Hsu, C.-S., *Chem. Rev.* **2009,** *109* (11), 5868-5923.

9. Chen, J.; Cao, Y., *Acc. Chem. Res.* **2009,** *42* (11), 1709-1718.

10. Dennler, G.; Scharber, M. C.; Brabec, C. J., *Adv. Mater.* **2009,** *21* (13), 1323-1338.

11. Nelson, J., *Mater. Today* **2011,** *14* (10), 462-470.

12. Facchetti, A., *Chem. Mater.* **2010,** *23* (3), 733-758.

13. Grimsdale, A. C.; Leok Chan, K.; Martin, R. E.; Jokisz, P. G.; Holmes, A. B., *Chem. Rev.* **2009,** *109* (3), 897-1091.

14. Thomas, S. W.; Joly, G. D.; Swager, T. M., *Chem. Rev.* **2007,** *107* (4), 1339-1386.

15. Yamamoto, T.; Zhou, Z.-h.; Kanbara, T.; Shimura, M.; Kizu, K.; Maruyama, T.; Nakamura, Y.; Fukuda, T.; Lee, B.-L.; Ooba, N.; Tomaru, S.; Kurihara, T.; Kaino, T.; Kubota, K.; Sasaki, S., *J. Am. Chem. Soc.* **1996,** *118* (43), 10389-10399.

16. Liu, Y.; Zhao, J.; Li, Z.; Mu, C.; Ma, W.; Hu, H.; Jiang, K.; Lin, H.; Ade, H.; Yan, H., *Nat Commun* **2014,** *5*.

17. Liu, C.; Yi, C.; Wang, K.; Yang, Y.; Bhatta, R. S.; Tsige, M.; Xiao, S.; Gong, X., *ACS Applied Materials & Interfaces* **2015,** *7* (8), 4928-4935.

18. Jeffries-El, M.; Kobilka, B. M.; Hale, B. J., *Macromolecules* **2014,** *47* (21), 7253-7271.

19. Gidron, O.; Diskin-Posner, Y.; Bendikov, M., *J. Am. Chem. Soc.* **2010,** *132* (7), 2148-2150.

20. Woo, C. H.; Beaujuge, P. M.; Holcombe, T. W.; Lee, O. P.; Fréchet, J. M. J., *J. Am. Chem. Soc.* **2010,** *132* (44), 15547-15549.

21. Hollinger, J.; Gao, D.; Seferos, D. S., *Isr. J. Chem.* **2014**, 10.1002/ijch.201400011, n/a-n/a.

22. Kobilka, B. M.; Hale, B. J.; Ewan, M. D.; Dubrovskiy, A. V.; Nelson, T. L.; Duzhko, V.; Jeffries-El, M., *Polymer Chemistry* **2013,** *4* (20), 5329.

23. Zou, Y.; Gendron, D.; Neagu-Plesu, R.; Leclerc, M., *Macromolecules* **2009,** *42* (17), 6361-6365.

24. Huo, L.; Hou, J.; Chen, H.-Y.; Zhang, S.; Jiang, Y.; Chen, T. L.; Yang, Y., *Macromolecules* **2009,** *42* (17), 6564-6571.

25. Cowan, S. R.; Roy, A.; Heeger, A. J., *Physical Review B* **2010,** *82* (24).

26. Yiu, A. T.; Beaujuge, P. M.; Lee, O. P.; Woo, C. H.; Toney, M. F.; Frechet, J. M., *J. Am. Chem. Soc.* **2012,** *134* (4), 2180-5.

27. Beaujuge, P. M.; Amb, C. M.; Reynolds, J. R., *Acc. Chem. Res.* **2010,** *43* (11), 1396-1407.

28. Ostroverkhova, O.; Shcherbyna, S.; Cooke, D. G.; Egerton, R. F.; Hegmann, F. A.; Tykwinski, R. R.; Parkin, S. R.; Anthony, J. E., *J. Appl. Phys.* **2005,** *98* (3), 033701.

29. Gierschner, J.; Ehni, M.; Egelhaaf, H. J.; Milian Medina, B.; Beljonne, D.; Benmansour, H.; Bazan, G. C., *J. Chem. Phys.* **2005,** *123* (14), 144914.

30. Wienk, M. M.; Turbiez, M.; Gilot, J.; Janssen, R. A. J., *Adv. Mater.* **2008,** *20* (13), 2556-2560.

31. Izumi, T.; Kobashi, S.; Takimiya, K.; Aso, Y.; Otsubo, T., *J. Am. Chem. Soc.* **2003,** *125* (18), 5286-5287.

32. Beaupré, S.; Belletête, M.; Durocher, G.; Leclerc, M., *Macromol. Theory Simul.* **2011,** *20* (1), 13-18.

33. Cardona, C. M.; Li, W.; Kaifer, A. E.; Stockdale, D.; Bazan, G. C., *Adv. Mater.* **2011,** *23* (20), 2367-71.

34. Khor, E.; Choon Ng, S.; Chze Li, H.; Chai, S., *Heterocycles* **1991,** *32* (9), 1805.

35. Hirono, Y.; Kobayashi, K.; Yonemoto, M.; Kondo, Y., *Chem. Commun.* **2010,** *46* (40), 7623-7624.

# CHAPTER 5

## LOW AND MEDIUM BANDGAP DONOR-ACCEPTOR COPOLYMERS UTILIZING PYRROLOPYRROLEDIONE AS A π-DONOR

*Benjamin J. Hale, Jon Stoffer, and Malika Jeffries-EL**

Department of Chemistry, Iowa State University, Ames, IA 50011, USA

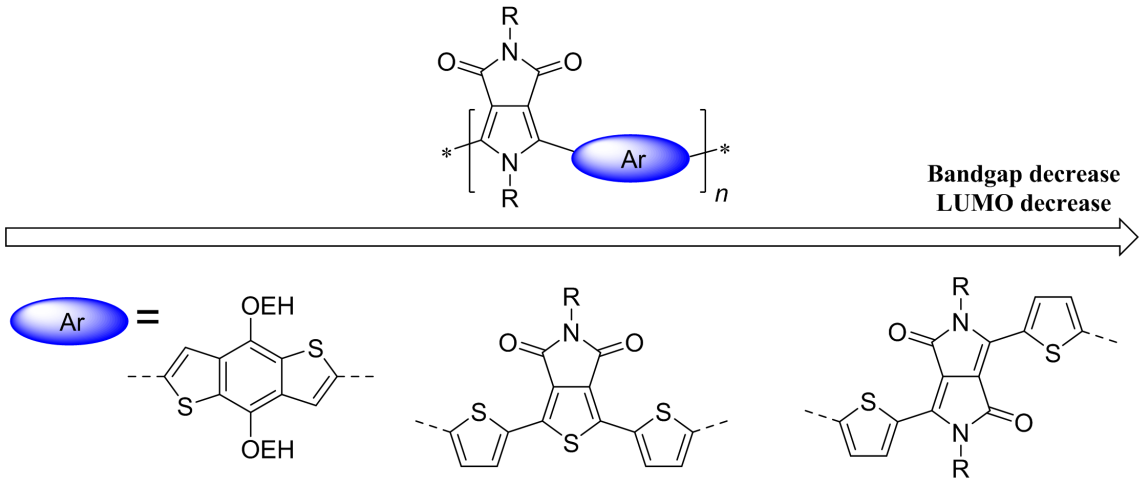


## 5.1 Abstract

Donor-acceptor copolymers comprised of the pyrrolo[3,4-*c*]pyrrole-1,3-dione (PPD) unit as a π-electron donor and pyrrolo[3,4-*c*]pyrrole-1,3-dione or diketopyrrolopyrrole as π-electron acceptors were synthesized by the Stille cross-coupling reaction. The optical and electrochemical properties were studied and compared to the polymer PBDT-PPD,

where PPD was used an acceptor. Although the PPD donor polymers suffered from low molecular weights and poor film forming properties, they displayed significantly lower bandgaps, broader optical absorption, and lower LUMO levels than PBDT-PPD. The improvements in optical absorption and energy levels give promise to the use of PPD as a donor in medium to narrow bandgap donor-acceptor copolymers.

## 5.2 Introduction

Research into organic semiconductors has grown exponentially since their discovery nearly forty years ago.[1-3] In that time, the field has grown to encompass organic light-emitting diodes, photovoltaics (OPVs), field-effect transistors, and non-linear optics, among others.[4-15] With the ever increasing need for energy, the development of high performance OPVs has become vital.[16] The use of conjugated donor-acceptor polymers, comprised of alternating π-electron rich and π-electron deficient arylene units, allows for energy levels that may be impossible to attain through the use of homopolymers.[8, 17-19] This technique has paved the way to materials with many desirable properties, such as deep highest occupied molecular orbital energy levels, broad optical absorption bands, LUMO levels with appropriate alignment to [6,6]-phenyl-$C_{71}$-butyric acid methyl ester ($PC_{71}BM$), and materials with relatively large dielectric constants.[20-25]

Heteroatom substitution in conjugated polymers can have a drastic impact on the physical, optical, and electronic properties of a material.[20, 26] Pyrrolo[3,4-*c*]pyrroledione (PPD) is a little studied unit that is structurally similar to the widely used thieno[3,4-*c*]pyrroledione (TPD). Incorporation of an electron rich pyrrole has multiple advantages, including the possibility of increased solubility, without the addition of π-spacers,

through nitrogen alkylation.[27] While this may increase solubility, the change in the electronics and polarizability of the monomer can have damaging effects on donor-acceptor copolymers. As shown in Chapter 4 of this dissertation, the substitution of the sulfur in TPD with a nitrogen, as in PPD, turns off intramolecular charge transfer (ICT) between the donor and the acceptor unit. This drastically decreases optical absorption, widens the optical bandgap, and destabilizes the highest occupied molecular orbital (HOMO). The homopolymer-like characteristics displayed by the use of PPD as an acceptor suggests it may be better suited as a π-electron donor.

Here, we report the synthesis and properties of two donor-acceptor copolymers incorporating the PPD unit as a π-electron donor and thieno[3,4-*c*]pyrroledione and diketopyrrolopyrrole as π-electron acceptors. Optical and electrochemical studies of the polymers showed significantly narrower bandgaps than PBDT-PPD. Both materials had lower LUMO levels of -3.79 and -3.95 eV, compared to the -3.10 eV of PBDT-PPD. As thin films, both polymers showed broad absorption bands, indicative of ICT.[17, 19] The presence of ICT, broad absorption, and low LUMO levels show potential for the incorporation of PPD into high efficiency materials.

## 5.3 Results and Discussion

The synthetic route to the PPD monomer is shown in Scheme 5.1. Compound **3** was prepared from diethyl fumarate and toluenesulfonylmethyl isocyanide according to literature procedure, followed by N-alkylation with 2-butyloctyl bromide to give **4**.[27] Bromination and subsequent soaponification of compound **4** gave the diacid **6**. Conversion of **6** to

the corresponding anhydride using acetic anhydride, ring opening with 2-butyloctylamine, and ring closure with thionyl chloride gave the final PPD monomer **7**.

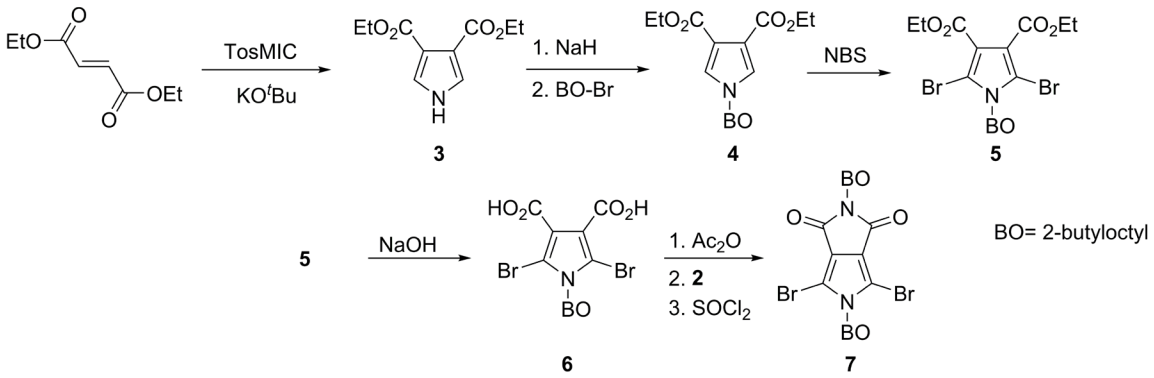


**Scheme 5.1.** Synthetic route to the PPD monomer **7**.

The synthesis of the donor-acceptor copolymers is shown in Scheme 5.2. The Stille cross-coupling reaction of **7** with bisstannanes **TPD-Sn** and **DPP-Sn** afforded the copolymers **P1** and **P2**, respectively. Both polymers were recovered in low yield after purification by soxhlet extraction and purification through a silica gel plug, even after attempts at catalyst and solvent optimization. One possible reason for the low yield of the polymers may be due to a slow reaction time. Stille coupling polymerizations are generally performed with the electron rich moiety as the stannane and the electron deficient as the dibromide.[21, 28] An electron deficient stannane may result in a slower transmetallation, increasing reaction time. The increased reaction time can lead to decomposition of the catalyst in the form of palladium black. Another possibility, with literature precedent, is the transfer of a methyl group instead of the TPD or DPP groups due to a stronger aryl-tin bond, caused by the electron withdrawing TPD and DPP units.[29-30] Both polymers displayed low solubility at room temperature in chloroform and **P2** showed even lower solubility in chlorobenzene.

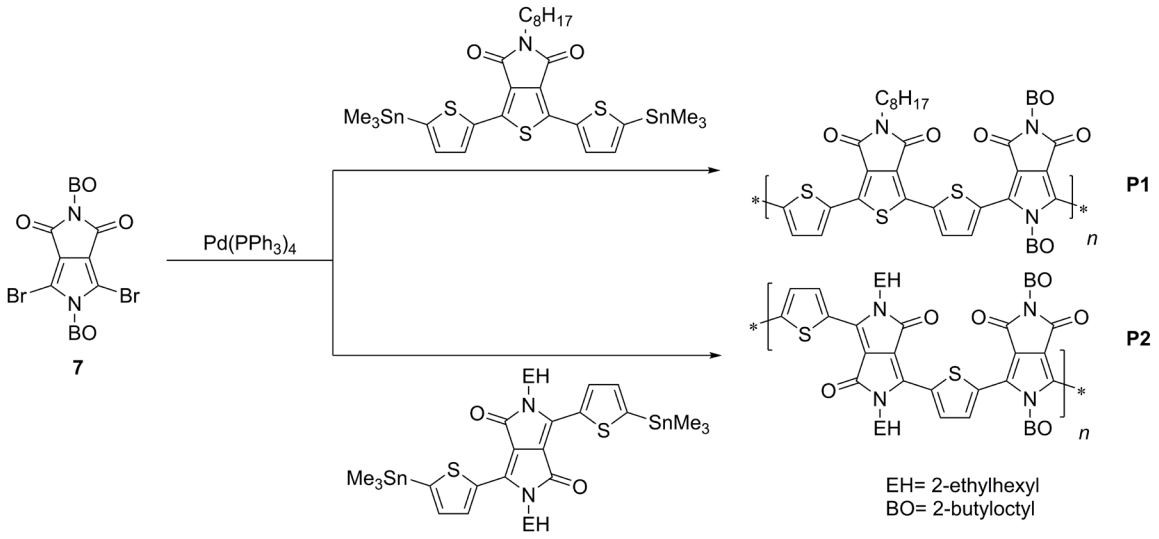


**Scheme 5.2.** Polymerization of **P1** and **P2**.

Molecular weights were estimated using gel permeation chromatography (GPC) with chloroform as the mobile phase against polystyrene standards. The weights of both **P1** and **P2** were exceptionally low, even with their low solubility in organic solvents. The number average molecular weight ($M_n$) of **P1** was 2.5 kDa with a dispersity (Đ) of 1.3, while **P2** had an $M_n$ of 3.0 kDa and a Đ of 1.4. **P1** and **P2** both showed low degrees of poymerization ($DP_n$) at 2.7 and 3.0, respectively. As discussed previously, these low degrees of polymerization are likely due to polymerization termination from methyl transfer and the low solubility of the materials in toluene. Thermal gravometric analysis was performed under air to evaluate the thermal stability of the polymers. Both **P1** and **P2,** with 5% weight loss onsets of 403.3 and 358.1 °C, respectively, show greater thermal stability than PBDT-PPD, even with their significantly lower degree of polymerization. Molecular weight and thermal properties are summarized in Table 5.1.

**Table 5.1.** Physical and thermal properties of PPD polymers.

| Polymer | Yield (%) | $M_n$ (kDa)[a] | Đ[b] | $DP_n$ | $T_d$[c] (°C) |
|---|---|---|---|---|---|
| PBDT-PPD[d] | 73 | 19.8 | 1.7 | 24.6 | 337.8 |
| P1 | 20 | 2.5 | 1.3 | 2.7 | 403.3 |
| P2 | 17 | 3.0 | 1.4 | 3.0 | 358.1 |

[a]Determined by GPC against polystyrene standards in chloroform at 40 °C. [b]Dispersity: $M_w/M_n$. [c]Temperature at 5% weight loss with a heating rate of 20 °C $min^{-1}$ under air. [d] Described in Chapter 4 of this dissertation.

The optical properties of the polymers in dilute $CHCl_3$ solution and thin film were examined using UV-Vis spectroscopy and are shown in Figure 5.1 and 5.2, respectively. In solution, both polymers show broad, low-energy absorption bands, with $\lambda_{max}$ for **P1** at 511 nm and **P2** at 719 nm, while **P2** also possesses a small higher energy transition near 410 nm. The high-energy band can be attributed to localized π-π* transitions, while the broad low-energy band is likely the result of intramolecular charge transfer (ICT) between the electron-donating PPD unit and the electron-deficient acceptor units.[17, 19] While structurally different, the absorption profiles of **P1** and PBDT-PPD are very similar in terms of $\lambda_{max}$, with **P1** also having slightly broader absorption.

Thin film absorption of **P1** and **P2** showed significant broadening of the low-energy transition, resulting in a red-shift in their absorption onsets of 95 and 45 nm for **P1** and **P2**, respectively, between solution and film. Film measurements also resulted in a red-shift of 18 nm in the $\lambda_{max}$ of **P1** and a blue-shift of 39 nm in **P2**. Both **P1** and **P2** show the presence of a slight shoulder in the solid state. Unlike in solution, the absorption of **P1** is

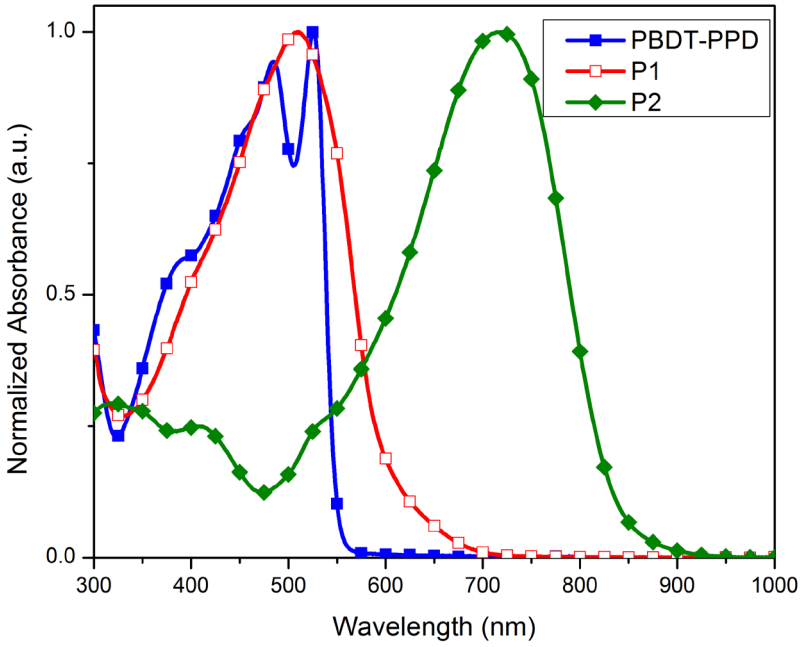


**Figure 5.1.** Normalized UV-vis absorption of PBDT-PPD, **P1**, and **P2** in $CHCl_3$.

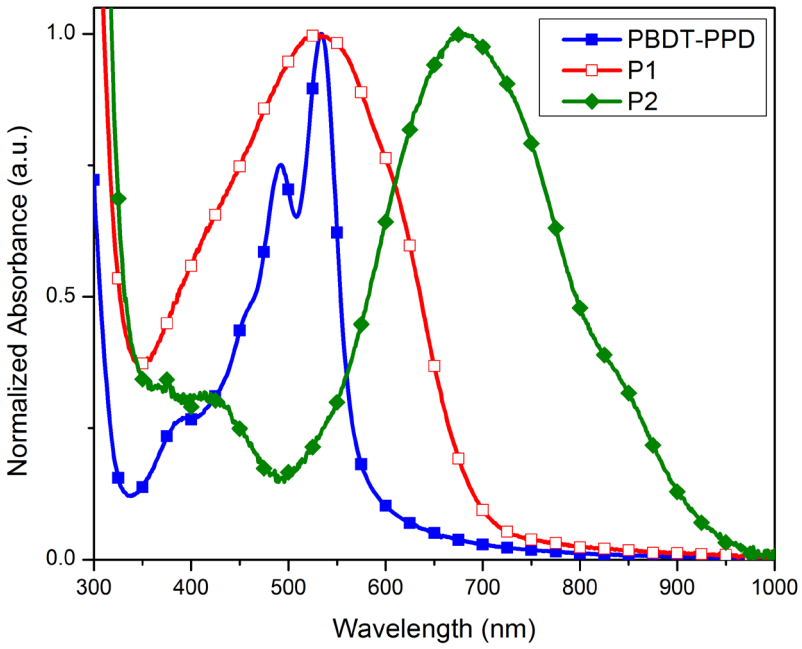


**Figure 5.2.** Normalized UV-vis absorption of PBDT-PPD, **P1**, and **P2** as thin films.

significantly broader than that of PBDT-PPD. The optical bandgap, calculated from the absorption onset in the thin film, was found to be 1.78 eV for **P1** and 1.40 eV for **P2**. The narrow bandgap of **P2** is typical of many DPP containing polymers.[7, 31-32] Both polymers had poor film forming properties when cast on glass slides, particularly **P2**. The poor film forming properties may be due to the low molecular weights, and not necessarily inherent to higher weight material.

**Table 5.2.** Optical and electrochemical properties of PPD polymers.

| Polymer | $\lambda_{\max}^{\text{soln}}$ (nm)[a] | $\lambda_{\max}^{\text{film}}$ (nm) | $E_g^{\text{opt}}$ (eV)[b] | $E_{\text{HOMO}}$ (eV)[c] | $E_{\text{LUMO}}$ (eV)[d] |
|---|---|---|---|---|---|
| PBDT-PPD[e] | 526 | 533 | 2.20 | -5.50 | -3.30 |
| P1 | 511 | 529 | 1.78 | -5.57 | -3.79 |
| P2 | 719 | 680 | 1.40 | -5.35 | -3.95 |

[a]Measured in chloroform. [b]Calculated from the absorption onset of the film spectra. [c]Calculated from the oxidation onsets using the equation $E_{HOMO}$ = -4.8 - $E_{ox}$. [d]Calculated from HOMO energy level and optical bandgap. [e]Described in Chapter 4 of this dissertation.

The electrochemical properties of the polymers were investigated by cyclic voltammetry. Both polymers exhibit irreversible oxidation processes and no discernible reduction (Figure S19, Supporting Information), regardless of initial scan direction. The HOMO energy levels were estimated from the onset of oxidation using the absolute energy level of ferrocene/ferrocenium as 4.8 eV under vacuum and are summarized in Table 5.2.[33] Both polymers had HOMOs below the air oxidation threshold, with **P1** at -5.57 eV and **P2** at -5.35 eV.[34] Lowest unoccupied molecular orbitals (LUMOs), calculated from

the sum of the HOMO and optical bandgap, were -3.79 and -3.95 eV for **P1** and **P2**, respectively. The low lying LUMO of both materials, matching well with that of PCBM, is optimal for use in photovoltaics as a donor material.[35-36] The significantly lower LUMO of **P1**, when compared to PBDT-PPD, allows for a significantly smaller bandgap while still maintaining oxidative stability. Unlike **P1**, **P2** showed a second oxidation peak which is likely due to decomposition of the polymer, as all successive experiments on the same film resulted in no signal.

## 5.4 Conclusions

Two donor-acceptor copolymers using pyrrolo[3,4-*c*]pyrrole-1,3-dione as the π-electron donor were synthesized and their optical and electrochemical properties studied and compared to the polymer PBDT-PPD reported in Chapter 4 of this dissertation. The polymerization with the isoelectronic thieno[3,4-*c*]pyrrole-1,3-dione as the π-electron acceptor gave a medium bandgap polymer, **P1**, with a relatively deep HOMO and similar absorption to PBDT-PPD. The polymerization of PPD with thienyldiketopyrrolopyrrole as the π-electron acceptor gave a narrow bandgap polymer, **P2**, with broad absorption from 500 – 900 nm. The absorption profiles of **P1** and **P2**, covering most of the solar spectrum, suggest they may be useful in tandem solar cells. The reduction in optical bandgap between PBDT-PPD and **P1** (0.42 eV) and **P2** (0.80 eV) indicates that the PPD unit has far greater potential as a π-electron donor than as an acceptor in donor-acceptor copolymers. Improved polymerization routes, such as direct arylation, may produce materials with weights viable for applications in organic electronics.

## 5.5 Experimental

### 5.5.1 Synthesis

**General polymerization procedure.** An oven dried two-neck flask was charged with **8** (1.0 equiv.), stannane (1.05 equiv.), and deoxygenated toluene (7 mL). The solution was sparged with argon for an additional 20 min and followed by the addition of tetrakis(triphenylphosphine)palladium(0) (8 mol%). The reaction mixture was refluxed for 3 days. The polymer was end-capped by refluxing with trimethyl(phenyl)tin (50 mg) for 4 h, followed by refluxing with iodobenzene (0.1 mL) overnight. After cooling to ambient temperature, the mixture was precipitated into methanol and filtered through a Soxhlet thimble. The polymer was washed with methanol (4 h), acetone (4 h), hexanes (12 h), and extracted with chloroform. The chloroform fraction was then concentrated and the polymer run through a short silica gel plug. The resulting fraction was then concentrated (~5 mL) and precipitated into cold methanol, filtered, and dried *in vacuo*.

**Synthesis of P1.** Following the general polymerization procedure using compounds **7** (119.3 mg, 0.19 mmol) and **TPD-Sn** (150.6 mg, 0.20 mmol) gave the expected polymers as a dark red solid (33.5 mg, 20%). $^1$H NMR (600 MHz, $CDCl_3$) δ 7.57, 6.84, 3.61, 1.68, 1.42 – 1.16, 0.89. GPC ($CHCl_3$, 40 °C): $M_n$ = 2.5 kDa, $M_w$ = 3.3 kDa, Đ = 1.3, $DP_n$ = 2.7. $T_d$ (5%) = 403.3 °C.

**Synthesis of P2.** Following the general polymerization procedure using compounds **7** (152.5 mg, 0.24 mmol) and **DPP-Sn** (217.1 mg, 0.26 mmol) gave the expected polymers as a black solid (22.8 mg, 15%). $^1$H NMR (600 MHz, $CDCl_3$) δ 8.99, 7.43, 4.06, 1.94, 1.61 – 1.08, 1.08 – 0.55. GPC ($CHCl_3$, 40 °C): $M_n$ = 3.0 kDa, $M_w$ = 4.3 kDa, Đ = 1.4, $DP_n$ = 3.0. $T_d$ (5%) = 358.1 °C.

## 5.6 Acknowledgements

This work was supported by the 3M Foundation and Iowa State University (ISU). We wish to thank Steve Veysey and the ISU Chemical Instrumentation Facility for training and assistance with the thermal analysis. We also thank Dr. Kamel Harrata and the ISU Mass Spectroscopy Laboratory for analysis. The OPVs were fabricated at the ISU Micro-electronics Research Center.

## 5.7 Supporting Information

### 5.7.1 Materials

Air- and moisture-sensitive reactions were performed using standard Schlenk techniques. Solvents used for palladium-catalyzed reactions were deoxygenated prior to use by sparging with argon for 30 minutes. 5-octyl-1,3-di(thiophen-2-yl)-4*H*-thieno[3,4-*c*]pyrrole-4,6(5*H*)-dione[37], 2,5-bis(2-ethylhexyl)-3,6-di(thiophen-2-yl)-2,5-dihydropyrrolo[3,4-*c*]pyrrole-1,4-dione[38] were prepared according to modified literature procedures. All other chemical reagents were purchased commercially and used without further purification unless otherwise noted.

### 5.7.2 Characterization

Nuclear magnetic resonance (NMR) spectra were collected on Varian VXR-300, Varian MR-400, or Bruker Avance III-600 spectrometers. $^{1}H$ NMR and $^{13}C$ NMR spectra were internally referenced to the residual solvent peak. In all spectra, chemical shifts are given in ppm (δ) relative to the solvent. Gel permeation chromatography (GPC) measurements were performed on a Shimadzu Prominence GPC with two 10 μm AM Gel columns connected in series (guard, 10,000 Å, 1,000 Å) in chloroform at 40 °C relative to polystyrene standards. Thermogravimetric analysis (TGA) was performed over an interval of 40 – 900 °C at a heating rate of 20 °C $min^{-1}$ under ambient atmosphere. Cyclic voltammetry (CV) measurements were carried out using an *e*-DAQ *e*-corder 410 potentiostat with a scanning rate of 100 mV $s^{-1}$. The polymer films were dropcast from 1 – 2 mg $mL^{-1}$ solutions in chlorobenzene onto a platinum working electrode. $Ag/Ag^{+}$ and Pt wire were used as the reference and auxiliary electrodes, respectively. The reported values were referenced to $Fc/Fc^{+}$ (-4.8 versus vacuum). All electrochemical experiments were performed in deoxygenated acetonitrile under an argon atmosphere using 0.1 M tetrabutylammonium hexafluorophosphate as electrolyte. Absorption spectra were obtained on a photodiode-array Agilent 8453 UV-visible spectrophotometer using polymer solutions in $CHCl_3$ and thin films. The films were cast by spin coating 25 x 25 x 1 mm glass slides using solutions of polymer (3.0 mg $mL^{-1}$) in chlorobenzene at a spin rate of 1200 rpm on a Headway Research, Inc. PWM32 spin-coater.

### 5.7.3 Synthesis

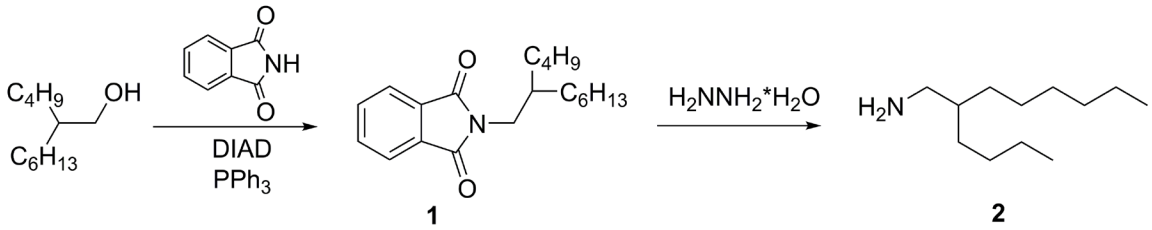


**2-(2-butyloctyl)isoindoline-1,3-dione (1)** Phthalimide (5.80 g, 39 mmol), 2-butyl-1-octanol (5.64 g, 30 mmol), and triphenylphosphine (10.28 g, 39 mmol) were dissolved in ether (30 mL). The solution was cooled to 0 °C, followed by the dropwise addition of diisopropyl azodicarboxylate (8 mL, 41 mmol) in ether (15 mL) and allowed to stir overnight at room temperature. The resulting precipitate was filtered, washed with ether, and the filtrate concentrated. The crude material was taken up in hexanes, washed with water, dried, and concentrated. The resulting yellow oil was further purified by silica gel chromatography using 1:4 ether/hexanes as eluent to afford the expected compound as a clear viscous oil (9.08 g, 95%). $^1$H NMR (400 MHz, $CDCl_3$) δ 7.84 (dd, $J$ = 5.4, 3.0 Hz, 2H), 7.71 (dd, $J$ = 5.4, 3.0 Hz, 2H), 3.57 (d, $J$ = 7.2 Hz, 2H), 1.95 – 1.81 (m, 1H), 1.38 – 1.21 (m, 16H), 0.87 (q, $J$ = 6.9 Hz, 6H).

**2-butyl-1-octylamine (2)** Compound **1** (9.08 g, 28.8 mmol) was dissolved in anhydrous EtOH (50 mL) followed by the dropwise addition of hydrazine monohydrate (4.4 mL, 91 mmol). The reaction was refluxed for two days before the addition of excess 6M HCl and EtOH (20 mL) and refluxed one additional hour. The resulting precipitate was washed with water, and the filtrate was rotovaped to remove the EtOH. Excess 6M NaOH was added, and the product extracted with ether, dried over $NaSO_4$, and concentrated to afford

the expected compound as a light yellow oil that was used without further purification (2.19 g, 97%).

**Diethyl 1*H*-pyrrole-3,4-dicarboxylate (3)** A suspension of potassium *tert*-butoxide (11.5 g, 102 mmol) in THF (100 mL) was stirred under argon in a flame dried two neck 500 mL round bottom flask. A solution of diethyl fumarate (8.8 g, 51.5 mmol) and *p*-toluenesulfonylmethyl isocyanide (10.0 g, 51.6 mmol) in THF (50 mL) was slowly added to the suspension and allowed to stir overnight. The reaction was then quenched with a saturated sodium chloride solution, extracted with THF (3 x 200 mL), and dried with anhydrous sodium sulfate. The solvent was removed under reduced pressure and the resulting solid dissolved methanol (50 mL). The product was then precipitated in water, filtered, and dried to afford the expected compound as an off-white solid (7.2 g, 67%). $^{1}$HNMR (600 MHz, DMSO-$d_6$) δ: 7.36 (s, 2H), 4.15 (q, $J$ = 7.0 Hz, 4H), 1.23 (t, $J$ = 7.1 Hz, 6H); $^{13}$CNMR (150 MHz, DMSO-$d_6$) δ: 163.41, 125.26, 115.03, 59.39, 14.20.

**Diethyl 1-(2-butyloctyl)-1*H*-pyrrole-3,4-dicarboxylate (4)** Compound **3** (3.19 g, 15.1 mmol) was dissolved in DMF (50 mL) and cooled to 0 °C. Sodium hydride (60% in mineral oil, 1.00 g, 25 mmol) was added slowly and the reaction allowed to stir at room temperature for 1 h, after which 2-butyloctyl bromide (6.26 g, 25.1 mmol) was added dropwise. After stirring overnight, the reaction was poured into water (100 mL) and extracted with ethyl acetate (3 x 75 mL). The organic fractions were combined, washed with water, and dried over $Na_2SO_4$. The solvent was removed and the resulting oil purified by silica gel chromatography using 17:3 hexanes/ethyl acetate as eluent to afford the expected

compound as a clear viscous oil (4.36 g, 76%). $^{1}$H NMR (400 MHz, $CDCl_3$) δ 7.36 (s, 2H), 4.39 (q, *J* = 7.1 Hz, 4H), 3.83 (d, *J* = 7.0 Hz, 2H), 1.91 – 1.80 (m, 1H), 1.44 (t, *J* = 7.1 Hz, 6H), 1.41 – 1.29 (m, 16H), 1.01 – 0.95 (m, 6H); $^{13}$C NMR (101 MHz, $CDCl_3$) δ 163.88, 128.28, 116.06, 60.31, 54.41, 39.62, 31.88, 31.23, 30.91, 29.62, 28.62, 26.39, 23.02, 22.76, 14.51, 14.22, 14.15; HRMS (ESI) m/z: $[M + H]^+$ calcd for $C_{22}H_{37}Br_2NO_4$, 380.2801; found, 380.2797; deviation, 1.1 ppm.

**Diethyl 2,5-dibromo-1-(2-butyloctyl)-1*H*-pyrrole-3,4-dicarboxylate (5)** Compound **4** (1.9 g, 5 mmol) was dissolved in DMF (50 mL), protected from light, and cooled to 0 °C. Freshly recrystallized NBS (1.98 g, 11.1 mmol) was added in two portions and the reaction stirred overnight at room temperature. The reaction mixture was poured into water (100 mL) and extracted with ether (3 x 75 mL). The combined organic fractions were washed with water, brine, and then dried over $Na_2SO_4$. The solvent was removed and the resulting orange oil purified by silica gel chromatography using 9:1 hexanes/ethyl acetate as eluent to give the expected compound as a clear viscous oil (2.54 g, 93%). $^{1}$H NMR (600 MHz, $CDCl_3$) δ 4.31 (q, *J* = 7.1 Hz, 4H), 3.96 (d, *J* = 7.6 Hz, 2H), 2.02 – 1.96 (m, 1H), 1.34 (t, *J* = 7.1 Hz, 6H), 1.32 – 1.17 (m, 16H), 0.88 (td, *J* = 7.0, 4.9 Hz, 6H); $^{13}$C NMR (151 MHz, $CDCl_3$) δ 163.04, 117.61, 107.58, 61.18, 52.41, 38.37, 31.93, 31.23, 30.98, 29.67, 28.71, 26.49, 23.10, 22.77, 14.29, 14.24, 14.18; HRMS (ESI) m/z: $[M + H]^+$ calcd for $C_{22}H_{35}Br_2NO_4$, 536.1006; found, 536.1011; deviation, -1.01 ppm.

**2,5-dibromo-1-(2-butyloctyl)-1*H*-pyrrole-3,4-dicarboxylic acid (6)** Compound **5** (2.54 g, 4.7 mmol) was dissolved in ethanol (50 mL). A solution of sodium hydroxide (1.62 g,

40.5 mmol) in water (50 mL) was added in one portion, and the reaction mixture refluxed overnight. Upon cooling, the reaction was poured into water (300 mL), acidified with excess 6M HCl, and extracted with ether (3 x 250 mL). The combined organic fractions were washed with excess water, brine, and dried over $Na_2SO_4$. Removal of the solvent gave the expected compound as a tacky off white solid (2.22 g, 98%). $^1$H NMR (400 MHz, DMSO-$d_6$) δ 3.96 (d, $J$ = 7.6 Hz, 2H), 1.94 (p, $J$ = 6.7 Hz, 1H), 1.33 – 1.13 (m, 16H), 0.84 (t, $J$ = 6.5 Hz, 6H); $^{13}$C NMR (101 MHz, DMSO-$d_6$) δ 163.80, 117.83, 107.32, 51.62, 37.48, 31.11, 30.61, 30.39, 28.92, 27.98, 25.73, 22.42, 22.08, 13.99, 13.87; HRMS (ESI) m/z: $[M + H]^+$ calcd for $C_{18}H_{27}Br_2NO_4$, 480.0380; found, 480.0373; deviation, 1.38 ppm.

**4,6-dibromo-2,5-bis(2-butyloctyl)pyrrolo[3,4-*c*]pyrrole-1,3(2*H*,5*H*)-dione (7)** Compound **6** (2.22 g, 4.6 mmol) was dissolved in acetic anhydride (35 mL) and refluxed overnight. After cooling, the reaction mixture was concentrated resulting in a dark tan solid. 2-butyl-1-octylamine (1.09 g, 5.6 mmol) in toluene (30 mL) was added in one portion and refluxed overnight. After cooling, the toluene was removed under vacuum and the resulting solid was taken up in thionyl chloride (25 mL) and refluxed 5 h. The reaction was cooled and the excess thionyl chloride removed under vacuum. Purification of the crude material by silica gel chromatography using 19:1 hexanes/THF as eluent gave the expected product as a dark yellow oil (2.37 g, 81%). $^1$H NMR (400 MHz, $CDCl_3$) δ 3.90 (d, $J$ = 8.0 Hz, 1H), 3.88 (d, $J$ = 7.7 Hz, 1H), 3.43 (d, $J$ = 7.2 Hz, 2H), 2.01 – 1.88 (m, 1H), 1.84 – 1.75 (m, 1H), 1.35 – 1.19 (m, 32H), 0.90 – 0.84 (m, 12H); HRMS (APCI)

m/z: $[M + H]^+$ calcd for $C_{30}H_{50}Br_2N_2O_2$, 629.2312; found, 629.2302; deviation, 1.56 ppm.

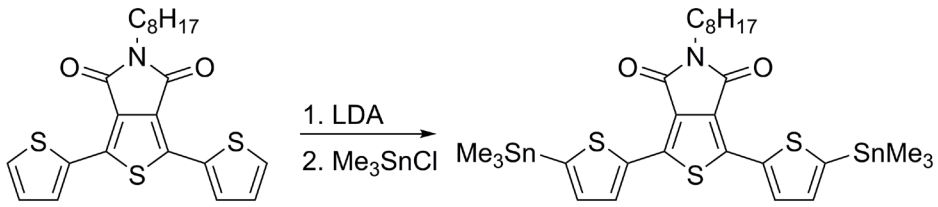


**5-octyl-1,3-bis(5-(trimethylstannyl)thiophen-2-yl)-4*H*-thieno[3,4-*c*]pyrrole-4,6(5*H*)-dione (TPD-Sn)** 5-octyl-1,3-di(thiophen-2-yl)-4H-thieno[3,4-*c*]pyrrole-4,6(5*H*)-dione (0.73 g, 1.7 mmol) was dissolved in THF (40 mL) and cooled to -78 °C. Freshly prepared LDA (5.5 mmol, 0.8 M in THF) was added dropwise and the reaction stirred at -78 °C for 2 h. Trimethyltin chloride solution (6.0 mL, 6 mmol, 1.0 M in THF) was added dropwise and the reaction stirred overnight at room temperature. The reaction was quenched with water (30 mL) and extracted with dichloromethane (3 x 75 mL). The combined organic layers were washed with water and dried over $Na_2SO_4$. After removal of the solvent, the crude material was recrystallized from ethanol to give the expected product as a dark yellow powder (0.63 g, 49%). $^1$H NMR (400 MHz, $CDCl_3$) δ 8.06 (d, $J$ = 3.5 Hz, 2H), 7.19 (d, $J$ = 3.5 Hz, 2H), 3.66 (t, $J$ = 7.4 Hz, 2H), 1.68 (p, $J$ = 14.8, 7.7, 6.9 Hz, 2H), 1.39 – 1.19 (m, 10H), 0.86 (t, $J$ = 6.6 Hz, 3H), 0.42 (s, 18H).; $^{13}$C NMR (101 MHz, $CDCl_3$) δ 162.94, 143.86, 138.02, 136.61, 136.41, 130.77, 127.83, 38.71, 31.94, 29.38, 29.33, 28.70, 27.15, 22.78, 14.25, -7.93; HRMS (ESI) m/z: $[M_2 + Na]^+$ calcd for $C_{56}H_{78}N_2O_4S_6Sn_4$, 1532.0281; found, 1532.0286; deviation, 0.3 ppm.

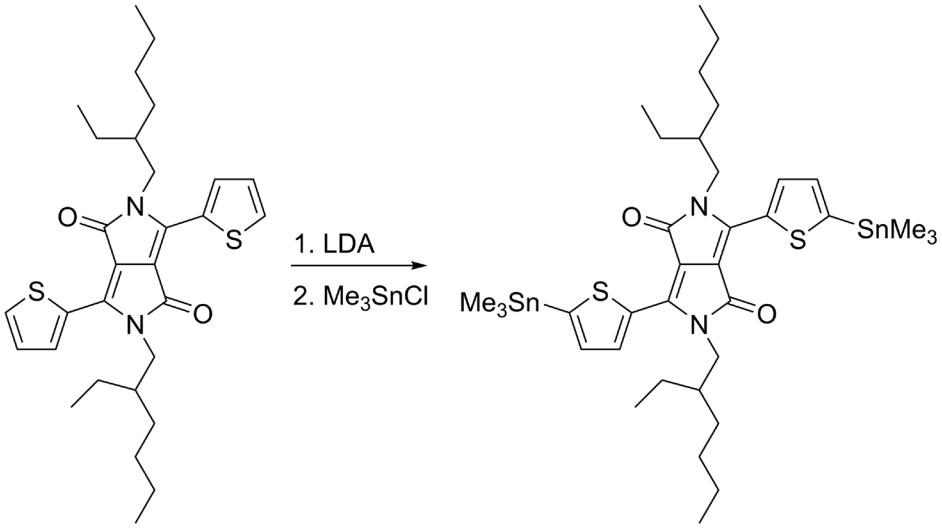


**2,5-bis(2-ethylhexyl)-3,6-bis(5-(trimethylstannyl)thiophen-2-yl)-2,5-dihydropyrrolo[3,4-*c*]pyrrole-1,4-dione (DPP-Sn)** 2,5-bis(2-ethylhexyl)-3,6-di(thiophen-2-yl)-2,5-dihydropyrrolo[3,4-*c*]pyrrole-1,4-dione (0.66 g, 1.3 mmol) was dissolved in THF (40 mL) and cooled to -78 °C. Freshly prepared LDA (4 mmol, 0.8 M in THF) was added dropwise and the reaction stirred at -78 °C for 2 h. Trimethyltin chloride solution (4.4 mL, 4.4 mmol, 1.0 M in THF) was added dropwise and the reaction stirred overnight at room temperature. The reaction was quenched with water (30 mL) and extracted with dichloromethane (3 x 75 mL). The combined organic layers were washed with water and dried over $Na_2SO_4$. Removal of the solvent gave the expected product as a dark purple solid (0.98 g, 92%). The stannane was used without further purification. $^1$H NMR (400 MHz, $CDCl_3$) δ 8.99 (d, $J$ = 3.7 Hz, 2H), 7.32 (d, $J$ = 3.6 Hz, 2H), 4.05 (t, $J$ = 7.7 Hz, 4H), 1.94 – 1.77 (m, 2H), 1.42 – 1.15 (m, 16H), 0.93 – 0.80 (m, 12H), 0.44 (s, 18H).

### 5.7.2 NMR Spectra and analytical data

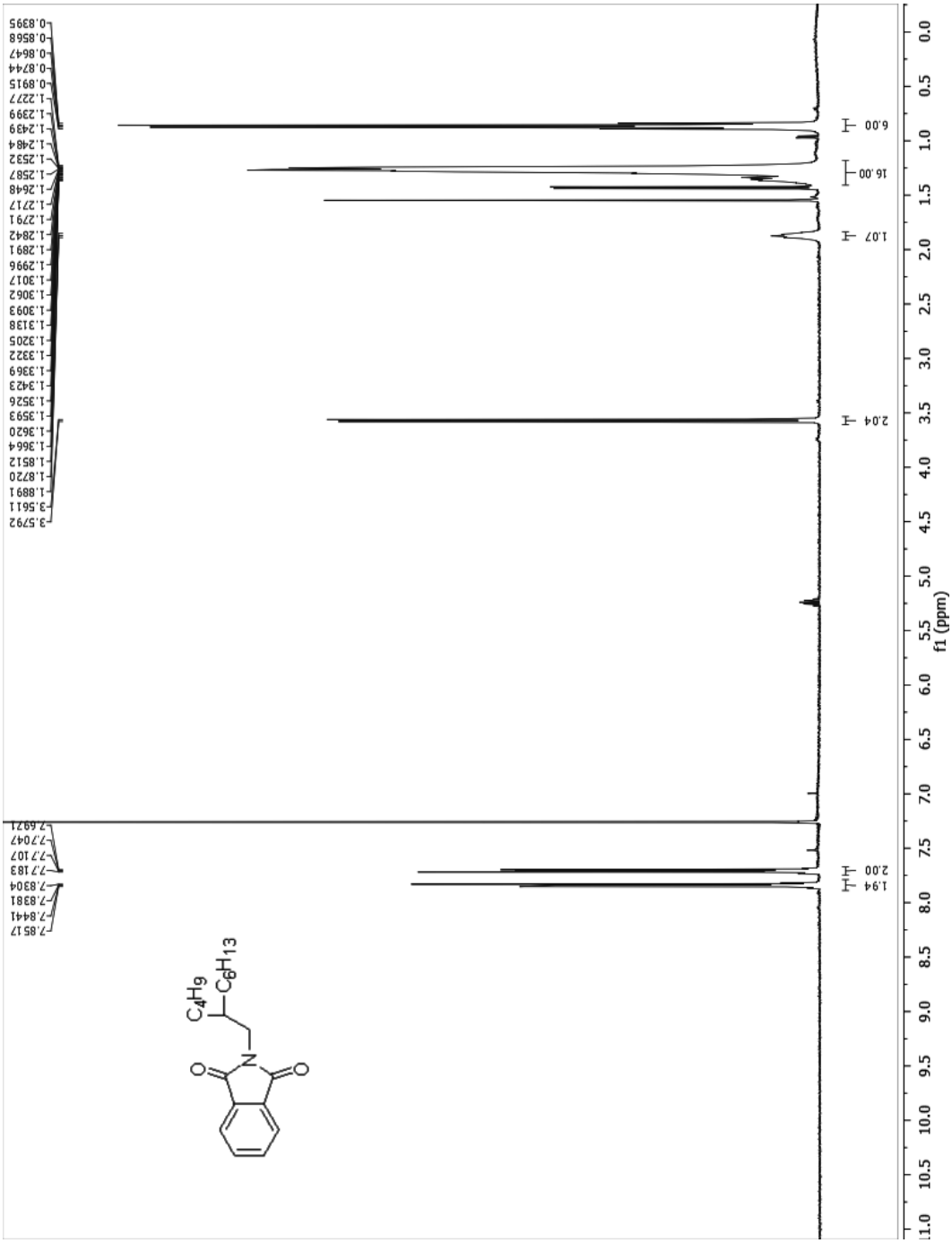


**Figure S5.1.** $^{1}$H NMR of **1**.

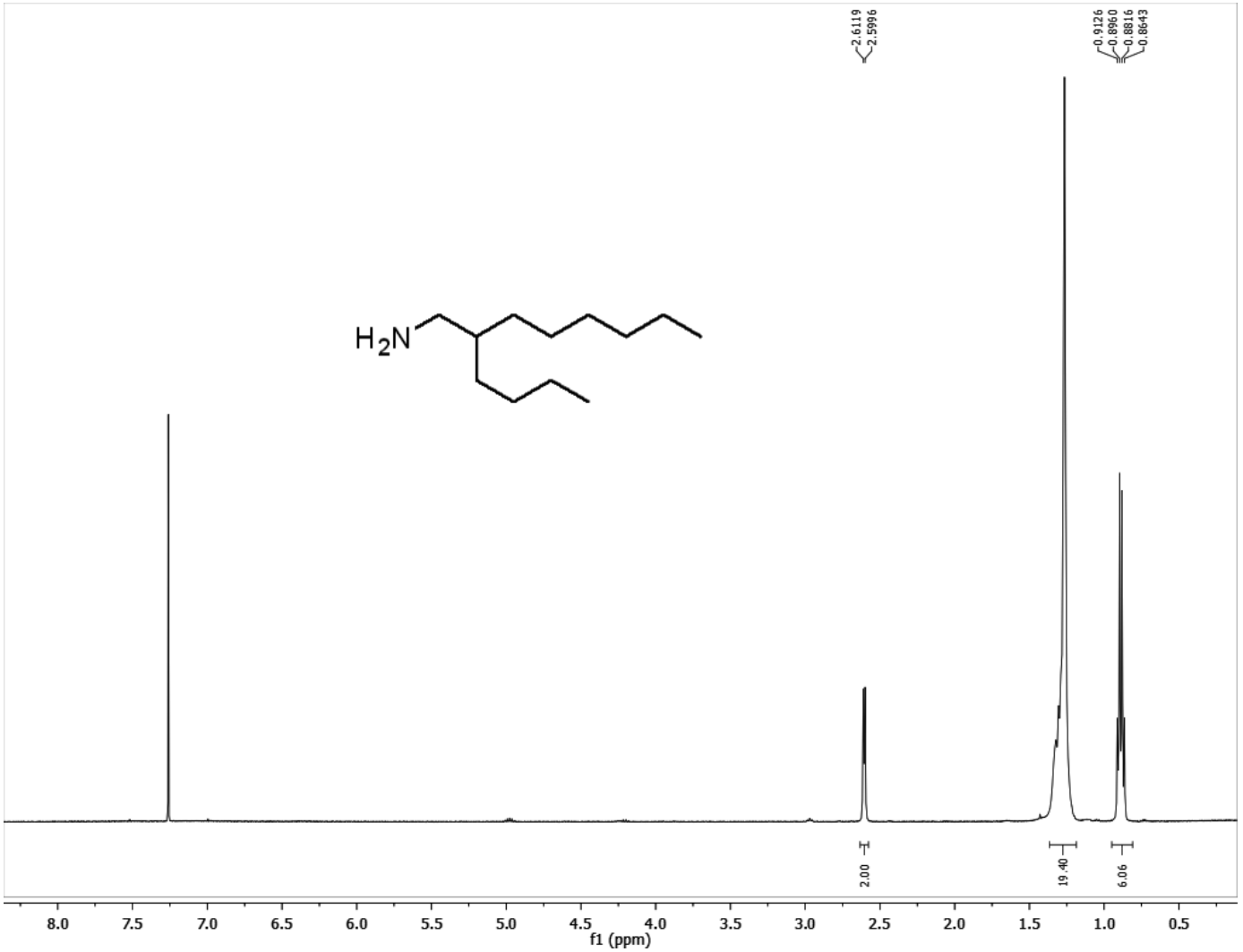


**Figure S5.2.** $^{1}$H NMR of **2**.

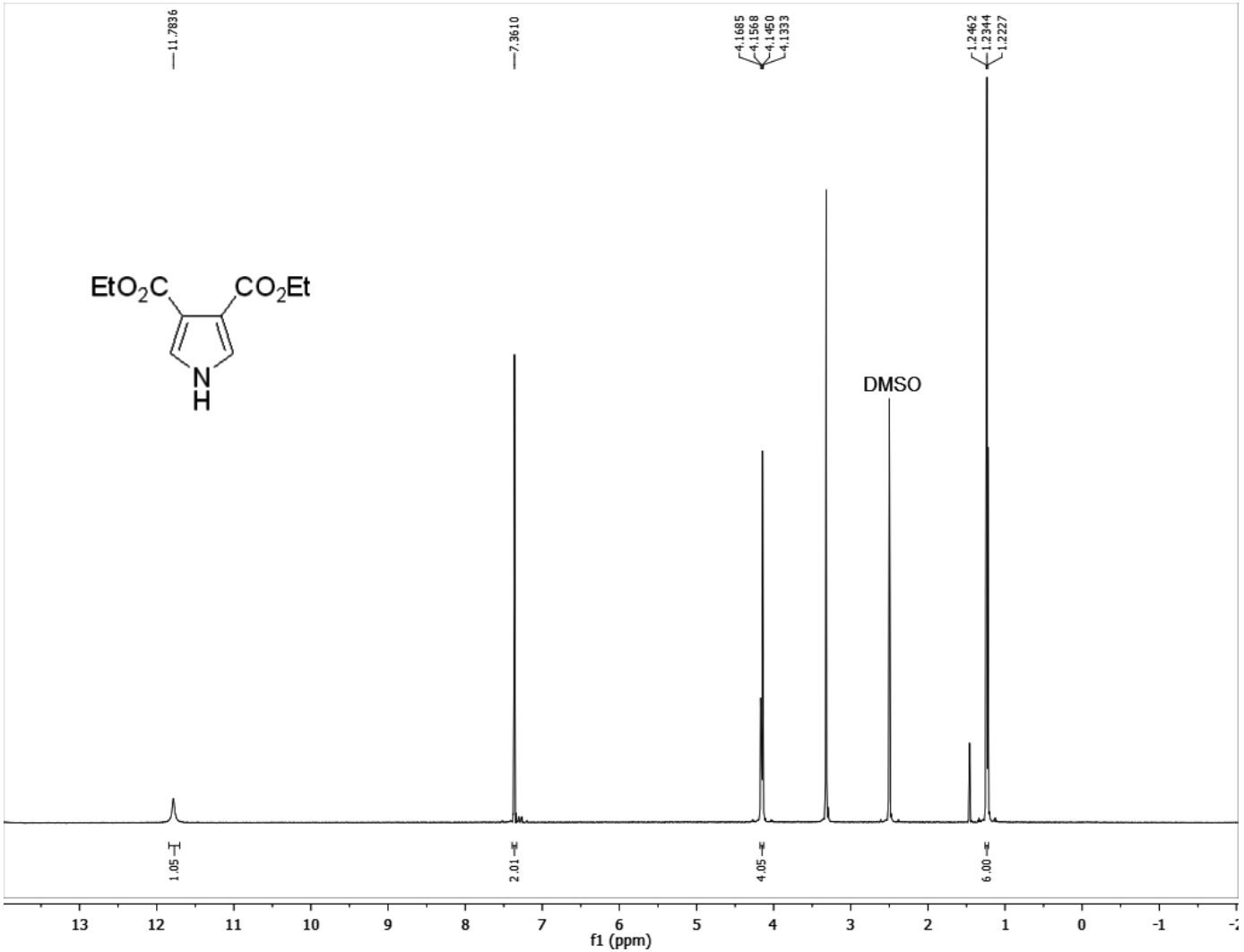


**Figure S5.3.** $^{1}$H NMR of **3**.

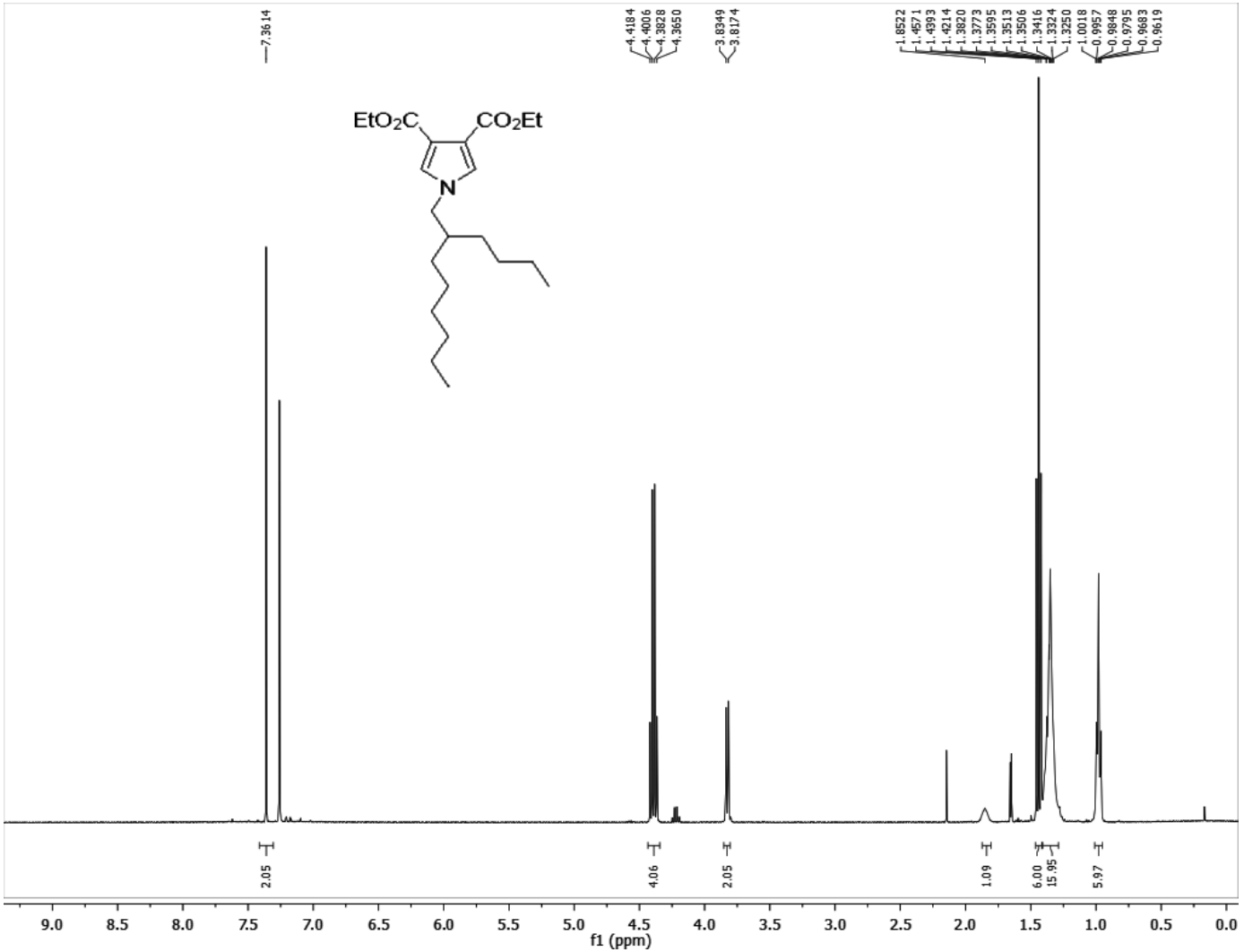


**Figure S5.4.** $^{1}$H NMR of **4**.

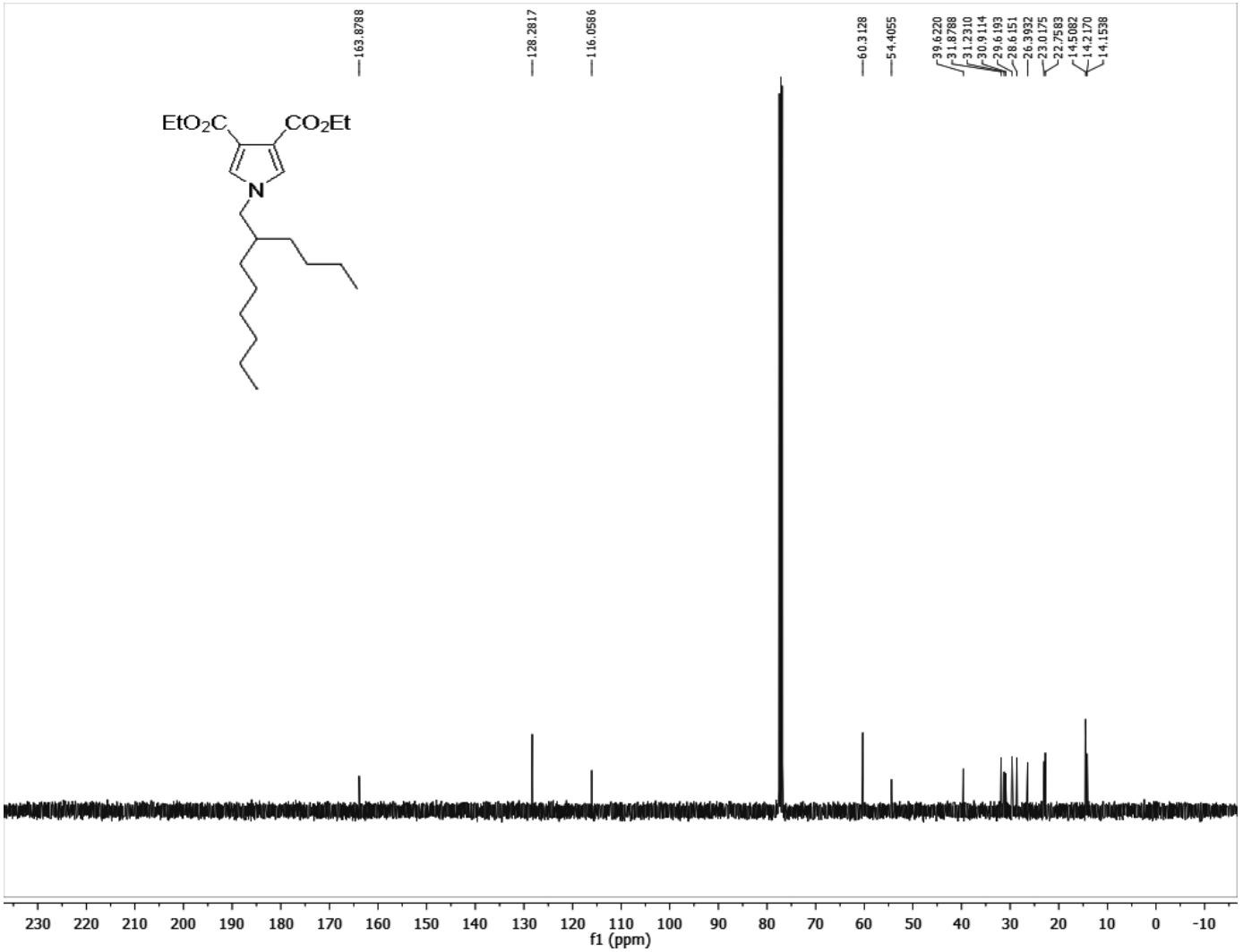


**Figure S5.5.** $^{13}$C NMR of **4**.

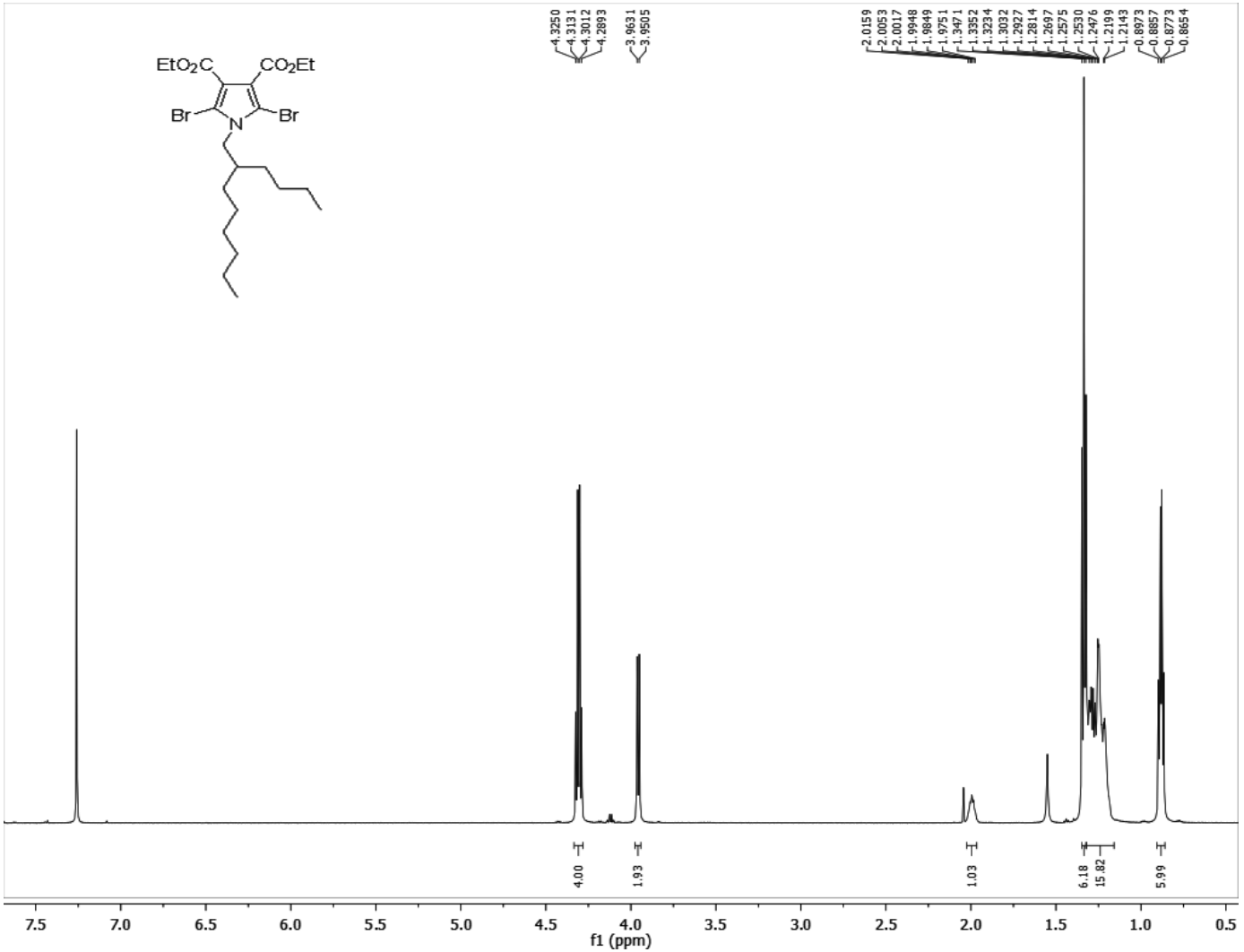


**Figure S5.6.** $^{1}$H NMR of **5**.

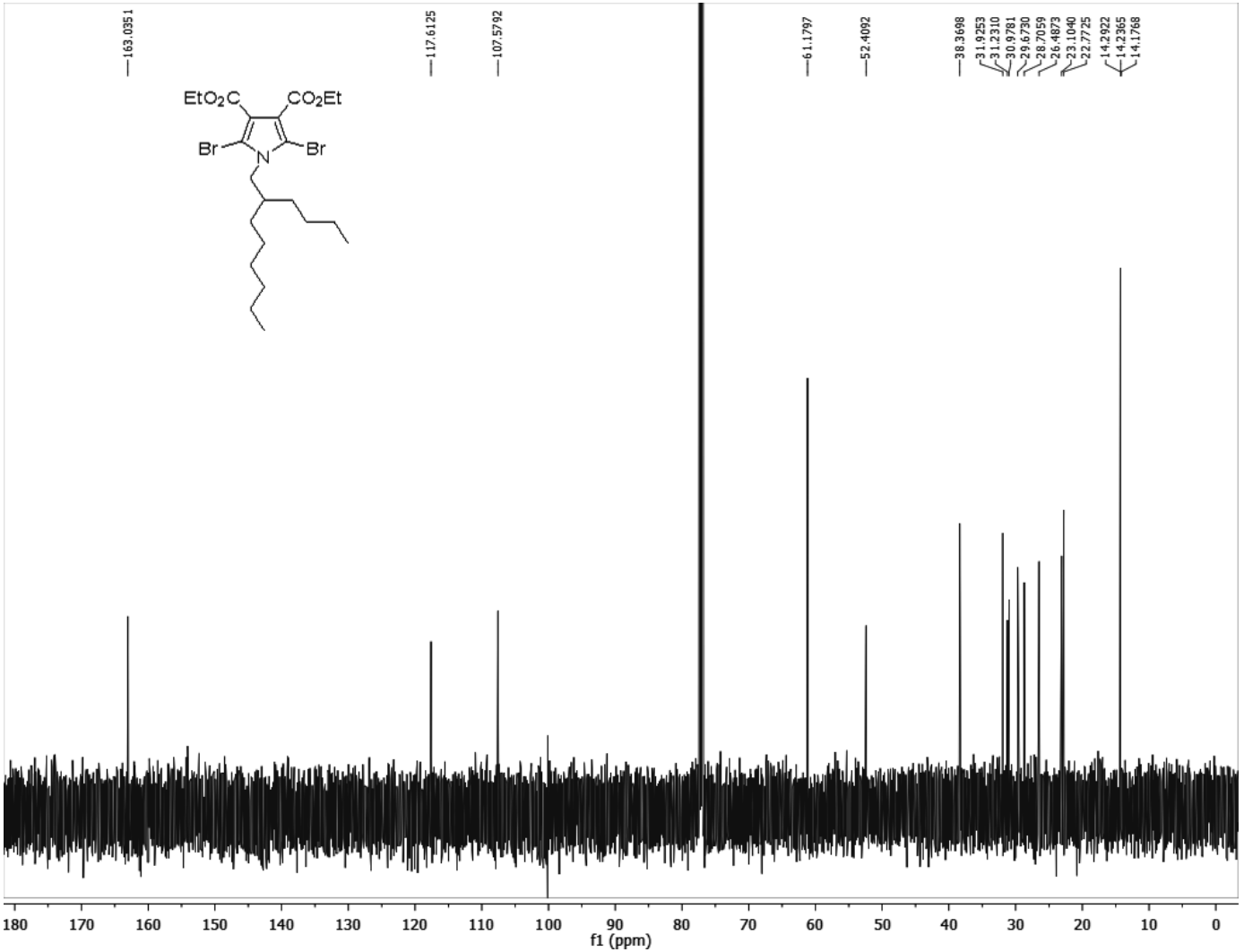


**Figure S5.7.** $^{13}$C NMR of **5**.

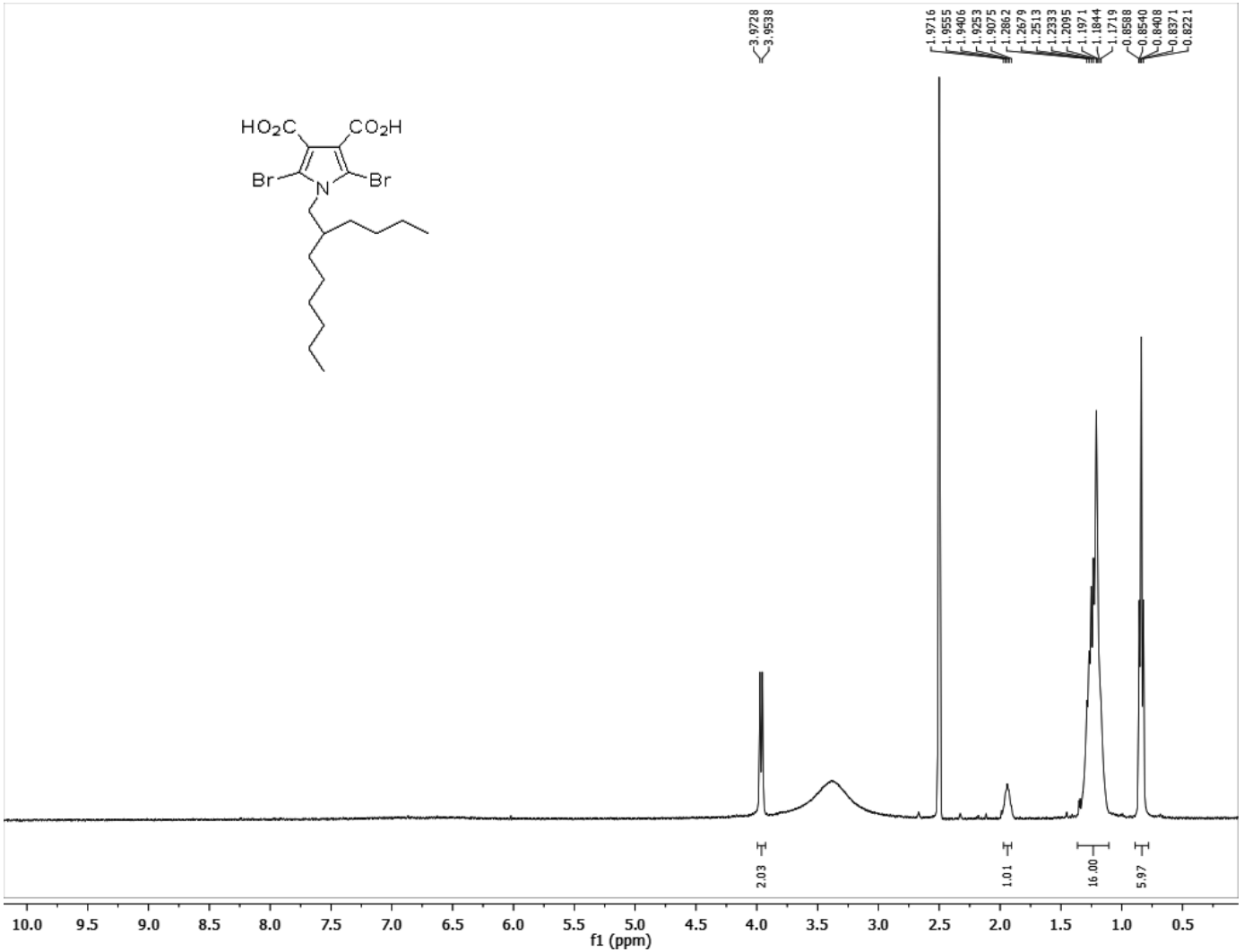


**Figure S5.8.** $^{1}$H NMR of **6**.

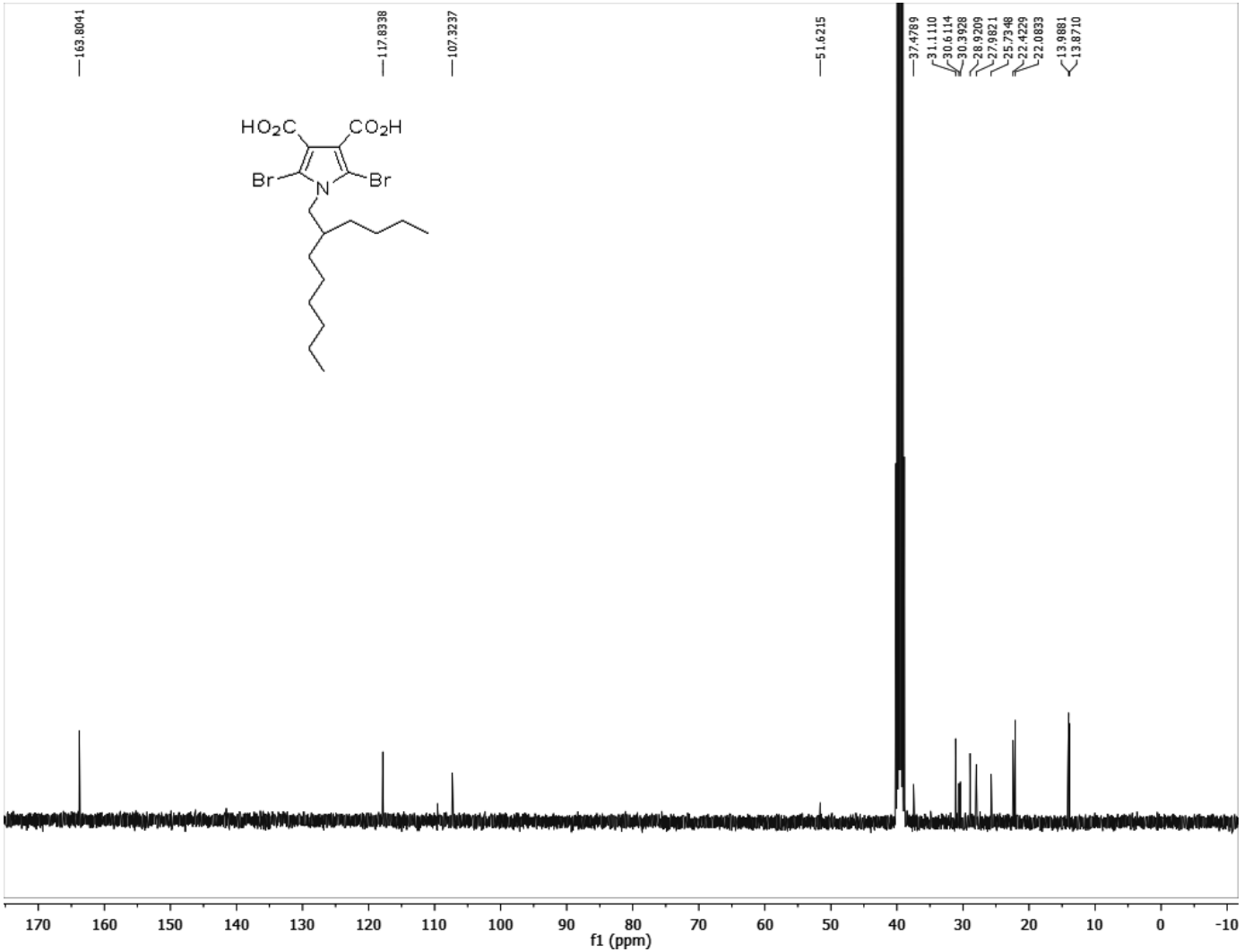


**Figure S5.9.** $^{13}$C NMR of **6**.

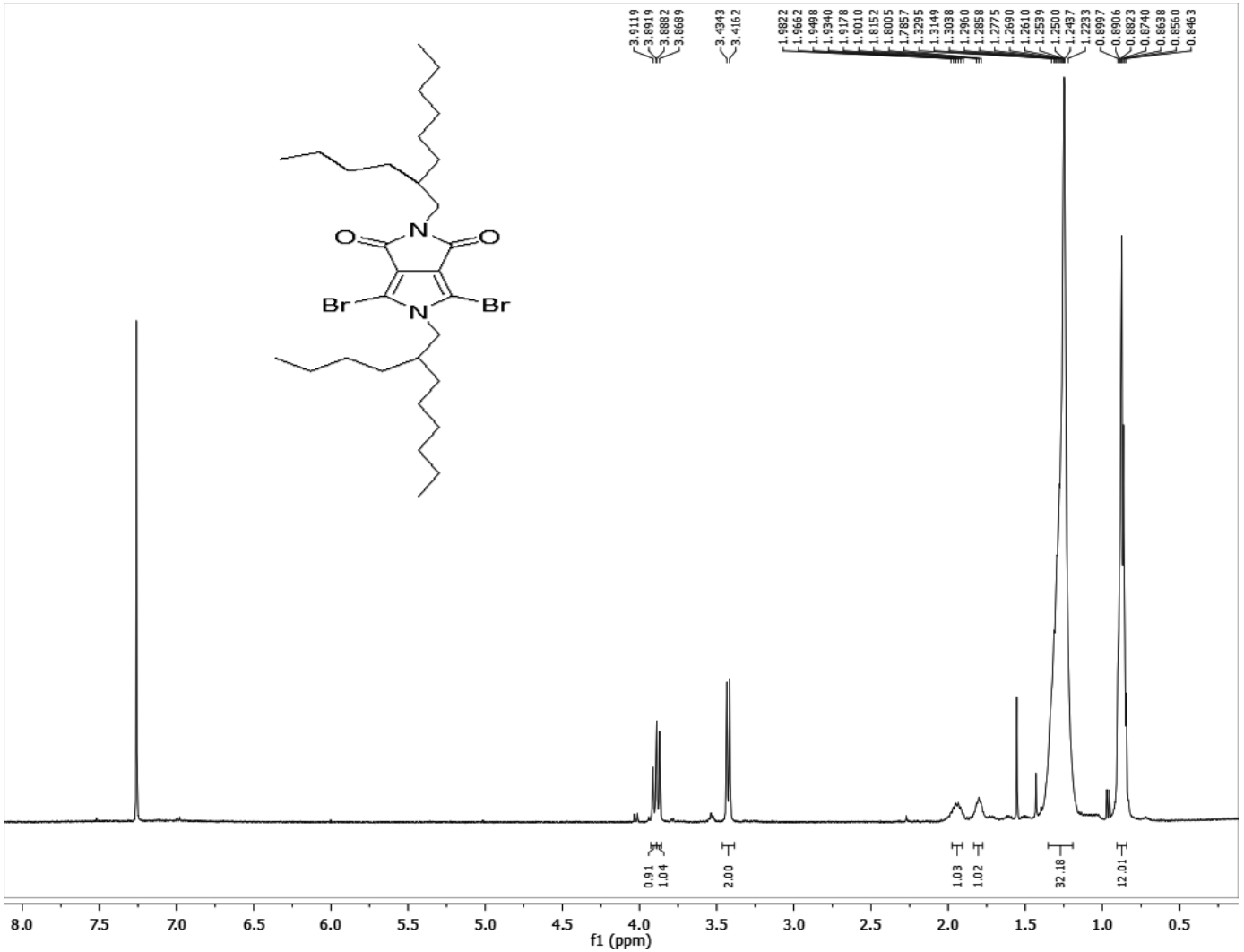


**Figure S5.10.** $^{1}$H NMR of **7**

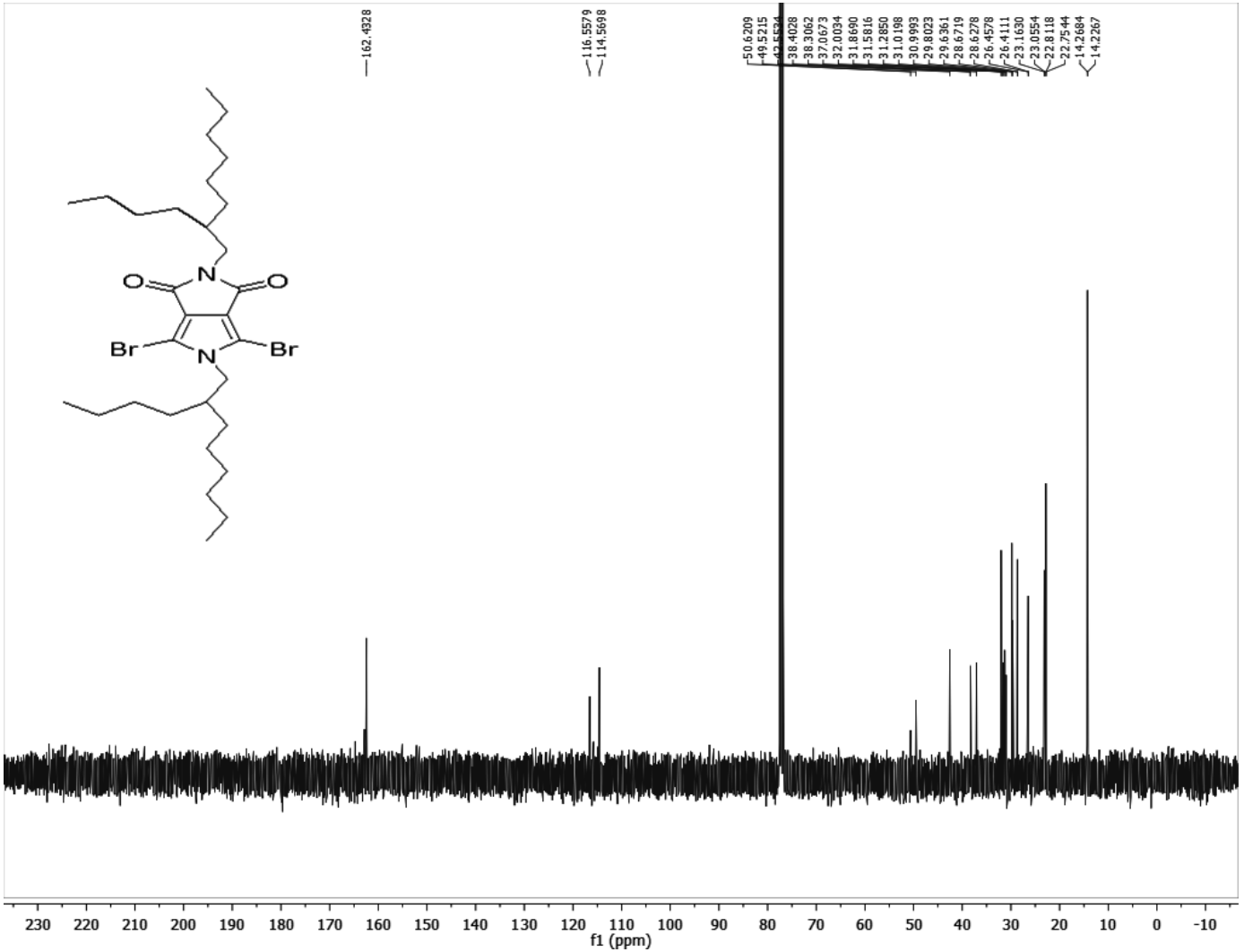


**Figure S5.11.** $^{13}$C NMR of **7**.

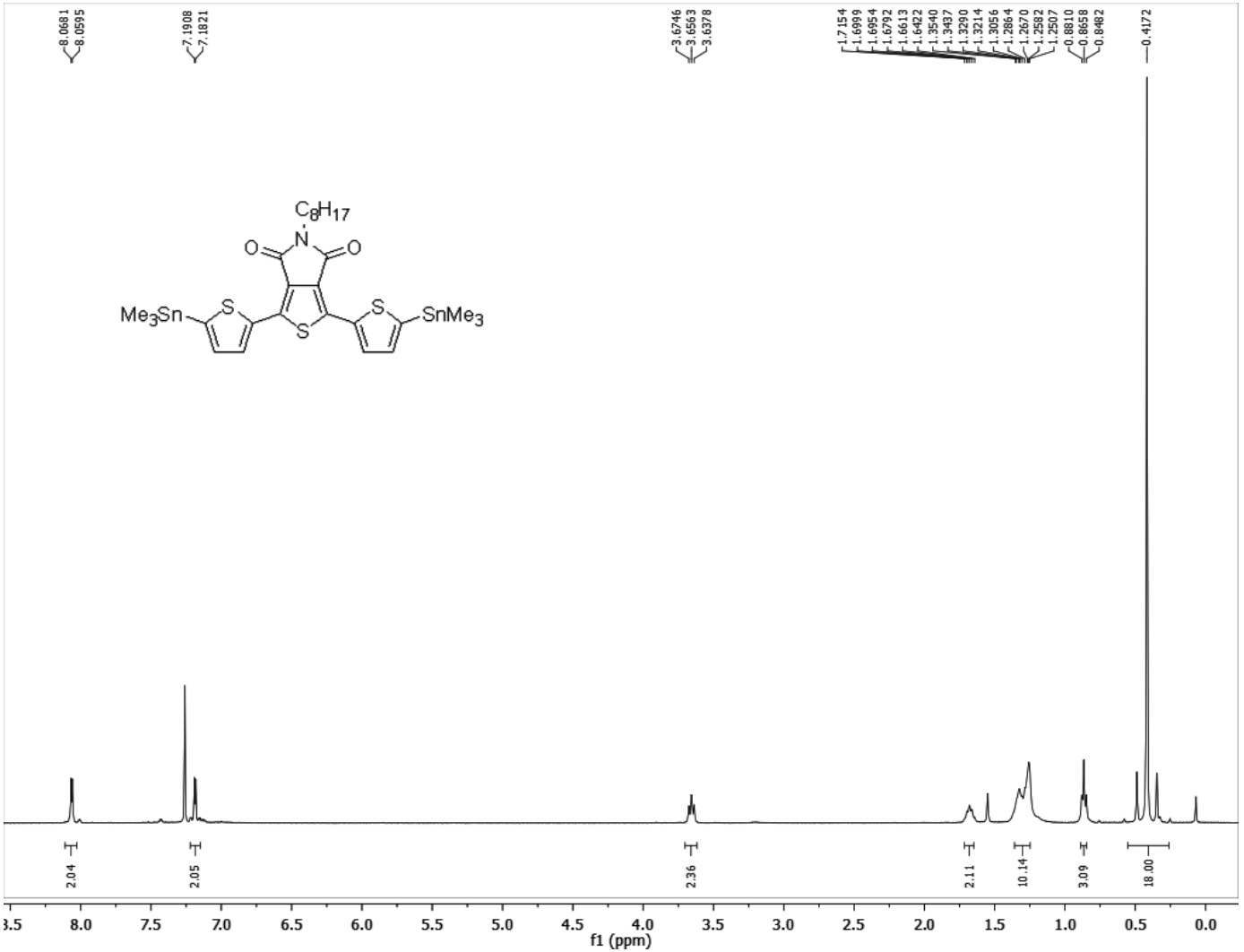


**Figure S5.12.** $^{1}$H NMR of **TPD-Sn**

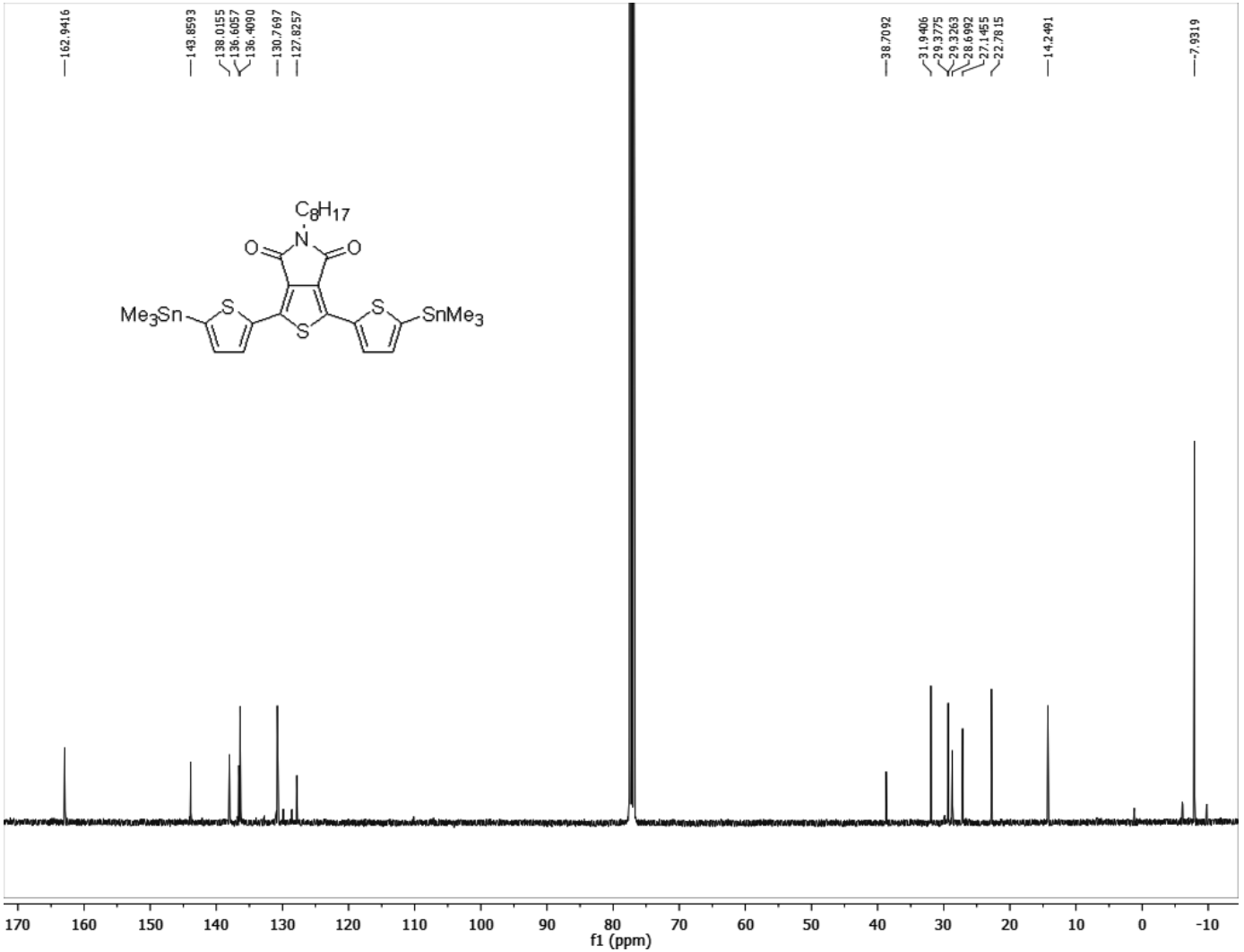


**Figure S5.13.** $^{13}$C NMR of **TPD-Sn**.

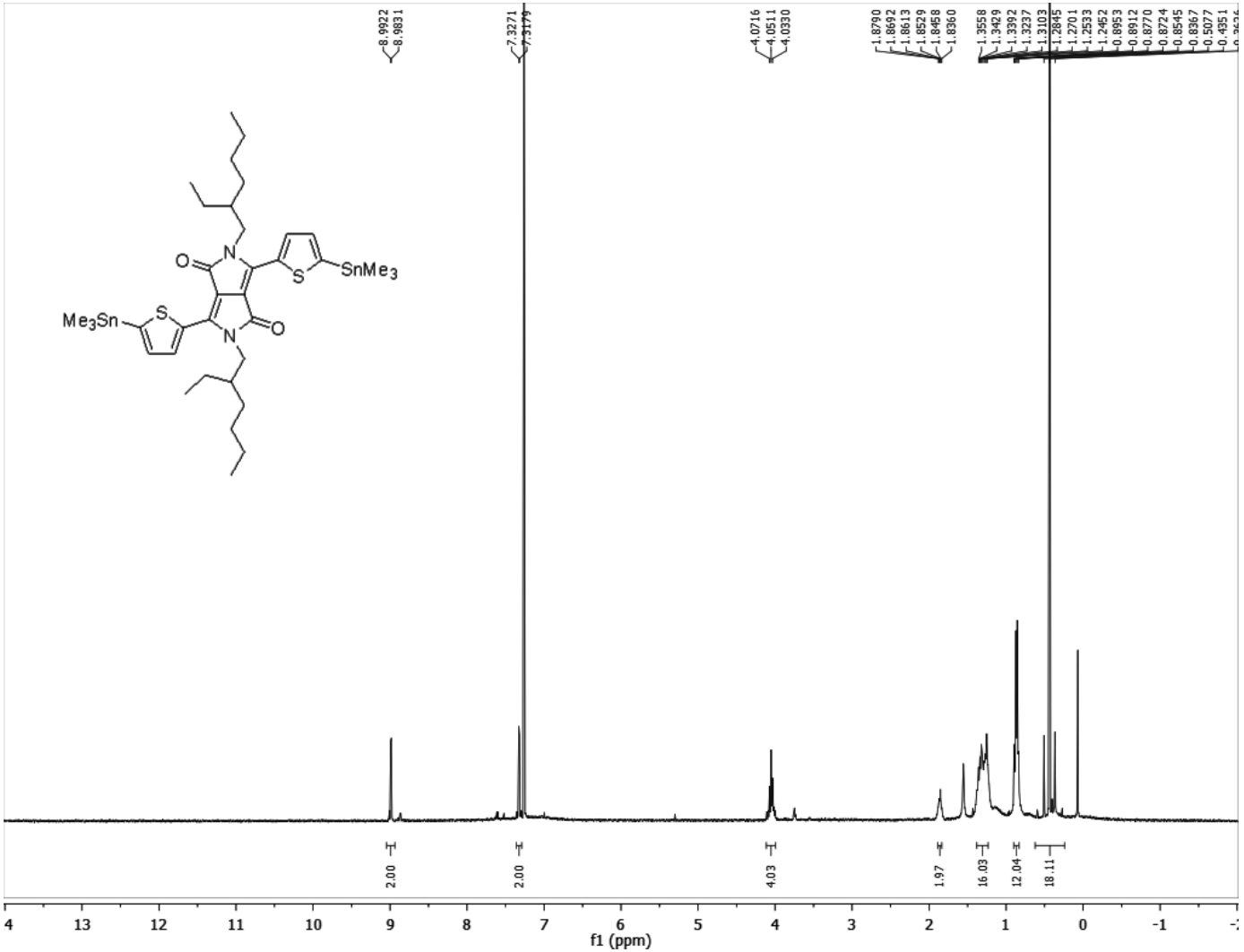


**Figure S5.15.** $^{1}$H NMR of **DPP-Sn**.

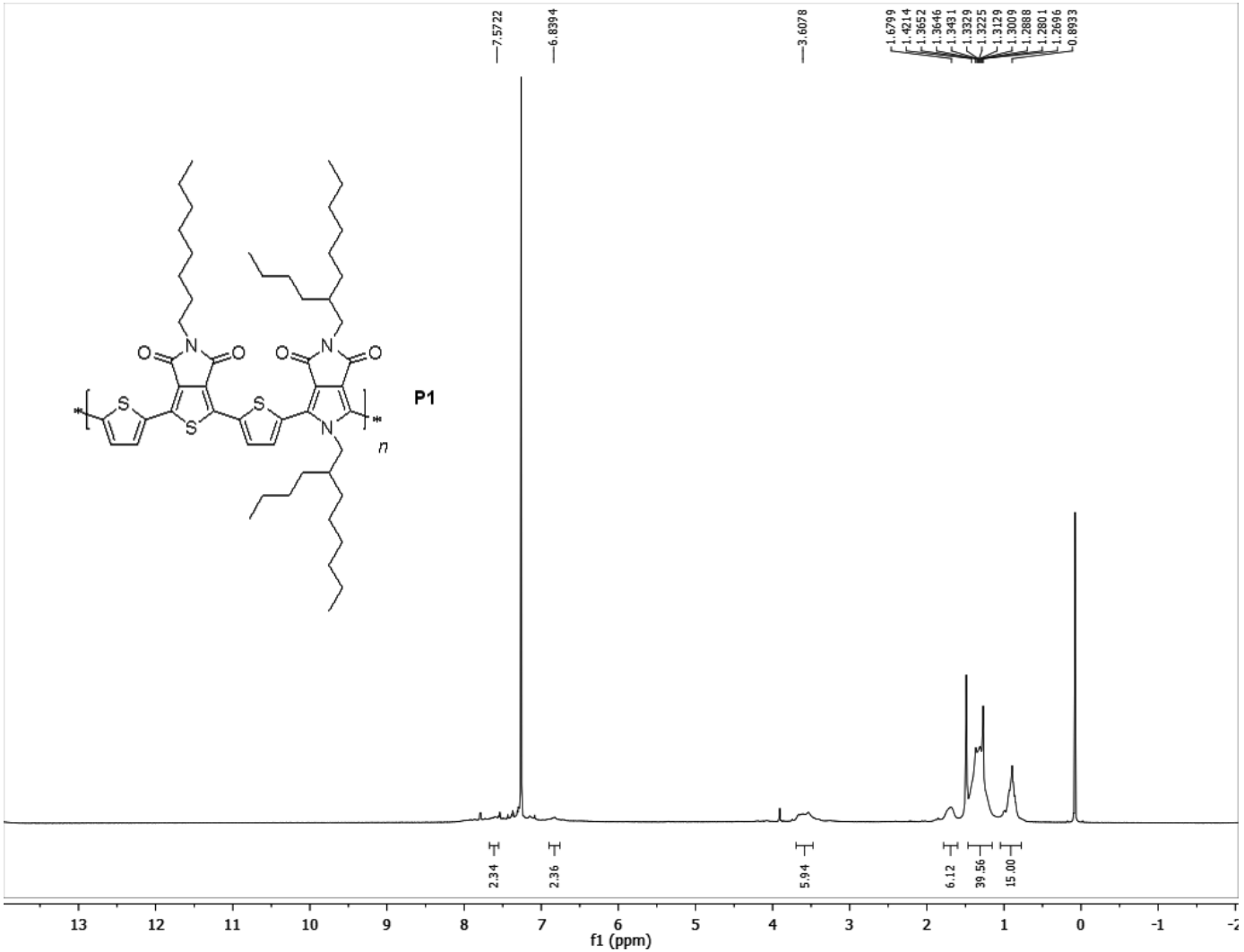


**Figure S5.15.** $^{1}$H NMR of **P1**.

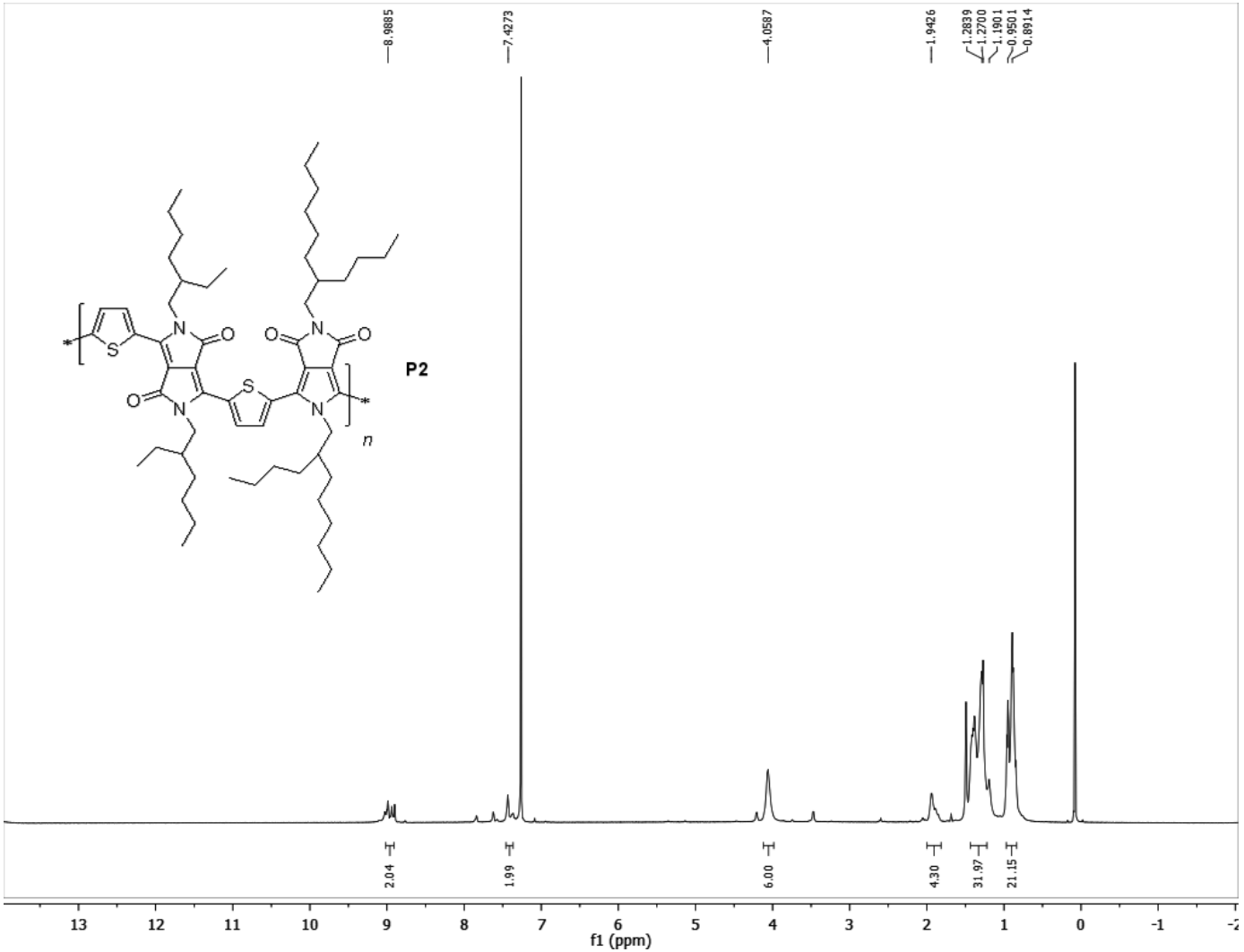


**Figure S5.16.** $^{1}$H NMR of **P2**.

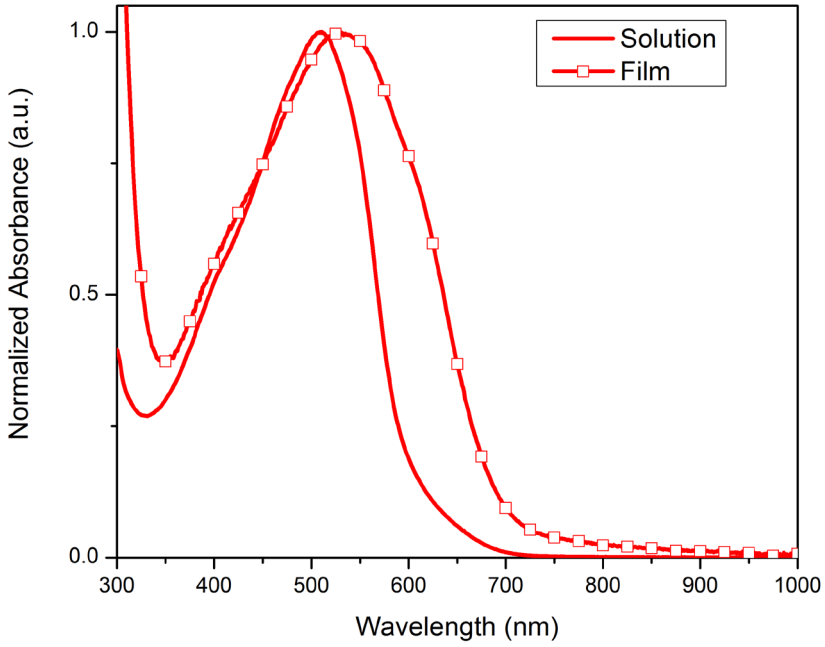


**Figure S5.17**. Normalized UV-vis absorption spectra of **P1**.

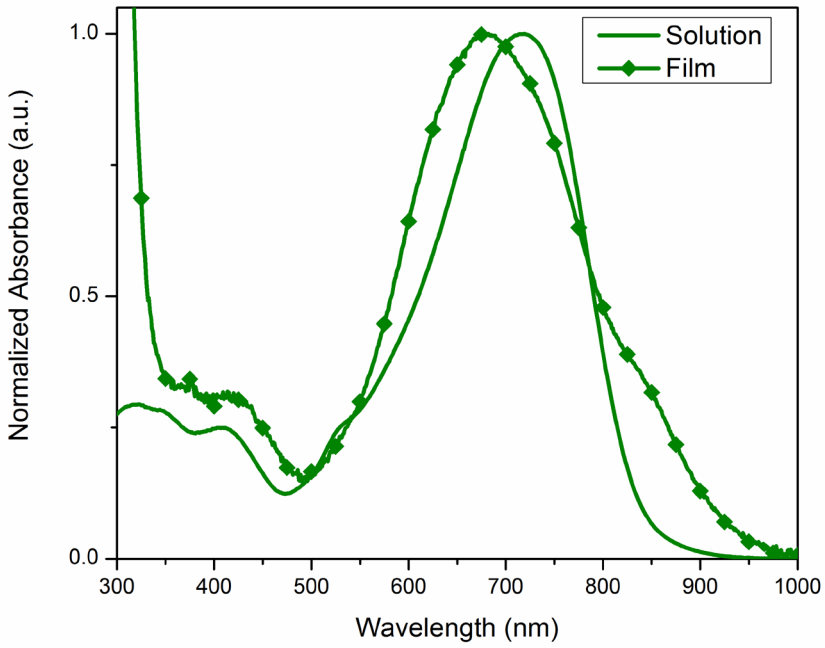


**Figure S5.18**. Normalized UV-vis absorption spectra of **P2**.

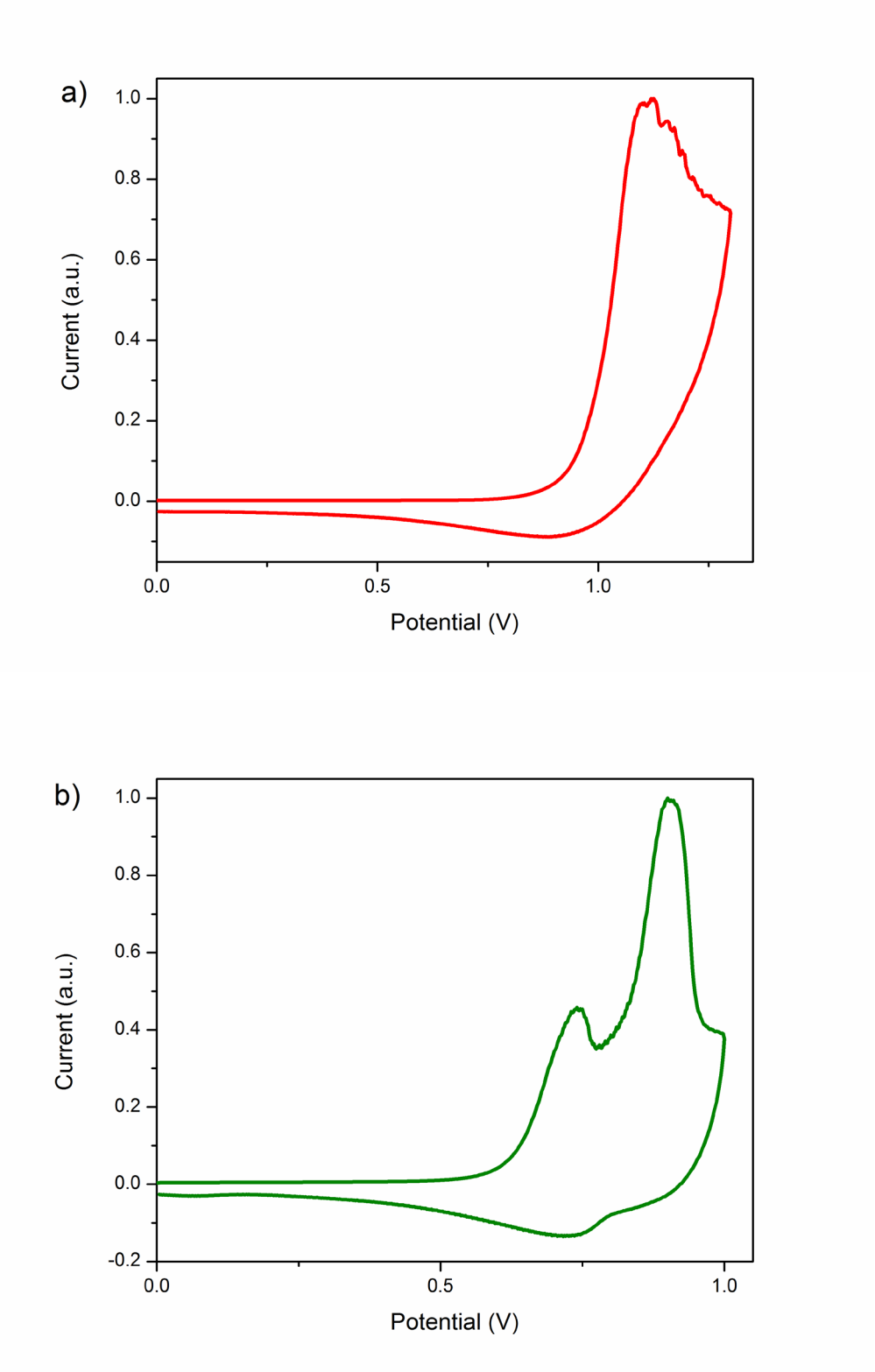


**Figure S5.19.** Cyclic voltammetry traces of a) **P1** and b) **P2**.

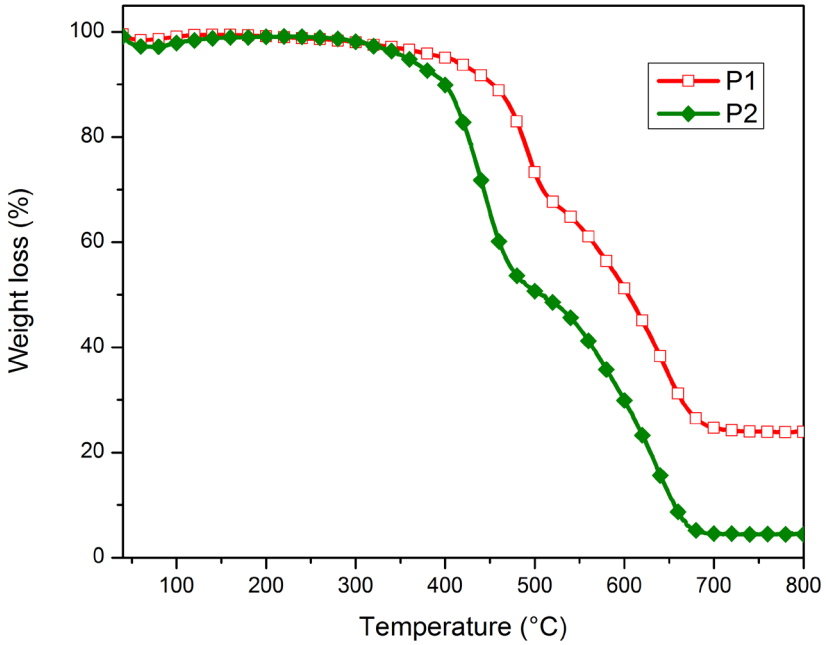


**Figure S5.20**. Thermal gravometric analysis of **P1** and **P2**.

## 5.8 References

1. Shirakawa, H.; Louis, E. J.; Macdiarmid, A. G.; Chiang, C. K.; Heeger, A. J., *J Chem Soc Chem Comm* **1977**, DOI 10.1039/c39770000578 (16), 578-580.

2. Chiang, C. K.; Fincher, C. R.; Park, Y. W.; Heeger, A. J.; Shirakawa, H.; Louis, E. J.; Gau, S. C.; MacDiarmid, A. G., *Phys. Rev. Lett.* **1977,** *39* (17), 1098-1101.

3. Heeger, A. J.; Sariciftci, N. S.; Namdas, E. B., *Semiconducting and Metallic Polymers*. OUP Oxford: 2010.

4. Shinar, J.; Shinar, R., 1.04 - An Overview of Organic Light-Emitting Diodes and their Applications. In *Comprehensive Nanoscience and Technology*, Wiederrecht, D. L. A. D. S. P., Ed. Academic Press: Amsterdam, 2011, pp 73-107.

5. Intemann, J. J.; Hellerich, E. S.; Tlach, B. C.; Ewan, M. D.; Barnes, C. A.; Bhuwalka, A.; Cai, M.; Shinar, J.; Shinar, R.; Jeffries-El, M., *Macromolecules* **2012,** *45* (17), 6888-6897.

6. Ego, C.; Marsitzky, D.; Becker, S.; Zhang, J.; Grimsdale, A. C.; Müllen, K.; MacKenzie, J. D.; Silva, C.; Friend, R. H., *J. Am. Chem. Soc.* **2003,** *125* (2), 437-443.

7. Kobilka, B. M.; Hale, B. J.; Ewan, M. D.; Dubrovskiy, A. V.; Nelson, T. L.; Duzhko, V.; Jeffries-El, M., *Polymer Chemistry* **2013,** *4* (20), 5329.

8. Beaujuge, P. M.; Fréchet, J. M. J., *J. Am. Chem. Soc.* **2011,** *133* (50), 20009-20029.

9. Beaujuge, P. M.; Amb, C. M.; Reynolds, J. R., *Acc. Chem. Res.* **2010,** *43* (11), 1396-1407.

10. Dimitrakopoulos, C. D.; Malenfant, P. R. L., *Adv. Mater.* **2002,** *14* (2), 99-117.

11. Facchetti, A., *Chem. Mater.* **2010,** *23* (3), 733-758.

12. Usta, H.; Facchetti, A.; Marks, T. J., *Acc. Chem. Res.* **2011,** *44* (7), 501-510.

13. Janiak, C., *Dalton Transactions* **2003**, 10.1039/b305705b (14), 2781-2804.

14. Entwistle, C. D.; Marder, T. B., *Chem. Mater.* **2004,** *16* (23), 4574-4585.

15. Camposeo, A.; Del Carro, P.; Persano, L.; Pisignano, D., *Adv. Mater.* **2012,** *24* (35), OP221-OP225.

16. Darling, S. B.; You, F., *RSC Advances* **2013,** *3* (39), 17633-17648.

17. Yamamoto, T.; Zhou, Z.-h.; Kanbara, T.; Shimura, M.; Kizu, K.; Maruyama, T.; Nakamura, Y.; Fukuda, T.; Lee, B.-L.; Ooba, N.; Tomaru, S.; Kurihara, T.; Kaino, T.; Kubota, K.; Sasaki, S., *J. Am. Chem. Soc.* **1996,** *118* (43), 10389-10399.

18. Li, Y., *Acc. Chem. Res.* **2012,** *45* (5), 723-733.

19. Lee, B.-L.; Yamamoto, T., *Macromolecules* **1999,** *32* (5), 1375-1382.

20. Cheng, Y.-J.; Yang, S.-H.; Hsu, C.-S., *Chem. Rev.* **2009,** *109* (11), 5868-5923.

21. Carsten, B.; He, F.; Son, H. J.; Xu, T.; Yu, L., *Chem. Rev.* **2011,** *111* (3), 1493-1528.

22. Lu, L.; Yu, L., *Adv. Mater.* **2014,** *26* (26), 4413-4430.

23. Yang, B.; Yuan, Y.; Sharma, P.; Poddar, S.; Korlacki, R.; Ducharme, S.; Gruverman, A.; Saraf, R.; Huang, J., *Adv. Mater.* **2012,** *24* (11), 1455-1460.

24. Carsten, B.; Szarko, J. M.; Lu, L.; Son, H. J.; He, F.; Botros, Y. Y.; Chen, L. X.; Yu, L., *Macromolecules* **2012,** *45* (16), 6390-6395.

25. Carsten, B.; Szarko, J. M.; Son, H. J.; Wang, W.; Lu, L.; He, F.; Rolczynski, B. S.; Lou, S. J.; Chen, L. X.; Yu, L., *J. Am. Chem. Soc.* **2011,** *133* (50), 20468-20475.

26. Jeffries-El, M.; Kobilka, B. M.; Hale, B. J., *Macromolecules* **2014,** *47* (21), 7253-7271.

27. Pollack, S. K.; Hijji, Y. M.; Kgobane, B., *Macromolecules* **1997,** *30* (21), 6709-6711.

28. Bao, Z.; Chan, W. K.; Yu, L., *J. Am. Chem. Soc.* **1995,** *117* (50), 12426-12435.

29. Coughlin, J. E.; Henson, Z. B.; Welch, G. C.; Bazan, G. C., *Acc. Chem. Res.* **2013,** *47* (1), 257-270.

30. Farina, V.; Krishnamurthy, V.; Scott, W. J.; Scott, W. J., *The Stille Reaction*. Wiley: 1998.

31. Rabindranath, A. R.; Zhu, Y.; Heim, I.; Tieke, B., *Macromolecules* **2006,** *39* (24), 8250-8256.

32. Woo, C. H.; Beaujuge, P. M.; Holcombe, T. W.; Lee, O. P.; Fréchet, J. M. J., *J. Am. Chem. Soc.* **2010,** *132* (44), 15547-15549.

33. Cardona, C. M.; Li, W.; Kaifer, A. E.; Stockdale, D.; Bazan, G. C., *Adv. Mater.* **2011,** *23* (20), 2367-71.

34. Beaupré, S.; Belletête, M.; Durocher, G.; Leclerc, M., *Macromol. Theory Simul.* **2011,** *20* (1), 13-18.

35. Allemand, P. M.; Koch, A.; Wudl, F.; Rubin, Y.; Diederich, F.; Alvarez, M. M.; Anz, S. J.; Whetten, R. L., *J. Am. Chem. Soc.* **1991,** *113* (3), 1050-1051.

36. Sariciftci, N. S.; Smilowitz, L.; Heeger, A. J.; Wudl, F., *Science* **1992,** *258* (5087), 1474-1476.

37. Najari, A.; Berrouard, P.; Ottone, C.; Boivin, M.; Zou, Y.; Gendron, D.; Caron, W.-O.; Legros, P.; Allen, C. N.; Sadki, S.; Leclerc, M., *Macromolecules* **2012,** *45* (4), 1833-1838.

38. Zhou, E.; Yamakawa, S.; Tajima, K.; Yang, C.; Hashimoto, K., *Chem. Mater.* **2009,** *21* (17), 4055-4061.

# CHAPTER 6

# GENERAL CONCLUSIONS

## 6.1 Dissertation Conclusions

Throughout this dissertation, the author has demonstrated how heterocycle substitution can have a dramatic, and potentially unintended, impact the physical, optical, electrochemical, and photovoltaic properties of donor materials used in organic electronics. A change as small as a heteroatom substitution up or down a group can selectively tune energy levels by either stabilizing or destabilizing them, resulting in wider or narrower bandgaps. Along the same lines, a substitution with a heteroatom from a different group can completely reverse the role of a building block from being π-electron acceptor, like TPD, to a π-electron donor, as in PPD. Full heterocycle substitution can further be used to tune the absorption of materials, by playing on strength of aromaticity. The use of thienothiophene in molecular donors resulted in materials that had a blue-shifted absorption, due to higher aromaticity, and larger degree of π-stacking than their bithiophene analogues. Replacing the bridging silicon of DTS with a carbon results in materials with red-shifted absorption and narrow bandgap, but lower current density when used in preliminary photovoltaic devices, thought to be the result of reduced structural order caused by the shorter covalent bonds.

While many of these materials are still in the process of being optimized in photovoltaic devices, their optical and electrochemical properties suggest they have the potential for significantly higher efficiencies than similar analogues that have been

previously reported. The alkyl chain effect being studied on the DPP based devices will give useful insight into judicious alkyl chain selection for future generations of materials. This work adds to the ever growing understanding of the importance heterocycle selection plays on the electronic, optical, and physical properties of materials for organic photovoltaics.

## 6.2 Acknowledgements

All of the work described in this dissertation, and even the writing of this dissertation itself, would not have been possible if it weren't for the unwavering support, love, and encouragement from my love, Clair Williams. She has not only made me want to become a better researcher, but a better person. Her willingness to tolerate the incredibly late hours (especially the last year), listen to my complaining about reactions not working, and ability to keep me grounded, among countless other things, has meant more to me than she may ever know. To my parents, Jim and Linda, and sisters, Jessica and Kimberly: I will always appreciate the love, support, and encouragement you've given me throughout my life and academic career.

I want to thank my advisor, Dr. Malika Jeffries-EL, for all she has done for me. Over the past six years, she has given me free reign to explore (most of) my ridiculous ideas in lab, and also prevented me on numerous occasions from recreating the iconic copier scene from Office Space with the seemingly constantly broken THF GPC. I'd like to show my gratitude for the current members of the Jeffries-EL group, particularly Dana Drochner, for the chemistry discussions the past year. To Dr. Jared Mike, Dr. Jeremy Intemann, Dr. Brandon Kobilka, Dr. Brian Tlach, and Dr. Achala Bhuwalka: Thank you for your guidance

and friendship throughout my time at ISU. I will be forever grateful. I would also like to thank Dr. Sumit Chaudhary, Dr. Moneim Elshobaki, and Ryan Gebhardt for their help with making solar cells and engineering discussions. I am thankful for the assistance of the great people at the ISU chemical instrumentation facility for all of their help characterizing my compounds and training me on instruments, especially Steve Veysey, Dr. Kamel Harrata, Dr. Shu Xu, Dr. Dave Scott, and Dr. Sarah Cady.

I want to thank the entire Williams family for their support the last few years and Dave "The Prairie Guy" Williams for help taking my mind off of lab with all the great fishing trips. I'd like to thank Dr. Randy Benedict, The Dr. Jesse Waldo, and Dr. Bernie Anding for all the chemistry discussions over the years as well as a multitude of non-chemistry discussions, video game marathons, and just all around fun. If it weren't for Dr. Andrew Korte, Dr. Christie Beck, Dr. Patrick Hanway, and Dr. Adam Klein – my first friends at ISU – who could say I would have even gotten past my prelim. I miss you all. I also want to thank all the friends I've made at ISU, that have long since gone their own way, that I haven't been able to mention here by name. You've all made my time in Ames memorable. As I sit here, finishing up this final section, I find myself reflecting on the past 6 years, and it occurs to me: What a long, strange trip it's been.

# APPENDIX

## LIST OF ACRONYMS AND DESCRIPTIONS

| Acronym | Description |
|---|---|
| A | Acceptor |
| AFM | Atomic force microscopy |
| APCI | Atmospheric-pressure chemical ionization |
| BDT | Benzo[1,2-*b*:4,5-*b′*]dithiophene |
| BHJ | Bulk-heterojunction |
| BLA | Bond lengthalternation |
| BT | 2,2'-bithiophene |
| CB | Chlorobenzene |
| CN | 1-chloronapthalene |
| CPDT | Cyclopenta[2,1-*b*;3,4-*b′*]dithiophene |
| CV | Cyclic voltammetry |
| D | Donor |
| D-A | Donor-acceptor |
| DIO | 1,8-diiodooctane |
| DFT | Density functional theory |
| $DP_n$ | Degree of polymerization |
| DPP | 1,4-diketopyrrolo[3,4-*c*]pyrrole |
| DTS | Dithieno[3,2-*b*:2',3'-*d*]silole |

| Acronym | Description |
|---|---|
| DSC | Differential scanning calorimetry |
| Đ | Dispersity |
| $E_g$ | Bandgap |
| $E_g^{opt}$ | Optical bandgap |
| $E_g^{EC}$ | Electrochemical bandgap |
| ESI | Electron-spray ionization |
| FBT | 5-fluoro-2,1,3-benzothiadiazole |
| FF | Fill factor |
| GPC | Gel permeation chromatography |
| HOMO | Highest occupied molecular orbital |
| HRMS | High resolution mass spectrometry |
| $I_{SC}$ | Current density |
| ICT | Intramolecular charge transfer |
| ITO | Indium tin oxide |
| $J$ | Current density |
| $J_{SC}$ | Short-circuit current density |
| LUMO | Lowest unoccupied molecular orbital |
| $M_n$ | Number-averaged molecular weight |
| MO | Molecular orbital |
| $M_w$ | Weight-averaged molecular weight |
| NMR | Nuclear magnetic resonance |
| *o*-DCB | 1,2-dichlorobenzene |

| Acronym | Description |
|---|---|
| OFET | Organic field-effect transistor |
| OLED | Organic light-emitting diode |
| OPV | Organic photovoltaic cell |
| P3HT | poly(3-hexylthiophene) |
| PCBM | [6,6]-phenyl-$C_{61}$-butyric acid methyl ester |
| PC[60]BM | [6,6]-phenyl-$C_{61}$-butyric acid methyl ester |
| PC[61]BM | [6,6]-phenyl-$C_{61}$-butyric acid methyl ester |
| $PC_{61}BM$ | [6,6]-phenyl-$C_{61}$-butyric acid methyl ester |
| $PC_{71}BM$ | [6,6]-phenyl-$C_{71}$-butyric acid methyl ester |
| PC[70]BM | [6,6]-phenyl-$C_{61}$-butyric acid methyl ester |
| PC[71]BM | [6,6]-phenyl-$C_{61}$-butyric acid methyl ester |
| PCE | Power conversion efficiency |
| PDI | Poly Dispersity Index |
| PEDOT:PSS | Poly(3,4-ethylenedioxythiophene) polystyrene sulfonate |
| PITN | Polyisothianaphthene |
| PPD | Pyrrolo[3,4-*c*]pyrrole-4,6-dione |
| PPP | Poly(para-phenylenevinylene) |
| PPV | Poly(phenylenevinylene) |
| PT | Polythiophene |
| PV | Photovoltaic |
| PVC | Photovoltaic Cell |
| SCE | Standard calomel electrode |

| Acronym | Description |
|---|---|
| SCLC | Space-charge limited current |
| $T_d$ | Thermal decomposition temperature |
| TGA | Thermal gravimetric analysis |
| TPD | Thieno[3,4-*c*]pyrrole-4,6-dione |
| TT | Thieno[3,2-*b*]thiophene |
| $V_{OC}$ | Open circuit voltage |
| ε | Molar absorptivity |
| $\lambda_{max}$ | Wavelength of maximum absorption |